3.2.1 Number of research papers published per teacher in the Journals notified on UGC CARE list during the year 2023-2024

Sr. No.	Title of paper	Name of the author/s	Department of the teacher	Name of journal	Page Nos.
1	Study Of Dolichos Lab-Lab L (Indian Bean) As A Natural Coagulant For The Treatment of River Water	Prof. TonneAkshata R.	Civil Engineering	Journal Of Emerging Technologies & Innovative Research	1 to 5
2	Dynamic Evaluation of A Circular & Rectangular Water Tanks With Non-Linear Time History Data	Prof. Bore Rutuja S.	Civil Engineering	International Journal of Science & Engineering Development Research	6 to 15
3	Study Of TrigonellaFoenumGraecum (Fenugreek Seeds) As A Natural Coagulant For The Treatment of	Prof. TonneAkshata R.	Civil Engineering	International Research Journal Of Engineering & Technology (IRJET)	16 to 21
4	Artificial Intelligence Techniques for Landslides Prediction using Satellite Imagery	Dr. Suhas G. Sapate	CSE	IEEE Access	22 to 38
5	Prediction of electrocoagulation treatment of tannery wastewater using multiple linear regression based ANN: Comparative study on plane and punched electrodes	Dr. Suhas G. Sapate	CSE	Desalination and Water Treatment	39 to 51
6	Political Flower Pollination Optimizer for age-related macular degeneration detection enabled Deep Maxout network using OCT images	Ir. Rahul.S.Nejk	CSE	Biomedical Signal Processing and Control	52 to 89
7	Recent Trends and Advances in Deep Learning Techniques for Classification of Landslides using Satellite Images	Dr. Suhas G. Sapate	CSE	IOP Conference Series: Earth and Environmental Science	90 to 99
8	A Comprehensive Survey of Machine Learning Techniques for Ear Recognition System	Dr. Suhas G. Sapate	CSE	International journal of Advanced Networking and Applications	100 to 111
9	Solar Based Automatic Grass Cutter	Prof. N.S. Jadhav	Electrical	The International Journal of Innovative Research in Science, Engineering and Technology (IJIRSET)	112
10	DESIGN & DEVELOPMENT OF PV MODULAR	Prof. Y. R. Naik	Electrical	International Research Journal of Modernization in Engineering Technology and Science	113
11	3 PHASE INDUCTION WITH SOFT START	Prof. V. M. Ghewari	Electrical	International Research Journal of Modernization in Engineering Technology and Science	114

3.2.1 Number of research papers published per teacher in the Journals notified on UGC CARE list during the year 2023-2024

Sr. No.	Title of paper	Name of the author/s	Department of the teacher	Name of journal	Page Nos.
12	SOLAR WIND HYBRID ELECTRIC VEHICLE	Prof. A. M. Bhandare	Electrical	International Research Journal of Modernization in Engineering Technology and Science	115
13	TO MODIFIED AND DESIGN SOLAR POWERED BASED ENERGY EFFICIENT PORTABLE WASHING MACHINE	Prof. V. T. Metkari	Electrical	International Research Journal of Modernization in Engineering Technology and Science	116
14	SOLAR BASED GPS TRACKING HANDICAPPED TRICYCLE	Prof. N.S. Jadhav	Electrical	International Research Journal of Modernization in Engineering Technology and Science	117
15	SMART SOLAR AUTOMATION	Prof. Y. R. Naik	Electrical	International Research Journal of Modernization in Engineering Technology and Science	118
16	AUTOMATIC POWER FACTOR CONTROLLER	Prof. B. S. Hebbale	Electrical	International Research Journal of Modernization in Engineering Technology and Science	119
17	DESIGN AND DEVELOPMENT OF SIGN LANGUAGE TO SPEECH CONVERSION	Prof. P.D. Pange	Electrical	INTERNATIONAL JOURNAL OF PROGRESSIVE RESEARCH IN ENGINEERING MANAGEMENT	120
18	SOLAR POWER CHARGE CONTROLLER USING ARDUINO	Prof. B. S. Hebbale	Electrical	International Research Journal of Modernization in Engineering Technology and Science	121
19	Vertical Injection Plastic Moulding Machine	Prof. A. M. Bhandare	Electrical	International Journal of Innovative Research in Science, Engineering and Technology	122
20	Performance analysis of sodium alanate hydride reactor with different nanofluids	Rahul U. Urunkar	Mechanical	International Journal of Hydrogen Energy	123

JETIR.ORG ISSN: 2349-5162 | ESTD Year : 2014 | Monthly Issue
JOURNAL OF EMERGING TECHNOLOGIES AND INNOVATIVE RESEARCH (JETIR)
An International Scholarly Open Access, Peer-reviewed, Refereed Journal

STUDY OF *DOLICHOS LABLAB-L* (INDIAN BEAN) AS A NATURAL COAGULANT FOR THE TREATMENT OF RIVER WATER

[1]Tonne Akshata R., [2]Dr. Chonde S. G., [3]Bhosale S. M.
1PG. Student Department of Technology, Shivaji University Kolhapur-416004, Maharashtra India.
2Assistant Prof. Krishna Institute of Allied Sciences, Krishna Vishwa Vidyapeeth Karad, Maharashtra, India.
3Assistant Prof. Department of Technology, Shivaji University Kolhapur-416004, Maharashtra India.
1Department of Technology, Shivaji University Kolhapur-416004, Maharashtra India.

Abstract : Water is the most essential element in all human activity. As a result of numerous human activities like population growth, climate change, and rising living standards, water supplies are steadily being depleted. Water bodies like streams, rivers, and oceans become contaminated as a result of local activity such untreated wastewater escaping from nearby industry, urbanization, agricultural activities, transportation on waterways, increasing population, etc. Present study involves the use of *Dolichos Lablab-L* (Indian Bean) as a natural coagulant for river water study. The powder of *Dolichos Lablab-L* (Indian Bean) seed was applies for river water to check the tests for natural coagulant.

All the physicochemical parameters including pH, EC, TDS, turbidity, acidity, alkalinity, chloride content, hardness, DO, and COD were measured before the treatment. When the water had been treated, the parameters including pH, turbidity, hardness, DO, and COD were maintained. As a result, turbidity reduced from 13-10 NTU at a dosage of 200mg, reduces hardness up to 15-20%, increases the DO from 4.4 – 5mg /l, & removes COD about 40% after the treatment.

Key Words: Natural Coagulation, Coagulants, *Dolichos Lablab-L*, River Water, etc.

I. INTRODUCTION

The usefulness of substances such as alum and ferric chloride as coagulants is well known. However, there are numerous drawbacks to using it, including high operational expenses, negative effects on human health, the formation of vast volumes of sludge, and the fact that it drastically affects the pH of treated water. As a result, it is preferable to replace these chemical coagulants with natural-based coagulants.*(Shamira Shaharom et al. 2019).* A naturally occurring, plant-based coagulant known as a "natural coagulant" can be employed in the coagulation-flocculation stage of wastewater treatment to lower turbidity of water is known as natural coagulation.

The purpose of this was to look at the potential of plant-based compounds as coagulants for surface water treatment. As natural coagulants, two types of locally available plant-based compounds were chosen.*(Muhamad et al., 2020)* The goal of this study was to apply natural treatment methods to obtain safe drinking water.*(Khagga et al., 2010)* The coagulation ability of *Dolichos lablab* (Hyacinth Bean) extract was evaluated using standard jar test measurements in different turbidities of water. *Dolichos lablab's* investigation as a natural coagulant was validated by its positive effective coagulation activity. An optimum dose of 200 mg of this coagulant produced 68% coagulation activity for water purification and bacteria inactivation in 60 minutes.*(Khagga et al., 2010)*. The Hyacinth Bean (*Dolichos lablab*), also called Indian Bean, is a species of bean in the family Fabaceae that is widespread as a food crop throughout the tropics, especially in Africa, India, and Indonesia. The seeds of *Dolichos lablab* were obtained in pods and only seeds from dry pods were used.(Khagga et al., 2010) This contains crude protein which helps in formation of floc and removes turbidity of water.

II. MATERIAL & METHODOLOGY

2.1 Materials

2.1.1 River Water Collection

For the present study purpose the water sample was collected from Krishna Ghat, Kurundwad which is situated in Kolhapur District. This sample was collected 1m deep from the water surface to avoid the floating matters, and the sample was collected in air tight container to preserve dissolved oxygen of the water. (16.6875° N, 74.6005° E.)

Fig. 1 River Water from 'Krishna Ghat Kurundwad'

2.1.2 Natural Coagulants Used for Study

2.1.2.1 Dolichos Lablab (L) (Indian Bean)

These seeds are brought from the grocery shop. The seeds are oven dried in the DOT's Environment Laboratory at 30°c for 24 hours. After that the powder is made using the grinder.

Fig. 2 Dolichos Lablab L (Indian Bean)

Fig 3 Dolichos Lablab L in Powdered form

2.1.3 Methodology Adopted

2.1.3.1 Physicochemical Characteristics Study of River Water Before Treatment

1. pH: pH stands for potential of hydrogen, i.e. H+ ion concentration present in the water which represents the nature of water i.e. acidic or basic state. The pH scale determines whether water is basic (alkaline) or acidic. From 0 (extremely acidic) to 14 (basic alkalinity), the pH scale is logarithmic (very alkaline).

2. Electrical Conductivity: Since dissolved solids split into positively and negatively charged ions, water's conductivity is a measure of how well it can carry an electric current.

3. Alkalinity: Natural water is typically alkaline because the bicarbonates are presence which creates the reactions in the soils that the water percolates through. It represents the buffering power of the water and measures its ability to neutralize acids. It may also be to blame, because it protects or acts as a buffer against abrupt pH changes, alkalinity is essential for fish and other aquatic life.

4. Acidity: The quantitative ability of water or solution to neutralize an alkali is known as its acidity. In plain English, this means that pH is a gauge of an aqueous solution's acidity or basicity. Acidic solutions are those with a pH under 7, and basic or alkaline solutions are those with a pH above 7. Low pH can cause copper in your household plumbing to leach into the water, leaving green stains on porcelain surfaces like bathroom sinks. Another possibility is that the water itself has a blue color.

5. Hardness: Hardness is an inherent property of water that can improve its flavour and consumer acceptability for drinking. Water's hardness is caused by calcium and magnesium minerals, which are found naturally in water. Poor soap lathering and scum are typical indicators of hard water. There are two types of hardness: temporary (carbonate) and permanent (non-carbonate). Water that has become temporarily hard can be easily made soft by boiling it.

6. Dissolved Oxygen: The volume of oxygen in the atmosphere (O2) that has been dissolved in water is known as dissolved oxygen. By aeration (rapid movement), diffusion from the surrounding air, and as a waste product from photosynthesis, enters in water. The majority of aquatic organisms require dissolved oxygen in order to survive and develop. Some organisms, like catfish, worms, and dragonflies, can survive in slightly lower concentrations of DO than others, such as fish and stoneflies, which require high concentrations of DO. Insufficient oxygen levels in water can cause adult and juvenile deaths, poor growth, failed egg or larval survival, and a shift in the species that live in a particular water body. When oxygen levels in a body of water

fall below 3 mg/L, the aquatic system's circulatory fluid balance is disturbed, which impairs cell function and ultimately results in death.

7. **Chemical Oxygen Demand:** The Chemical Oxygen Demand (COD) formula calculates the amount of oxygen needed to oxidize the organic material present in a water body at a specific temperature and time. COD is an essential indicator of water quality because it offers a baseline for determining the impact that wastewater discharge will have on the environment. Higher COD levels signify the presence of more oxidizable organic matter in the sample, and as this material degrades, the water body will once more experience low oxygen conditions. The proportion of organic material in the water that can be broken down by environmental microorganisms is shown by the BOD to COD ratio.

2.1.4 Coagulation Study Using Jar Test

1. The collected river water was tested before the treatment for various physico-chemical analysis which includes pH, E.C., TDS, Turbidity, Acidity, Alkalinity, Chloride content, Hardness, DO, COD, etc. The *Dolichos Lablab L* powder was prepared & it was tested for river water at the conc. dose of 200mg, 400mg, 600mg, 800mg, & 1000mg, for coagulation purpose with the help of jar test.
2. The sample is kept for 4 -5 minutes for mixing the coagulant and rotated about 100 rpm.
3. Switch off the apparatus and give the containers 30 to 45 minutes to settle.
4. Stirring should be reduced to 25 to 35 rpm, and mixing should go on up to 15 minutes to 20 minutes. In order to create larger flocs, particle collisions are enhanced by the slower mixing speed.
5. Then, the residual turbidity is plotted against the coagulant dose to identify the ideal circumstances.
6. The jar test was performed at different concentration of coagulant *Dolichos Lablab L* & the best coagulant dose was identified on the basis of physico-chemical characteristics of water after the treatment.

Fig. 4 Jar Test Using Natural Coagulant *DOLICHOS LABLAB L* (Indian Bean)

III. OBSERVATIONS FOR RIVER WATER SAMPLE

DOSAGE OF *Dolichos Lablab L*						
TESTS	**Control**	**200mg**	**400mg**	**600mg**	**800mg**	**1000mg**
pH	7.693	6.637	6.653	6.63	6.502	6.522
EC (µs)	394	462	490	518	546	574
TDS (mg/l)	207	232	245	259	273	287
TURBIDITY (NTU)	13	10	12	15	18	20
ACIDITY (mg/l)	30	45	52	55	61	69
ALKALINITY (mg/l)	90	40	40	45	50	50
CHLORIDE (mg/l)	25	25.5	27.5	30	32.5	35
HARDNESS (mg/l)	67.5	55	57.5	60	62.5	65
DO (mg/l)	4.4	5	5.3	5.4	5.5	5.6
COD (mg/l)	320	196	168	142	120	98

Table 1 Dolichos Lablab L (Indian Bean) Powder Coagulation in River Water Sample

RIVER WATER SAMPLE

Parameters	Before Treatment	After Treatment
pH	7.693	6.637
EC (µs)	394	462
TDS (mg/l)	207	232
TURBIDITY (NTU)	13	10
ACIDITY (mg/l)	30	45
ALKALINITY (mg/l)	90	40
CHLORIDE (mg/l)	25	25.5
HARDNESS (mg/l)	230	185
DO (mg/l)	4.4	5
COD (mg/l)	320	196

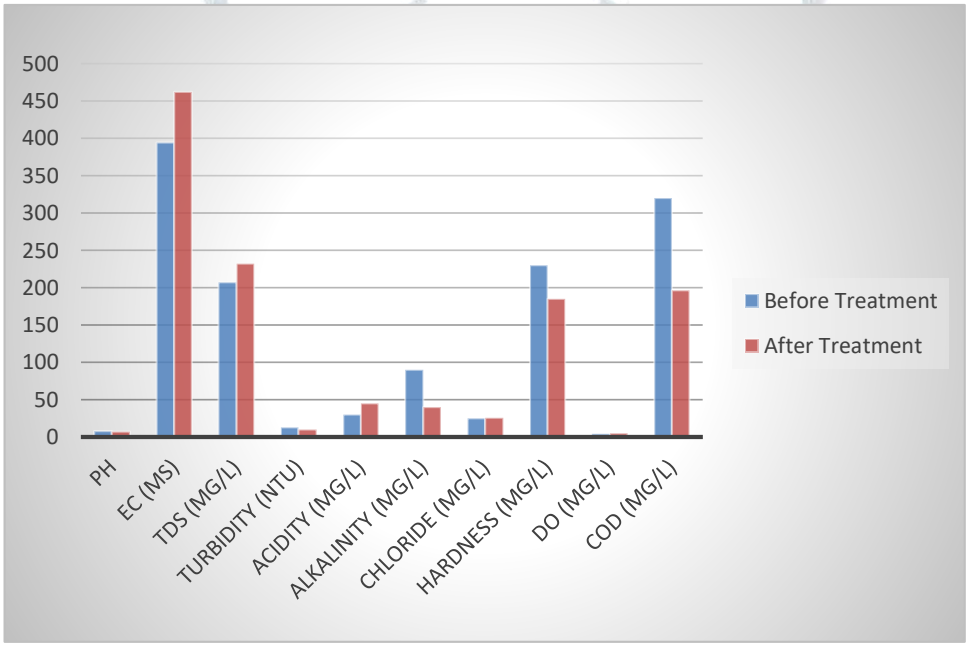

Graphical Representation of Optimum Dosage of Dolichos Lablab L (Indian Bean) Powder in River Water Sample

Parameters	River Water Sample Before Treatment	River Water Sample After Treatment (Optimum Dosage of 200mg)	WHO Standards
pH	7.693	6.637	6.5 - 8.5
EC	394	462	50 - 500 µs/cm
TDS	207	232	500 mg/l
TURBIDITY	13	10	1 - 5 NTU
ACIDITY	30	45	No Guidelines
ALKALINITY	90	40	200 - 600 mg/l
CHLORIDE	25	25.5	250 mg/l
HARDNESS	230	185	500 mg/l
DO	4.4	5	No Guidelines
COD	320	196	No Guidelines

Table 2 Comparison with WHO Standards & Results Obtained by Natural Coagulation with Effective Dose For River Water Sample

RESULT AND DISCUSSION

From the above study the optimum dosage for the coagulation process using *Dolichos lablab L* seed powder is 200 mg/l. The pH of Sample before treatment is 7.693 and it becomes 6.637 after the coagulation process. Electric conductivity gets increases due to presence of organic matter in the form of natural coagulant. TDS also little bit more than raw water sample. Turbidity gets reduced by 24%, alkalinity reduces up to 56% after the treatment, hardness also gets reduced up to 20%, D.O. before the treatment is 4.4 mg/l and it becomes 5 mg/l after the treatment, it shows better results for the removal of COD, it reduces nearby 70% after the treatment i.e. it was 320mg/l before treatment ad reduced up to 196mg/l after treatment.

CONCLUSION

From the above study it can be concluded that *Dolichos lablab* seeds was found to be good for water treatment. *Dolichos lablab* seed powder has effective coagulant properties. It is reasonably priced to make locally. It keeps the pH within an acceptable range, lowers physicochemical characteristics like turbidity, acidity, alkalinity, chlorides, hardness, and COD, and maintains the DO within a permitted range for selected water samples.

As it is a low-cost natural coagulant it will be very useful for household drinking water treatment especially in rural areas.

REFERENCES

1) *II Sampling*. ([s.d.]).
2) Ilyas, Z., & Ashfaq, M. ([s.d.]). *Water Sampling, Testing techniques and Water Borne diseases Cement Factories of Pakistan And Contact Details View project History of Major Earthquakes in pakistan and Effects on Building Structures View project*. https://doi.org/10.13140/RG.2.2.32165.22249
3) *jar test*. ([s.d.]). Recuperado 10 de junho de 2023, de https://www.owp.csus.edu/glossary/jar-test.php
4) Khagga, M., Unnisa, S. A., Deepthi, P., & Mukkanti, K. (2010). Efficiency studies with Dolichos lablab and solar disinfection for treating turbid waters. Em *JOURNAL OF ENVIRONMENTAL PROTECTION SCIENCE* (Vol. 4). https://www.researchgate.net/publication/268288918
5) Muhamad, N. A. N., Juhari, N. F., & Mohamad, I. N. (2020). Efficiency of natural plant-based coagulants for water treatment. *IOP Conference Series: Earth and Environmental Science*, *616*(1). https://doi.org/10.1088/1755-1315/616/1/012075
6) Shamira Shaharom, M., & Siti Quraisyah Abg Adenan, D. (2019). POTENTIAL OF ORANGE PEEL AS A COAGULANT FOR WATER TREATMENT. Em *Infrastructure University Kuala Lumpur Research Journal* (Vol. 7, Número 1).

Dynamic Evaluation of a Circular and Rectangular Water Tanks with Non-Linear Time History Data

[1]Miss. Rutuja Vitthal Sabale, [2]Prof. Mr. Ravindra Desai

[1]Student, M.Tech Structural Engineering, [2]Professor
Dept. of Civil Engineering
Sanjay Ghodawat University, Kolhapur.

***Abstract*- Elevated water tank is a water storage facility supported by a tower and constructed at an elevation to provide useful storage and pressure for a water distribution system. The height of the tower provides the pressure for the water supply system. During the high peak hours of the water system, the static potential reserved in the tank will be used to provide the pressure in the water pipes and helps the pumping systems by maintaining the necessary water pressure without increasing pumping capacity. They also present enough water pressure for firefighting when the pumping systems are not sufficient to provide large amount of water needed for fire extinguishing. In public water distribution system, Elevated water tanks are generally used being an important part of a lifeline system. Due to post earthquake functional needs, seismic safety of water tanks is of most important. Elevated water tanks also called as elevated service reservoirs (ESRs) typically consists of a container and a supporting tower. In major cities and also in rural areas elevated water tanks forms an Integral part of water supply system. The elevated water tanks must remain functional even after the earthquakes as water tanks are most essential to provide water for drinking purpose. These paper analysis and design of elevated water tank of different type such as rectangular and circular water tank by using software SAP2000 by using various bracing system.**

***Keywords*: Elevated Water tank, SAP 2000, Bracing System, Circular, Rectangular.**

I. INTRODUCTION

Elevated water tanks are commonly used in public water distribution system. Being an important part of lifeline system, and due to post earthquake functional needs, seismic safety of water tanks is of considerable importance. Elevated water tanks also called as elevated service reservoirs (ESRs) typically comprises of a container and a supporting tower (also called as staging). Staging in the form of reinforced concrete shaft and in the form of reinforced concrete column-brace frame are commonly deployed. The column-brace frame type of staging is essentially a 3D reinforced concrete frame which supports the container and resists the lateral loads induced due to earthquake or wind.

A. Performance of elevated water tank

Geological and seismological discoveries during the 20thcentury have helped in initiating the development of seismic building codes and earthquake resistant buildings and structures. The improvement in seismic design requirements has led to more robust, safe and reliable buildings. Due to the earthquake many buildings collapsed killing thousands of people. Therefore, to protect the earthquake effects/earthquake damages to the buildings and to protect the life of people, it's important to use seismic control techniques. The base isolators are provided at the basement level to absorb the earthquake energy or earthquake forces. Not only important buildings such as Museum, Shopping Mall, Hospital, Water tanks, Dams, and Airports etc. are provided with base isolator, but if the occurrence of the earthquake is more often it can be provided for all types of buildings.

B. Nonlinear Time History Analysis:

Nonlinear Time History Analysis can be used for all isolation systems regardless of height, size, geometry, location, and nonlinearity of the isolation system. Time-History analysis is a step-by-step procedure where the loading and the response history are evaluated at successive time increments. During each step, the response is evaluated from the initial conditions existing at the beginning of the step (displacements and velocities) and the loading history in the interval. Nonlinear time history analysis is the dynamic analysis in which the loading causes significant changes in stiffness. With this method, the non-linear behaviour may be easily considered by changing the structural properties (e.g. stiffness, (k) from one step to the next. Therefore, this method is one of the most effective for the solution of non-linear response. Non-linear time history analysis utilizes the combination of ground motion records with a detailed structural model, Response of base isolated structure on liquefiable soil. Therefore, is capable of producing results with relatively low uncertainty. In nonlinear dynamic analyses, the detailed structural model subjected to a ground-motion record produces estimates of component deformations for each degree of freedom in the model and the modal responses are combined using schemes such as the square-root-sum-of-squares.

Table 1: Properties of Ground Motion

Earthquake Area	Magnitude	Record/ Component	PGA
EI-Centro (1940)	7.2	El-Centro 1940,	0.35 g
Bhuj (2001)	7.7	Bhuj (2001), India	0.38 g
Uttarkashi	6.6	Uttarkashi (2001), India	0.31 g

(2001)			
Koyna (1967)	6.5	Koyna(1967)	0.31g
Chamoli (1999)	6.8	Chamoli(1999)	0.31g

II. METHODOLOGY

The main objective of this study is to examine the behaviour of overhead circular water tank supported on frame staging considering different modelling systems. All the above cases are analysed for five different earthquake records i.e. time history analysis. The analysis is carried out using SAP 2000 software.

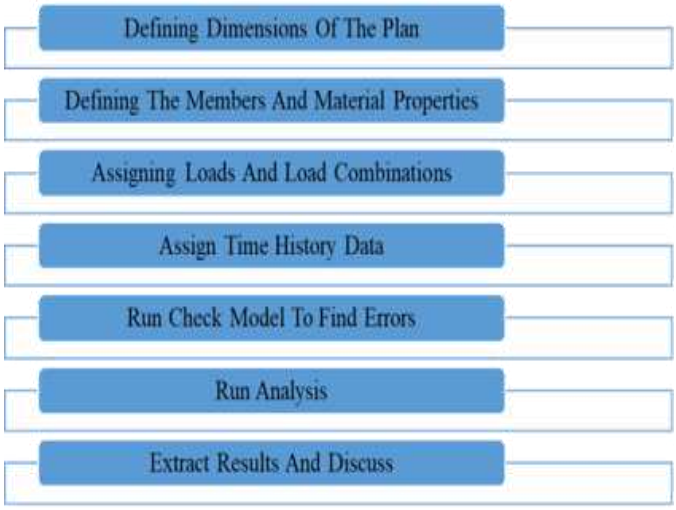

A. Types of bracing

- **Single diagonals**

Trussing, or triangulation, is formed by inserting diagonal structural members into rectangular areas of a structural frame, helping to stabilise the frame. If a single brace is used, it must be sufficiently resistant to tension and compression

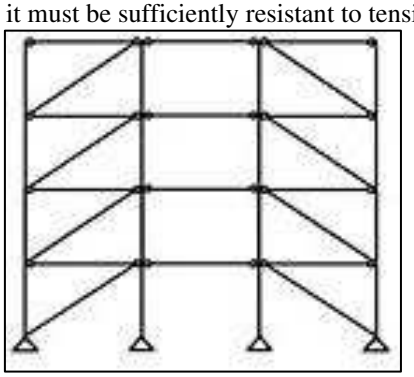

Fig 1. Single bracing

- **Cross-bracing**

Cross-bracing (or X-bracing) uses without diagonal members crossing each other. These only need to be resistant to tension, one brace acting to resist sideways forces at a time depending on the direction of loading. As a result, steel cables can also be used for cross-bracing.

Fig 2 Cross bracing

- **K-bracing**

Braces connect to the columns at mid-height. This frame has more flexibility for the provision of openings and results in the least bending in floor beams. K-bracing is generally discouraged in seismic regions because of the potential for column failure if the compression brace buckles

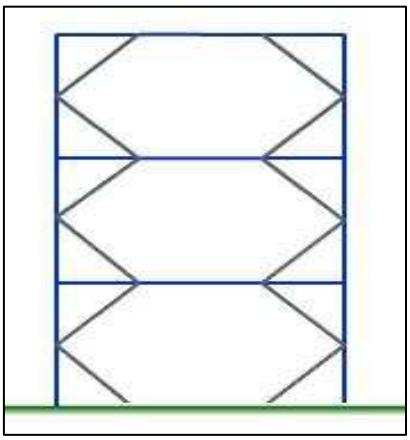

Fig 3 K-bracing

III. PROBLEM STATEMENT

A. Model input Data

- **Size of Rectangular Water Tank**
  - L = 9m
  - B = 4.5m
  - H= 4m
- **Size of Circular Water Tank**
  - Diameter - 7m
  - H= 4m
  - Staging Height=20m
  - Beam size - 230x600
  - Column size - 230x650
  - Earthquake zone - III
  - Time history – Bhuj
  - Soil – Medium stiff
  - Depth of Foundation - 1.5m
  - Concrete – M30
  - Bracing BRB- A buckling-restrained brace (BRB) is a structural brace, designed to allow the structure to withstand cyclical lateral loadings, typically earthquake-induced loading. It consists of a slender steel core, a concrete casing designed to continuously support the core and prevent buckling under axial compression, and an interface region that prevents undesired interactions between the two.

Table 2 Models

Model No.1	Rectangular water tank without bracing
Model No.2	Rectangular water tank with single bracing
Model No.3	Rectangular water tank double bracing
Model No.4	Rectangular water tank knee bracing
Model No.5	Circular water tank without bracing
Model No.6	Circular water tank with single bracing
Model No.7	Circular water tank double bracing
Model No.8	Circular water tank knee bracing

IV. MODEL DESCRIPTION

1) Rectangular Water Tank (Plain)

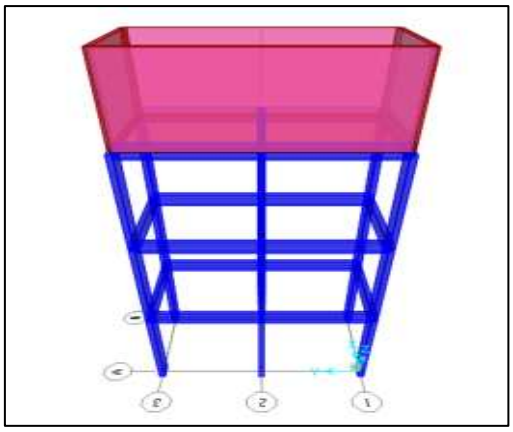

Fig 4 Rectangular water tank without Bracing

2) Rectangular Water Tank with Single Bracing

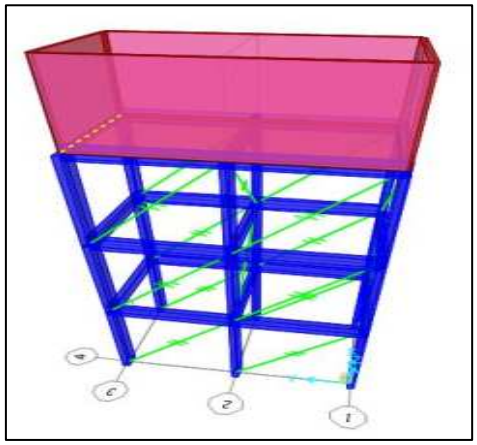

Fig 5 Rectangular water tank with Single Bracing

3) Rectangular Water Tank with Knee Bracing

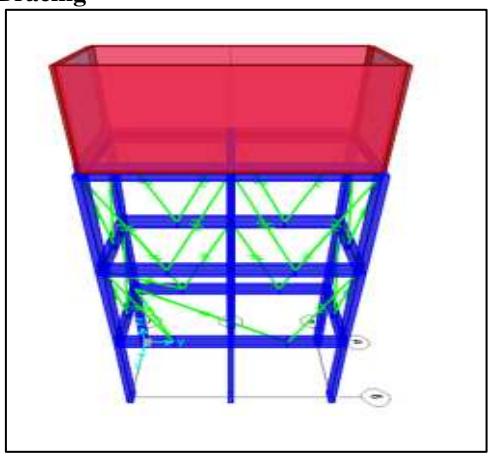

Fig 6 Rectangular water tank Knee Bracing

4) Rectangular Water Tank with Cross Bracing

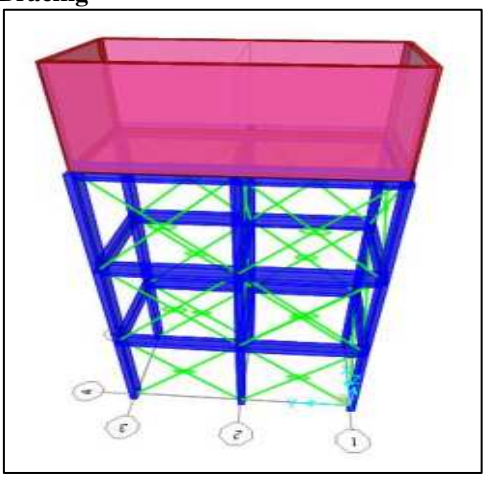

Fig 7 Rectangular water tank with Cross Bracing

5) Circular Water Tank (Plain)

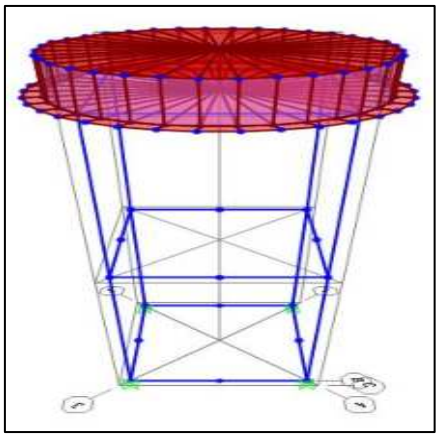

Fig 8 Circular water tank without Bracing

6) Circular Water Tank with Single Bracing

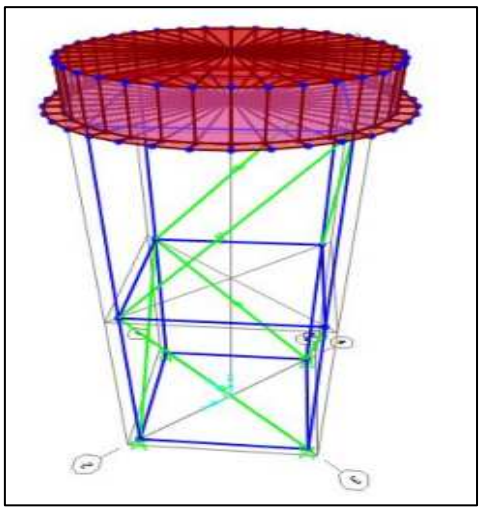

Fig 9 Circular water tank with Single Bracing

7) Circular Water Tank with Knee Bracing

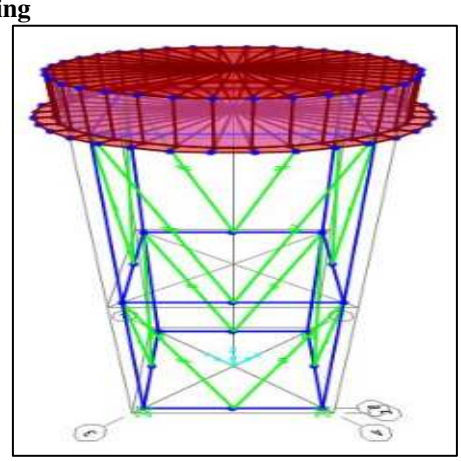

Fig 10 Circular water tank Knee Bracing

8) Circular Water Tank with Cross Bracing

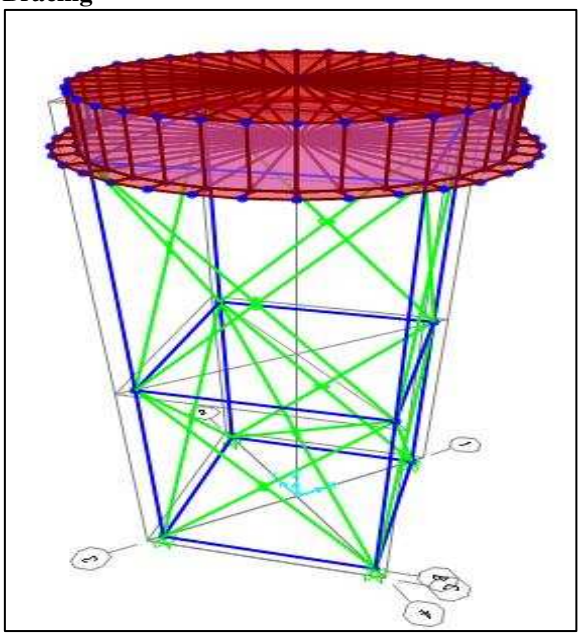

Fig 11 Circular water tank with Cross Bracing

V. RESULT AND DISCUSSION

The result of analytical parameter such as story drift, base shear, and time history analysis of Composite frame are carried out. These results are shown in tabular form. The interpretations of this result are compared graphically. Also soil structure interaction comparison of composite element with element are done by tabular form.

A. Analysis Parameter for Rectangular Water Tank

Table 2 Time History Deformation

Time History Deformation-X mm			
RT Without Bracing	RT With Cross Bracing	RT With Single Bracing	RT With Knee Bracings
4.6	2.268	1.09	1.74

Graph 1 Time History Deformation X mm

In this graph maximum deformation is 4.6 mm rectangular tank without bracing difference between Rectangular Tank without Bracing and rectangular tank with Single Bracing is 30%.

Table 3 Time Period For RT

TIME PERIOD				
MODE NO	RT Without Bracing	RT With Cross Bracing	RT With Single Bracing	RT With Knee Bracings
1	1.95	1.59	1.25	0.90
2	1.19	1.12	1.00	0.91
3	1.05	0.88	0.63	0.44
4	0.48	0.40	0.29	0.20
5	0.34	0.31	0.25	0.21
6	0.26	0.23	0.21	0.18

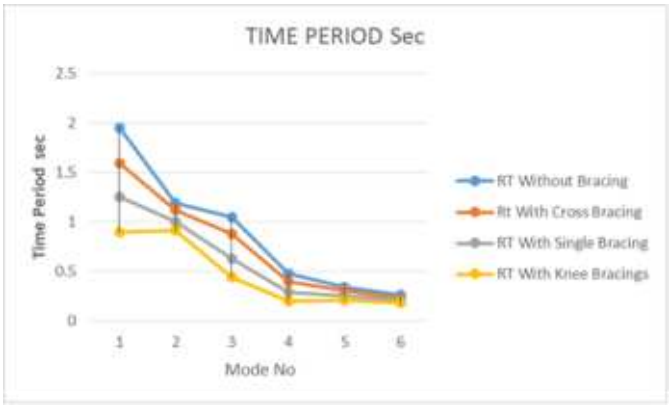

Graph 2 Time Period For RT

In this graph max Time Period is 1.95 sec. for rectangular tank without bracing. Difference between rectangular tank without bracing and rectangular with single bracing is 15%, the economic results given by model RT with Knee Bracings.

B. Analysis Parameter for Circular Water Tank

Table 4 Time History Deformation

Time History Deformation-X mm			
CT Without Bracing	CT With Cross Bracing	CT With Single Bracing	CT With Knee Bracings
7.49	6.64	6.28	6.66

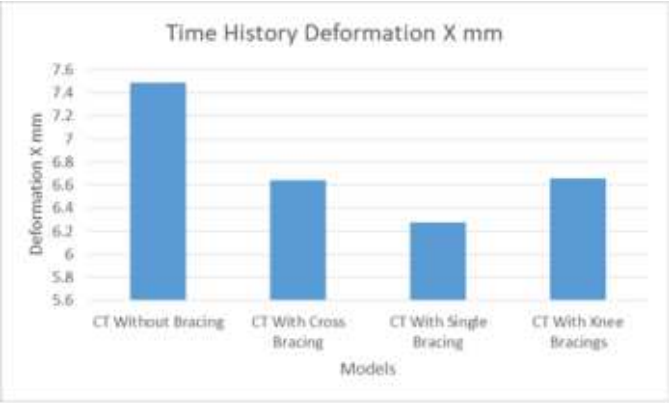

Graph 3 Time History Deformation

In this graph max deformation is 7.49 Circular tank without bracing. Difference between Circular tank without bracing and with single bracing is 15%.

Table 5 Time Period Sec CT

TIME PERIOD				
MODE NO	CT Without Bracing	CT With Cross Bracing	CT With Single Bracing	CT With Knee Bracings
1	2.44	1.98	1.57	1.12
2	1.49	1.39	1.24	1.13
3	1.31	1.10	0.79	0.55
4	0.60	0.49	0.36	0.25
5	0.43	0.39	0.32	0.26
6	0.33	0.29	0.27	0.23

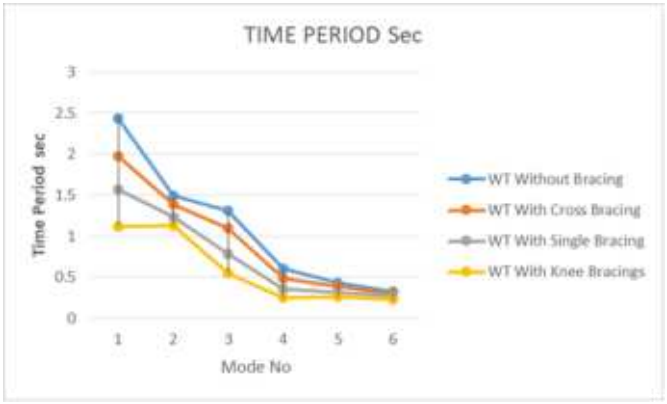

Graph 4Time Period Sec

In this graph max Time Period is 2.44 sec. for Circular tank without bracing. Difference between rectangular tank without racing and rectangular with single bracing is 20%, the economic results given by model RT with Knee Bracings.

C. Model Results For All Time History Data

Table 6 Time History Deformation-X mm (RT)

Time History Deformation-X mm				
Earthquake Area	RT Without Bracing	RT With Cross Bracing	RT With Single Bracing	RT With Knee Bracings
El-Centro 1940	3.91	1.93	0.93	1.48
Bhuj (2001)	4.60	2.27	1.09	1.74
Uttarkashi (2001)	3.32	1.64	0.79	1.26
Koyna(1967)	3.16	1.56	0.75	1.19
Chamoli(1999)	3.49	1.72	0.83	1.32

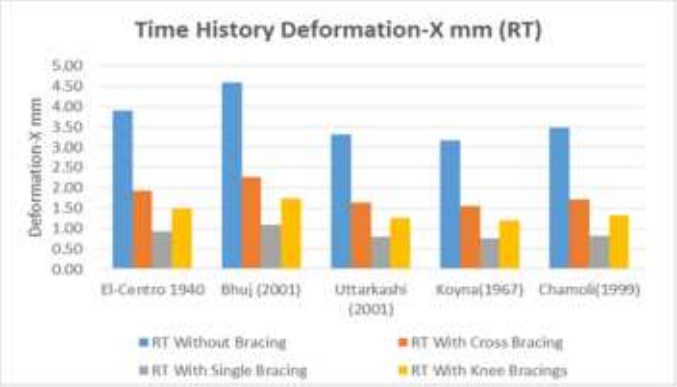

Graph 5 Time History Deformation-X mm (RT)

Above graph shows the deformation for the rectangular water tank with different Earthquake data, the continuously economic results given by model RT with Knee Bracings in every data.

Table 7 Time History Deformation-X mm (CT)

Time History Deformation-X mm				
Earthquake Area	CT Without Bracing	CT With Cross Bracing	CT With Single Bracing	CT With Knee Bracings
El-Centro 1940	6.37	5.64	5.34	5.66
Bhuj (2001)	7.49	6.64	6.28	6.66
Uttarkashi (2001)	5.41	4.80	4.54	4.81
Koyna(1967)	5.14	4.56	4.31	4.57
Chamoli(1999)	5.68	5.04	4.76	5.05

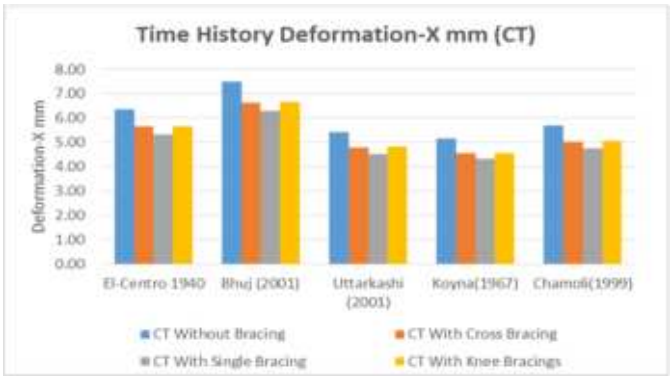

Graph 6 Time History Deformation-X mm (RT)

Above graph shows the deformation for the circular water tank with different Earthquake data, the continuously economic results given by model CT with Knee Bracings in every data.

VI. CONCLUSION

In the given study the elevated water tank with various bracing systems are studied for staging height 20m.Firstly water tank model is designed for 150m3 capacity and for time history analysis bhuj earthquake is considered. Various models of bracing systems are proposed and following conclusions are made.

For the time-displacement results in SAP 2000, difference between rectangular water tank without bracing and rectangular water tank with single bracing is 42%, because the diagonal bracings increase resistance to lateral bracings

By performing the analysis of circular and rectangular water tanks with different bracing systems we came to the conclusion that rectangular water tank is more sustainable as compared to circular water tank in accordance to displacement. And the displacement of circular and rectangular water tank is 6.28mm and 2.26mm respectively.

In accordance to velocity and acceleration parameter circular water tank gives better results than rectangular water tank.

A. Future Scope

As known from very upsetting experiences, elevated water tanks were heavily damaged or collapsed during earthquake Hence different configurations of liquid storage tanks have been constructed. Water tanks are play an important role in municipal water

supply and fire fighting systems. Due to post earthquake useful desires, seismic safety of water tanks is most important. In the current study time history analysis of rectangular and circular elevated water storage tank were analysed using SAP 2000 software. In further study the concrete baffle wall should use to reduce sloshing effect of the water tank. The tank responses such as maximum nodal displacement, base shear and result should compared for empty and full tank water fill condition.

REFERENCES:

1. 01 G. W. Housner (1963), "The dynamic behaviour of water tanks", Bulletin of the Seismological Society of America, Vol.53, No.2, pp 381-387.
2. 02 B. Devadanam and M K Ratnam (2015), "Effect of staging height on the seismic performance of RC elevated water tank",International Journal of Innovative Research in Science, Engineering and Technology (An ISO 3297: 2007 Certified Organization) Vol. 4, Issue 1, January 2015.
3. 03 S.C. Dutta, S.K. Jain, and C.V.R. Murty (2000), "Assessing the seismic torsional vulnerability of elevated tanks with RC frame-type staging", Soil Dynamics and Earthquake Engineering, Vol.19 (2000) pp183–197.
4. 04 R. Livaoğlu andA. Doğangünk (2008), "Sloshing response of the cylindrical elevated tanks with frame staging system on different soil conditions", Technical University, Department of Civil Engineering. 61080,Gumushane, Turkey. Institute of Thermo mechanics, Prague, 2008.
5. 05 S. M. Maidankar, G.D. Dhawale, and S.G. Makarande (2015), "Seismic analysis of elevated circular water tank using various bracing systems", International Journal of Advanced Engineering Research and Science Vol-2, Issue-1, Jan.- 2015
6. 06 P. M.Vijay and A. Prakash (2014), "Analysis of sloshing impact on overhead liquid storage structures", IMPACT: International Journal of Research in Engineering & Technology Vol. 2, Issue 8, Aug 2014, pp127-142
7. 07 M.M. Ranjbar and R. Madan (2013), "Seismic Behavior Assessment of Concrete Elevated Water Tanks", Journal of Rehabilitation in Civil Engineering pp 69-79.
8. 08 K. J. Dona Rose, M. Sreekumar and A. S. Anumod (2015), "A Study of Overhead Water Tanks Subjected to Dynamic Loads", International Journal of Engineering Trends and Technology (IJETT) – Volume 28 Number 7 - October 2015.
9. 09 S. A. Patil, A. H. Kumbhar, and T. F. Mujawar (2016), "Elevated Water Tank Under Sloshing Effect", International Journal for Scientific Research & Development Vol. 4, Issue 05, 2016
10. 10 M. V. Waghmare and S. N. Madhekar (2013), "Behaviour of Elevated Water Tank Under Sloshing Effect", International Journal of Advanced Technology in Civil Engineering, Vol.-2, Issue-1, 2013.
11. 11 M. R.Wakchaure and S. S. Besekar (2014), "Behaviour of Elevated Water Tank Under Sloshing Effect", International Journal of Engineering Research & Technology (IJERT) Vol. 3 Issue 2, February – 2014.
12. 12 S. K. Jangave and P. B. Murnal (2014), "Structural Assessment of Circular Overhead Water Tank Based on Frame Staging Subjected to Seismic Loading", International Journal of Emerging Technology and Advanced Engineering, Vol. 4, Issue 6, June 2014.
13. 13 D. Virkhare and L. Vairagade (2015), "Pushover Analysis of Water Tank Staging", Civil Engineering Department, G.H.R.A.E.T N Structural Consultant, Techpro Consultancy, Nagpur, Maharashtra, India IRJET/July 2015.
14. 14 M. Masoudi, (2012), "Evaluation of Response Modification Factor (R) of Elevated Concrete Tanks", Engineering Structures, Vol.39 (2012) pp199-209.
15. 15 F. Omidinasab and H. Shakib(2008), "Seismic Vulnerability of Elevated Water Tanks Using Performance Based-Design" The 14th Withoutrld Conference on Earthquake Engineering, October 12- 17, 2008, Beijing, China.
16. 16 A. M. Jabar and H. S. Patel (2012), "Seismic behaviour of RC elevated water tank under different staging pattern and earthquake characteristics", International Journal of Advanced Engineering Research and Studies, Vol.1 April-June, 2012, pp293-296.
17. 17 S.C. Dutta, S.K. Jainb and C.V.R. Murty (2000), "Assessing the seismic torsional vulnerability of elevated tanks with RC frame-type staging",Soil Dynamics and Earthquake Engineering , Vol.19 (2000) pp183–197.
18. 18 P. K.Malhotra, T.Wenk and M.Weiland , "Simple Procedure of Seismic Analysis of liquid-Storage Tanks", Structural Engineering, Vol. 3, pp197–201.
19. 19 D.C. Rai (2001), "Performance Of Elevated Tanks In Mw 7.7 Bhuj Earthquake of January 26, 2001",International Conference on Seismic Hazard With Particular Reference to Bhuj Earthquake of January 26, 2001, Oct. 3–5, New Delhi.

IS Codes

1. IS 456-2000 Indian Standard Code of Practice for Plain and Reinforced Concrete, Bureau of Indian Standards, New Delhi.
2. IS: 1893 (Part 1), (20016), Indian Standard Criteria for Earthquake Resistant Design of Structures, Bureau of Indian Standards, New Delhi.
3. IS: 875 (Part 2) – 1987: Imposed loads.
4. IS 3370- (2009) – Concrete Structures For Storage Of Liquids-Code Of Practice.

International Research Journal of Engineering and Technology (IRJET) e-ISSN: 2395-0056
Volume: 10 Issue: 12 | Dec 2023 www.irjet.net p-ISSN: 2395-0072

Study of *Trigonella Foenum-Graecum* (Fenugreek Seeds) & *Carica Papaya L* (Papaya Seeds) As A Natural Coagulant for Treatment of River Water

Tonne Akshata R.[1], Dr. Chonde S. G.[2], & Bhosale S. M.[3]

[1,3]*Department of Technology, Shivaji University Kolhapur – 416004, Maharashtra, India*
[2]*Krishna Institute of Medical Science, Karad, Maharashtra, India*

Abstract - *The usefulness of substances like alum and ferric chloride as chemical coagulants is well known. However, there are numerous drawbacks to using it, including high operational expenses, adverse consequences on human health, the formation of vast volumes of sludge, and the fact that it drastically affects the pH of treated water. To avoid the stated difficulties, it is preferable to substitute these chemical coagulants with natural-based coagulants derived from plants. All physicochemical parameters, including pH, EC, TDS, turbidity, acidity, alkalinity, chloride content, hardness, DO, and COD, were measured before and after adding Trigonella Foenum-*Graecum *(fenugreek seeds) and Carica Papaya L (papaya seeds) powder to the river water for treatment. The water's characteristics, such as pH, turbidity, hardness, DO, and COD, were preserved after treatment. It removes turbidity about 70%, & decreases COD near about 60-65%.*

***Key Words*: Natural Coagulation, Coagulants, *Trigonella Foenum-Graecum*, *Carica Papaya L,* River Water, etc.**

1.INTRODUCTION

One of the necessary components for life is water. Water is a necessity for all living things to survive. Water is utilised for many things, such as drinking, cooking, irrigating, and manufacturing. Although more than 70% of the surface of the Earth is covered by water, less than 1% of that resource is available as fresh water, and even that is not distributed equally over the globe*. (S. Shaharom et al., 2019)*.

Natural coagulation is the process of lowering water turbidity by using a naturally occurring, plant-based coagulant known as a "natural coagulant" during the coagulation-flocculation stage of wastewater treatment*. (Ang et al., 2020)*. The coagulation procedure for treating water can use a natural substance called a plant-based coagulant. This research was done to find out whether plant-based substances could be used as coagulants to remediate surface water.

(Muhamad et al., 2020).

Two types of locally available plant-based materials were selected as natural coagulants are *Trigonella Foenum-Graecum* (Fenugreek Seeds) & *Carica Papaya L* (Papaya Seeds). Processes for coagulation and flocculation are frequently employed in the treatment of water and wastewater. Its primary goals are to eliminate colloidal particles that are suspended in water and to lessen turbidity. *(Hariz Amran et al., 2018).* Due to their advantages and the fact that they generally alleviate the problems that go along with utilising chemical coagulants, natural coagulants have gained popularity over the past few years. Plant-based natural coagulants, which can be derived from diverse plant components, carry out coagulation either by polymer bridging or charge neutralisation.*(Hariz Amran et al., 2018).*

There is a great desire to identify an alternative coagulant, preferably a natural coagulant, due to the numerous issues caused by utilising the synthetic coagulants, such as the widely used aluminium sulphate. Normal assumptions about the safety of naturally occurring coagulants for humans. *(Binayke & Jadhav, 2013).* The use of natural coagulants is a viable remedy due to widespread worries about the negative effects. In order to determine whether plant-based natural coagulants could take the place of chemical coagulants in the treatment of water, this study was carried out. *(Muda et al., n.d.).*

A chemical found in fenugreek seeds possesses coagulation properties and is water soluble, making it suitable for cleaning water and wastewater. Fenugreek seeds which belongs from *Pea Family (Faaceae)*, contain a chemical that is water soluble and has coagulation capabilities such as mixture of pectic polysaccharide, non-polysaccharide, and natural electrolytes, particularly divalent cation types such as Ca^{+2} and Mg^{+2}, suitable for wastewater and water treatment.

Carica Papaya L belong's from *Caricaceae Family* and also collected from the farmer who kept it for the cultivation. Papaya seeds act as a coagulant by forming bonds with particles that are negatively charged (such as silt, clay, bacteria, and toxins) thanks to the presence of positively charged proteins. The resulting flocs settle and produce pure water by adsorption and charge neutralization.

2. MATERIAL AND METHODOLOGY

2.1 Materials

I. River Water Collection

The water sample for the treatment is collected from the Krishna Ghat Kurundwad. It is situated on the banks of Krishna - Panchaganga river (16.6875° N, 74.6005° E.)

Fig - 1 River Water from 'Krishna Ghat Kurundwad'

ll. Natural Coagulants Used for Study

- ***Trigonella Foenum-Graecum*** **(Fenugreek Seeds)**

These seeds are brought from the grocery shop. The seeds are oven dried in the DOT's Environment Laboratory at 30°c for 24 hours. After that the powder is made using the grinder.

Fig - 2 Trigonella Foenum-Graecum (Fenugreek Seeds)

Fig - 3 Trigonella Foenum-Graecum in Powder Form

- ***Carica Papaya L*** **(Papaya Seeds)**

The papaya seeds were collected from farmer who kept it for the cultivation. It is washed and oven dried for 24 hours and fine powder is made for the treatment.

Fig - 4 Carica Papaya L (Papaya Seeds)

Fig - 5 Carica Papaya L in Powder Form

2.2 Methodology Adopted

l. Physicochemical Characteristics Study of River Water Before Treatment

- **pH:** pH stands for potential of hydrogen, i.e. H+ ion concentration present in the water which represents the nature of water i.e. acidic or basic state. The pH scale determines whether water is basic (alkaline) or acidic. From 0 (extremely acidic) to 14 (basic alkalinity), the pH scale is logarithmic (very alkaline).

- **Electrical Conductivity:** Since dissolved solids split into positively and negatively charged ions, water's conductivity is a measure of how well it can carry an electric current.

- **Alkalinity:** Natural water is typically alkaline because the bicarbonates are presence which creates the reactions in the soils that the water percolates through. It represents the buffering power of the water and measures its ability to neutralize acids. It may also be to blame, because it protects or acts as a buffer against abrupt pH changes, alkalinity is essential for fish and other aquatic life.

- **Acidity:** The quantitative ability of water or solution to neutralize an alkali is known as its acidity. In plain English, this means that pH is a gauge of an aqueous solution's acidity or basicity. Acidic solutions are those with a pH under 7, and basic or alkaline solutions are those with a pH above 7. Low pH can cause copper in your household plumbing to leach into the water, leaving green stains on porcelain surfaces like bathroom sinks. Another possibility is that the water itself has a blue color.

- **Hardness:** Hardness is an inherent property of water that can improve its flavour and consumer acceptability for drinking. Water's hardness is caused by calcium and magnesium minerals, which are found naturally in water. Poor soap lathering and scum are typical indicators of hard water. There are two types of hardness: temporary (carbonate) and permanent (non-

carbonate). Water that has become temporarily hard can be easily made soft by boiling it.

- **Dissolved Oxygen:** The volume of oxygen in the atmosphere (O2) that has been dissolved in water is known as dissolved oxygen. By aeration (rapid movement), diffusion from the surrounding air, and as a waste product from photosynthesis, enters in water. The majority of aquatic organisms require dissolved oxygen in order to survive and develop. Some organisms, like catfish, worms, and dragonflies, can survive in slightly lower concentrations of DO than others, such as fish and stoneflies, which require high concentrations of DO. Insufficient oxygen levels in water can cause adult and juvenile deaths, poor growth, failed egg or larval survival, and a shift in the species that live in a particular water body. When oxygen levels in a body of water fall below 3 mg/L, the aquatic system's circulatory fluid balance is disturbed, which impairs cell function and ultimately results in death.

- **Chemical Oxygen Demand:** The Chemical Oxygen Demand (COD) formula calculates the amount of oxygen needed to oxidize the organic material present in a water body at a specific temperature and time. COD is an essential indicator of water quality because it offers a baseline for determining the impact that wastewater discharge will have on the environment. Higher COD levels signify the presence of more oxidizable organic matter in the sample, and as this material degrades, the water body will once more experience low oxygen conditions. The proportion of organic material in the water that can be broken down by environmental microorganisms is shown by the BOD to COD ratio.

ll. Coagulation Study Using Jar Test

The following methodology is adopted

- The sample was taken from Krisha - Panchaganga Ghat in Kurundwad. The sample is taken from the water's surface at a depth of 1 m using an airtight sampling bottle.
- The natural coagulants were gathered and dried in an oven for 24 hours at 30°C.
- After that, it is ground into a fine powder.
- Before performing the jar test, the sample was subjected to preliminary physicochemical characteristics.
- After that, the coagulant dosage, which will be used to treat the water sample utilising jar test equipment, is decided upon: 0.2gm, 0.4gm, 0.6gm, 0.8gm, & 1gm.
- The sample is rotated at a speed of around 100 rpm for 4 to 5 minutes while the coagulant is mixed.
- Reduce the speed of the stirring to 25 to 35 rpm, and continue mixing for up to 15 to 20 minutes. The slower mixing speed increases particle collisions, resulting in larger flocs.
- Following that, the optimal conditions are determined by plotting the residual turbidity versus the coagulant dose.
- Based on the results, the ideal dosage is decided.
- Let the containers to settle for 30 to 45 minutes after turning off the machinery.

3. OBSERVATIONS

Fig - 6 Jar Test Using Natural Coagulant TRIGONELLA FOENUM – GRAECUM (Fenugreek Seeds)

Table - 1 Trigonella Foenum - Graecum (Fenugreek Seeds) Powder Coagulation in River Water Sample

DOSAGE OF *TRIGONELLA FOENUM – GRAECUM*						
TESTS	**0 gm**	**0.2 gm**	**0.4 gm**	**0.6 gm**	**0.8 gm**	**1.0 gm**
pH	7.693	6.865	6.865	6.866	6.867	6.867
EC	394	471	484	497	511	524
TDS	207	250	242	248	255	262
Turbidity	13	4	10	12	14	16
Acidity	30	35	37	40	43	49
Alkalinity	90	60	60	55	50	50
Chloride	25	32.5	33	33.5	34	35
Hardness	67.5	62.5	65.5	69	71.5	75
DO	4.4	8	7.9	7.5	7.2	6.9
COD	320	128	156	182	203	296

Table - 2 Optimum Dosage of Trigonella Foenum - Graecum (Fenugreek seed) Powder in River Water Sample.

TESTS	BEFORE	AFTER
pH	7.693	6.865
EC	394	471
TDS	207	250
Turbidity	13	4
Acidity	30	35
Alkalinity	90	60
Chloride	25	32.5
Hardness	67.5	62.5
DO	4.4	8
COD	320	128

Chart - 1 Graphical Representation of Optimum Dosage of Trigonella Foenum -Graecum (Fenugreek seed) Powder in River Water Sample

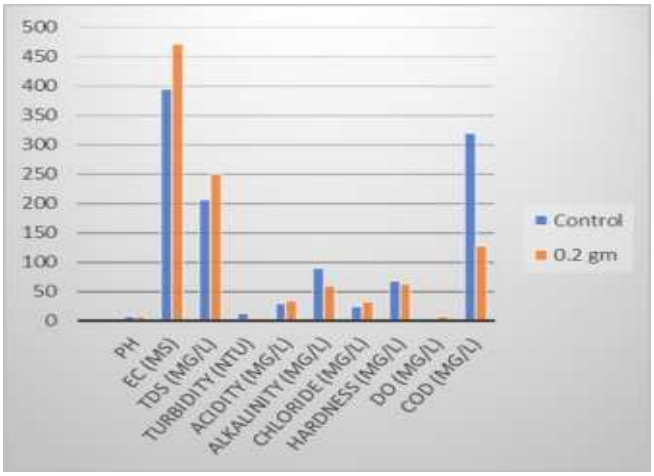

Fig - 7 Jar Test Using Natural Coagulant CARICA PAPAYA L (Papaya Seeds)

Table - 3 Carica Papaya L (Papaya Seeds) Powder Coagulation in River Water Sample

DOSAGE OF *TRIGONELLA FOENUM – GRAECUM*						
TESTS	**0 gm**	**0.2 gm**	**0.4 gm**	**0.6 gm**	**0.8 gm**	**1.0 gm**
pH	7.693	6.316	6.294	6.211	6.147	6.054
EC	394	500	548	595	644	691
TDS	207	250	274	298	322	345
Turbidity	13	5	9	12	15	16
Acidity	30	35	37	39	48	56
Alkalinity	90	30	30	35	40	40
Chloride	25	20	20.5	21	21.5	22.5
Hardness	67.5	62.5	65.5	69	71.5	75
DO	4.4	5	4.9	4.8	4.7	4.6
COD	320	96	184	272	360	448

Table - 4 Optimum Dosage of Carica Papaya L (Papaya Seeds) Powder in River Water Sample.

TESTS	BEFORE	AFTER
pH	7.693	6.316
EC	394	500
TDS	207	250
Turbidity	13	5
Acidity	30	35
Alkalinity	90	30
Chloride	25	20
Hardness	67.5	62.5
DO	4.4	5
COD	320	96

Chart - 2 Graphical Representation of Optimum Dosage of Carica Papaya L (Papaya Seeds) Powder in River Water Sample

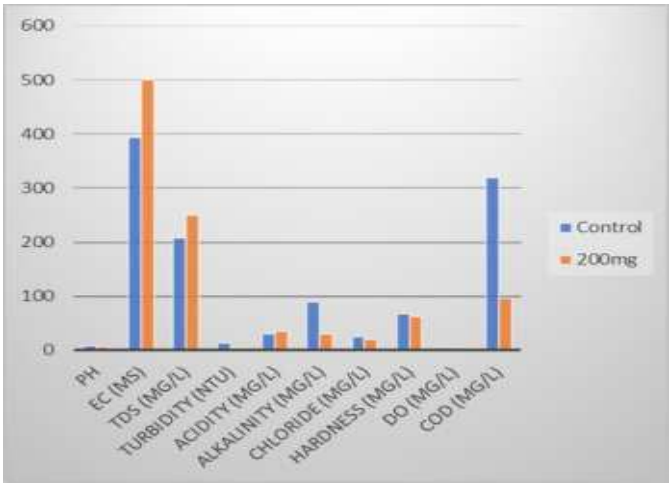

Table - 5 Comparison Between The Results Obtained By Trigoenlla Foenum Graecum & Carica Papaya L At The Optimum Dosage Of 200 Mg

TESTS	River Water Sample Before Treatment	River Water Sample After Treatment (Optimum Dosage of 200mg)	
		Trigonella Foenum-Graecum	Carica Papaya L
pH	7.693	6.865	6.316
EC	394	471	500
TDS	207	250	250
Turbidity	13	8	5
Acidity	30	35	35
Alkalinity	90	60	30
Chloride	25	32.5	20
Hardness	67.5	62.5	62.5
DO	4.4	8	5
COD	320	128	96

Chart - 3 Graphical Representation of Comparison between Optimum Dosage of Coagulant For Treating River Water

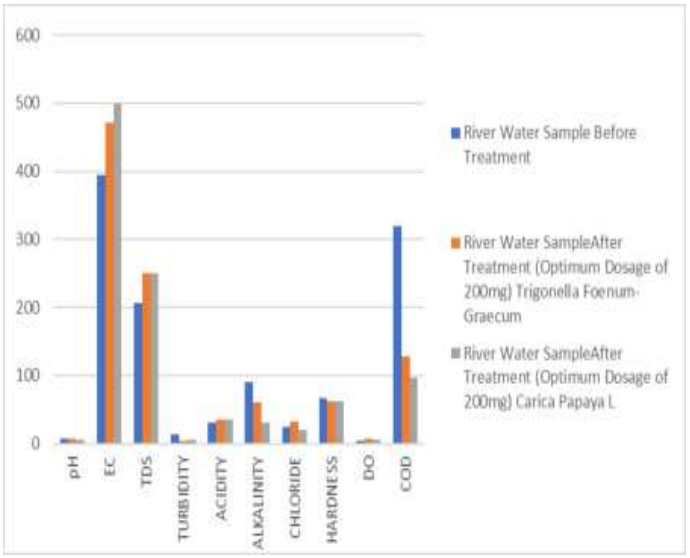

4. RESULT AND DISCUSSION

1) **pH:** When Trigonella Foenum-Graecum (Fenugreek Seeds) are used as natural coagulant it shows better results after the treatment. The pH of the Sample is 7.693 prior to treatment, and it is 6.865 following the coagulation procedure at a dosage of 0.2 gm. While Carica Papaya L (Papaya Seeds) is used in the powdered form as an alternative to synthetic coagulant it gives effective outcomes after the process. Before the treatment, the pH of the Sample is 7.693, and after coagulation at a dosage of 0.2 gm, it is 6.316.

2) **EC:** Electric Conductivity is the term related to water which pass the electric flow through it. Natural coagulants doesn't contribute for reduction of electric conductivity of water because it contains organic matter which carries electric flow through it.The presence of organic matter in the form of a natural coagulant causes an increase in electric conductivity. So, the EC gets increased up to 20-30%.

3) **TDS:** It is the term which contains all the organic and inorganic dissolved matters present in the liquid. TDS increases with the increasing dosage of coagulant. TDS increases because we are adding the coagulants which is already in powdered form increases the solids present in liquid.TDS is slightly higher than that of untreated water sample. It is increased near about 20%.

4) **Turbidity:** Turbidity is the term that related to water which contains large amount of particles which causes cloudiness to water and also affects the quality and

clarity of water. It decreases near about 40-60% at the effective dosage of 200 mg/l.

5) **Acidity:** When acidity parameter taken into consideration coagulation process doesn't play any important role in removal of acidity. It gets increased up to 17% after addition of coagulant.

6) **Alkalinity:** When natural coagulation process is employed on river water sample, it reduces alkalinity near about 30-70 after treatment.

7) **Chloride Content:** Chloride content present in water increases the waters electric conductivity which leads the water to make it corrosive in nature. When *Trigonella Foenum - Graecum* is used the chloride content increases up to 30% on the other hand in case of *Carica Papaya L* it gets reduced up to 20%.

8) **Hardness:** Hardness of water cannot be removed just by coagulation process, it needs to be boiling if they contain bicarbonates of calcium & magnesium. If water contains bicarbonates of chlorides & sulphates, they cannot be removed just by boiling. When natural coagulants are introduced to river water it reduces the hardness near about 10%.

9) **DO:** When concerning about dissolved oxygen it is the most important factor in treating water. It helps to oxidize the organic matter present in water sample. The freshness of water also depends on the oxygen content in it. After coagulation process DO gets increases up to 80%.

10) **COD:** It is the term where the decomposition of organic matter is done chemically in presence of oxygen. COD removal is improved, with a reduction of almost 60-70% following the treatment.

5. CONCLUSION

A powder made from the seeds of *Trigonella Foenum-Graecum* (fenugreek seeds) and *Carica Papaya L* (papaya seeds) was used to reduce the turbidity of the water. Powder made from the seeds of *Trigonella Foenum-Graecum* (fenugreek seeds) and *Carica Papaya L* (papaya seeds) has considerable coagulant qualities. It maintains the pH. TDS is moderately higher than that of the sample of untreated water. *Trigonella Foenum-Graecum* (Fenugreek Seeds) exhibits more effective outcomes than *Carica Papaya L* (Papaya Seeds) in lowering turbidity. *Trigonella Foenum-Graecum* (Fenugreek Seeds) is not as effective in removing alkalinity as *Carica Papaya L* (Papaya Seeds). *Carica Papaya L* (Papaya Seeds) contributes significantly more than *Trigonella Foenum-Graecum* (Fenugreek Seeds) in removing COD from the sample, but both help to raise the DO in water following the treatment.

When both the coagulants are taken into consideration *CaricaPapaya L* Shows better results than *Trigonella Foenum-Graecum,* because it forms a gelatinous layer over it which has coagulation properties that helps in maintaining the physicochemical parameters within permissible limit.

6. REFERENCES

1) Ang, T. H., Kiatkittipong, K., Kiatkittipong, W., Chua, S. C., Lim, J. W., Show, P. L., Bashir, M. J. K., & Ho, Y. C. (2020). Insight on extraction and characterisation of biopolymers as the green coagulants for microalgae harvesting. In *Water (Switzerland)* (Vol. 12, Issue 5). MDPI AG. https://doi.org/10.3390/W12051388.

2) BINAYKE, R. A., & Jadhav, M. (2013). APPLICATION OF NATURAL COAGULANTS IN WATER PURIFICATION. *International Journal of Advanced Technology in Civil Engineering*, 65–70. https://doi.org/10.47893/ijatce.2013.1063.

3) Hariz Amran, A., Syamimi Zaidi, N., Muda, K., & Wai Loan, L. (2018). Effectiveness of Natural Coagulant in Coagulation Process: A Review. In *International Journal of Engineering & Technology* (Vol. 7, Issue 3). www.sciencepubco.com/index.php/IJET

4) Muda, K., Shahidah, N., Ali, A., Abdullah, N., & Sahir, A. B. (n.d.). Potential Use of Fruit Seeds and Plant Leaves as Coagulation Agent in Water Treatment. In *Journal of Environmental Treatment Techniques* (Vol. 2020, Issue 3). http://www.jett.dormaj.com.

5) Muhamad, N. A. N., Juhari, N. F., & Mohamad, I. N. (2020). Efficiency of natural plant-based coagulants for water treatment. *IOP Conference Series: Earth and Environmental Science*, *616*(1). https://doi.org/10.1088/1755-1315/616/1/012075

6) Shamira Shaharom, M., & Siti Quraisyah Abg Adenan, D. (2019). POTENTIAL OF ORANGE PEEL AS A COAGULANT FOR WATER TREATMENT. In *Infrastructure University Kuala Lumpur Research Journal* (Vol. 7, Issue

7) ShariffM, I., & Rani NR, A. (2021). *Evaluation of wastewater Treatment using Hyacinth bean peel powder as Natural coagulant*

IEEE Access

Date of publication xxxx 00, 0000, date of current version xxxx 00, 0000.

Digital Object Identifier 10.1109/ACCESS.2024.Doi Number

Artificial Intelligence Techniques for Landslides Prediction using Satellite Imagery

Akanksha Sharma[1] , Shakti Raj Chopra[2] , Suhas G Sapate[3] , Krishan Arora[2], Mohammad Khalid Imam Rahmani[4], Senior Member, IEEE, Sudan Jha[5*], Senior Member, IEEE, Sultan Ahmad[6*,7], Member, IEEE, Md Ezaz Ahmed[4*], Hikmat A. M. Abdeljaber[8] and Jabeen Nazeer[6]

[1]Electronics and Communication Department, Lovely Professional University Jalandhar, 144001, India
[2]School of Electronics and Electrical Engineering, Lovely Professional University Jalandhar, 144001, India
[3]Department of Computer Science and Engineering, Sanjeevan Engineering and Technology Institute Somwar Peth, Panhala , 416201, India
[4]College of Computing and Informatics, Saudi Electronic University, Riyadh 11673, Saudi Arabia
[5]Department of Computer Science and Engineering, School of Engineering, Kathmandu University, Banepa, Kathmandu, Nepal
[6]Department of Computer Science, College of Computer Engineering and Sciences, Prince Sattam Bin Abdulaziz University, P. O. Box. 151, Alkharj 11942, Saudi Arabia
[7]University Center for Research and Development (UCRD), Department of Computer Science and Engineering, Chandigarh University, Gharuan, Mohali 140413, Punjab, India
[8]Department of Computer Science, Faculty of Information Technology, Applied Science Private University, Amman 11937, Jordan

Corresponding authors: Md Ezaz Ahmed (email: m.ezaz@seu.edu.sa), Sudan Jha (email: jhasudan@ieee.org), Sultan Ahmad (email: s.alisher@psau.edu.sa).

ABSTRACT In hilly areas, landslides can occur due to natural factors such as heavy rainfall, earthquakes, moisture in soil , or man-made factors like unplanned constructions. Landslides can be disastrous leading to a huge loss of property and lives which can be avoided using automatic prediction. Recently, machine learning algorithms have been applied to automatically identify landslides. Numerous feature extraction and classification-based approaches have been implemented on satellite images for semiautomatic detection and prediction of landslides. However, limited research has been done on fully automatic detection with acceptable accuracy. The most challenging task in the classification and prediction of landslides from satellite images is to find an appropriate database for training and yield highly accurate testing results. The primary agenda of a comprehensive study of various techniques used for the detection and classification of landslides using satellite images is to identify the research gap. The secondary objective aims to propose a prototype of novel approach for the same task. Fifty papers based on machine learning and deep learning algorithms from reputed journals are considered for analysis. This article summarizes the performances of different classification techniques from recent literature followed by comparison and discussion with respect to accuracy. Based on the gap identified an effective prototype of the landslide classification approach is proposed. A slightly modified version of the deep learning model ResNet-101 is proposed which yields an accuracy of 96.88% when tested on an augmented Beijing dataset of 770 satellite images. The article also offers the researchers the latest status, overview, and potential avenues of machine and deep learning algorithms for landslide detection. The techniques discussed will serve as a valuable resource for identifying research gaps, guiding new researchers, and fostering innovative exploration in the field of landslide classification using satellite images.

INDEX TERMS Landslide classification, satellite image classification, support vector machine, fuzzy-based classification, landslide prediction, landcover classification.

I. INTRODUCTION

In today's era, the utmost importance is to protect life and infrastructure from natural disasters like landslides and earthquakes. As more mountain areas are getting populated, there is an increase in national initiatives towards the safety of lively beings in the landslide susceptible areas. Landslides can cause tremendous amounts of damage to life as well as property. Landslides pose significant demographic and economic concerns in diverse countries, underlining the need for proactive risk management and international collaboration to avoid disaster-related losses [1]. In India, 12.6% of covered land except snow-covered areas is prone

to landslides. About 0.32 million sq. km area falls under the Himalayan range which is further categorized into Northeast Himalaya and North West Himalaya. Darjeeling and Sikkim fall under the North East Himalayas and cover 0.18 million sq. km area prone to landslides. North West Himalaya covers Uttarakhand, Himachal Pradesh and Jammu and Kashmir comprising 0.14 million sq. Km. Western Ghats cover Tamil Nadu, Kerala, Karnataka, Goa, and Maharashtra contributing 0.09 million sq. km and Eastern Ghat contributes 0.01 sq. km of total landslide-prone area [2]. Himalayan range lies in earthquake Zone IV and V, these areas are susceptible to landslides initiated by earthquakes [3]. The estimated loss of infrastructure due to landslides is 1-2 % of the gross national product in most developing countries [4]. Estimating and minimizing the damage caused by landslides is a challenging task for the government authorities and technical teams in developing countries as approximately 80% of the casualties due to landslides are reported from these countries [5].

Developing counties follow a steep increase in construction. Remote areas are connected to roads, railway tracks, bridges, tunnels etc. Constructions in the morphological area cause a problem in the ecosystem environment and create hazards like landslides. The danger of landslides along road alignments in North Sikkim Himalayas is evaluated by geospatial analysis utilizing thematic weighting. The results show that 65.3% of landslides occur in very high-hazard zones, which informs construction design to reduce the likelihood of future disasters [6]. A landslide is a natural and manmade disaster that causes loss of life. Being a developing country, construction cannot be stopped and natural parameters that trigger landslides cannot be controlled. Therefore, an early alarm system can save lives from such hazards. Satellite image databases can be pre-processed to extract the feature to train the model for the detection of landslides with artificial intelligence. AI and machine learning are essential in the digital age for utilizing a variety of data sources and supporting spatial information analysis for catastrophe risk reduction. Recurrent and convolutional neural networks, for example, have achieved above 90% accuracy in their analyses [7].

Landslide classification has three main stages, the first stage is the collection of images or creating datasets from satellite data. Initially, a landslide-prone area is selected, and satellite images of landslides and non-landslides related to those areas are collected and created a database. There are few ready-to-use data sets available for training and testing algorithms [8]. The next step is to preprocess the collected data by removing noise, increasing brightness, and segmenting the area of interest. The image segmentation process is an important step in image pre-processing. The result of segmentation depends on the quality of the images. High-resolution images and machine learning algorithms provide reliable results of segmentation that are useful for selecting interest objects [9].

Satellite remote sensed data is highly effective for the prediction of landslides and reducing the risk of disaster. Data acquired by remotely sensed satellites help in support of keeping inventories of landslides, majorly in periods of risk assessment and during the prevention of landslides [10]. Satellite data is also useful for creating an alert during emergencies and observing current ground situations [11]. Machine learning can allow easy, yet accurate classification and prediction of landslides based on satellite images. Timely prediction of landslide incidents can help the disaster management team to save human lives and avoid loss of property. Machine Learning models are extensively used for landslide susceptibility mapping due to the complex relationships between landslides and causative factors. Many ML models achieve high reliability in generating susceptibility maps, with an Area Under the Curve (AUC) value exceeding 0.90 [12].

The major primary objectives of this article are as follows.

1. To analyze and categorize different machine learning algorithms and compare these algorithms in terms of performance with diverse types of datasets and types of satellites from where data is collected with accuracy.
2. To identify the research gap from the literature on machine learning classification of landslides available in the last few years.
3. To test and verify whether artificial intelligence algorithms can provide a better classification for landslide and non-landslide data.
4. To propose a prototype of a new artificial intelligence-based technique for the classification of landslides with better accuracy.

This study identified several key concerns regarding this work, which encompass

1. Selecting appropriate and latest articles from the available literature.
2. Identify common ground and parameters for evaluating and comparing performances of existing solutions.
3. Use a common strategy to compare different machine learning techniques.

For this comprehensive study, we have selected 50 research papers based on machine learning algorithms for automatic and semiautomatic classification of landslides from various sources such as IEEE Explore, Springer, Remote Sensing Journal, landslide Journal, IEEE and Science Direct etc. Enough care is taken to ensure that the research articles cover a variety of datasets from various landslide-prone countries all over the world. This will allow the researcher to understand the changing trend of datasets and techniques so that a new robust technique can be developed to predict the landslide from any dataset accurately.

The remaining part of this article is arranged as follows. Section 2 summarizes the research work categorized according to the type of algorithm. The important findings and research gaps are identified in Section 3. Based on the research gap identified, Section 4 proposes an optimized artificial intelligence-based classification algorithm. Section 5 concludes the articles.

II. RELATED WORK

This section takes a comprehensive review of different machine-learning algorithms and methodologies for landslide detection and classification using satellite data.

The literature studied reveals that the entire Machine learning algorithm used for landslide detection or classification can be divided into four main categories: supervised learning-based algorithms, unsupervised learning-based algorithms, Fuzzy classification algorithms and combination or hybrid classification algorithms. Hence, we have grouped the methodologies and their summaries in four different sub-sections as below.

A. SUPERVISE LEARNING-BASED ALGORITHM

This subsection summaries all Machine learning techniques under supervised learning-based algorithms as below:

Utsav Kumar Malviya *et al.* [13] used learning-based Extended Local Binary Patterns [ELBP] and SVM for the classification of 24 different class satellite images. Two major issues with satellite image processing were discovered in this paper: noise is more noticeable in satellite images and different satellite images have unique properties. The SVM algorithm is used to estimate the noise pattern and Local Binary Pattern used for segmentation. In this research, the researcher considers only four different classes of pictures for training the framework with three algorithms; Radial Kernel-based Support Vector Machine (RKSVM), Linear Kernel base Support Vector Machine (LKSVM), extended Local Binary Patterns (ELBP). Extended Local Binary Patterns (ELBP) is preferred which correctly classify all 24 images. The overall 94% accurate result was obtained by the ELBP SVM algorithm for satellite image classification. Satellite images are of unique features and have varieties in texture and quite difficult to propose one strategy for all images. Still, work needs to be done to design a more accurate algorithm to give improved results for the classification of different classes of satellite images. Only a few images for training cannot guarantee better accuracy. The robustness of technique with more dataset is not attempted which may be the bottleneck in its applicability.

Young Gi Byun *et al.* [14] proposed a landcover classification multispectral image approach based on the Seeded Region Growing (SRG) approach. Efficient image segmentation techniques and high-resolution pan-sharpened images were used. The modified SRG approach combines the multispectral and gradient information of images for homogeneous image regions with accurate and close boundaries. In the noise removal process of multispectral images multi-valued anisotropic diffusion method was used to collect edge information for extracting seed points local minima. Two datasets Quick Bird image and GeoEye-1 were used for experimental results. The result of the proposed technique was compared with three algorithms: the conventional region growing algorithm, the toboggan watershed algorithm, and the mean shift algorithm. At a threshold value of 0.5 and mean square spectral error, the proposed algorithm provided the best result and has an accuracy of 91.15% and the kappa coefficient is 96.70%. MSRG can use multi-feature information including edge and multi-spectral information. This proposed method uses a threshold value for seed selection which cannot provide the best result of seed section for every image. The work needs to be done in an area that is more efficient in segmentation.

Chanika Sukawattanavijit *et al.* [15] developed GA SVM algorithm for the classification of multi-frequency images from RADARSAT-2 (RS2), Synthetic Aperture Radar (SAR) and Thaichote (THEOS) MS images. SVM classifier was used for the classification of land cover. To obtain the best input feature GA was used. Function classification accuracy and the number of features in the selected subset were used to define the fitness of the function. Two datasets THEOS & LANDSAT8 of MS images were used for experiments. To convert the intercorrelated MS band into a set of non-correlated components PCA was used. Training sets and testing sets were developed by using the ENVI program GA-SVM algorithm was compared with the grid search algorithm based on parameter searching.GA-SVM algorithm has 85.02% accuracy for THEOS images and 95% accuracy with combined RS2 and THEOS images. The genetic algorithm along with SVM provides better results as compared to grid search but the Genetic algorithm can be computationally intensive and time-consuming for large datasets. High classification accuracy was achieved with fused RS2 and THEOS images and performance might be different with other testing datasets.

Xin Huang *et al.* [16] proposed a multi-feature model-based SVM that combines multiple spatial and spectral features both for object and pixel levels. Differential morphological profiles Gray-level, co-occurrence matrix and an urban complexity index, are three features that were used. Probabilistic fusion, object-based semantics and certainty voting three algorithms were proposed to add multiple features. Two WorldView-2 datasets and DC Mall dataset were used for training and testing. In DC Mall 50 samples were used in the training process and 19332 in testing. WorldView 2350 samples were used for training and 68706 samples were used for testing. For the classification of high-resolution imagery data, one optimal feature for different images was impossible to select. In the proposed multi-feature, SVM was based on multi classifier system that contain a series of spatial and spectral features for high-resolution image classification. Newly developed SVM has 94.4% accuracy with GLCM on DC Mall dataset. With the

Worldview-2 dataset developed SVM has 92.8% accuracy. This work is limited to training sets and knowledge base rules for construction. Two datasets used in the experimental result used a limited number of datasets for training does not provide efficient results. Semantic analysis was used for the post-processing feature system and depended on segmentation quality which can reduce the overall classification accuracy.

Dericks P. Shukla *et al.* [17] discussed the survey of different LSZ map approaches for preparing landslide susceptibility zonation maps with support vector machine by considering one case study on the area of Garhwal. The datasets were prepared from the survey of India toposheet. To finalize the tectonic map of the selected area, Landsat satellite images of 30 m resolution were used. Data is pre-processed with ArcGIS software to generate parameters such as soil, aspect ratio, drainages, and elevation of the study area. The vector layer of 30*30 m resolution data set was converted into Raster data and raster to ASCII format to use Matlab for SVM. To test the trained SVM Model Ukhimath river basin data were used which was prepared by the geologic survey of India. The trained proximal SVM model to classify more area in landslides susceptible zone have classification higher accuracy of 84.2% and prediction accuracy of 81.15%. Landslide susceptibility zonation maps play an important role in assessing the risk in those zones. Preparing landslides susceptibility zonation map for an area that is sensitive to landslide is most important. The focus of such kind of map prepared with a Support vector machine is to identify the landslide-prone areas.

Kadir Sabanci *et al.* [18] compared the results of K-Nearest Neighbor Algorithm and multilayer perceptron (MLP) for the classification of varied forest types to classify the dataset data mining methods used. A dataset of ASTER satellite images was created and the collected images were processed in three parts: Classification, regression, and clustering along with association rules. Advanced Spaceborne Thermal Emission and Reflection Raido meter Satellite images with a resolution 15m in forest land were used in creating training and testing datasets. To train the model, training sets of ASTER Satellite images were used to classify the sample images into different classes. The collected ASTER Satellite data from the University of California, Irvine (UCI) forest is divided into two classes one was for training and the other one was for testing the model. A total of 524 images were used of which 38% data was used for training and 62% was for testing. The machine learning algorithm MLP yielded a classification accuracy of 90.43% and KNN produced 89.10% accuracy. KNN and MLP have the best classification accuracy. In this research training set is only 38 % and by increasing the ratio of a training set the result can be further improved.

B. BAYESIAN MODEL BASED LANDCOVER CLASSIFICATION TECHNIQUES

This subsection area summarizes all Machine learning techniques under Bayesian model-based algorithms as below.

Fereidoun A. Mianji *et al.* [19] proposed a modified supervised classification method in which the feature reduction technique combined with Bayesian learning-based probabilistic spare kernel method. To increase the distance between the classes, hyperspectral data was first transferred to low-dimensionality feature space and processed with a multiclass RVM classifier. The proposed method uses a dataset of AVIRIS with a resolution of 10nm and wavelength of 0.4 to 2.5micro m images for training and testing the model. This dataset used contains two datasets Indian Pine and San Diego dataset. The experiment was performed for both Linear [FLDA+RVM] and nonlinear [GNDA+RVM] and the performance of the proposed methods was evaluated on varying trains to test the sample. The overall accuracy of Linear FLDA+RVM and GNDA+RVM was 98.01% and 99.04% when the train-to-test sample ratio is 1:30 respectively. Real Hyperspectral data is used for verifying the effectiveness of this proposed supervise classification method. The result is compared with the SVM algorithm and this proposed method gives better performance over SVM.

Jun Li *et al.* [20] investigated an active sampling supervised Bayesian approach with active learning for the segmentation of Hyperspectral images. A multinomial logistic regression model based on logic regression was used for class posterior probability distribution learning Unbiased multilevel logistic prior (MLP)was used to encode spatial information and segment the hyperspectral images. Active learning is useful for reducing number of labelled samples. The performance of the proposed algorithm was assessed by simulating a real hyperspectral dataset. Gaussian RBF kernel is applied for all experiments to normalize the input hyperspectral data. The LORSAL algorithm was used to learn MLR (multinomial logistic regression). The Multilevel logistic (MLL) prior model was adopted for smooth segmentation. The researcher designed an algorithm that combines LORSAL, MLL and active learning. To evaluate proposed algorithm datasets Indian pines, AVIRIS and ROSIS Pavia were used for experimental results. The proposed algorithm yielded 86.72% accuracy on 3921 labelled sample. Overall accuracy Based on experimental results MBT approach gives unbiased sampling and better classification. In this paper, the main dominating factor is a limited dataset for training and testing of the algorithm. The result can be modified with more training samples.

Pablo Ruiz *et al.* [21] proposed a method for Remote sensing image classification based on nonparametric & interference paradigms. This approach allows dealing with infinite dimension features. For both fine and infinite dimension feature space this method is useful. This scheme provides point-wise class prediction and confidence interval prediction. This method is efficiently used for supervised and active learning. The experimental result of this proposed algorithm was performed over two multispectral images for

supervised and active learning classification. Landsat images of Rome city were acquired for supervised classification and ROSIS images of Pavia city were used for active classification. Multispectral and synthetic aperture radar data is used to test this algorithm and Hyperspectral images are used for multiclass land cover classification. The proposed method has 96.80% overall accuracy in supervised mode. For active learning minimum normalized distance (BAL-3) has 97.34% accuracy and running time is 9s. In the supervised mode, proposed algorithm provides the same result as compared to SVM but an improvement is observed in active learning. This work can provide pointwise class prediction and confidence intervals. To an extent this work can use multitemporal image segmentation for better results.

Zhaobin Cui *et al.* [22] suggested a novel classification method for multispectral (MS) images and this approach was based on nonparametric supervised classification. To provide a digital vector number of different class statistic distributions were followed. In MS image high posterior probability was calculated only when an unknown pixel digital number is the same as this pixel in a training class. In accordance with the statistical characteristics of the DN vector, each class vector must follow Gaussian mixture distribution. To estimate the maximum posterior optimized simulated algorithm was used in the proposed method. Spectral classification of the proposed approach yielded 85.30% accuracy and 0.799 Kappa coefficients for the first dataset. Spectral Spatial classification of the proposed approach yielded 94.78% accuracy and 0.92 Kappa coefficient for the first dataset. Three datasets of multispectral images acquired from the SPOT6 satellite have four bands and each band has a spatial resolution of 2m. The overall accuracy result of the proposed classification model was compared with the state–of–the–art classification methods and suggested that the proposed approach outperformed in kappa coefficient and overall accuracy. The proposed Bayesian approach has good results in comparison with the traditional approach. This approach uses the Gaussian Mixture model for fitting the training dataset instead traditional single Gaussian model to provide better results.

C. DECISION TREE BASED LANDCOVER CLASSIFICATION TECHNIQUES

This subsection area summaries all Machine learning techniques under Decision tree based algorithms as below

Dennis C. Duro *et al.* [23] explored a multiscale object-based image analysis (MOBIA) approach based on an RF classifier for EO imagery. MOBIA can produce more than a dozen variables for classification as compared to the pixel-based approach. The use of object features to evaluate information from multispectral bands vegetation index and digital elevation model or other input layers is possible with MOBIA. For object-based classification, object features are used for calculating individual image objects and provide a segmentation process. Maximum likelihood classification (MLC) and K-nearest neighbor (k-NN) are traditional classification algorithms used for MOBIA classification. As compared to modern or parametric algorithms MLC gives poor classification results. In nonparametric algorithms, the RF classifier is more faster and reliable for MOBIA. Two datasets from SPOT-5 high-resolution geometrics sensors and LANDSat-5's thematic mapper sensor were used for testing and training. For multisource, multi-sensor data RF classifier accuracy is 90%. This approach consistently gives 85% accuracy with RF algorithm. The data used is of high resolution of 10 m and quite complex to collect data for the training process. This algorithm can be implemented with more datasets to improve the result.

Lena Albert *et al.* [24] introduced a classification approach for land cover and land use (LCLU). This classification approach focuses on spatial and semantic context for LCLU classification simultaneously. In land cover land use classification conditional random field was applied. Nodes are used as super-pixels in the land cover layer and nodes represent the object in the land use layer. An iterative inference procedure was introduced to enable inference in high-order Conditional Random Forest (CRF). Aerial images were used as input for this proposed classification approach. Two test sets located in Germany were used for testing the algorithm and all these pictures were of orthophoto with four channels and 0.2m ground sampling distance. The result is homogenous for land cover classification and the classification result is improved for similar land use. The overall accuracy for the first test set is 83.7% and for the second set is 82.5%. The size of the super-pixel is very useful for good classification results. As compared to the non-contextual classifier proposed approach gives better experimental results.

Javier A. Montoya Zegarra *et al.* [25] proposed approach is multi-class semantic segmentation with class-specific for high-resolution aerial images. This research includes prior knowledge about the layout in the CRF model. The first step starts with a Pixel-wise prediction of the class likelihood. For better results, the appearance feature sampled from the neighborhood of each pixel was considered. From object specifies the assumption high-level representation at the level of the object was added. The hypothesis was for road segments and buildings. In the classifier stage, all pixels that belong to the hypothesis were assigned the same level. Experimental results were performed on 1000x1000 pixels file generated from dense matching from Vaihingen dataset. This model consists of three steps: The first step is the input of aerial data, then passes through a multilevel classifier with good appearance feature extraction and the last is the recovery step. In the second step large window of the classifier is used because of this building boundaries get blurred and boundaries get mixed even if buildings are close enough. Overall 82.42% accuracy was achieved with experimental results. This classifier Accuracy is given by CRF for buildings, roads, grass, tree and background. Classifiers give more than 80% accuracy but the boundaries of roads and buildings were blurred. The proposed approach

is useful for urban planning and environmental monitoring. The complexity, computational cost, and sensitivity to extreme variations of objects are a few disadvantages that can be improved by improving datasets.

D. NEURAL NETWORK BASED LANDCOVER CLASSIFICATION TECHNIQUES

This subsection area summaries all Machine learning techniques under Neural Network supervised learning based algorithms as below.

Nur Anis Mahmon *et al.* [26] surveyed different algorithms which were backpropagation and K mean algorithm for the classification of satellite images with different classification methodologies. ANN's classifier approach was compared with convolutional classifier techniques which are Maximum Likelihood (ML) and unsupervised (ISODATA). To cover the different types of area, present work categorized the LU/LC into three different classes. Either output of k means clustering image output or ground truth data samples were used as a training set. The training set was selected randomly in this research. Accuracy and kappa coefficient were used to compare the result of image classification. Overall accuracy is 89.3% and the kappa coefficient is 0.820.

Rachid Sammouda *et al.* [27] introduced a Hopfield Neural Network for agriculture satellite images. Pixel clustering-based segmentation was performed on Satellite images which is quite difficult due to poor resolution, poor illumination and environmental conditions. Characteristics such as population density, ecological distribution etc. were used to find exact bee forage locations with Hopfield Neural Network. Geo Eye satellite images dataset with 0.5m resolution was used for clustering. Hopfield Neural Network is giving good results when using three, four and five clusters in terms of classification sensitivity and accuracy.

Wei Zhao *et al.* [28] presented a Convolutional Neural Network (CNN) model for multispectral and panchromatic image classification. The convolutional Neural Network (CNN) model introduced in this paper was a super pixel-based multiple local CNN. A very high-resolution multispectral and panchromatic images were fused together to achieve results. The introduced CNN model was valid for two datasets one was prepared from the DEIMOS-2 satellite for Vancouver images and the other was prepared from Quick Bird Satellite for China images. Both dataset images were MS remote-sensing and panchromatic images. For the segmentation of MS images and to collect super pixel linear clustering algorithm was used. Super-pixel multiple region joint representation method was introduced to collect all spatial and environmental information of super-pixel. Super pixels were taken as basic units. To improve the classification performance of the proposed algorithm that combines detailed information and semantic information. The overall accuracy for classification was 94.4% and kappa coefficient was 0.92. Further, this experiment can be extended to semi-supervised and unsupervised deep learning. The processing time may increase due to the complexity of the SML-CNN model. This work will be more helpful in urban planning, environment monitoring and vegetation.

E. Fuzzy BASED CLASSIFICATION ALGORITHM

This subsection area summaries all Machine learning techniques under Fuzzy based algorithms as below:

Tao Lei *et al.* [29] proposed an unsupervised change detection using fuzzy c mean clustering for landslide mapping. For VHR remote sensing image change detection approach based on image segment was used for landslide mapping. Gaussian pyramid-based fast fuzzy c mean clustering algorithm is used to get better spatial information for landslide regions and for accurate landslide region difference of image structure information. Three datasets of biotemporal images of 0.5 m resolution were prepared from aerial survey system. The result was compared with existing three algorithms in terms of higher accuracy, fewer parameters, and short execution time. The proposed CDFFCM model yields 79%, 80%, and 62% accuracy for three data sets, respectively. The proposed approach work on spatial information to achieve better difference image and also have better computational time due to Gaussian pyramid method. This algorithm also reduces the sensitivity to a threshold for segmentation and requires fewer parameters. Post-event images have complex information and still this algorithm needs to be modified for post-event images. More landslide images and ground truth are required to improve the accuracy.

D.G. Stavrakoudis *et al.* [30] developed a classification approach for VHR multispectral images based on Boosted Genetic Fuzzy Classifier. The classification procedure followed two stages, one was fuzzy rule-based which is followed by the genetic tuning stage. The fuzzy rule is useful in local feature selection and it is allowed to select the feature by repeating Boosted Genetic algorithm. The next stage was the tuning stage used to improve the classification by using an Evolutionary Algorithm. An IKONOS satellite database with 1m spatial resolution was used for experimental results. The testing performance of BGFC is 84.87%. The main aim was to increase the overall classification performance of the algorithm and the proposed algorithm was good in handling complex multidimensional classification.

Dinh Sinh Mai *et al.* [31] proposed a method that combines the fuzzy probability theory and fuzzy clustering classification algorithm to overcome the disadvantages like low accuracy and instability of other satellite image classification algorithms. This proposed method initially calculates the number and coordinates of cluster-based Fuzzy probability and then for classification applies a fuzzy algorithm. Landsat 7 Satellite datasets were used for experimental results. The experimental results show that the developed fuzzy clustering algorithm gives a Classification

entropy of 0.13 and a kappa coefficient of 0.9156 for one dataset and a Classification entropy of 0.14 and a kappa coefficient of 0.8599 for the second dataset. This method yields high classification accuracy on multispectral satellite images as compared to the various developed algorithms.

Long Thanh Ngo *et al.* [32] developed an Interval Type 2 C-mean clustering scheme for multi-spectral satellite imagery. The dataset for experimental results was taken from LANDSAT7 imagery which includes rivers, rocks, fields, jungles planted forests. To generate NDVI image of the chosen study area, two channels were used : Near Infrared and the other is visible red. NDVI is classified by IT2FCM to define different types of land covers. For some undefined pixels, the IT2FCM algorithm can handle uncertainty. Further, this algorithm can be implemented with a hyperspectral image for better results.

F. DEEP LEARNING METHODS

Many literature surveys and Comprehensive review on deep learning and its application applications carried out in number of researches are available [33-43]. This research discusses the challenge of high quality datasets, impact of model complexity on computational resources and limitations of model interpretabilityThis subsection area summaries all Deep learning techniques under hybrid algorithms as below:

Shunping JI *et al.* [35] presented a large-scale landslide dataset based on Bijie City to address the problem of an accurate remote sensing dataset along with a boosted attention module to enhance the feature map in CNN. Experimental results show that ResNet50 boosted by the 3D attention module yields the best performance in landslide detection with a 96.62% F1 score. To extend this work, need for more sophisticated CNN architecture is required to recover different representations of landslides from complicated backdrops.

Silvia Liberata Ullo *et al.* [36] presented a Mask R-CNN pixel-based segmentation model trained with transfer learning and ResNet 101 ResNet50 as a backbone network. Experimental results claim precision 1 and 0.97 FI of the model with ResNet 101 as a backbone network. The dataset used in model training was only 160 samples collected from open-source landslide UAV photographs.Aadityan Sridharan *et al.* [37] evaluated landslide near debris scars.Three deep learning algorithms : ResNet, AlexNet, NASNet-large yields 96%,92%,98% accuracy. The findings suggest potential for modifying and deploying these algorithms to develop landslide hazard risk maps globally.

Qi Zang *et al.* [38] undertook a theoretical comparative framework of Artificial intelligence, Machine learning, and Deep learning emphasizing their major component and learning approaches. Filippo Catani [39] Discussed the implementation of convolutional neural networks (CNNs) for discerning mass movement patterns using transfer learning to attain higher classification than existing architectures Gang Chang *et al* [40] discussed the application of deep learning model in landslide recognition. This work emphasizes the incorporation of a transformer into ResU-Net to improve context modeling utilization of large and different sources of data for better identification. This study shows deep learning with InSAR shows promise for early landslide prediction

Shun Yang *et al.* [41] proposed a semantic segmentation model for automatic landslide detection. Three semantic models: U-Net, DeepLab3+, and PSPNet were combined with different deep learning models (ResNet50, ResNet 101) to evaluate experimental results. Among all combinations, PSPNet with ResNet 50 as the backbone network yields 91.18% mIoU. This paper indicates high accuracy in landslide recognition but further needs to improve landslide boundary segmentation and dataset. DEM data and remote sensing data can be integrated to enhance segmentation accuracy. Tong Liu *et al.* [42] developed a landslide detection mapping model based on three networks: Convolutional neural network, residual neural network, and dense convolutional neural network. DenseNet with RS images and CF's reveals the promising experimental result on landslide detection. Rao FU *et al.* [43] proposed a study to evaluate the size of post-earthquake seismic landslides with unmanned air vehicle remote sensing images. Mask R-CNN uses ResNet50, ResNet101, and Swin Transformer as the backbone network was trained with post-quake UAV images that claimed 0.93 precision. To reduce training time and increase generalization transfer learning was used in this research.

G. OTHER CLASSIFICATION

This subsection area summaries all Machine learning techniques under hybrid algorithms as below:

Tapas R. Martha *et al.* [44] presented an algorithm uses spectral, contextual and shape information of images for landslide detection. For object-oriented analysis, multispectral images were segmented and objects collected from these images were used as a classifying unit. The main objective was to correctly identify the landslide using OOA. Complex landslides were difficult to segment because of different characteristics like low contrast and overlap shadow. To identify the false positive landslides shape and morphological information were combined. A landslide is categorized by the base material and movement of flow. To identify landslide Resources at 1 and LISS IV multispectral data sets were used. For testing the algorithm images of the area in Himalayan in India were selected and test the algorithm with 5.8 m MS data from Resources at 1 and 2.5 m Cartosat1. 76.4% recognition is possible with the proposed algorithm and classification accuracy is 69.1%. This algorithm yields more efficient and accurate landslide detection by utilizing object-based classification. The main challenge in the work is to distinguish landslides from another object with similar spectral properties like soil and water.

Thomas Blaschke *et al.* [45] used a semi-automated object-based image analysis methodology to detect landslides. Object-based image analysis has gained an important role in remote sensing. IRS-ID and SPOT 5 satellite image database were used for the detection process. For landslide detection NDVI, brightness and textural features of satellite images were fused with slop and flow direction. Digital Elevation and gray-level co-occurrence matrices were used to collect slop and flow directions. In object-based image analysis multi multi-resolution segmentation was applied for selecting the feature and classifying the object. The segmented object was processed with their spatial, spectral, and textural parameters. The landslide class was defined on the base of its morphological characteristics. Research aimed to integrate the spectral, spatial, and morphometric characteristics of landslides. The inventory database of 109 landslide events was used as proof to validate the results and according to rule-based classification, the area above 1600m (about 5249.34 ft) with a slope greater than 7% is considered landslide affected area. The brightness threshold is set for a database created from IRS-ID and SPOT 5 satellite images**.** The combinations of these parameters indicated that an overall accuracy of 93.07% was achieved for landslide detection. This method will be useful to detect landslides even without proper landslide inventory.

Sansar Raj Meena [46] Used U-Net and machine learning approaches for automatic detection of landslides by landslide event-based inventory of triggering events and occurrence landslides. The major issue lies in mapping performances among interpretations in the event-based inventory. In this research, two datasets: Dataset 1 from RapidEye satellite imagery and Dataset 2 combine RapidEye and ALOS-PALSAR. 239 data samples were used in several training zone and one testing zone to evaluate the model. Experiments were performed over fully convolutional U-Net, Support Vector Machine (SVM), Random Forest (RF), K-nearest neighbour. Among all machine learning models, U-Net performs best result of 76.59%MCC. The performance of the U-Net model further can be increased by increasing the sample size for training samples.

Haojie Wang *et al.* [47] presented a 11-layer deep convolutional neural network (DCNN-11) model for landslide identification using ML& deep learning. Promising results from a case study of Hongkong City were achieved on three databases: Recent Landslide Database (RecLD), Relict Landslide, Database (RelLD) and Joint Landslide Database (JLD). Experimental result reveals that DCNN-11 is very effective model among Support Vector Machine (SVM), Random Forest (RF), and logistic regression.DCNN-11 has highest area accuracy 92.5% with RecLD database. Further, it is observed that the performance of DCNN can be improved by considering the inconsistency in terrain, landslide, inaccuracy in database and necessity for more complicated CNN's in the future owing to computational restrictions. Soumik Saha *et al.* [48] also investigates landslide susceptibility in the Garhwal Himalaya using machine learning models, with Deep learning neural network (DLNN) demonstrating good accuracy. Omid Ghorbanzadeh *et al.* [49] compares Artificial neural network(ANN) , Support vector machine(SVM), Random forest (RF) Convolutional neural network (CNN) for landslide detection.Optical data from Rapid Eye satellite were used for experimental result. CNNs are used for effective feature representation in image recognition and have better accuracy for small window size.
Mahnaz Naemitabar *et al.* [50] undertook a comparative study on four machine learning models: Support vector machine(SVM), the Random Forest (RF), the boosted regression trees (BRT) model and a Logistic Model Tree (LMT) for identification of landslide prone area. The models SVM and RF yield higher reliability in assessing landslide susceptibility, with factors like lithology, slope, and land use identified as crucial. Experimental results shows that SVM and RF model have AVC 0.86 and 0.89 respectively.

Jie Dou *et al.* [51] presented an automatic method for landslide detection. This approach combines three different approaches namely Genetic algorithm, object-oriented analysis, and case-based reasoning. In object-based analysis, segmentation plays a very important role. High resolution of the image provides correct information about the landslide and was helpful in the better result of the segmentation process. To obtain the object of interest in object-oriented analysis multi-segmentation was preferred on collected images. The genetic algorithm was applied for the feature section. Geographical features classify and enhance the accuracy with case-based reasoning. The case-based reasoning is achieved with different techniques like k nearest neighbour etc. In this paper, Quickbird images of 0.6 m spatial resolution were used for image segmentation and feature selection. Roadside landslides were more exposed to high damage due to landslides and caused difficulties in day-to-day life. Spot 5 and DEM datasets were also used for experimental results. All data were rectified to remove the distortion and noise. Object-oriented image analysis gives 75% accuracy for the detection of landslides and fused Object-oriented image analysis with a case-based reasoning and genetic algorithm (GA) yields 87% accuracy in the detection of landslides. The proposed technique provides benefits over a knowledge-based section for the detection of landslides. This technique helps in creating inventory that will be helpful for providing specifications for future landslides.

Tapas R. Martha *et al.* [52] designed a new approach to detect landslides using bitemporal multispectral images. Multispectral images were used to collect the object from post-landslide images. For the analysis of high-resolution images, a tool is developed which makes input data in a user-defined grid. Multispectral images were collected from the Resourcesat-2 LISS-IV satellite for a defined study area. These two datasets have three bands and are useful for object-based change detection techniques to recognize

landslides. For the detection of landslides 10m DEM from Cartosat1 satellite data was used. For good quality images auto-rectified Resourcesat-2 LISS-IV satellite images are further processed to achieve high pixel match. Top atmospheric reflectance calculations were performed in the preprocessing step of images to overcome weather conditions like sunlight. Pre and post-landslide image reflectance differences identify the landslide. Image segmentation was performed with knowledge-based approach. Object-based change detection was used to detect landslides. The developed graphic user interface (GUI) tool provides overall good accuracy in landslide detection. Combined spectral and morphometric parameters have 89% accuracy in the detection of landslides with 10m DEM from Cartosat-1 satellite images. This work can further be modified for the shadow of clouds in pre-landslide images. Some landslides were not identified due to small clouds over the pre-landslide images.

Tapas R. Martha *et al.*[53] presented a comparison of the pixel-based approach and object-oriented approach for landslide detection. Very high resolutions of 0.5m remotely sensed images were used to compare the results of the two algorithms. An inventory was created with 115 field-based landslides fused with 0.5m spatial resolution for comparative analysis. Unsupervised classification was used in pixel base classification and images were classified in eleven different classes. For non-landslide and landslide pixel binary analysis was used and assigned zero and unity for landslide and non-landslide, respectively. In object-oriented analysis k mean clustering was used to remove regions based on brightness to detect landslides and object properties were used to reduce false positive results. Object-oriented analysis has 96.5% and Pixel-based unsupervised classification has 94.3% accuracy. In this paper, further investigation on challenges associated with OOA needs to be discussed for improvement.

Filippo Vecchiotti *et al* .[54] presented a semi-automatic image classification technique for landslides caused by rainfall. This approach combines pixel-based classification with remotely sensed images multi multi-parameters for landslide detection. Vegetation change in pre and post-image will identify the landslide event. In the method, bitemporal pixel change detection was applied. It was a double classification technique. Terra ASTER L2 data sets were used for the defined study area. 110 landslides which were recognized accurately with this semiautomatic image classification technique. This double classification workflow gives 81.5% producer accuracy coupled with a more than acceptable 68.9% accuracy and 72.9% kappa coefficient. With its data set cloud detection was not performed but it can be overcome with SPOT and SENTINEL-2 for a better view of scenes.

A comparative analysis of the review is shown in Table 1

TABLE 1 : COMPARATIVE ANALYSIS

REF	Technique	Data Set	Type of Images	Accuracy
[12]	SVM &ELBP	Different class images	All type satellite images	94% accuracy
[13]	Seed Region Growing Approach	1.Quick Bird 2. Geo Eye	Pan sharpened High Resolution satellite image.	accuracy 91.15% and the kappa coefficient is 96.70%.
[14]	GA-SVM	RADARSAT-2 (RS2), Thaichote(THEOS) & LANDSAT 8	MS images	95% Accuracy with RADARSAT-2 (RS2) THEOS
[15]	Multi feature Model Based SVM approach	DC Mall data set World View -2 data set	Hyper spectral digital imagery	Improved accuracy 1-4%
[17]	MLP&KNN	ASTER Satellite Image 15m resolution	524 images	MLP has 90.43% classification rate and KNN has 89 %
[18]	Feature reduction technique combined with Bayesian Learning sparse kernel model.	San Diego and Indian Pine data set	Hyperspectral images	Real time hyperspectral images give better result over SVM
[22]	Non parametric RF classifier for multiscale object based image analysis.	LandSat 5, Spot .5	Landsat 5 thematic mapper sensor, Spots high resolution geometrics .	85% RF classifier accuracy
[34]	The automatic method fused three techniques: OOIA),GA, CB technique.	High-resolution Quickbird, SPOT 5	Spatial resolution 0.6 m	Proposed OOIA-GA-CBR gives 87%
[35]	Multi-resolution segmentation (MRS) technique	Resoursesat-2 LISS-IV	Multispectral Images	80.9% accuracy

[36]	Compare pixel-based and object-oriented analysis for landslide detection	aerial images	Very high-resolution (VHR)	OOA gives 96.5% accuracy and pixel-based unsupervised has 94.3%accuracy

III. FINDING AND RESEARCH GAP

The primary tendency of all research papers that have been reviewed in this paper is to observe the performance of classification on landslide detection. In this literature survey the analysis is based on the accuracy of the classification, satellite-based datasets used for detection and algorithms used for classification. During this survey, we find different observations that will be helpful for future research directions, concluded in this section.

A. CHALLENGES WHICH ARE DISCUSSED

Numerous researches have been done with semi-automatic classification of landslides and a few with automatic detection. The most important stage is the data collection. The high-quality image provides a better result for feature extraction. The review concludes that two different images are fused to give a better feature selection. Earth-observing satellites are two types: active satellites and passive satellites [55]. Satellite data provides images and features are extracted based on the following points:

- Active satellites are microwave remote sensing and have their own source of energy. Active satellites have controlled illumination and have the least effect of weather.
- In Active satellite Day and night operations are possible. ESA satellite, Canada RadarSet, Indian satellite (RISAT) and Japanese satellite (ALSO) is a type of active satellite. ESA's sentinel-1 is an active microwave remote sensor and is useful in providing data for all types of disasters like floods, earthquakes, and landslides.
- Passive remote sensing is more useful nowadays and does not assign any external source of energy. These types of satellites measure either reflected radiation from the sun or emitted radiation from the earth. Reflected radiation depends on sunlight so it works on the daytime only and suffers various illumination conditions like weather play a major role. NOVA AVHRR, LANDSAT, SPOT, IRS, Cartosat, and IKNOS are some examples of passive satellites.
- To image segmentation, compare object-based and pixel-based image classification.
- To classify multispectral images and multi-frequency images

B. CHALLENGES WHICH ARE NOT DISCUSSED

There are few challenges which are not discussed:

- Real-time remote sensing data: Automatic detection of landslide require real-time data which based on satellite imagery need highly efficient algorithms for real-time computation**.**
- Limited training data set: Acquiring large-scale data sets for training the model in a machine learning algorithm is a challenging task, which can hinder the ability of the trained model to detect landslides accurately**.**
- Feature extraction: for automatic detection and classification of landslides, need to extract the feature from the database and the feature should be relevant so that model can accurately differentiate between landslide and non-landslide images.
- Environmental factor: landslide depends on various environmental factors like rainfall, soil type, topography etc. By considering these parameters machine learning model require a more careful feature selection algorithm

C. RESEARCH GAP

For natural areas like soil hills and forests, experimental segmentation results are good . Overall accuracy is good due to feature testing but if the number of samples increases accuracy will decrease, it is relative accuracy than the actual accuracy. For the seed selection process threshold value is used, it gives a suitable result but also limits the best results [16]. A combination of high spectral and spatial resolution images was used. It is challenging to classify images that have the same spectral properties and spectral reflection as water and shadow. The suggested C voting and P fusion technique must ensure that the high-resolution picture knowledge base rule is accurately interpreted [18].

The SVM-based approach for landslide segmentation could not provide better results due to dependency on the threshold. SVM and RF learning methods could not achieve classification accuracy [56] For the seed selection process threshold value is used, it gives a suitable result but also limits the best results[15]. Three models random forest (RF), classification and regression tree (CART) and multivariate adaptive regression spline (MARS) were compared in testing, training, and validity accuracy. Random forest gives high accuracy in testing but does not give high accuracy in validating runs. The result shows that one model that provides good results in testing does not provide high accuracy in validating runs. Preference is always provided to the one mode that gives high accuracy in the prediction of events [57]

D. OBSERVATION

This review survey is based on 50 research papers which shows 70% used passive sensor-based satellite databases for training and testing, 22% papers used active sensor-based satellite data base for training and testing and 8% papers used

aerial images for experimental results. The different type of satellites used in different research work as shown in Figure.1

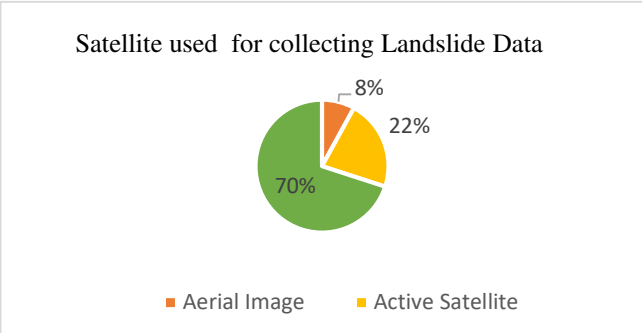

Figure 1: Various types of satellites used for collecting Landslide data

Analysis carried out on the basis of accuracy shows that an accuracy range between 95%-100% is obtained in three research papers, 90%-94% is obtained in seven research papers, 85%-89% is obtained in seven research papers, 80%-84% is obtained in four research papers and below 80% is obtained in two research papers as shown in Figure2.

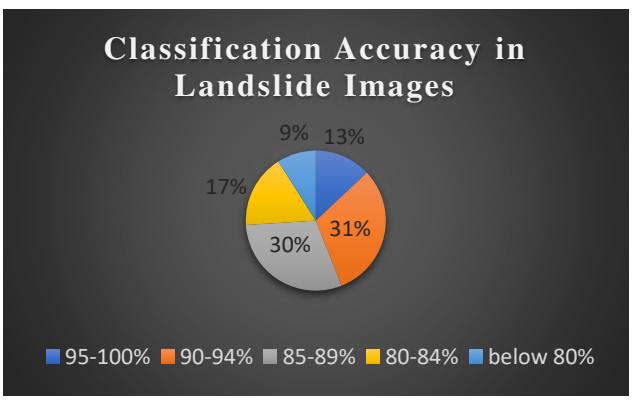

Figure 2: Accuracy of classification in different algorithms

Classification algorithms are categorized into six different classes. This survey paper reviewed twenty-six research papers, six papers are based on SVM classifier, four papers are based on Bayesian classifier, three papers are based on a decision tree classifier, three papers are based on neural networks, four papers are based on fuzzy and the remaining are hybrid algorithms that combine different classifier algorithms. Figure 3 shows the different algorithms-based research papers.

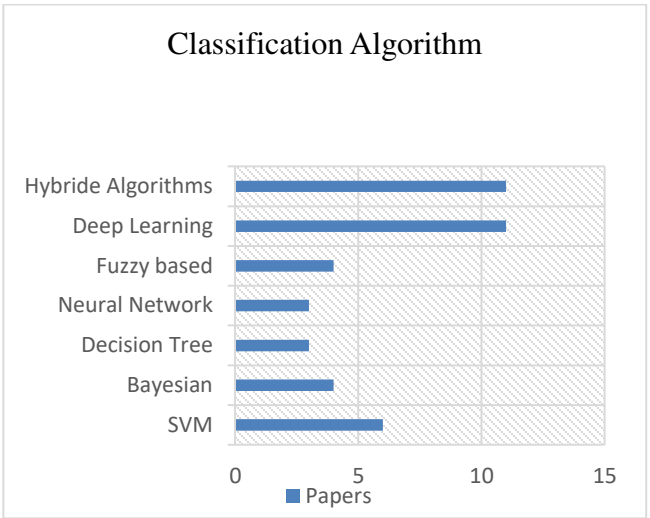

Figure.3: Classification Algorithms used in recent research works

IV. PROPOSED CLASSIFICATION ALGORITHM

Automatic detection and classification of landslides using satellite images play a very important role. Classification has two approaches: The classical machine learning based approach and the Deep Learning model-based approach. For feature extraction and feature selection Machine learning uses an explicit whereas deep learning uses an implicit approach for classification. Deep learning model extracts and selects the features automatically without any supervision using hidden network layers so the results are more accurate. Based on the results of previous research work, automatic detection and classification of landslides using satellite images need tuning of trainable parameters during the training phase. The optimization algorithm used in deep learning will improve the model efficiency in terms of accuracy and learning speed in the training process. Figure 4 presents a flow chart describing the proposed prototype model for landslide detection. This proposed work uses the Bijie dataset which contains 770 landslide and 2000 non-landslide satellite images. The dataset is prepared with the preprocessing of images. Image augmentation is used to increase the sample size in the database. All the images are kept in the same size and format. The data set is divided into two classes: landslide and non-landslide. 70% of data is used to train the model and 30% of the data is used to test the model. Images in the training dataset are not included in the testing set to maintain the originality of the result. The train and test ratio impacts the model's learning rate which is the response of estimated error when updating the weights of the model. We consider hyperparameters: batch size, learning rate, momentum, epoch, to train the network. In the proposed model we use an attention mechanism to emphasize the feature map with ResNet 101 as a backbone convolutional network.

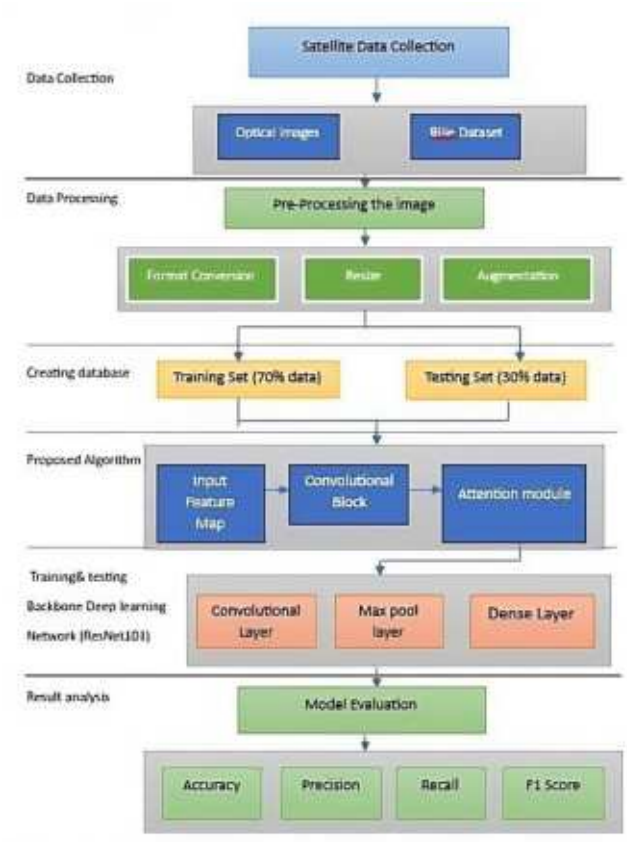

Figure 4: Proposed Deep Learning Prototype Model

V. EXPERIMENTAL RESULT

A. DATASETS

Dataset plays an important role in deep learning CNN algorithms. In the proposed work we select Bijie Landslide dataset. This dataset is first open remote sensing dataset based on landslide and non-landslide images [33] This dataset contains images of Bijie City, China and covers 26,853 square km area. These images were from TripleSat satellite with 0.8m resolution. More than 2770 images were classified into two sets, the landslide set contains 770 images and the non-landslide images contain 2003 images. In our experiment, we used this data set for training and testing the result. In our proposed work 70:% images from the dataset were used for training and 30% of images for testing the model. The figure 5, shows some images of landslides in our training set. To evaluate the performance of proposed model non of images in the test participate in training set.

Figure 5: Example of landslide samples from Bijie dataset

B. EXPERIMENTAL RESULTS AND ANALYSIS

A deep learning-based CNN model along with optimization algorithms are used to modify the loss function, learning rate, weights, bias, and accuracy. The model is shown in figure 6

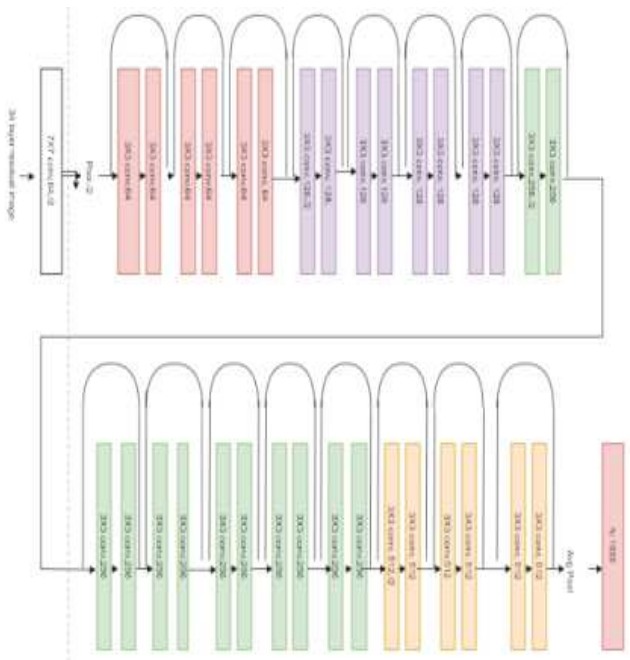

Figure 6: ResNet-101 Architecture

Different deep learning optimizers like adaptive gradient descent, Stochastic Gradient descent, Adam, and Root mean square can be used for increasing the efficiency of deep learning-based CNN models for detecting and classifying landslides.

For landslide detection and prediction initial stage is data collection. We consider the Bijin dataset for experimental results. This set of data contain two class of data one is landslide and other is non landslide. Google Collaboratory is used for python code. Model trained with ResNet 101 as backbone network with batch size to 32 and 64.

The main advantage of ResNet's is that it allows the training of very deep networks through its skip connections, which mitigate the problem of vanishing gradient. The architecture

of ResNet-101 is quite straightforward and computationally efficient compared to others such as DenseNet.

Experimental results of ResNet-101 are shown in Table 2.

Table 2: Results of Proposed Architecture

ResNet-101Parameter		Precision	Recall	F1-Score	Accuracy
Training Set 70 Testing set 30	Batch Size 32	96.4%	96.36%	96.36%	96.88%
	Batch Size 64	91.40%	90.90%	90.88%	92.86%
Training Set 80 Testing set 20	Batch Size 32	95.2%	94.86%	95.14%	94.86%
	Batch Size 64	90.85%	91.36%	91.18%	91.24%

The proposed model uses deep learning CNN network ResNet101 as a backbone to produce the best landslide recognition effect with an accuracy value of 96.4% and obtain the highest precision index 96.4%. The graphical analysis of the results are shown in Figure 7.

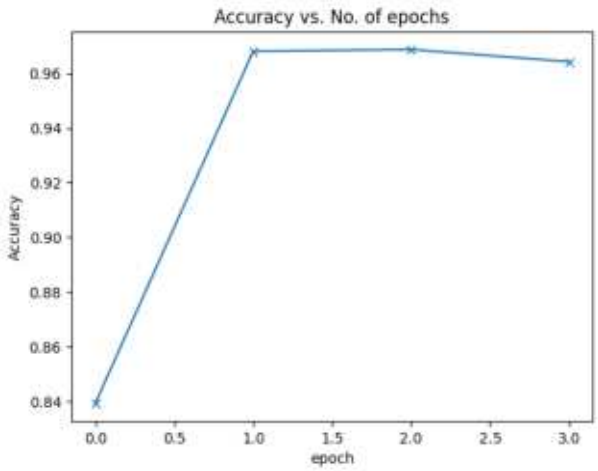

Figure 7 a) ResNet 101 Accuracy vs number of epochs

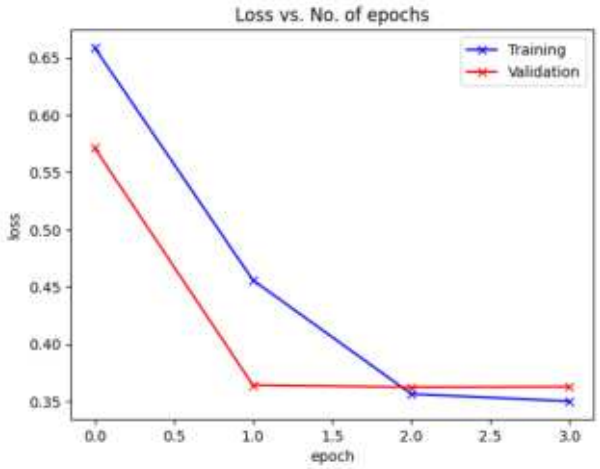

Figure 7 b) ResNet 101 Loss Vs Number of Epochs

VI. OBSERVATION AND DISCUSSION

The batch size is an important hyperparameter in deep learning which works as a trade-off between speed and accuracy. If batch size is large, it may lead to faster training. However, this may result in less accuracy and overfitting. A special care is taken to implement Regularization Techniques such as dropout and weight decay to prevent overfitting, which can be particularly problematic when training with less size. On the other hand, if batch size is smaller it can yield better accuracy, but it is computationally expensive as well as time-consuming.

It is observed that a smaller batch size than 32 is leading to few random fluctuations in the training data. Whereas, the larger batch size than 64 is found more resistant to the fluctuations and converges very slowly.

Another important hyperparameter "number of epochs" is found yielding maximum accuracy of 96.4% at epoch = 1 with moderate loss around 0.45 as shown in Figure 7b. The accuracy is slightly declining with the increased number of epochs. As shown in Figure 7a, at epoch=3, accuracy is declining and showing as 96% but the loss is also minimal. At epoch =1 onwards, the loss is almost constant and not reducing which indicates that the model stops improving on the validation set. Thus, the experiment has been stopped at maximum 3 number of epochs.

VII. CONCLUSION

This article provides an overview of important classification algorithms based on machine learning and compares the results of different algorithms used for landslide detection. In selected articles 22% paper used active sensor based satellite database and 70% use passive sensor based satellite. The accuracy in selected articles was found between 90% to 95%. This review survey reveals that a hybrid combination of different algorithms gives better classification results as compared to a single algorithm.

Based on the literature review, proposed a technique with deep learning a CNN model can be designed with optimization algorithms for classification and results can be

compared with existing accuracy results. The proposed model uses deep learning CNN network ResNet101 as the backbone to produce the best landslide recognition effect with an accuracy value of 96.88% and obtain the highest precision index of 96.4% with well-thought-tuned hyperparameters.

REFERENCES

[1] A. K. Turner, "Social and environmental impacts of landslides," *Innovative Infrastructure Solutions*, vol. 3, no. 1. Springer, Dec. 01, 2018. https://doi.org/10.1007/s41062-018-0175-y

[2] "Geological survey of India." [Online]. Available: https://www.gsi.gov.in

[3] N. Singh, S.K.Gupta and.P. Shukla. "Analysis of Landslide Reactivation Using satellite data: a case study of kotrupi landslide, mandi, himachal pradesh, India," *International Archives of the Photogrammetry, Remote Sensing and Spatial Information Sciences - ISPRS Archives*, pp. 137–142, 2020. https://doi.org/10.5194/isprs-archives-XLII-3-W11-137-2020

[4] E. Pollock and J. Wartman, "Human Vulnerability to Landslides" *Geohealth*, vol.4, no. 10,2020, https://doi.org/10.1029/2020GH000287

[5] D. Petley, "Global Patterns of Loss of Life From Landslides" *Geology*, vol.40,no.10 ,pp.927-930, 2012, https://doi.org/10.1130/G33217.1

[6] B. Koley, A. Nath, S. Saraswat, S. Bhattacharya, B.C. Ray, T. Choudhury and J. Um, "Landslide hazard zones differentiated according to thematic weighting:Road alignment in North Sikkim Himalayas, India", *Spatial Information research*, vol. 32, pp. 29-44, ,2024, https://doi.org/10.1007/978-3-031-18471-0_16

[7] A. Goel, A.K. Goel andA. Kumar , " The role of artificial neural network and machine learning in utilizing spatial information" , *Spatial Information research.* Vol. 31, pp. 275-285, 2022 https://doi.org/10.1007/s41324-022-00494-x

[8] A. Sharma, K.K.Sharma and S.G. Sapate, "A prototype model for detection and classification of landslides using satellite data" presented in *Journal of Physics: Conference Series, Institute of Physics*. 2327, 2022 https://doi.org/0.1088/1742-6596/2327/1/012029

[9] S. Dridi , "Unsupervised Learning-A Systematic Literature Review" 2021 . https://doi.org/10.13140/RG.2.2.16963.12323

[10] N. Casagli, "Landslide mapping and monitoring by using radar and optical remote sensing: Examples from the EC-FP7 project SAFER. *Remote Sens Appllications:society and environment,* vol. 4, pp.92–108, 2016 https://doi.org/10.1016/j.rsase.2016.07.001

[11] M.M. Jaber, M.H. Ali,S.K.,Abd, M.M. Jassim,A. Alkhayyat., B.A. Alreda, A.R.Alkhuwaylidee, and S.Alyousif, "A Machine Learning-Based Semantic Pattern Matching Model for Remote Sensing Data Registration", *Journal of the Indian Society of Remote Sensing*, vol. **50**, no.12, pp. 2303-2316, 2023, https://doi.org/10.1007/s12524-022-01604-w

[12] M. Ado *et al.*, "Landslide Susceptibility Mapping Using Machine Learning: A Literature Survey," *Remote Sensing*, vol. 14, no. 13. MDPI, Jul. 01, 2022. https://doi.org/10.3390/rs14133029

[13] U.K. Malviya and R. Gupta, "Satellite image classification method using ELBP and SVM classifier" Proceedings of the 2021 1st International Conference on Advances in Electrical, Computing, Communications and Sustainable Technologies, ICAECT 2021, Institute of Electrical and Electronics Engineers Inc. 10.1109/ICAECT49130.2021.9392509.

[14] Y.G. Byun, Y.K. Han and T.B. Chae, "A multispectral image segmentation approach for object-based image classification of high resolution satellite imagery", *KSCE Journal of Civil Engineering*, vol. 17, no.2, pp. 486–497, 2013, https://doi.org/10.1007/s12205-013-1800-0

[15] C.Sukawattanavijit, J. Chen and H. Zhang, "GA-SVM Algorithm for Improving Land-Cover Classification Using SAR and Optical Remote Sensing Data. *IEEE Geoscience and Remote Sensing Letters*,vol.14, no3, pp. 284–288, 2017 , https://doi.org /10.1109/LGRS.2016.2628406

[16] X. Huang, and L. Zhang, "An SVM ensemble approach combining spectral, structural, and semantic features for the classification of high-resolution remotely sensed imagery" .*IEEE Transactions on Geoscience and Remote Sensing*, vol.51, no.1, pp. 257–272, 2013 https://doi.org/10.1109/TGRS.2012.2202912

[17] D.P. Shukla, S. Gupta, C.S. Dubey, and M. Thakur, "Geo-spatial Technology for Landslide Hazard Zonation and Prediction." *Environmental Applications of Remote Sensing*, 2016, https://doi.org/10.5772/62667

[18] K. Sabanci, M. Fahri, and K. Polat, "Classification of different forest types with machine learning algorithms", *Research For Rural Development*, vol. 1,pp.254-260, 2016 https://hdl.handle.net/11492/3918

[19] F.A. Mianji and Y. Zhang, " Robust hyperspectral classification using relevance vector machine" , *IEEE Transactions on Geoscience and Remote Sensing*. vol.49, no. 6, pp. 2100–2112., 2011, https://doi.org/10.1109/TGRS.2010.2103381

[20] J. Li, J.M. Bioucas-Dias and A.Plaza, "Hyperspectral image segmentation using a new bayesian approach with active learning", *IEEE Transactions on Geoscience and Remote Sensing*, vol.49, no. 10, pp. 3947–3960,2011 , https://doi.org/ 10.1109/TGRS.2011.2128330

[21] P.Ruiz, J. Mateos,G. Camps-Valls, R. Molina and A.K. Katsaggelos, , "Bayesian active remote sensing image classification", *IEEE Transactions on Geoscience and Remote Sensing*, vol.52, no.4, pp.2186–2196., 2014, https://doi.org/10.1109/TGRS.2013.2258468

[22] Z.Cui, Y.Wang, X.Gao, J. Li and Y. Zheng, "Multispectral image classification based on improved weighted MRF Bayesian.", *Neurocomputing*, vol. 212, pp. 75–87, 2016 https://doi.org/10.1016/j.neucom.2016.03.097

[23] D.C.Duro, S.E. Franklin, and M.G.Dubé, "Multi-scale object-based image analysis and feature selection of multi-sensor earth observation imagery using random forests", *International Journal of Remote Sensing*, vol.33, no. 14, pp. 4502–4526, 2012 https://doi.org/10.1080/01431161.2011.649864

[24] L.Albert, F. Rottensteiner, C. Heipke, "A higher order conditional random field model for simultaneous classification of land cover and land use", *ISPRS Journal of Photogrammetry and Remote Sensing*, vol. 130, pp.63–80, 2017, https://doi.org/10.1016/j.isprsjprs.2017.04.006

[25] J.A.M. Zegarra, J.D.Wegner, L. Ladický and K.Schindler, "Semantic segmentation of aerial images in urban areas with class-specific higher-order cliques" , *ISPRS Annals of the Photogrammetry, Remote Sensing and Spatial Information Sciences*, pp.127–133, 2015 https://doi.org/10.5194/isprsannals-II-3-W4-127-2015

[26] N.A.Mahmon and N. Ya'acob , " Review on Classification of Satellite Image Using Artificial Neural Network (ANN)" *IEEE 5th Control and System Graduate Research Colloquium*, pp. 153-157 , 2014

[27] R. Sammouda, N. Adgaba, A. Touir, and A. Al-Ghamdi, "Agriculture satellite image segmentation using a modified artificial Hopfield neural network" *Computer Human Behaviour*, vol. 30, pp. 436–441, 2014 https://doi.org/10.1016/j.chb.2013.06.025

[28] W. Zhao, "Superpixel-based multiple local CNN for panchromatic and multispectral image classification" , *IEEE Transactions on Geoscience and Remote Sensing*, vol.55, no. 7, pp. 4141–4156, 2017, https://doi.org/10.1109/TGRS.2017.2689018

[29] T. Lei, D. Xue,,Z. Lv, S. Li, Y. Zhang, and A. K. Nandi, "Unsupervised change detection using fast fuzzy clustering for landslide mapping from very high-resolution images" *Remote Sensing*, vol. 10, no. 9, 2018, https://doi.org/10.3390/rs10091381

[30] D.G. Stavrakoudis, J.B. Theocharis. " An evolutionary fuzzy classifier for satellite image classification." Presented in *Proceedings of 17th IEEE Mediterranean Conference on Control and Automation (MED'09)*, pp.383–388, 2009.

[31] M.D.Sinh, L.H. Trinh and N.T. Long, "Combining fuzzy probability and fuzzy clustering for multispectral satellite imagery classification." *Vietnam Journal of Science Technol*, vol. 54, no.3, pp. 300,2016, https://doi.org/10.15625/0866-708x/54/3/6463

[32] L.T. Ngo, D.D. Nguyen, " Land cover classification using interval type- 2 fuzzy clustering for multi-spectral satellite imagery*", Institute of Electrical and Electronics Engineers. and M. IEEE Systems, Proceedings 2012, IEEE International Conference on Systems, Man and Cybernetics (SMC)*, pp. 2371–2376.2012

[33] Z. qiang Yang, W. wen Qi, C. Xu, and X. yi Shao, "Exploring deep learning for landslide mapping: A comprehensive review," *China*

Geology, vol. 7, no. 2, pp. 330–350, Apr. 2024, doi: https://doi.org/10.31035/cg2024032

[34] A. Sharma, S. R. Chopra, S. G. Sapate, and P. B. Bhagawati, "Recent Trends and advances in deep learning techniques for the classification of landslides using satellite images: comprehensive survey," in *IOP Conference Series: Earth and Environmental Science*, Institute of Physics, 2024 https://doi.org/10.1088/1755-1315/1285/1/012024O

[35] S. Ji, D.Yu, C. Shen, W. Li and Q. Xu, "Landslide detection from an open satellite imagery and digital elevation model dataset using attention boosted convolutional neural networks. *Landslides*, vol.17, no.6, pp. 1337–1352, 2020, https://doi.org/10.1007/s10346-020-01353-2

[36] S. Ullo *et al.*, "A New Mask R-CNN-Based Method for Improved Landslide Detection," *IEEE J Sel Top Appl Earth Obs Remote Sens*, vol. 14, pp. 3799–3810, 2021, doi: 10.1109/JSTARS.2021.3064981.

[37] A. Sridharan, A.S.R. Ajai and S. Gopalan, "Landslide Susceptibility for Communities Based on Satellite Images Using Deep Learning Algorithms," in *Intelligent Systems and Sustainable Computing. Smart Innovation, Systems and Technologies*, vol 289. Springer, Singapore 2022. https://doi.org/10.1007/978-981-19-0011-2_41

[38] Q. Zhang and T. Wang, "Deep Learning for Exploring Landslides with Remote Sensing and Geo-Environmental Data: Frameworks, Progress, Challenges, and Opportunities," *Remote Sensing*, vol. 16, no. 8. Multidisciplinary Digital Publishing Institute (MDPI), Apr. 01, 2024. doi: 10.3390/rs16081344

[39] F. Catani, "Landslide detection by deep learning of non-nadiral and crowdsourced optical images," *Landslides*, vol. 18, no. 3, pp. 1025–1044, Mar. 2021, doi: 10.1007/s10346-020-01513-4.

[40] G. Cheng *et al.*, "Advances in Deep Learning Recognition of Landslides Based on Remote Sensing Images," *Remote Sens (Basel)*, vol. 16, no. 10, May 2024, doi: 10.3390/rs16101787.J

[41] S. Yang *et al.*, "Automatic Identification of Landslides Based on Deep Learning," *Applied Sciences (Switzerland)*, vol. 12, no. 16, Aug. 2022, doi: 10.3390/app12168153.

[42] T. Liu, T. Chen, R. Niu, and A. Plaza, "Landslide Detection Mapping Employing CNN, ResNet, and DenseNet in the Three Gorges Reservoir, China," *IEEE J Sel Top Appl Earth Obs Remote Sens*, vol. 14, pp. 11417–11428, 2021, doi: 10.1109/JSTARS.2021.3117975.

[43] R. Fu *et al.*, "Fast Seismic Landslide Detection Based on Improved Mask R-CNN," *Remote Sens (Basel)*, vol. 14, no. 16, Aug. 2022, doi: 10.3390/rs14163928.

[44] T.R.Martha, N. Kerle, V. Jetten, C.J. Westen and K.V. Kumar, "Characterising spectral, spatial and morphometric properties of landslides for semi-automatic detection using object-oriented methods", *Geomorphology*, vol.116 no. 1–2, pp. 24–36,2010, https://doi.org/10.1016/j.geomorph.2009.10.004

[45] T. Blaschke, B. Feizizadeh and D. Hölbling, "Object-based image analysis and digital terrain analysis for locating landslides in the Urmia Lake basin, Iran", *IEEE Journal Selected Topic Applied Earth Observation Remote Sensing*, vol. 7, no.12, pp. 4806–4817, 2014, https://doi.org/10.1109/JSTARS.2014.2350036

[46] S. R. Meena *et al.*, "Landslide detection in the Himalayas using machine learning algorithms and U-Net," *Landslides*, vol. 19, no. 5, pp. 1209–1229, May 2022, https://doi.org/10.1007/s10346-022-01861-3

[47] H. Wang, L. Zhang, K. Yin, H. Luo, and J. Li, "Landslide identification using machine learning," *Geoscience Frontiers*, vol. 12, no. 1, pp. 351–364, Jan. 2021, https://doi.org/10.1016/j.gsf.2020.02.012.C

[48] S. Saha, P. Majumdar, and B. Bera, "Deep learning and benchmark machine learning based landslide susceptibility investigation, Garhwal Himalaya (India)," *Quaternary Science Advances*, vol. 10, Apr. 2023, https://doi.org/10.1016/j.qsa.2023.100075

[49] O. Ghorbanzadeh, T. Blaschke, K. Gholamnia, S. R. Meena, D. Tiede, and J. Aryal, "Evaluation of different machine learning methods and deep-learning convolutional neural networks for landslide detection," *Remote Sens (Basel)*, vol. 11, no. 2, Jan. 2019, https://doi.org/10.3390/rs11020196

[50] M. Naemitabar and M. Zanganeh Asadi, "Landslide zonation and assessment of Farizi watershed in northeastern Iran using data mining techniques," *Natural Hazards*, vol. 108, no. 3. Springer Science and Business Media B.V., pp. 2423–2453, Sep. 01, 2021. https://doi.org/10.1007/s11069-021-04805-7.

[51] J. Dou *et al.* ,"Automatic case-based reasoning approach for landslide detection: Integration of object-oriented image analysis and a genetic algorithm" *Remote Sensing (Basel)*, vol. 7, no. 4, pp. 4318–4342, 2015 https://doi.org/10.3390/rs70404318

[52] T.R. Martha, P. Kamala, J. Jose, V. Kumar and G.J. Sankar, "Identification of new Landslides from High Resolution Satellite Data Covering a Large Area Using Object-Based Change Detection Methods", *Journal of the Indian Society of Remote Sensing*, vol. 44, no.4, pp. 515–524. 2016, https://doi.org/10.1007/s12524-015-0532-7

[53] R.N. Keyport, T. Oommen, T.R. Martha, K.S. Sajinkumar and J.S. Gierke, "A comparative analysis of pixel- and object-based detection of landslides from very high-resolution images", *International Journal of Applied Earth Observation and Geoinformation*, vol.64, pp. 1–11, 2017, https://doi.org/10.1016/j.jag.2017.08.015

[54] F.Vecchiotti, N. Tilch and A. Kociu, "The use of Terra-Aster satellite for landslide detection" *Geosciences (Switzerland)*, vol. 11, no.6, 2021 https://doi.org/10.3390/geosciences11060258

[55] A.Sharma, K.K. Sharma, "A Review on Satellite Image Processing for Landslides Detection. Artificial Intelligence and Machine Learning in Satellite Data Processing and Services" Lecture Notes in Electrical Engineering. Vol. 970, pp.123-129, 2022 Springer, Singapore. https://doi.org/10.1007/978-981-19-7698-8_14

[56] A.B. Gavade and V.S. Rajpurohit, " Systematic analysis of satellite image-based land cover classification techniques: literature review and challenges. *International Journal of Computers and Applications*, vol. 43, no. 6, pp.514–523, 2021, https://doi.org/10.1080/1206212X.2019.1573946

[57] M. Ahmadlou, M. Delavar, A. Basiri, and M. Karimi, "A Comparative Study of Machine Learning Techniques to Simulate Land Use Changes. *Journal of the Indian Society of Remote Sensing.* vol.47, no. 2, 2018, https://doi.org/10.1007/s12524-018-0866-z

Bibliography

AKANKSHA SHARMA is working toward the Ph.D degree in Electronic and Communication Engineering at Lovely Professional University. She has completed her master's degree in Electronics and Communication Engineering from Chandigarh Engineering College, Landran in 2013. She graduated from Lovely Professional University Jalandhar in the year 2011 and was awarded with bachelor's degree in Electronics and communication. Her area of interest is Neural Networks and digital image processing. She has done research work in medical image processing in her master's degree. Currently, she is giving her services as an Assistant Professor at Government Engineering College in Himachal Pradesh, India.

SHAKTI RAJ CHOPRA has completed his Ph.D. in the area of Electronics and Electrical Engineering from Lovely Professional University, Phagwara. He did his M.Tech in Control and Instrumentation from NIT Allahabad and MBA in IT and Marketing from Agra University. He is associated with Lovely Professional University as a Professor with more than eighteen years of experience in academics. He worked at different levels including Head of Department, Wireless Communication in the School of Electronics and Electrical Engineering, at Lovely Professional University. He has published more than 45 research papers in refereed IEEE, Springer, and IOP Science Journals and Conferences. He has organized several workshops, summer internships, and expert lectures for students. He has supervised more than 18 Postgraduate Thesis and more than 50 undergraduate student projects. He has taken and completed 10 Non-Government and Consultancy Projects. He has attended/Participated in twenty-four National/International Online webinars. His areas of expertise

include Massive MIMO, Cognitive Radio, Block Chain, AI, and Machine learning. He has taught various courses to UG and PG levels like Advanced Wireless Communication Systems, Electromagnetic field theory, Microwave and Antenna, Digital Electronics, and many more. He is the reviewer of most reputed journals like Applied Soft Computing, IEEE Access, China Communication, etc.

SUHAS GAJANAN SAPATE completed his B.E. and M.E in CSE from Walchand College of Engineering, Sangli in the year 2000 and 2007 respectively. He earned his Ph.D. in CSE at "Center of Excellence in signal and image processing" of SGGS IE&T Nanded during Sept 2014 to Sept 2017. He has taught many UG and PG courses at Mumbai University, Visveswaraya Technological University, Belgaum, DBATU Lonere and Shivaji University, Kolhapur. He has published 10 journal articles including his research work on automatic breast cancer detection in Springer's Medical Imaging in Clinical Applications, Elsevier's Computer Methods and Programs in Biomedicine, Elsevier's Biocybernetics and Biomedical Engineering. He has published his 8 research articles in national conferences and 14 articles in international conferences. Dr. Suhas is approved PhD research co-supervisor in Lovely Professional University Phagwara Punjab, one student has completed his PhD under his supervision and other two are working. He is also approved PhD research co-supervisor at Visvesvaraya Technological University Belagavi Karnataka and two students are working under his supervision. Dr. Sapate is reviewer of few international peer reviewed journals of good repute including Computers in Biology and Medicine, Computer Methods and Programs in Biomedicine etc..He is member of Technical Program Committee of few reputed international conferences including IEEE ICBDS. Currently, he is working as professor in CSE department, Dean, Research and Development as well as Vice Principal of Sanjeevan Engineering and Technology Institute Panhala Dist Kolhapur in Maharashtra.

KRISHAN ARORA has completed his Ph.D. in the area of Electrical Engineering from MM (Deemed to be) University, Ambala. He did his M.Tech in Electrical Engineering from IKG Punjab Technical University, Punjab, and B.Tech in Electrical and Electronics Engineering from IKG Punjab Technical University, Punjab. He is associated with Lovely Professional University as an Associate Professor with more than seventeen years of experience in academics. He is currently Head of Department, Power Systems in School of Electronics and Electrical Engineering, Lovely Professional University from February 2017. He has published more than 70 research papers in refereed IEEE, Springer and IOP Science Journals and Conferences. He has organized several workshops, summer internships, International Conferences, and expert lectures for students. He has supervised more than 10 Postgraduate Thesis and more than 30 undergraduate student's projects. He has taken and completed 15 Non-Government and Consultancy Projects. He has attended/Participated in twenty-four National/International Online webinars. His area of expertise includes Electrical Machines, Non-Conventional Energy Sources, Load Frequency Control, Automatic Generation Control and Modernization of Smart Grids. He has taught various courses to UG and PG level like Power Electronics, Non-Conventional Energy Sources, Electric Drives, Induction and Synchronous Machines and Digital Electronics.

MOHAMMAD KHALID IMAM RAHMANI (SMIEEE) was born in Patherghatti, Kishanganj, Bihar, India in 1975. He received a B.Sc. (Engg.) and an M.Tech. degrees in Computer Engineering from Aligarh Muslim University, India in 1998 and Maharshi Dayanand University Rohtak in 2010 respectively, and a Ph.D. degree in Computer Science Engineering from Mewar University, India, in 2015. From 1999 to 2006, he was a Lecturer at Maulana Azad College of Engineering and Technology, Patna. From 2006 to 2008, he was a Lecturer and Senior Lecturer with Galgotias College of Engineering and Technology, Greater Noida. From 2010 to 2011, he was an Assistant Professor at MVN, Palwal. Presently, he is working as an Associate Professor in the Department of Computer Science, College of Computing and Informatics, Saudi Electronic University, Riyadh, Saudi Arabia. His research interests include Algorithms, IoT, Cryptography, Image Retrieval, Pattern Recognition, Machine Learning, and Deep Learning. He has published more than 75 research papers in journals and conferences of international repute, 3 book chapters, and holds one USA patent and another Australian patent of innovation.

SUDAN JHA is a Senior IEEE Member and Principal Scientist in the Himalayan Country Nepal. Presently, he is working as a Professor at the School of Engineering, Kathmandu University, Banepa, Kathmandu, Nepal. He received his Ph.D. degree in 2015 and Graduation/ Post-graduation in Engineering from MNREC (Motilal Nehru Regional Engineering College), Allahabad, India in 2001. He has around 75 accepted and published research papers and book chapters in reputed SCI, SCIE, ESCI, and SCOPUS-indexed journals, and conferences. He is an Editor-in-Chief of an international journal published in South Korea. He has two patents in his name. Additionally, he has authored and edited 6 books for recent advanced topics in IoT, 5G, and AI for publishers like Elsevier, CRC, and AAP. He is an Internationally Acclaimed Keynote Speaker at several international conferences, Resource Person in National/International Faculty Development Programs, and Short Term Training Programs for faculties and students. He has served as Guest Editor in several SCIE and ESCI journals, and Reviewer/TPC Member in various conferences and journals.

SULTAN AHMAD (Member, IEEE) received a Ph.D. degree in CSE from Glocal University and a Master of Computer Science and Applications degree (Hons.) from Aligarh Muslim University, India, in 2006. He is currently a Faculty Member of the Department of Computer Science, College of Computer Engineering and Sciences, Prince Sattam Bin Abdulaziz University, Al-Kharj, Saudi Arabia. He is also an Adjunct Professor at Chandigarh University, Gharuan, Punjab, India. He has more than 15 years of teaching and research experience. He has around 105 accepted and published research papers and book chapters in reputed SCI, SCIE, ESCI, and SCOPUS-indexed journals and conferences. He has an Australian patent and a Chinese patent in his name also. He has authored four books that are available on Amazon. He has presented his research papers at many national and international conferences. His research interests include distributed computing, big data, machine learning, and the Internet of Things. He is a member of IACSIT and the Computer Society of India.

MD EZAZ AHMED received the M.E. (Master of Engineering) degree in Computer Science & Engineering from MDU University Rohtak, Haryana India, in 2008, and the Ph.D. degree in Computer Science from Jodhpur National University, India, in 2013. He was with NCU, (North Cap University) earlier Known as ITM University Gurgaon Haryana, India as an Assistant Professor, and another rank from 2002 to 2013. Since 2014, he has been with the Department of Computer Science, College of Computing and Informatics, Saudi Electronic University, as an Assistant Professor. His research interests include Data mining, Web Technology, machine learning, deep learning, Data Science and IoT.

HIKMAT A. M. ABDELJABER is Asst. Professor in Department of Computer Science, Faculty of Information Technology, Applied Science Private University, Amman, Jordan. He was born in Kuwait, in 1967. He received a Ph.D. degree in information sciences and technology in 2010 from the Universiti Kebangsaan Malaysia, UKM, Malaysia. He has published papers on information retrieval and artificial intelligence. His research interests include information retrieval, semantic web technology, data mining, and machine learning.

JABEEN NAZEER is working as faculty in the Department of Computer Science, College of Computer Engineering and Sciences, Prince Sattam Bin Abdulaziz University, Al-Kharj, Saudi Arabia. She has more than 20 years of teaching and research experience. She received her master's degree in computer applications in the year 2001. She is a distinction holder from Osmania University, Hyderabad. She was working as Head of the Department at Princeton College of Engineering till 2006. In 2006, she joined as a Grade H lecturer at the Higher College of Technology, Muscat, Oman. She published many research papers in reputed journals and conferences. Her research areas include software engineering, big data, data science, and the Internet of Things. She has presented her research papers at many national and international conferences.

Desalination and Water Treatment 319 (2024) 100530

Contents lists available at ScienceDirect

Desalination and Water Treatment

journal homepage: www.sciencedirect.com/journal/desalination-and-water-treatment/

Prediction of electrocoagulation treatment of tannery wastewater using multiple linear regression based ANN: Comparative study on plane and punched electrodes

Prashant Basavaraj Bhagawati[a,*], Kiran Kumar H S.[b], Lokeshappa B.[c], Farideh Malekdar[d], Suhas Sapate[e], Abideen Idowu Adeogun[f,*], Sharanappa Chapi[g], Lalit Goswami[h], Sayedali Mirkhalafi[i,*], Mika Sillanpää[j,k]

[a] Department of Civil Engineering, S. G. Balekundri Institute of Technology, Belagavi, Karnataka 590010, India
[b] Department of Civil Engineering, G M Institute of Technology, Davangere, Karnataka 577004, India
[c] Department of Civil Engineering, University B.D.T College of Engineering, Davangere, Karnataka-577004, India
[d] Department of Civil, Environmental and Architectural Engineering, University of Padova, Padova, Veneto, Italy
[e] Department of Computer Science and Engineering, Sanjeevan Engineering and Technology Institute, Panhala 416201, India
[f] Department of Chemistry, Federal University of Agriculture, Abeokuta 110101, Nigeria
[g] Department of Physics, B.M.S. College of Engineering, Bull Temple Road, Bangalore 560019, India
[h] Center for the Environment, Indian Institute of Technology Guwahati, Guwahati, Assam 78109, India
[i] Faculty of Engineering and Technology, School of Civil Engineering and Built Environment, Liverpool John Moores University (LJMU), Liverpool L3 3AF, UK
[j] Department of Chemical Engineering, School of Mining, Metallurgy and Chemical Engineering, University of Johannesburg, P. O. Box 17011, Doornfontein 2028, South Africa
[k] Functional Materials Group, Gulf University for Science and Technology, Mubarak Al-Abdullah, 32093 Kuwait, Kuwait

ARTICLE INFO

Keywords:
Tannery wastewater
Electrocoagulation
Artificial Neural Network
Multiple Linear Regression
Chromium removal

ABSTRACT

This study investigated the electrocoagulation (EC) treatment of tannery wastewater using plane and punched aluminum and iron electrodes at the optimum condition of pH 9, voltage 20 V, electrode distance of 1 cm and 90 min electrolysis duration. The efficiency of the EC process was determined by evaluating the levels of biochemical oxygen demand (BOD), chemical oxygen demand (COD), and Chromium (Cr) in the treated effluents. The experiment utilized both linear regression and Artificial Neural Network (ANN) models for modeling, with the ANN model validating the predicted model from the experimental design with 95 % confidence. The use of plane aluminum electrodes resulted in an optimum removal efficiency of BOD (89.66 %), COD (96.21 %), Cr (96.05 %), and TDS (95.77 %). On the other hand, the punched electrodes achieved a removal efficiency of 90.86 % (BOD), 98.62 % (COD), 96.94 % (Cr), and 96.92 % (TDS). Similarly, when using plane iron electrodes, the removal efficiency of BOD, COD, Cr and TDS was 87.57 %, 94.77 % 93.42 % and 93.08 %, respectively, while punched iron electrodes removed 89.01 % of BOD, 96.59 % of COD, 94.66 % of Cr and 95 % of TDS. The results demonstrate that the proposed ANN effectively predicts effluent BOD, COD, Cr and TDS, addressing economic and environmental sustainability concerns.

1. Introduction

India ranks as the third largest leather producer globally, following China and Italy [1]. Tanning, the process of converting rawhide or skin protein into durable, non-decomposing material, is the key technique used in leather production [2]. Tanning processes required a lots of chemical substances for their accomplishment, thus, the tannery effluents are characterized by strong colour, excessive COD, high pH, and high dissolved solids [3]. Two widely used tanning methods are vegetable tanning and chrome tanning. Vegetable tanning, although not frequently used due to its chemical intensity leading to high contamination levels and low treatability, produces biodegradable leather [4]. Chromium sulfate is widely utilized in chrome tanning processes due to its excellent mechanical strength, impressive dyeing capabilities, and superior resistance to hydrothermal conditions compared to vegetable tanning. However, only a small amount of the salts is required during the process, with any excess salts ending up in the effluents [5]. Considering the huge amount and the low biodegradability of chemicals

* Corresponding authors.
E-mail addresses: prashantbhagawati@gmail.com (P.B. Bhagawati), S.mirkhalafi@2024.ljmu.ac.uk (S. Mirkhalafi).

https://doi.org/10.1016/j.dwt.2024.100530
Received 29 April 2024; Received in revised form 30 May 2024; Accepted 7 June 2024

in the tannery wastewater, the discharge of untreated wastewater to the stream will result in high inorganic solids, with attendance hardness and high alkalinity [6]. Elevated levels of BOD can reduce the amount of dissolved oxygen in streams, posing a threat to aquatic life. Increased suspended solids can overload treatment plants, and degradable matter can contribute to the spread of pathogens. Chromium is carcinogenic to humans and animals, and its accumulation in plants near waterways can pose a risk to the food chain. Additionally, it can lead to soil pollution, impacting soil fertility by altering pH levels. The excessive organic materials cause soil clogs, which in turn negatively affect soil structure and lead to degradation. The discharge of tannery wastewater poses a significant risk to the environment. Therefore, it is crucial to develop and enhance treatment methods for tannery industry effluents in order to safeguard the ecosystem from immense damage [7]. Tannery effluents are conventionally treated by adopting various physicochemical and biological methods. Such methods includes biodegradation [8], adsorption [9], ion exchange [10], chemical oxidation/precipitation [11], coagulation/flocculation [12], electro-floatation [13], bio electrochemical [14] system and advanced oxidation processes [15]. The traditional methods used for treating tannery wastewater are frequently inadequate in fully eliminating contaminants and result in increased production of sludge. Electrocoagulation (EC) on the other hand plays a prominent role in pollutants removal and also proves to be efficient with useful by-products such as manure [16]. EC involves the application of electric current to an aqueous medium in an electrochemical cell. The process is based on the reaction of water contaminants to strong electric fields and electrically induced oxidation and reduction reactions. Direct current is used to remove undesirable contaminants through chemical reactions and precipitation. The electrodes used in this process include Aluminum, Zinc, Copper, and Iron.

The EC process usually involves: (i.) the sacrificing the anode material under the influence of an electric current, leading to the generation of metal ion (Cations) as well as (ii.) the generation of hydroxyl ions at the cathode; this is followed by (iii.) the formation of metal hydroxides with good adsorption properties that bind pollutants. The next important step is (iv.) the oxidation of pollutants to less toxic products followed by (v.) the neutralization of charged pollutants with metal ions then (vi.) the aggregation of neutralized pollutants and their adsorption followed by (vii) the flotation using the gases produced in the system [17].

When an external power source applies potential, the anode material oxidizes, while the cathode undergoes reduction. The electrochemical reactions involving metal M as the anode are summarized as follows [18].

Reactions at anode:

$$M_{(s)} \rightarrow M^{n+}_{(aq)} + ne^- \quad (1)$$

$$2H_2O_{(l)} \rightarrow O_2 + 4H^+ + 4e^- \quad (2)$$

Reactions at cathode:

$$2H_2O_{(l)} + 2e^- \rightarrow H_{2(g)} + 2OH^- \quad (3)$$

Metal ions formed by dissolving the anode material react with hydroxyl ions generated at the cathode, forming hydroxides that are good adsorbents. Iron and aluminum are most often used to produce anodes, due to the formation of polyvalent ions and various hydrolysis products, which depend on the pH of the solution as well as the possibility of forming polynuclear complexes.

The effectiveness of EC is significantly impacted by the pH level of the solution. As the pH level of the solution increases, the reaction continues and leads to the creation of more products. Iron exists in the solution as Fe^{3+} at lower pH (< 3), but as the pH increases from 3 to 4, its presence shifts to $Fe(OH)^{2+}$. Between pH range of 4 to 6, it exists as $Fe(OH)^{2+}$, and from pH 6 to 9.5, the hydroxyl form $Fe(OH)_3$ will be the dominant form in the solution. Above pH of 9.5, iron will mainly be in the form of $Fe(OH)_4^-$ in the solution. In the same way, aluminum will undergo hydrolysis reactions when in aqueous solutions resulting in the formation of Al^{3+}, $Al(OH)^{2+}$, $Al(OH)_2{}^+$ and $Al(OH)_3$ as the main species in acidic, neutral and slightly alkaline solutions. In contrast, $Al(OH)_4^-$ will be found in alkaline solutions. These hydroxides and polyhydroxides settle as a precipitate, the insoluble forms, $Fe(OH)_3$ and $Al(OH)_3$ remain in the solution as destabilizers for the contaminants by electrostatic attraction forces. The destabilization of contaminants occurs through two mechanisms: (i) the neutralization of negatively charged colloidal particles by cation hydrolysis products, and (ii) the elimination of pollutants in the form of an amorphous hydroxide [19,20]. Eqs. (4–11) are carried out for aluminum and iron electrodes:

Reactions at the anode (for coagulation):

$$Al_{(s)} \rightarrow Al^{3+}_{(aq)} + 3e^- \quad (4)$$

$$Fe_{(s)} \rightarrow Fe^{2+}_{(aq)} + 2e^- \quad (5)$$

$$2H_2O_{(l)} \rightarrow O_2 + 4H^+ + 4e^- \quad (6)$$

Reactions at the cathode (for flotation):

$$2H_2O_{(l)} + 2e- \rightarrow H_2(g) + 2OH- \quad (7)$$

Overall reactions at bulk (for precipitation):

$$Al^{3+}_{(aq)} + 3OH^- \rightarrow Al(OH)_3 \quad (8)$$

$$4Fe^{2+} + 8OH- \rightarrow 4Fe(OH)_2 \quad (9)$$

$$4Fe(OH)_2 + 2H_2O + O_2 \rightarrow 4Fe(OH)_3 \quad (10)$$

$$Fe(OH)_3 \rightarrow FeOOH + H_2O \quad (11)$$

EC using iron as the sacrificial anode can effectively remove waste water containing Cr^{6+} (CrO_4) ions. In the reaction solution, ferrous ion (Fe^{2+}) is generated and can reduce Cr^{6+} to Cr^{3+} under alkaline conditions. The Cr^{3+} (aq) ions are subsequently precipitated as $Cr(OH)_3$(s) by increasing the pH of the solution [21].

At pH < 6.5:

$$HCrO_4^- + 3Fe^{2+} + 7H^+ \rightarrow Cr^{3+} + 3Fe^{3+} + 4H_2O \quad (12)$$

$$Cr_2O_7{}^{2-} + 6Fe^{2+} + 14H^+ \rightarrow 2Cr^{3+} + 6Fe^{3+} + 7H_2O \quad (13)$$

At 6.5 < pH < 7.5:

$$CrO_4{}^{2-} + 3Fe^{2+} + 4H_2O \rightarrow 3Fe^{3+} + Cr^{3+} + 8OH^- \quad (14)$$

At pH > 7.5:

$$CrO_4{}^{2-} + 3Fe(OH)_2 + 4H_2O \rightarrow Cr(OH)_3 + 3Fe(OH)_3 + 2OH^- \quad (15)$$

Methods of artificial intelligence, including artificial neural networks (ANN), adaptive neuro-fuzzy inference systems (ANFIS), support vector regression (SVR), and metaheuristic algorithms like genetic algorithms (GA) and particle swarm optimization (PSO), have become popular for modeling and optimizing nonlinear processes [23]. These models rely on empirical data and connections between input and output variables of a process, rather than on process knowledge. Recent research has demonstrated the use of AI models in electrochemical processes for water and wastewater treatment with a satisfactory level of precision [24,25]. According to the literature, there are few published papers that have compared the use of punched and plate electrodes made of two different materials for treating tannery wastewater using the artificial neural network. Here, for the first time, this work studies as proof of concept the performance of iron and aluminum electrodes in EC process for removing pollutants namely COD, BOD, TDS, and Cr. The performance of the process was predicted using the artificial neural network based on the multiple linear regression.

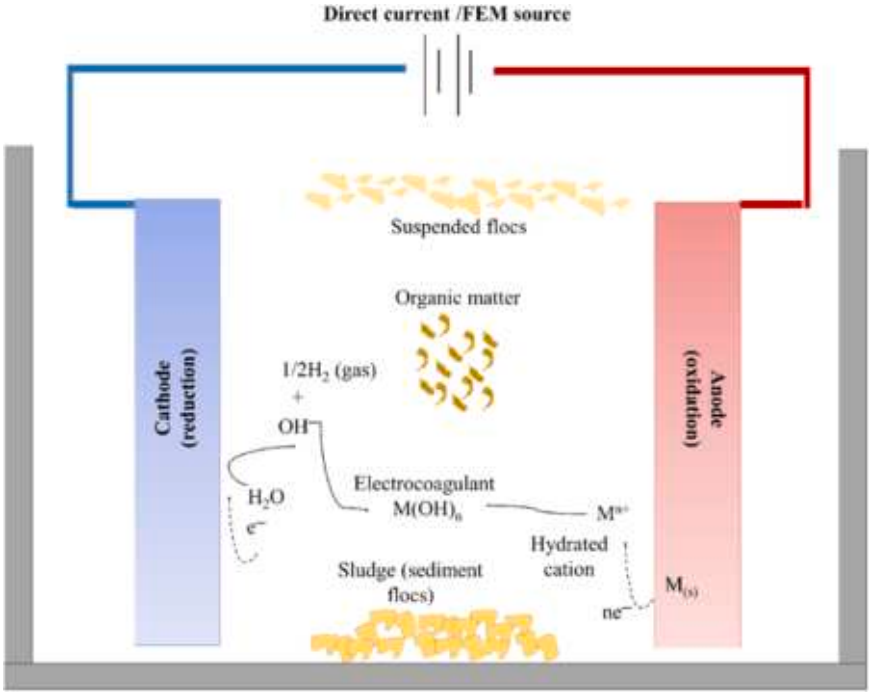

Fig. 1. Schematic A depiction of a basic EC reactor operating in batch mode. Reprinted with permission from Ref. [22]. Copyright (2021), Springer.

2. Materials and methods

2.1. Tannery wastewater sampling

Effluent from the tannery was gathered in accordance with established protocols from a shared treatment facility at the Vanitec tannery wastewater treatment plant in Tamil Nadu, India. The sample was kept at 6 °C and transported to the laboratory in a sealed flask. The tannery wastewater collected then was filtered and analyzed for color, temperature, pH, turbidity, total dissolved solid (TDS), electrical conductivity (EC), chemical oxygen demand (COD), biological oxygen demand (BOD), and chromium (Cr). COD was determined using a digestion reactor (LT200, HACH, USA) and direct reading spectrophotometer (HACH 2700) at 620 nm according to standard test methods (5220 D, closed reflux colorimetric). Collected samples were analysed for total chromium content by Spectrophotometer (HACH 2700) spectrophotometer at 540 nm according to the International Electrotechnical Commission standard test methods (IEC 62321). TDS Meter (Eutech EcoTestr) was used for determining the TDS. EC and pH were measured using digital multi-parameter electrochemistry meter (HQ 40D, HACH). Furthermore, BOD was measured according to the Standard Methods (5210B). The composition of the tannery wastewater is presented in Table 1.

Table 1
Initial Characteristics of Raw Tannery Wastewater.

Parameter	Unit	Average
Color		Brown
Temperature	°C	24
pH	-	8.4
Turbidity	NTU	727
TDS	ppm	26000
EC	S/m	38806
BOD	mg/L	2156
COD	mg/L	6100
Chromium	mg/L	14.6

2.2. Experimental Setup

The electrocoagulation experiments utilized flat and perforated aluminum and iron electrodes measuring 15 cm x 5 cm x 0.2 cm. A rectangular prism reactor, with dimensions of 22 cm x 11 cm x 10 cm and a 2-liter working capacity, was constructed from plexiglass material for the experiments. The electrocoagulation reactor consisted of monopolar electrodes connected to the direct current power supply (Applab 7711 multi-output) to provide an adjustable voltage (0–30 V) and applied current (0–2 A) using a monopolar configuration. The experimental arrangement is shown in Fig. 2.

In order to establish the optimum condition, the electrocoagulation process was carried out at varying electrodes distance (1 cm, 2 cm, 3 cm), pH [7-9], voltage (10 V, 15 V, 20 V) and process time of 90 min with sample analysis at interval of 30 minus using 2 liters of 10 % diluted tannery wastewater.

2.3. Design of Experiment and Statistical Analysis

The simultaneous influence of pH, electrode distance, applied voltage and duration of electrolysis as well as the interactions of these factors on the pollutants (TDS, BOD, COD and Cr) removal efficiencies were investigated based on Design of Experiment in a Face Central Composite (FCC) method. The Start-Ease Design Expert software (version 11.1.2.0) was utilized to create the design as outlined in Table 2.

The obtained experimental data were analyzed using a three-layer artificial neural network with sigmoid transfer functions to effectively model the practical function of interest [26]. The input layers contain four [4] nodes, each for the independent variable with an output layer generating the scaled estimated values for the removal efficiencies of the pollutants. Multiple linear regression model (MLR) was used to model the impacts of the four independent factors on the removal efficiencies of the pollutants according to Eq. [16]:

$$y = \beta_0 + \sum_{i=1}^{n} \beta_i x_i + \varepsilon \quad (16)$$

Fig. 2. Laboratory experimental setup used in the present study.

Table 2
The coded levels and range of the studied variables.

Variable	Unit	Factor code /Notation	Range and level of factors		
			-1	0	+ 1
pH	-	x_i	7	8	9
Distance	cm	x_{ii}	1	1.5	2
Voltage	V	x_{iii}	10	20	30
Duration	min	x_{iv}	30	60	90

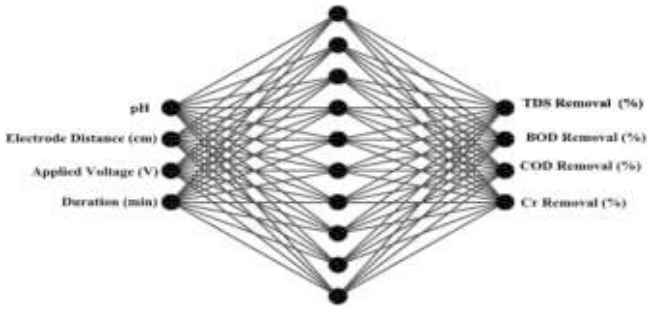

Fig. 3. Artificial Neural Network architecture.

The predicted value of the dependent variable y is determined by the MLR model, with βi (i = 1,…,n) representing the partial regression coefficients and xi (i = 1,…,n) representing the independent variables (inputs), while ε represents the random or unexplained error [18]. The performance of the ANN and MLR models was statically evaluated using mean square error (MSE), root mean square error (RMSE), mean absolute error (MAE), sum square error (SSE), and the coefficient of determination (R^2) [27]. The MATLAB R2015a (The MathWorks, Inc. ver. 8.5.0) computing environment was utilized for the neural network toolbox and fitml (x,y) command to generate the ANN and MLR from the data.

3. Results and discussions

3.1. Effects of pH on removal efficiency

The pH of the electrocoagulation media plays vital roles in the process, the chemistry of the species, electrodes as well as the pollutants depends on this important factor. Fig. 4(a and b) shows the effects of pH on the removal efficiencies of pollutants parameters (TDS, BOD, COD and Chromium) of the tannery effluent using Al and Fe electrode, respectively. The highest COD removal efficiency was obtained at pH 8, with Al electrodes, the COD was reduced to 84.18 while the final COD in Fe electrode was 208.01 mg/g from initial COD of 6100 mg/L, representing efficiency of 98.62 % and 96.59 % for Al and Fe electrodes, respectively. The decrease in removal efficiency observed at pH 9 for both electrodes may be attributed to the formation and predominance of inefficient flocculants (i.e. monomeric $Al(OH)_4^-$ and $Fe(OH)_4^-$anions) under alkaline conditions [28,29]. At higher pH, flocks deposits on the anode surface form making it to become inert, thus leading to a reduced conducting layer which resulted to an increasing ohmic drop and increase in the electrical consumption with reduction efficiency. Also, soluble monomeric cations are converted to insoluble flocs at higher pH by precipitation kinetics which remains in treated wastewater leading to decrease removal efficiency above pH 9. Similarly, Emamjomeh et al. [30] found that complete removal efficiency of COD was achieved at pH 8 to carwash wastewater treatment using aluminum electrodes and at higher values of pH 8 the removal rates gradually decreased, which is in consistence with the present study.

3.2. Effects of Voltage on Removal Efficiency

The effects of applied voltage on removal efficiencies of the pollutants are as shown in Fig. 5(a and b). As shown, the increase in voltage lead to increase in the removal efficiency. The Al electrodes reduced the COD to 193.98 mg/L while the final COD in Fe electrode was 246.44 mg/L, representing efficiency of 96.82 % and 95.96 % for Al and Fe electrodes, respectively at applied voltage of 20 V. The reason for this is that a higher electrode potential leads to an increase in the number of coagulant ions, resulting in a higher rate of pollutant recovery [31,32]. Conversely, voltage density dictates the rate and quantity of hydroxyl ion generation. The greater the rate of hydroxyl ion production, the higher the removal efficiency [33]. Increasing the electrical voltage speeds up the elimination of COD. When the voltage of the cell is increased, a greater amount of hydrogen bubbles is produced at the cathode, resulting in a higher upward flow, and leading to a faster reduction in COD [34]. Increased bubble generation will lead to a greater deposition of organic matter. Higher applied voltage values result in higher allowance percentages. Hence, it can be inferred that the most effective reduction in COD concentration occurs at a voltage of 20 V, leading to COD removal efficiencies of 98.62 % and 96.59 % for Al and Fe electrodes, respectively. Amri et al. demonstrated that as the voltage increased, the removal of COD and TSS also increased. They observed the most significant reduction at 24 V, leading to a 91 % decrease in COD from 3000 mg/L to 270 mg/L, and a 90 % decrease in TSS from 1220 mg/L to 120 mg/L [35]. However, the results of other

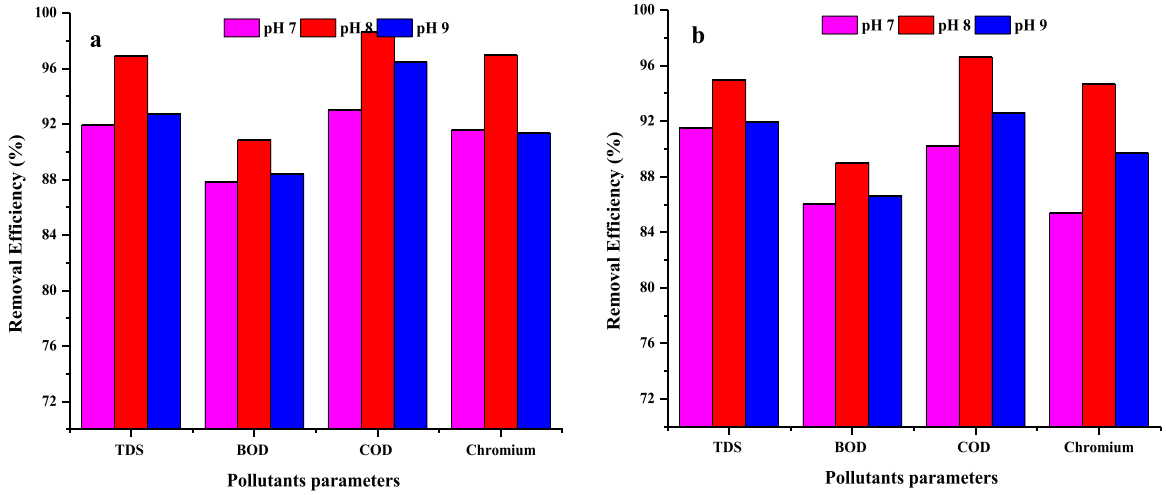

Fig. 4. Effect of pH on Removal of the pollutants using: (a) Al and (b) Fe Electrodes.

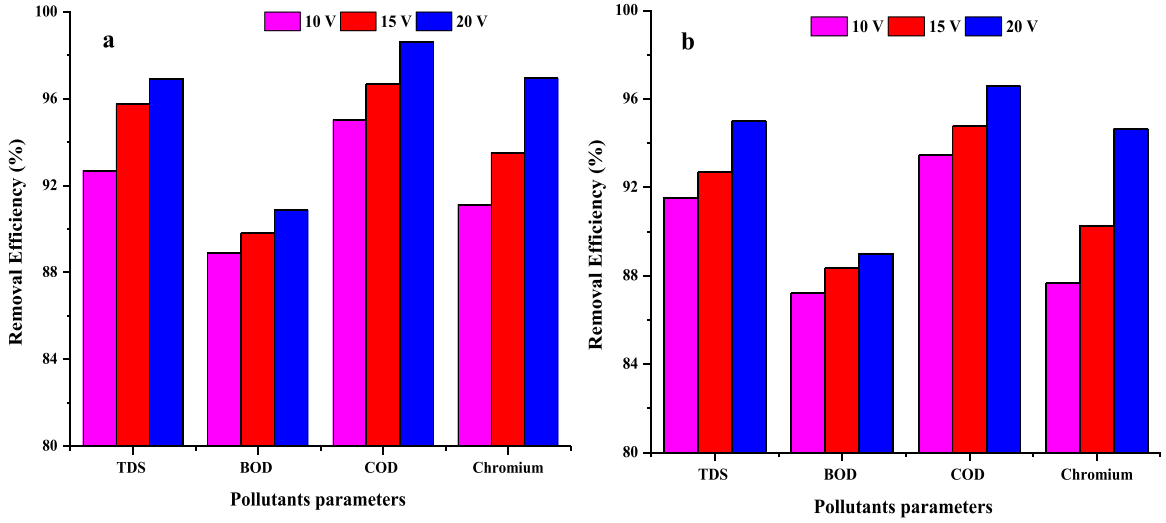

Fig. 5. Effect of Applied Voltage on Removal of the pollutants using: (a) Al (b) Fe Electrodes.

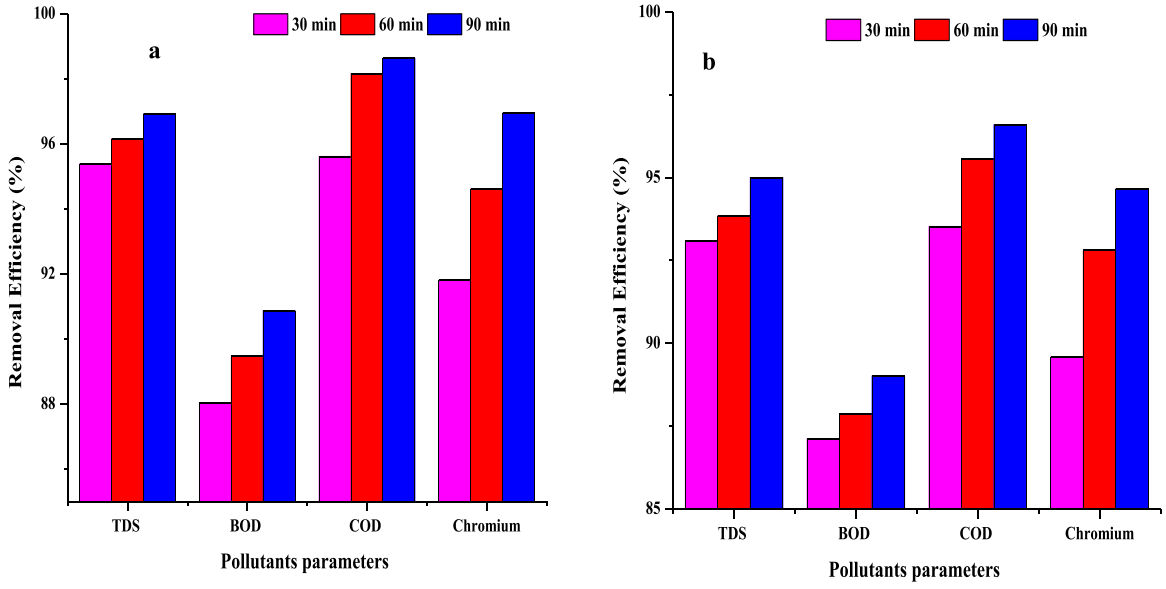

Fig. 6. Effect of electrolysis time on Removal of the pollutants using: (a) Al (b) Fe Electrodes.

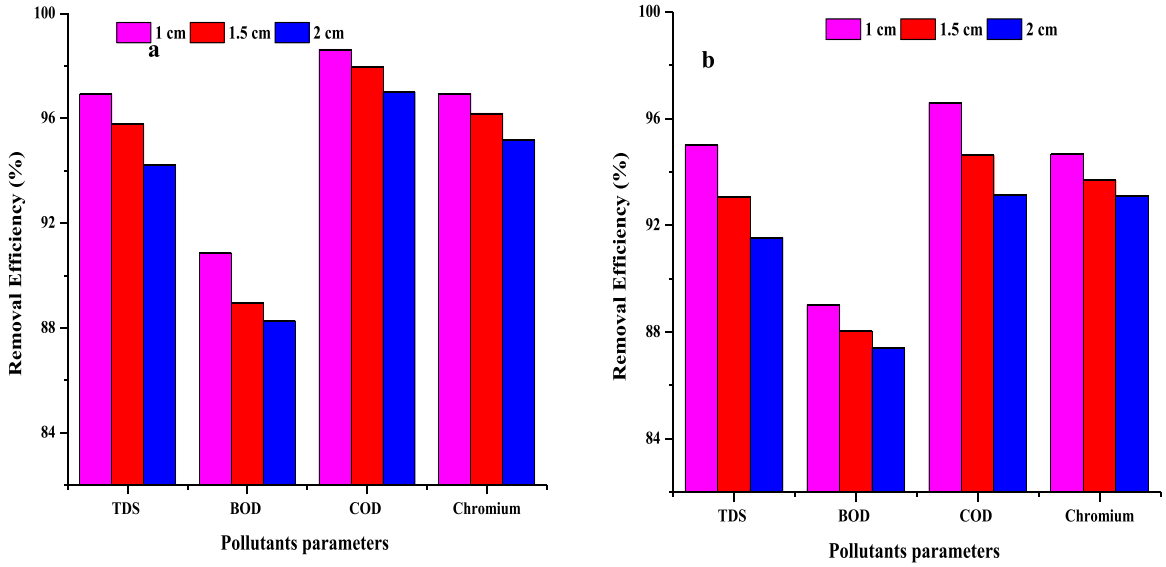

Fig. 7. Effect of Electrode Distance on Removal Efficiency for (a) Al and (b) Fe Electrodes.

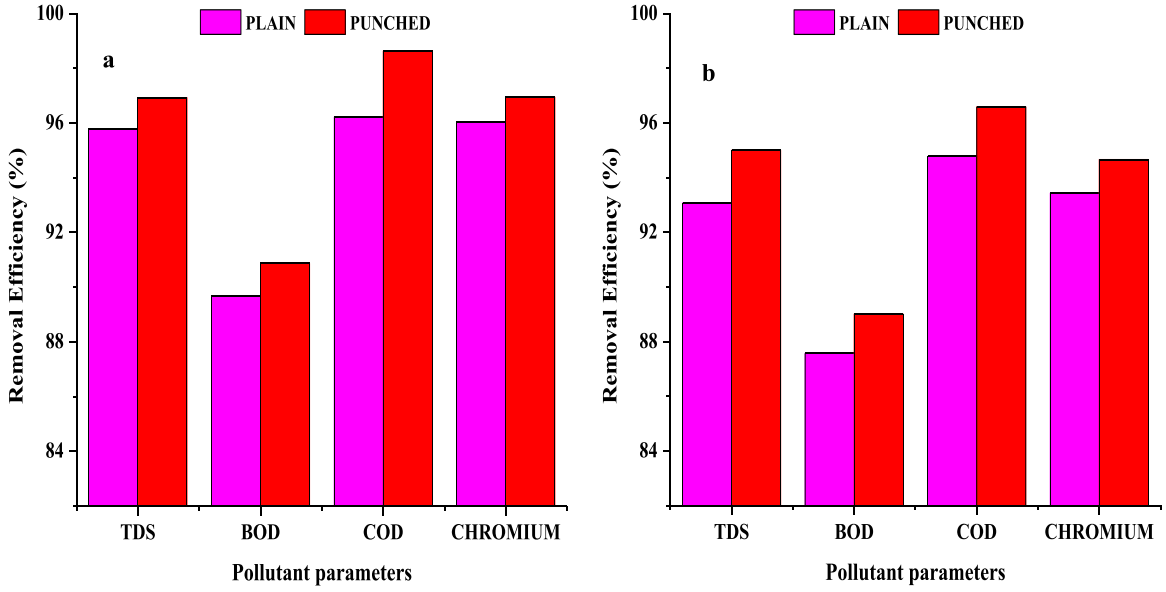

Fig. 8. Effect of Electrode Shape on Removal Efficiency for (a) Al and (b) Fe Electrodes.

studies indicated that high voltage (20 v) was not efficient in removing COD using EC due to the extended electrolysis duration [36,37], which is inconsistent with the present study. Fig. 5(a and b) depicts that the TDS reduction from tannery wastewater is influenced by the electrical voltage of 10 V, 15 V, and 20 V changes in TDS removals of 92.68 %, 95.85 %, and 97.2 % using Al electrodes and 91.9 %, 93.34 %, and 95.1 % using Fe electrodes. The findings showed that Al electrode at voltage of 20 V had high performance rather than Fe electrode.

The interaction between the electrodes and voltage during the EC process results in the formation of flocs that effectively bind pollutants. The effectiveness of the EC process increases with the production of more flocs. Aluminum hydroxide is produced as a result of the hydrolysis of Al^{3+} ions, and this sludge has a correlation with TDS [38]. When at the anode electrode, it will undergo oxidation to form Al^{3+} ions and bind OH^- to create $Al(OH)_3$ compounds that can trap pollutants, while at the cathode it will generate hydrogen gas to help raise the formed flocs to the surface.

At the anode electrode, it will undergo an oxidation reaction to anions (negative ions) to form Al^{3+} and bind OH^- to form $Al(OH)_3$ compounds which can bind pollutants, while at the cathode it will produce hydrogen gas which functions to lift the formed flocs to the surface. The flocs will become larger and settle to the bottom of the EC cell, leading to an increase in the procedure's effectiveness in reducing the quantity of TDS. When varying the voltage to 10 V, 15 V, and 20 V for Cr reduction using an Al electrode, the removal efficiency increased to 86.5 %, 90 %, and 94.5 %, respectively. Similarly, in the study by Villabona-Ortíz et al. [37], it was observed that the efficiency of Cr removal reached 92.9 % when treated for 30 min at 20 V. This removal occurred because the hydrolysis products of aluminum caused destabilization of Cr(VI) in the solution, leading to agglomeration and improved separation of the solution through sedimentation or flotation.

3.3. Effects of electrolysis time on removal efficiency

Fig. 6(a and b) illustrates that 267.79 mg/L of COD was remaining in the solution (translating to 95.61 % COD removal efficiency) after 30 min of electrolysis time. After 90 min of electrocoagulation process, the COD of the solution was found to have been reduced to 8.54 and 145.79 mg/L in Al and Fe electrodes system, respectively, corresponding to removal efficiencies of 99.86 % and 97.61 % in Al and Fe

Table3

Experimental design matrix for the electrocoagulation treatment of tannery wastewater using Al Electrodes.

				Plane Aluminum Electrodes												PunchedAluminum Electrodes											
								ANN				LINEAR REGRESSION								ANN				LINEAR REGRESSION			
pH	Elect space (cm)	Voltage (V)	Duration (min)	TDS (%)	BOD (%)	COD (%)	Chromium (%)	TDS (%)	BOD (%)	COD (%)	Chromium (%)	TDS (%)	BOD (%)	COD (%)	Chromium (%)	TDS (%)	BOD (%)	COD (%)	Chromium (%)	TDS (%)	BOD (%)	COD (%)	Chromium (%)	TDS (%)	BOD (%)	COD (%)	Chromium (%)
7	1	10	30	88.85	82.93	88.16	78.49	89.11	84	88.78	78.61	90.06	84.32	89.36	79.39	90	85.99	90.11	80.23	90.31	85.76	90.37	80.11	91.17	86.15	90.55	80.7
7	1	10	60	89.23	85.11	89.08	80.16	89.2	85.49	89.3	79.85	90.47	85.2	90.18	82.49	90.38	86.87	91.33	82.01	90.52	86.43	90.78	81.32	91.62	87.06	91.5	83.68
7	1	10	90	89.62	85.62	89.85	83.03	89.59	86	89.97	82.58	90.87	86.08	91	85.6	90.77	87.2	91.31	83.86	90.69	87.29	91.55	83.5	92.08	87.96	92.46	86.65
8	1	10	30	91.15	86.04	91.69	82.14	91.41	86.2	92.2	83.36	90.43	85.5	91.59	82.26	91.92	87.38	92.74	83.99	91.65	87.11	92.55	84.03	91.62	86.69	92.66	83.74
8	1	10	60	91.15	87.2	93.36	85.43	91.79	87.15	92.75	85.75	90.84	86.38	92.41	85.36	92.31	88.13	94.59	87.01	92.66	88.5	93.88	87.5	92.07	87.59	93.62	86.71
8	1	10	90	91.54	88.08	93.97	89.95	92.52	87.86	93.84	89.79	91.24	87.26	93.23	88.46	92.69	88.91	95.02	91.12	93.44	89.46	94.65	89.99	92.53	88.49	94.57	89.69
9	1	10	30	90.77	86.18	94.21	85.77	91	86.51	93.71	85.86	90.8	86.68	93.81	85.12	92.69	87.2	95.02	87.69	92.93	87.32	95.12	87.57	92.07	87.22	94.78	86.77
9	1	10	60	91.15	87.01	94.72	90.43	91.45	87.14	94.73	90.51	91.21	87.56	94.63	88.23	93.08	87.99	96.61	92.21	93.52	87.82	96.08	91.76	92.52	88.12	95.73	89.75
9	1	10	90	91.54	87.8	95.18	92.14	91.82	87.95	95.21	91.9	91.61	88.45	95.45	91.33	93.46	88.73	96.8	92.9	94.21	88.52	96.49	91.88	92.98	89.02	96.69	92.72
7	1.5	10	30	88.46	79.56	85.77	74.75	88.14	79.92	85.75	74.49	88.91	81.11	86.23	76.29	89.23	82.84	88.38	76.51	89.27	82.47	88	76.71	89.88	83.24	88.37	78.1
7	1.5	10	60	88.85	81.11	86.87	78.38	88.33	81.84	86.74	76.44	89.31	81.99	87.05	79.4	89.62	83.3	89.26	80.14	89.72	83.26	88.91	79.78	90.34	84.14	89.33	81.08
7	1.5	10	90	88.85	82.46	87.92	80.16	88.7	82.43	87.69	80.56	89.72	82.87	87.87	82.5	90	84.32	89.9	81.92	90.1	84.42	89.89	82.06	90.79	85.04	90.29	84.05
8	1.5	10	30	90	84.3	89.48	80.16	89.96	83.64	89.75	80.38	89.28	82.29	88.46	79.16	90.77	84.46	90.33	81.92	90.27	84.62	90.49	82.04	90.33	83.77	90.49	81.14
8	1.5	10	60	90.38	84.54	90.26	83.45	90.53	84.59	90.67	83.38	89.68	83.17	89.28	82.26	91.15	85.25	92.03	85.21	91.1	86.03	91.52	85.13	90.79	84.67	91.44	84.11
8	1.5	10	90	90.77	85.36	91.87	87.76	91.15	85.46	91.73	87.58	90.09	84.05	90.09	85.36	91.92	86.46	93.02	89.52	91.84	86.92	92.37	89.15	91.24	85.57	92.4	87.09
9	1.5	10	30	89.62	83.81	91.44	84.48	89.59	83.87	91.19	84.3	89.65	83.47	90.68	82.03	91.15	84.65	93.57	86.24	91.44	84.63	93.13	86.33	90.78	84.3	92.6	84.17
9	1.5	10	60	90	83.44	91.89	88.17	90.08	84.45	92.24	88.63	90.05	84.35	91.5	85.13	91.15	85.34	94.52	89.93	91.79	85.18	94.03	90.41	91.23	85.2	93.56	87.15
9	1.5	10	90	90.38	84.88	92.08	89.82	90.35	85.21	92.63	89.83	90.46	85.23	92.32	88.23	91.54	85.9	95.28	91.58	92.53	85.89	94.46	90.45	91.69	86.11	94.51	90.12
7	2	10	30	87.31	75.5	81.84	70.68	87.35	75.37	82	70.68	87.75	77.9	83.1	73.2	88.46	78.43	86	72.19	88.68	78.69	85.6	72.63	88.59	80.32	86.2	75.5
7	2	10	60	87.31	77.24	83.2	74.73	87.48	77.72	82.98	72.73	88.16	78.78	83.92	76.3	88.85	79.64	86.85	76.23	88.75	79.7	86.59	76.2	89.05	81.22	87.16	78.48
7	2	10	90	87.69	78.75	83.92	76.99	87.83	78.48	83.86	76.74	88.57	79.66	84.74	79.4	89.23	81.08	87.03	78.49	89.12	81.01	87.66	78.53	89.5	82.13	88.11	81.45
8	2	10	30	88.85	80.81	85.87	75.55	88.88	80.57	85.79	75.67	88.12	79.08	85.32	76.06	89.62	81.59	88.28	78.42	89.79	81.66	88.48	78.33	89.04	80.86	88.31	78.54
8	2	10	60	89.23	81.08	87.2	79.52	89.51	81.2	86.73	79.23	88.53	79.96	86.14	79.16	89.62	83.16	89.26	82.4	90.29	83.08	89.42	82.1	89.5	81.76	89.27	81.52
8	2	10	90	90	82	87.38	83.42	89.97	81.98	87.46	83.14	88.94	80.84	86.96	82.26	90.38	84	89.7	86.3	90.36	83.99	89.91	86.23	89.95	82.66	90.23	84.49
9	2	10	30	88.85	80.75	87.2	80.27	88.78	81.13	87.21	80.38	88.49	80.26	87.55	78.93	90.38	81.73	89.93	83.15	90.06	81.77	90.77	83.04	89.49	81.39	90.43	81.58
9	2	10	60	89.62	81.54	88.44	84.38	89.34	81.66	88.27	84.14	88.9	81.14	88.37	82.03	90.77	82.47	91.18	87.26	90.49	82.05	91.55	87.17	89.95	82.29	91.38	84.55
9	2	10	90	90	82.33	88.92	85.75	89.53	82.43	88.68	85.7	89.3	82.02	89.19	85.13	91.15	82.47	91.57	88.63	91.18	82.81	92.27	88.3	90.4	83.19	92.34	87.53
7	1	15	30	89.23	84.14	88.9	79.13	89.44	84.19	89.14	80.19	90.63	84.55	89.9	81.15	90.38	85.99	90.67	81.8	90.63	86.41	90.96	81.3	91.72	86.46	91.32	82.48
7	1	15	60	89.62	86.27	89.59	82.35	89.47	85.72	89.6	81.96	91.04	85.43	90.72	84.25	90.77	87.34	91.34	83.31	90.82	87.18	91.69	83.62	92.17	87.36	92.28	85.45
7	1	15	90	90	86.6	90.79	83.92	89.99	86.24	90.41	85.19	91.44	86.31	91.54	87.36	91.15	87.76	91.97	84.75	90.99	87.61	91.84	85.17	92.63	88.26	93.24	88.43
8	1	15	30	93.85	86.64	92.08	85.91	92.87	86.86	93.11	85.63	91	85.73	92.12	84.02	94.62	87.8	94.2	86.66	93.83	87.71	94.51	86.85	92.17	86.99	93.44	85.51
8	1	15	60	94.62	87.71	93.97	90.5	93.34	87.69	93.99	89.73	91.41	86.61	92.94	87.12	95	89.05	96.03	91.39	94.63	88.96	95.87	91.29	92.62	87.89	94.39	88.49
8	1	15	90	95	88.73	94.33	92.76	93.94	88.61	94.85	93.17	91.81	87.49	93.76	90.22	95.77	89.8	96.67	93.51	95.46	90.04	96.93	93.27	93.08	88.79	95.35	91.46
9	1	15	30	90.38	86.09	93.97	84.95	90.35	85.88	93.5	84.64	91.37	86.91	94.35	86.88	92.31	87.01	94.67	86.6	91.89	86.69	94.69	86.14	92.62	87.52	95.55	88.55
9	1	15	60	90.77	86.83	94.51	88.58	90.78	86.46	94.45	89.03	91.78	87.79	95.17	89.99	92.69	87.76	95.72	89.75	92.38	87.47	95.67	89.51	93.07	88.42	96.51	91.52
9	1	15	90	91.15	87.24	94.98	90.5	90.99	87.22	94.77	90.29	92.18	88.67	95.99	93.09	93.08	88.31	96	91.39	92.89	88.42	96.5	91.19	93.53	89.33	97.46	94.5
7	1.5	15	30	88.85	80.38	86.43	77.9	88.46	80.25	86.47	76.98	89.48	81.34	86.77	78.05	89.62	83.3	89.03	79.66	89.69	83.2	88.97	79.43	90.43	83.54	89.15	79.88
7	1.5	15	60	89.23	81.59	87.56	79.54	88.57	82.07	87.37	79.87	89.88	82.22	87.59	81.16	90	84.52	89.61	81.3	90.04	84.03	89.6	81.37	90.89	84.44	90.11	82.85
7	1.5	15	90	89.62	82.51	88.61	81.18	89.12	82.66	88.4	83.89	90.29	83.1	88.41	84.26	90.38	85.53	90.3	82.95	90.27	84.99	90.2	83.53	91.34	85.35	91.06	85.83
8	1.5	15	30	91.92	84.4	90.25	83.17	91.26	84.41	90.86	83.2	89.85	82.52	88.99	80.92	92.31	84.79	91.98	84.93	91.87	85.36	92.08	84.78	90.88	84.08	91.26	82.91
8	1.5	15	60	92.69	84.78	91.59	87.76	91.81	85.19	91.98	88.02	90.25	83.4	89.81	84.02	93.08	86.13	93.72	89.52	92.87	86.38	93.53	90.27	91.33	84.98	92.22	85.89
8	1.5	15	90	93.08	85.56	92.28	90.02	92.4	86.15	92.78	90.79	90.66	84.28	90.63	87.12	93.46	87.38	94.62	91.78	93.95	87.28	94.46	91.78	91.79	85.88	93.18	88.86
9	1.5	15	30	88.85	83.4	91.23	83.31	88.94	83.26	91.04	82.99	90.22	83.7	91.22	83.79	89.62	84.16	93.03	85.07	90.23	84.14	92.85	84.28	91.33	84.61	93.38	85.95
9	1.5	15	60	88.85	83.72	92.23	86.18	89.3	83.77	91.91	87.03	90.62	84.58	92.04	86.89	90	84.99	94.16	87.95	90.59	84.87	93.82	88.07	91.78	85.51	94.33	88.92
9	1.5	15	90	89.23	84.32	92.43	87.97	89.54	84.34	92.24	87.83	91.03	85.46	92.85	89.99	90.38	86.04	94.46	89.73	91.36	85.68	94.71	90.21	92.24	86.41	95.29	91.9
7	2	15	30	87.69	76.42	82.25	74.38	87.51	75.62	82.31	72.53	88.32	78.12	83.63	74.96	88.85	79.36	86.69	75.89	88.73	79.68	86.61	75.39	89.14	80.63	86.98	77.28
7	2	15	60	87.69	77.78	83.59	75.41	87.73	77.89	83.44	75.43	88.73	79	84.45	78.06	89.23	80.47	87.25	76.92	89	80.51	87.13	77.26	89.6	81.53	87.93	80.25
7	2	15	90	88.08	78.81	84.16	79.18	88.22	78.79	84.43	79.47	89.13	79.88	85.27	81.16	89.62	81.73	87.77	80.68	89.52	81.64	88.14	80.58	90.05	82.43	88.89	83.23
8	2	15	30	89.62	80.92	86.77	78.49	89.88	81	86.58	78.56	88.69	79.31	85.86	77.82	90.38	83.07	89.7	81.37	90.66	82.55	89.69	81.51	89.59	81.16	89.09	80.32
8	2	15	60	90.38	81.35	87.69	83.7	90.47	81.56	87.65	83.48	89.1	80.19	86.68	80.92	90.77	83.63	91.57	86.58	91.06	83.47	90.69	86.95	90.05	82.06	90.05	83.29
8	2	15	90	91.15	82.22	88.33	86.23	90.96	82.32	88.28	86.34	89.5	81.07	87.5	84.02	91.54	84.6	92.34	89.11	91.9	84.25	91.45	88.86	90.5	82.96	91.00	86.27
9	2	15	30	88.46	80.43	87.11	78.9	88.18	80.58	87.13	79.18	89.06	80.49	88.08	80.69	89.23	80.47	90.74	81.78	89.21	81.31	90.95	81.34	90.04	81.69	91.20	83.35
9	2	15	60	88.46	81.12	88.07	82.74	88.53	81.1	88.05	82.94	89.47	81.37	88.9	83.79	89.62	82.05	91.95	85.62	89.4	81.92	91.89	85.74	90.49	82.59	92.16	86.33
9	2	15	90	88.85	82.19	88.52	84.11	88.82	81.59	88.64	84.17	89.87	82.25	89.72	86.89	90	82.65	92.52	86.99	89.87	82.73	92.49	87.05	90.95	83.49	93.12	89.3
7	1	20	30	89.62	84.79	89.98	81.53	90.22	84.58	89.64	81.8	91.2	84.77	90.44	82.91	91.15	86.64	91.3	83.58	91.7	87	91.84	83.76	92.27	86.76	92.10	84.25
7	1	20	60	90	85.67	90.33	83.86	90.32	86.01	90.2	84.42	91.61	85.65	91.25	86.01	91.54	87.52	92.07	87.14	91.98	87.57	92.6	86.96	92.72	87.66	93.06	87.23
7	1	20	90	90.77	86.73	90.77	89.82	90.75	86.62	91.02	88.77	92.01	86.53	92.07	89.12	91.92	87.85	93.02	91.6	92.08	87.77	93.02	91.54	93.18	88.57	94.01	90.2
8	1	20	30	95.38	87.71	94.54	90.77	95.06	87.78	94.36	88.36	91.57	85.96	92.66	85.78	95.38	88.03	95.61	91.8	95.79	88.23	95.97	91.6	92.72	87.3	94.21	87.29
8	1	20	60	95.38	88.78	95.64	93.99	95.61	88.53	95.44	93.4	91.98	86.84	93.48	88.88	96.15	89.47	98.15	94.61	96.5	89.72	97.32	94.69	93.17	88.2	95.17	90.26
8	1	20	90	95.77	89.66	96.21	96.05	96.02	89.56	96.08	96.55	92.38	87.72	94.3	91.98	96.92	90.86	98.62	96.94	97.05	90.88	98.47	97.04	93.63	89.1	96.13	93.24
9	1	20	30	90	85.25	93.62	84.34	90	85.6	93.54	84.8	91.94	87.14	94.89	88.64	91.92	86.87	94.31	86.39	91.38	86.55	94.48	86.72	93.16	87.83	96.33	90.32
9	1	20	60	90.38	86.22	93.85	87.49	90.43	86.13	94.39	88.62	92.35	88.02	95.7	91.75	92.31	87.2	95.43	89.13	91.75	87.4	95.38	89.48	93.62	88.73	97.28	93.3
9	1	20	90	90.77	86.83	94.33	90.36	90.63	86.68	94.76	90.27	92.75	88.9	96.52	94.85	92.69	88.4	96.44	91.32	92.17	88.29	96.2	91.45	94.08	89.63	98.24	96.27
7	1.5	20	30	89.23	80.77	87.26	79.4	89.13	80.63	87.23	79.54	90.05	81.56	87.3	79.81	90.38	83.74	89.57	81.16	90.37	83.82	89.66	81.37	90.98	83.85	89.93	81.65
7	1.5	20	60	89.62	82.12	88.26	83.79	89.31	82.25	88.27	83.67	90.45	82.44	88.12	82.92	90.77	84.73	90.36	85.55	90.58	84.7	90.5	84.7	91.43	84.75	90.88	84.63
7	1.5	20	90	90	82.85	88.97	87.97	89.83	83.02	89.19	87.71	90.86	83.32	88.94	86.02	91.15	85.39	91.00	89.73	90.71	85.29	90.79	88.09	91.89	85.65	91.84	87.6
8	1.5	20	30	93.46	84.88	92	87.35	93.37	85.38	92.25	86.33	90.42	82.74	89.53	82.68	94.23	85.39	93.8	89.11	94.15	85.66	93.94	89.16	91.43	84.38	92.04	84.69
8	1.5	20	60	94.23	85.8	93.2	91.73	93.91	86.09	93.38	91.55	90.82	83.62	90.35	85.78	95.00	86.64	95.87	93.49	95.01	86.97	95.41	93.06	91.88	85.28	93.00	87.66
8	1.5	20	90	94.62	85.99	93.39	93.72	94.31	87	93.97	94.25	91.23	84.5	91.17	88.88	95.77	87.66	96.92	95.48	95.68	88.23	96.69	95.34	92.34	86.18	93.95	90.64
9	1.5	20	30	88.46	82.98	91.08	82.21	88.44	82.85	90.98	82.5	90.79	83.93	91.75	85.55	89.23	83.86	92.67	83.97	89.47	84.04	92.65	83.83	91.88	84.91	94.15	87.73
9	1.5	20	60	88.85	83.58	91.77	86.01	88.78	83.29	91.72	85.91	91.19	84.81	92.57	88.65	89.62	84.36	93.79	87.77	89.98	84.66	93.61	87.52	92.33	85.81	95.11	90.7
9	1.5	20	90	89.23	83.86	92.52	88.03	88.97	83.62	92.12	87.61	91.6	85.69	93.39	91.75	90.00	85.3	94.56	89.79	90.51	85.52	94.49	89.69	92.79	86.71	96.07	93.68
7	2	20	30	87.69	76.86	83.08	76.78	88.03	76.05	82.84	74.5	88.89	78.35	84.17	76.72	88.85	79.96	86.9	78.29	89.07	80.41	87.21	77.13	89.69	80.93	87.75	79.06
7	2	20	60	88.08	78.37	85.02	79.79	88.32	78.12	84.27	79.46	89.3	79.23	84.99	79.82	89.23	80.84	88.2	81.3	89.45	81.25	88.15	81.32	90.15	81.83	88.71	82.03
7	2	20	90	88.85	79.18	85.16	83.01	88.89	79.27	85.18	82.6	89.7	80.11	85.81	82.92	90.00	81.68	88.7	84.52	89.73	82	88.38	84.21	90.6	82.73	89.67	85.01
8	2	20	30	91.54	81.46	87.9	81.99	91.74	81.66	87.74	81.87	89.26	79.53	86.4	79.58	92.69	83.26	91.25	84.86	92.4	82.92	91.38	85.19	90.14	81.46	89.87	82.09
8	2	20	60	91.92	82.49	89.11	87.12	92.24	82.18	88.81	87.31	89.67	80.41	87.21	82.68	93.08	84.18	93.33	90	93.15	84.04	92.86	89.79	90.59	82.37	90.82	85.07
8	2	20	90	92.69	82.7	89.56	89.73	92.68	82.81	89.39	89.8	90.07	81.29	88.03	85.78	94.23	85.25	94.54	92.6	94.17	85.04	94.26	92.67	91.05	83.27	91.78	88.04
9	2	20	30	88.08	79.87	87.02	77.67	87.59	80.15	87.13	78.28	89.63	80.71	88.62	82.45	88.85	81.63	90.51	80.55	88.43	81.29	90.89	80.7	90.59	82	91.98	85.13
9	2	20	60	88.46	80.71	87.21	82.12	87.91	80.66	88	81.62	90.04	81.59	89.44	85.55	89.23	82.24	92.07	85	88.51	81.93	91.73	84.54	91.04	82.9	92.94	88.1
9	2	20	90	88.85	81.54	88.92	84.38	88.19	81.05	88.69	83.32	90.44	82.47	90.26	88.65	89.62	82.98	92.54	87.26	88.83	82.78	92.53	86.78	91.5	83.8	93.89	91.08

Table 4
Experimental design matrix for the electrocoagulation treatment of tannery wastewater using Fe Electrodes.

				Plane Iron Electrodes												Punched Iron Electrodes											
								ANN				LINEAR REGRESSION								ANN				LINEAR REGRESSION			
pH	Electrode space (cm)	Voltage (V)	Duration (min)	TDS (%)	BOD (%)	COD (%)	Chromium (%)	TDS (%)	BOD (%)	COD (%)	Chromium (%)	TDS (%)	BOD (%)	COD (%)	Chromium (%)	TDS (%)	BOD (%)	COD (%)	Chromium (%)	TDS (%)	BOD (%)	COD (%)	Chromium (%)	TDS (%)	BOD (%)	COD (%)	Chromium (%)
7	1	10	30	88.08	77.09	84.97	78.08	88.48	76.28	84.57	78.86	88.40	79.93	86.76	78.26	88.85	80.24	87.5	78.08	88.27	80.39	87.01	78.38	89.39	82.55	88.62	80.20
7	1	10	60	88.46	77.88	86.03	80.14	88.55	77.59	85.88	80.15	88.84	81.18	88.00	80.68	88.85	81.59	88.73	82.26	88.80	81.37	88.04	81.36	89.82	83.72	89.72	82.49
7	1	10	90	88.46	78.9	87.08	81.58	88.66	78.72	87.22	81.32	89.27	82.44	89.23	83.10	89.23	82.75	89.05	84.04	89.34	82.60	88.92	83.83	90.25	84.89	90.81	84.79
8	1	10	30	89.62	82.93	90.33	81.16	89.82	81.83	88.24	81.49	89.41	81.46	88.81	81.14	90.38	84.79	90.84	84.11	90.55	85.02	90.82	84.16	90.20	83.75	90.28	82.96
8	1	10	60	90	84.04	91.74	83.63	89.73	83.24	90.57	83.93	89.85	82.71	90.05	83.56	90.77	86.33	92.18	86.85	91.32	86.27	92.10	86.35	90.63	84.92	91.38	85.25
8	1	10	90	90.38	86.18	92.82	85.34	90.25	84.49	91.51	85.60	90.28	83.97	91.28	85.98	91.54	87.21	93.46	87.67	91.96	87.77	93.08	87.17	91.06	86.09	92.47	87.54
9	1	10	30	90.77	83.96	91.66	84.93	90.59	84.04	91.32	84.91	90.42	82.99	90.86	84.02	91.54	85.81	92.48	85.55	91.52	85.75	92.08	85.77	91.01	84.94	91.94	85.72
9	1	10	60	91.15	84.9	92.61	87.81	90.76	85.57	92.97	87.08	90.86	84.24	92.10	86.44	91.92	86.64	93.34	88.7	92.28	86.05	93.47	88.50	91.44	86.11	93.04	88.01
9	1	10	90	91.54	85.78	93.34	89.45	91.28	86.94	93.90	88.83	91.29	85.49	93.33	88.86	91.92	87.57	94.25	90.41	92.50	87.01	93.94	89.13	91.87	87.29	94.13	90.30
7	1.5	10	30	87.69	74.26	83.2	72.12	88.10	74.55	82.88	75.22	87.84	76.90	83.96	74.31	88.08	77.69	85.46	75.07	87.69	77.84	84.78	75.30	88.56	79.39	85.96	77.49
7	1.5	10	60	87.69	75.46	84.48	76.37	88.14	75.85	84.00	76.51	88.27	78.15	85.19	76.73	88.46	78.76	86.25	79.32	88.16	78.91	86.07	78.90	88.99	80.56	87.06	79.78
7	1.5	10	90	88.08	76.3	85.84	78.15	88.09	77.05	85.60	78.30	88.71	79.40	86.43	79.15	88.46	79.87	87.34	81.1	88.46	80.33	86.94	81.38	89.41	81.74	88.15	82.08
8	1.5	10	30	88.85	79.92	86.05	78.15	89.36	80.62	85.96	78.43	88.85	78.43	86.01	77.19	89.62	82.29	88.41	81.1	89.47	82.23	88.28	81.28	89.37	80.59	87.62	80.25
8	1.5	10	60	89.23	81.26	87.77	81.37	89.31	82.06	88.31	81.00	89.28	79.68	87.24	79.61	90	83.63	89.46	84.32	90.00	83.33	89.63	83.86	89.80	81.76	88.72	82.54
8	1.5	10	90	89.62	83.25	89.89	82.53	89.72	83.30	89.44	82.78	89.72	80.93	88.48	82.03	90.38	84.97	90.89	85.48	90.41	84.83	90.61	84.91	90.22	82.93	89.81	84.84
9	1.5	10	30	90.38	81.96	88.9	81.37	90.24	81.13	88.73	81.54	89.86	79.96	88.06	80.07	90.38	82.51	90	84.32	90.19	82.69	89.70	84.34	90.18	81.79	89.28	83.01
9	1.5	10	60	90.77	82.56	90.1	83.56	90.38	82.44	90.53	83.97	90.29	81.21	89.29	82.49	90.77	83.35	91.36	86.51	90.79	83.48	91.11	86.95	90.61	82.96	90.38	85.30
9	1.5	10	90	90.77	83.63	91.05	85.68	90.80	83.59	91.42	85.54	90.73	82.46	90.53	84.91	91.15	83.86	92.44	88.63	91.09	84.67	91.88	88.05	91.04	84.13	91.47	87.59
7	2	10	30	87.31	72.4	80.44	67.26	87.38	72.25	80.20	67.46	87.28	73.87	81.15	70.36	87.69	74.35	82.57	71.85	87.05	74.29	81.72	70.92	87.73	76.24	83.30	74.78
7	2	10	60	87.31	74.03	81.54	70.41	87.53	73.81	81.41	70.23	87.71	75.12	82.39	72.78	87.69	75.97	83.2	76.85	87.58	75.39	83.21	74.95	88.15	77.41	84.40	77.07
7	2	10	90	87.69	75.23	82.88	72.67	87.35	75.13	83.16	73.18	88.14	76.37	83.62	75.20	88.08	77.18	84.21	77.88	87.98	77.07	84.41	77.89	88.58	78.58	85.50	79.37
8	2	10	30	88.85	76.48	82.89	73.49	88.68	76.48	82.66	73.42	88.29	75.40	83.20	73.24	89.23	78.43	85.1	76.58	88.86	78.67	85.20	77.11	88.54	77.43	84.96	77.54
8	2	10	60	89.23	78.01	84.79	76.58	88.86	77.94	84.91	76.52	88.72	76.65	84.44	75.66	89.62	79.96	86.33	80.48	89.56	79.68	86.94	80.48	88.96	78.60	86.06	79.83
8	2	10	90	89.62	79.45	85.93	78.15	89.15	79.11	86.27	78.58	89.16	77.90	85.67	78.08	90	81.4	88.1	81.51	89.89	81.48	87.96	81.71	89.39	79.78	87.15	82.13
9	2	10	30	89.62	77.18	85.18	78.77	89.93	76.96	85.55	77.83	89.30	76.93	85.25	76.12	90	79.13	86.95	81.99	89.96	78.96	86.98	82.12	89.35	78.63	86.62	80.30
9	2	10	60	90	78.15	86.54	81.3	90.08	78.03	87.47	80.61	89.73	78.18	86.49	78.54	90.38	80.1	87.97	84.38	90.35	79.95	88.12	84.31	89.78	79.80	87.72	82.59
9	2	10	90	90.38	78.9	88.25	82.81	90.49	79.05	88.35	82.28	90.17	79.43	87.72	80.96	90.77	80.84	89.18	85.55	90.57	81.09	88.91	85.68	90.20	80.97	88.81	84.88
7	1	15	30	89.23	79.13	85.87	78.97	88.92	79.16	86.39	79.97	89.01	80.56	87.20	79.42	89.62	81.77	87.98	80.27	89.44	81.87	88.17	80.06	89.90	83.13	89.10	81.39
7	1	15	60	89.62	80.29	86.69	81.99	89.45	80.58	87.09	81.22	89.45	81.81	88.44	81.85	90	82.93	88.81	82.88	89.96	82.66	89.18	82.67	90.33	84.30	90.20	83.68
7	1	15	90	90	81.63	88.15	82.53	89.68	81.61	88.06	82.50	89.88	83.06	89.67	84.27	90.38	84.51	89.35	83.84	90.34	84.12	89.78	84.00	90.75	85.48	91.30	85.98
8	1	15	30	90.38	84.04	91.05	84.93	90.63	83.78	90.91	85.23	90.02	82.09	89.25	82.31	91.15	85.97	92.48	86.92	91.37	86.05	92.05	87.06	90.71	84.33	90.76	84.15
8	1	15	60	91.54	85.39	92.48	86.92	91.23	85.20	92.15	87.47	90.46	83.34	90.49	84.73	91.92	87.11	93.7	89.32	92.09	87.22	93.27	89.14	91.14	85.50	91.86	86.44
8	1	15	90	91.92	86.82	93.54	88.7	91.54	86.21	93.71	89.50	90.89	84.59	91.72	87.15	92.69	88.36	94.77	90.27	92.76	88.48	94.34	90.36	91.56	86.67	92.96	88.74
9	1	15	30	90.38	82.56	89.85	82.74	90.48	82.78	90.19	83.01	91.03	83.62	91.30	85.19	91.15	85.08	91.49	85.48	91.29	85.22	91.64	84.59	91.52	85.53	92.42	86.91
9	1	15	60	90.77	84.23	92.24	85.48	90.75	84.12	92.12	85.57	91.47	84.87	92.54	87.61	91.54	85.91	92.62	87.33	91.98	85.48	92.93	87.12	91.95	86.70	93.52	89.20
9	1	15	90	91.15	85.11	92.69	88.77	91.44	85.43	93.02	87.63	91.90	86.12	93.77	90.03	91.54	86.54	93.59	88.08	92.23	86.27	93.46	88.04	92.37	87.87	94.61	91.50
7	1.5	15	30	88.08	75.97	84.16	73.77	88.07	75.77	83.87	73.96	88.45	77.53	84.40	75.47	88.46	79.22	86.31	76.71	88.69	79.73	86.00	77.43	89.07	79.98	86.44	78.68
7	1.5	15	60	88.46	77.09	85	77.12	88.62	77.62	84.89	76.31	88.88	78.78	85.63	77.90	88.85	80.66	87.18	80.07	89.05	80.63	87.17	80.47	89.49	81.15	87.54	80.98
7	1.5	15	90	88.85	79.17	86.08	79.25	89.06	79.16	85.83	78.66	89.32	80.03	86.87	80.32	89.23	82	87.9	82.19	89.16	82.14	87.76	81.91	89.92	82.32	88.64	83.27
8	1.5	15	30	89.62	82.17	88.21	81.3	89.93	81.67	88.22	81.20	89.46	79.05	86.45	78.36	90	83.12	89.28	84.25	90.28	83.35	89.61	84.76	89.88	81.17	88.10	81.44
8	1.5	15	60	90.38	82.6	89.79	84.04	90.59	83.21	89.53	83.79	89.90	80.31	87.68	80.78	90.77	84.14	90	86.99	90.80	84.36	90.93	87.22	90.30	82.34	89.20	83.73
8	1.5	15	90	90.77	84.37	91.38	85.41	90.98	84.29	91.21	86.23	90.33	81.56	88.92	83.20	91.15	85.58	91.82	88.36	91.25	85.62	91.99	88.60	90.73	83.52	90.30	86.03
9	1.5	15	30	90	80.57	88.08	80.41	90.11	80.43	87.77	79.96	90.47	80.58	88.50	81.24	90	81.91	89.23	83.36	89.89	81.99	89.15	83.01	90.69	82.37	89.76	84.20
9	1.5	15	60	90.38	81.96	89.07	82.6	90.32	81.48	89.47	82.22	90.91	81.84	89.73	83.66	90.38	82.79	90.48	85.55	90.49	82.87	90.52	85.56	91.11	83.54	90.86	86.49
9	1.5	15	90	90.77	82.88	90.26	83.36	90.99	82.51	90.34	84.20	91.34	83.09	90.97	86.08	90.77	83.86	91.52	86.3	90.89	84.03	91.44	87.06	91.54	84.71	91.96	88.79
7	2	15	30	87.69	74.21	80.92	69.93	87.20	72.93	80.93	68.30	87.89	74.49	81.59	71.52	88.08	76.16	83.34	73.08	87.99	76.45	83.00	73.39	88.23	76.82	83.78	75.97
7	2	15	60	88.08	75.46	82.49	72.12	87.74	75.08	82.20	71.98	88.32	75.75	82.83	73.95	88.46	77.41	84.1	77.33	88.40	77.35	84.30	76.69	88.66	77.99	84.88	78.27
7	2	15	90	88.46	76.99	83.17	74.79	88.38	76.75	83.02	74.75	88.76	77.00	84.06	76.37	88.85	78.94	85.07	78.49	88.65	78.95	85.26	78.75	89.09	79.16	85.98	80.56
8	2	15	30	89.23	78.11	84.08	75.68	89.23	77.76	84.54	75.60	88.90	76.02	83.64	74.41	89.62	80.06	86.21	81.99	89.80	79.84	86.64	81.25	89.04	78.02	85.44	78.73
8	2	15	60	89.62	79.45	85.66	78.22	89.84	79.25	85.85	78.31	89.33	77.27	84.88	76.83	90.38	81.4	86.93	84.38	90.46	80.65	88.25	84.36	89.47	79.19	86.54	81.02
8	2	15	90	90	80.1	87.51	80.14	90.29	80.42	87.55	81.24	89.77	78.53	86.11	79.25	90.77	82.05	89	85.55	90.78	82.10	89.23	85.75	89.90	80.36	87.64	83.32
9	2	15	30	89.62	75.48	84.66	76.78	89.89	76.10	84.78	76.89	89.91	77.55	85.69	77.29	89.62	77.42	86.15	81.23	89.61	77.88	86.04	80.74	89.85	79.21	87.10	81.49
9	2	15	60	90	77.24	85.64	78.84	90.02	76.92	86.13	78.58	90.34	78.80	86.93	79.71	90	79.19	87.16	83.15	90.02	78.95	87.20	83.03	90.28	80.38	88.20	83.78
9	2	15	90	90.38	77.92	87.21	79.45	90.52	77.79	87.06	80.22	90.78	80.06	88.16	82.13	90.38	79.87	88.52	83.56	90.30	80.10	88.12	84.77	90.71	81.56	89.30	86.08
7	1	20	30	89.62	81.08	87.15	78.7	89.58	81.40	87.45	80.92	89.63	81.18	87.64	80.59	90.38	82.93	88.95	81.58	90.01	83.02	89.00	81.42	90.40	83.71	89.58	82.58
7	1	20	60	90	82.51	87.59	82.19	90.03	82.35	87.76	82.24	90.06	82.43	88.88	83.01	90.77	84.18	89.66	84.25	90.71	84.04	90.28	84.37	90.83	84.89	90.68	84.88
7	1	20	90	90.38	84.59	88.19	84.38	90.26	83.48	88.56	84.69	90.49	83.68	90.11	85.43	91.54	86.02	90.18	85.41	91.20	85.94	91.02	85.57	91.26	86.06	91.78	87.17
8	1	20	30	91.15	85.71	92.59	87.81	91.73	85.74	92.90	88.76	90.64	82.71	89.69	83.47	93.08	87.11	93.53	89.59	92.70	86.97	93.42	90.13	91.22	84.91	91.24	85.34
8	1	20	60	92.31	86.83	93.34	91.51	92.41	86.93	93.64	90.58	91.07	83.96	90.93	85.89	93.85	87.85	95.56	92.81	93.52	88.27	94.82	92.71	91.64	86.08	92.34	87.64
8	1	20	90	93.08	87.57	94.77	93.42	92.69	88.08	95.21	93.14	91.50	85.21	92.16	88.32	95	89.01	96.59	94.66	94.34	89.41	96.18	94.95	92.07	87.25	93.44	89.93
9	1	20	30	90.77	80.98	89.23	81.71	90.59	81.15	89.38	81.88	91.65	84.24	91.74	86.36	91.15	84.93	90.7	83.56	91.15	84.77	91.32	83.72	92.03	86.11	92.90	88.10
9	1	20	60	91.15	82.28	90.54	84.11	91.31	82.50	90.38	84.14	92.08	85.49	92.98	88.78	91.54	85.29	91.75	86.64	91.74	85.00	92.47	85.97	92.45	87.28	94.00	90.39
9	1	20	90	91.54	83.3	91.59	86.85	91.51	83.87	92.68	87.49	92.51	86.74	94.21	91.20	91.92	86.64	92.61	89.73	91.97	85.66	93.00	86.94	92.88	88.45	95.10	92.69
7	1.5	20	30	88.46	78.11	85.21	75.07	88.64	78.20	85.06	74.67	89.06	78.15	84.84	76.64	88.85	80.61	87.07	78.01	89.39	80.45	86.73	78.52	89.57	80.56	86.92	79.87
7	1.5	20	60	88.85	79.62	85.95	79.18	89.21	79.63	85.59	77.25	89.50	79.40	86.07	79.06	89.23	81.68	88.11	82.12	89.85	81.48	88.04	81.63	90.00	81.73	88.02	82.17
7	1.5	20	90	89.23	80.84	87.03	80.21	89.52	81.05	86.56	80.58	89.93	80.65	87.31	81.48	89.62	83.72	88.97	83.15	90.05	83.25	88.76	83.03	90.43	82.90	89.12	84.46
8	1.5	20	30	90.77	83.16	90.07	84.86	90.99	82.41	90.17	84.68	90.07	79.68	86.89	79.52	91.15	84.51	90.77	87.81	91.34	84.45	90.90	88.05	90.38	81.75	88.58	82.63
8	1.5	20	60	92.31	84.42	91.23	88.15	91.81	83.67	90.97	86.98	90.51	80.93	88.12	81.94	91.92	85.67	92.59	91.1	92.01	85.69	92.50	91.21	90.81	82.93	89.68	84.93
8	1.5	20	90	92.69	85.67	92.74	90.21	92.29	85.04	92.51	90.27	90.94	82.18	89.36	84.37	93.08	86.64	94.13	93.15	92.63	86.99	93.87	93.57	91.24	84.10	90.78	87.22
9	1.5	20	30	90.38	78.8	87.36	78.63	90.15	79.02	86.89	78.77	91.08	81.21	88.94	82.41	90	81.45	88.84	81.58	89.63	81.32	88.61	81.79	91.19	82.95	90.24	85.39
9	1.5	20	60	90.77	79.82	88.67	81.3	90.94	80.11	87.60	80.83	91.52	82.46	90.17	84.83	90	82.28	89.74	84.25	90.19	82.23	89.91	84.17	91.62	84.12	91.34	87.68
9	1.5	20	90	91.15	81.26	89.84	84.45	91.18	81.39	89.88	84.33	91.95	83.71	91.41	87.25	90.38	83.4	90.87	87.4	90.66	83.37	90.89	85.85	92.05	85.29	92.44	89.98
7	2	20	30	88.08	74.95	81.9	71.58	87.79	74.83	82.36	71.56	88.50	75.12	82.03	72.69	88.46	76.9	84.08	74.52	88.76	76.88	83.62	74.30	88.74	77.40	84.27	77.16
7	2	20	60	88.46	75.97	83.15	74.04	88.53	76.34	82.98	74.28	88.93	76.37	83.27	75.11	88.85	77.92	85.28	76.58	89.21	77.92	84.97	77.49	89.17	78.57	85.36	79.46
7	2	20	90	88.85	77.46	83.69	77.53	89.00	77.66	84.01	77.17	89.37	77.62	84.50	77.53	89.23	79.41	86.23	79.93	89.56	79.62	86.07	79.68	89.59	79.74	86.46	81.75
8	2	20	30	90.38	79.13	86.23	78.22	90.17	78.82	86.47	78.39	89.51	76.65	84.08	75.57	90.77	81.08	88	84.93	90.73	81.00	87.77	84.89	89.55	78.60	85.93	79.92
8	2	20	60	91.15	80.19	87.48	80.89	91.06	80.32	87.37	81.44	89.95	77.90	85.32	78.00	91.92	82.14	89.15	88.63	91.53	81.94	89.58	88.62	89.98	79.77	87.02	82.22
8	2	20	90	91.92	81.73	89.49	86.3	91.68	82.21	89.10	86.01	90.38	79.15	86.55	80.42	91.54	83.67	90.48	90.96	92.00	83.35	90.78	90.83	90.40	80.94	88.12	84.51
9	2	20	30	90	74.49	83.77	75.55	89.73	74.95	83.89	75.30	90.52	78.18	86.13	78.46	89.23	76.44	85.28	78.63	89.21	76.74	85.03	79.21	90.36	79.79	87.58	82.68
9	2	20	60	90.38	75.93	84.9	78.42	90.48	75.94	84.41	77.00	90.96	79.43	87.37	80.88	89.62	77.88	86.25	81.3	89.64	77.92	86.23	81.56	90.79	80.97	88.68	84.98
9	2	20	90	90.77	77.37	86.31	80.62	90.74	77.36	86.66	80.50	91.39	80.68	88.60	83.30	90	79.31	87.72	82.67	89.98	79.17	87.30	83.57	91.21	82.14	89.78	87.27

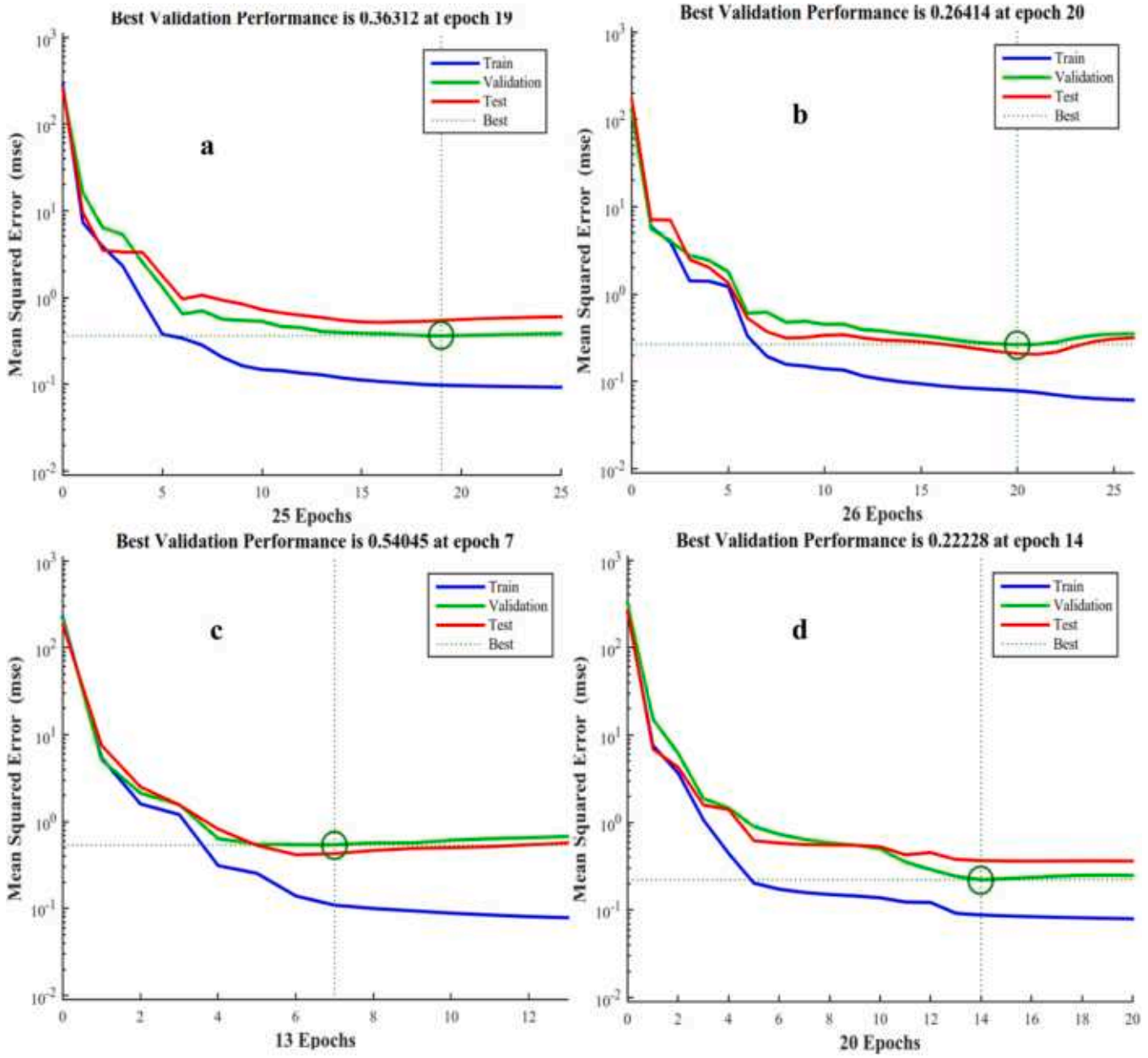

Fig. 9. The Validation performances of the Training Algorithms: ((a) Plane Al (b) Punched Al (c) Plane Fe and (d) Punched Fe) Electrodes.

electrodes, respectively. The duration of electrolysis varies linearly with consumption of electrode (anode) materials, thus longer electrolytic process increases the operational cost. The stability of the passive layer of an electrode is affected by the changing concentration of certain pollutants over time, resulting in the accumulation of cations and sludge particles on the electrode material. This accumulation forms an oxide layer that prevents the metal from dissolving, ultimately reducing the electrode's efficiency and removal capacity [39].

3.4. Effects of electrode distance on removal efficiency

The impact of electrode spacing on the removal efficiencies of TDS, BOD, COD, and Chromium using Al and Fe electrodes is illustrated in Fig. 7. A distance of 1 cm between the electrodes gives the highest reduction of the COD. In Al electrode, the COD reduced to 15.54 and 95.79 mg/L in Fe electrodes system respectively, corresponding to removal efficiencies of 99.75 % and 95.79 % in Al and Fe electrodes, respectively. As the distance between the electrodes increases, the removal efficiency decreases due to the decrease in faradaic yield and potential difference. The farther the electrodes are from each other, the lower the removal efficiency because of the reduced faradaic yield and potential difference. Consequently, this leads to a decrease in the quantity of metal that dissolves into the solution. Additionally, shorter inter-electrode distances create an electric field with a high potential gradient and low resistance to ion motion, leading to faster formation of hydroxide species ($Al(OH)_3$ or $Fe(OH)_3$) and quicker collision of electrode cations with pollutants in the solution [40,41]. In the same vein, Kumar et al. [42] found that at an electrode distance of 1 cm, the COD removal efficiency was 98 %, which is in consistence with the present study.

3.5. Effects of electrode materials and shape on removal efficiency

Fig. 8 depicts the effect of electrodes shapes on removal efficiencies of the pollutants, with plain aluminum and iron electrodes the COD reduction to 231.19 and 319.03 mg/L were observed respectively for

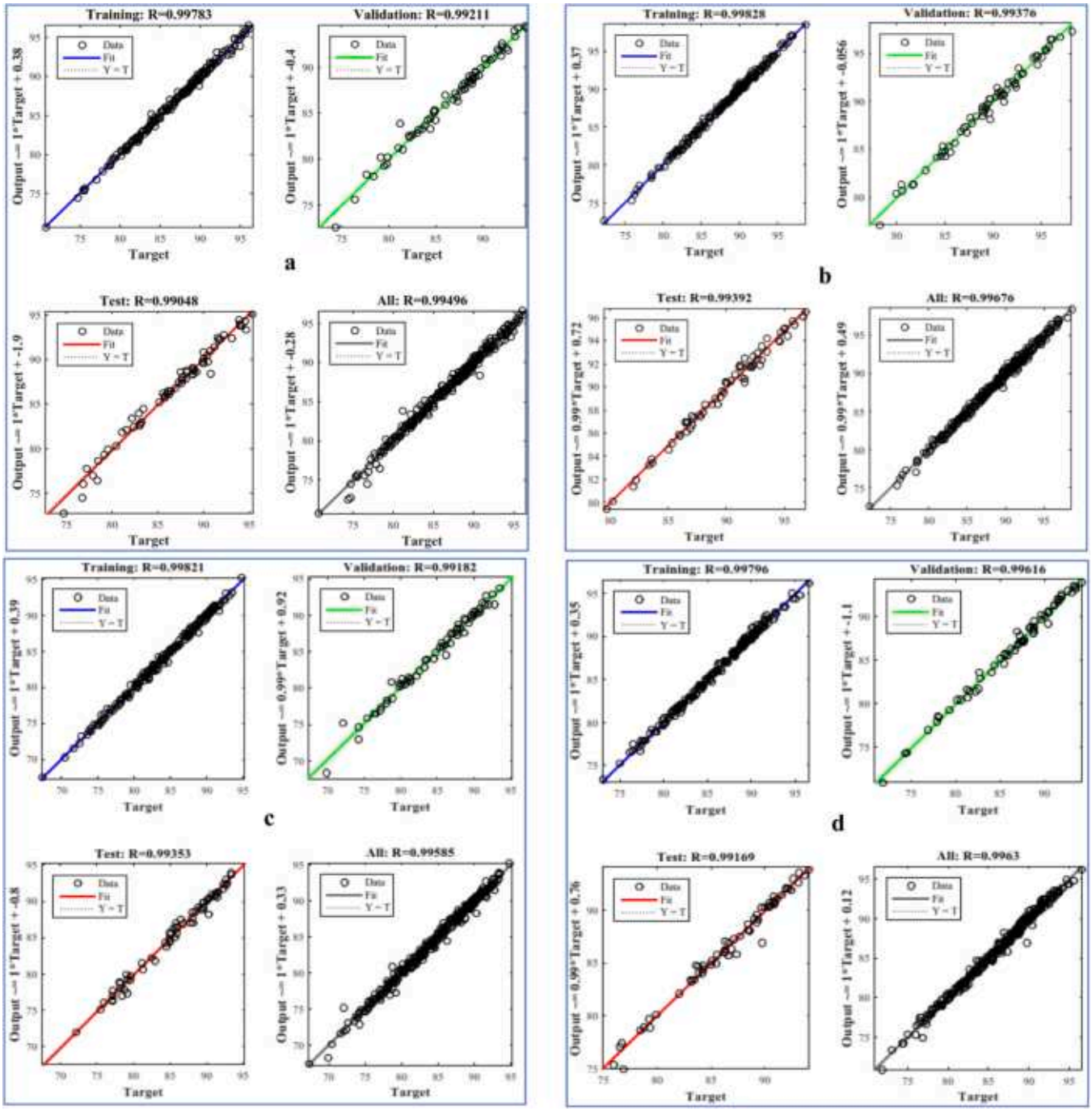

Fig. 10. The Regression plots for Training, Validation and Testing of ANN Algorithms: (a) Plane Aluminum (b) Punched Aluminum (c) Plane Iron and (d) Punched Iron Electrodes.

the electrodes, (equivalent to COD removal efficiencies of 96.21 % and 94.77 %) while the punched electrodes reduced the COD to 84.18 and 208.01 mg/L, equivalent to COD removal efficiencies of 98.62 % and 96.59 %, respectively. The small improvement in the effectiveness of the punched electrodes is due to the larger surface area compared to the flat electrodes. Additionally, the electron density is higher at the sharp edges and there is more electron accumulation at the holes and edges, leading to increased reactions in the solution and higher efficiency. Perforated electrodes expose more surface area, leading to increased electric field intensity at the edges and higher current discharge. It was found that the processes using aluminum electrodes were more effective in removing all the pollutant parameters compared to those using iron electrodes. This finding is a result of the fact that iron hydroxides are not as effective as aluminum hydroxides in the coagulation process, especially when paired with the higher faradaic yield of aluminum electrodes [43].

3.6. Statistical and machine learning modeling

The data obtained from the design of experiments are as shown in Tables 3 and 4, respectively. The data were used for the ANN and MLR analysis.

3.6.1. Artificial neural network analysis

The training algorithm with 10 hidden layer neurons architecture was adopted for the study. Fig. 3 is a 4:10:4 ANN architecture applied

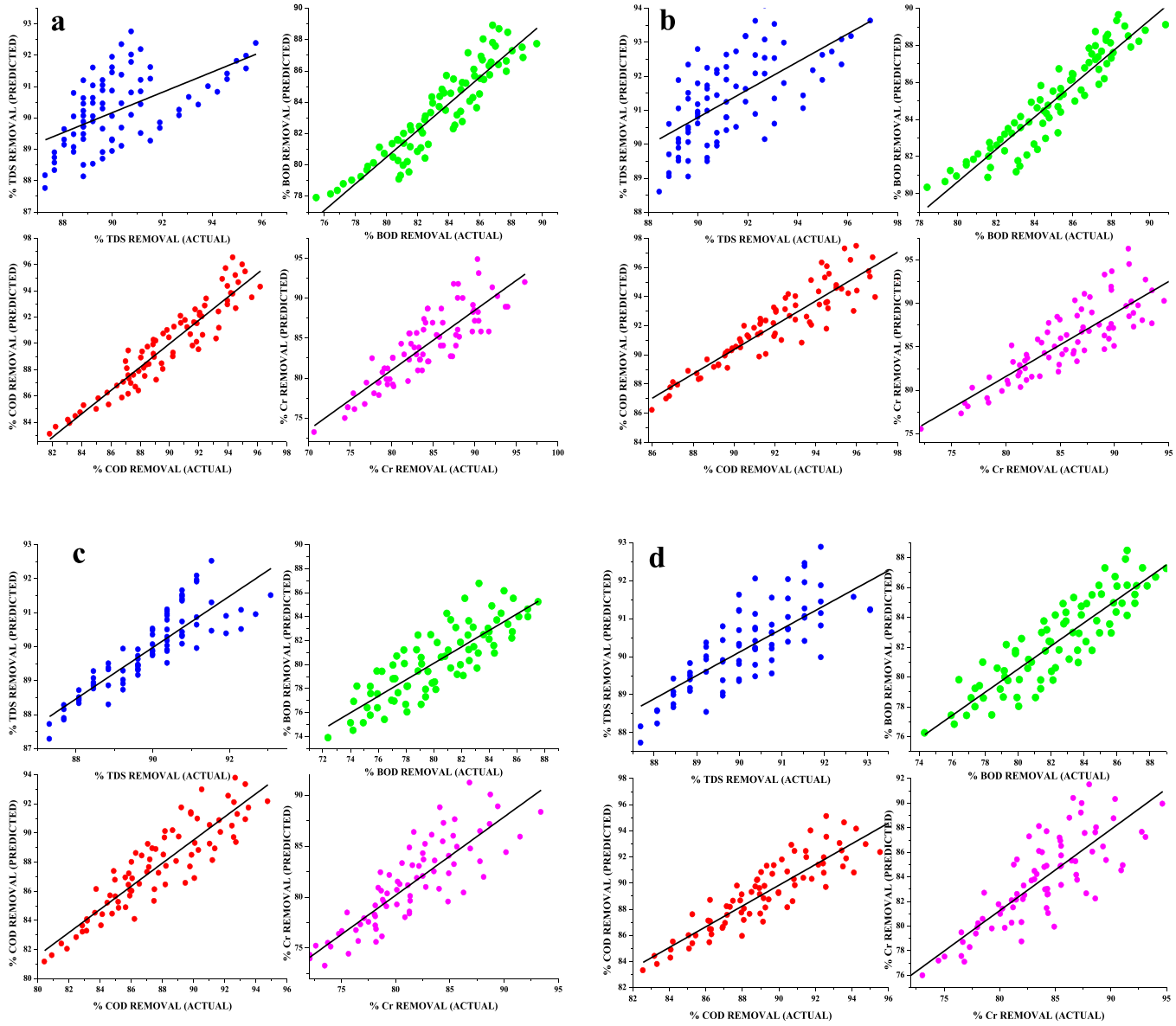

Fig. 11. Plots of the predicted vs. experimental removal of the pollutants (a) Plane Aluminum (b) Punched Aluminum (c) Plane Iron and (d) Punched Iron Electrodes.

Table 5
Statistical Evaluations of the models.

	Plane Aluminum Electrode		Punched Aluminum Electrode	
	ANN	MLR	ANN	MLR
MSE	0.264	8.64E-06	0.403	5.25E-06
MAE	0.321	1.385	0.2882	1.3055
R^2	0.995	0.825	0.997	0.8351
	Plane Iron Electrode		Punched Iron Electrode	
MSE	0.0071	3.09E-06	0.115	2.78E-06
MAE	0.351	1.366	0.286	1.3495
R^2	0.996	0.866	0.996	0.8419

for the data modelling based on Levenberg–Maquardt inbuilt MATLAB function using NN tools input menu. The output also consists of the 4 nodes, each for modelled removal efficiencies of the pollutants (TDS, BOD, COD and Cr).

The data for this modelling consisted of 80 experimental trials each, the input factors were the pH, electrode distance, voltage and duration of the electrocoagulation process while the removal efficiencies of TDS, BOD, COD and Cr were the target variables. The data were randomly divided into 60 % (40 data set) for training, 20 % [20] for testing and 20 % for validation. The initial optimization of the ANN model focused on identifying the most effective architecture. The testing dataset yielded the highest R^2 value and lowest MSE at 10 hidden neurons, leading to the use of the standard Levenberg–Maquardt algorithm for the training process.

The ideal electrocoagulation process topology was determined using R^2 and MSE values, as depicted in Figs. 9 and 10. The ANN model achieved a strong correlation with the training data for the optimized structure, as shown in Fig. 10, and it also demonstrated good performance in the validation and testing phases. The predicted values from the ANN model aligned well with the experimental dataset, as evidenced in Tables 3 and 4.

3.6.2. Multiple linear regression analysis

Multiple linear regression was used to predict the effects of the experimental variables on the efficiency of the electrocoagulation removal of the pollutants, the equations of regressions relating the efficiencies with the variables were formed from the empirical data using MINITAB 16 [44,45]. The prediction values were calculated by using Eq. [16] [41,46]. The related results are presented below while the plot of the experimental against the predicted values are presented in Fig. 11.

Plane Aluminum Electrodes:

TDS (%) = 88·2 + 0·370 pH - 2·31Electrode space + 0·114Voltage + 0·0135Duration (17)

BOD (%) = 81·1 + 1·18 pH - 6·42Electrode space + 0·0453Voltage + 0·0293Duration (18)

COD (%) = 78·2 + 2·22 pH - 6·27 Electrode space + 0·107 Voltage + 0·0273Duration (19)

Chromium (%) = 58·9 + 2·87 pH - 6·20 Electrode space + 0·352Voltage + 0·103Duration (20)

Punched Aluminum Electrodes:

TDS (%) = 89·1 + 0·449 pH - 2·58 Electrode space + 0·110 Voltage + 0·0152 Duration (21)

BOD (%) = 86·8 + 0·532 pH - 5·83 Electrode space + 0·0609 Voltage + 0·0300 Duration (22)

COD (%) = 77·6 + 2·11 pH - 4·35 Electrode space + 0·155 Voltage + 0·0319 Duration (23)

Chromium (%) = 58·1 + 3·04 pH - 5·20Electrode space + 0·355Voltage + 0·0992Duration (24)

Plane Iron Electrodes:

TDS (%) = 80·8 + 1·01 pH - 1·12Electrode space + 0·122Voltage + 0·0145Duration (25)

BOD (%) = 72·8 + 1·53 pH - 6·06Electrode space + 0·125Voltage + 0·0417Duration (26)

COD (%) = 75·9 + 2·05 pH - 5·61Electrode space + 0·0878Voltage + 0·0412Duration (27)

Chromium (%) = 61·2 + 2·88 pH - 7·90Electrode space + 0·233Voltage + 0·0807Duration (28)

Punched Iron Electrodes:

TDS (%) = 83·9 + 0·811 pH - 1·67Electrode space + 0·101Voltage + 0·0142Duration (29)

BOD (%) = 78·1 + 1·20 pH - 6·31Electrode space + 0·116Voltage + 0·0391Duration (30)

COD (%) = 80·3 + 1·66 pH - 5·32Electrode space + 0·0964Voltage + 0·0366 Duration (31)

Chromium (%) = 61·6 + 2·76 pH - 5·42Electrode space + 0·238Voltage + 0·0764Duration (32)

3.6.3. Evaluation of developed models by ANN and MLR techniques

The created models were assessed using statistical measures such as Mean Square Error (MSE), Mean Average Error (MAE), and Pearson regression coefficient (R^2) [47,48]. The accuracy assessment of the proposed models (Table 5) indicates that the ANN model demonstrates superior predictive capability compared to the MLR model for all electrodes utilized in this research. Consequently, the ANN model proves to be an effective tool for predicting the removal efficiency of pollutants in this study.

3.7. Energy consumption and cost analysis

The Energy consumption of the electrocoagulation process can be estimated from the voltage-time data according to the expression below [41–45] and reported as EC (kWh/$kg_{[COD]}$).

$$EC = \frac{Current \times Voltage \times time}{([COD]_0 - [[COD]_t) \times V_L} \quad (33)$$

Thus, for the 90 min of electrocoagulation, which witnessed the highest removal efficiency, the EC (kWh/$kg_{[COD]}$) were estimated to be 3.5 and 0.21 KWh/$kg_{[COD]}$ for Aluminum and Iron electrodes respectively.

Cost of Commercial electricity = ₹8.57/1 kWh.

Cost of Aluminum sheet is = ₹ 200/kg.

Cost of Iron sheet is = ₹ 60/kg.

Amount of Al used for 1 h operation at 2 amp = 0.672 kg.

Amount of Fe used for 1 h operation at 2 amp = 2.083 kg.

Cost of Al used for one hour operation is = 0.672 kg x ₹ 200/kg = ₹134.

Cost of Fe used for one hour operation is = 2.083 kg x ₹ 60/kg = ₹124.98.

The cost of electrocoagulation removal of 1 kg COD using Al electrode = Cost of electricity + Cost of Al used = (₹8.57/1 kWh x 3.5 KWh/$kg_{[COD]}$) + ₹134 = ₹160.57/ $kg_{[COD]}$.

Thus, the cost of electrocoagulation removal of 1 kg COD using Fe electrode = Cost of electricity + Cost of Fe used = (₹8.57/1 kWh x 2.083 KWh/$kg_{[COD]}$) + ₹124 = ₹141.85/ $kg_{[COD]}$.

The above estimates indicate that electrocoagulation is a cost-effective method for removing pollutants from tannery effluents, especially when compared to using commercially available adsorbents and other necessary accessories for the process, as well as other chemical processes.

4. Conclusion

Electrocoagulation removal of pollutants from tannery water was successfully conducted in this study. The results showed that the performance of Aluminum electrodes were slightly higher than that of Iron electrodes, while the punched electrodes performed better than the plane electrodes. The optimum performing condition for the process was obtained at 90 min of electrolysis duration, voltage of 20 V, at a distance of 1 cm and pH 9 with punched aluminium and iron electrodes. The modelling of the experimental results showed that ANN better modified the results than MLR. Thus, the process can be adapted for better purification of tannery effluents for improve COD, BOD, TDS and Chromium removal before the wastewater is released into the environment. The model demonstrated high statistical quality as evidenced by the strong correlation between experimental and model outcomes. This model has the potential to assess a full-scale wastewater treatment system, manage process variables, and decrease both time and costs associated with treatment. Consequently, the ANN model can be utilized to assess input parameters and enhance the wastewater treatment process by removing COD, BOD, TDS, and Chromium. Future study could be applied the developed ANN-MLR model to optimize EC treatment of other industrial wastewater streams including pharmaceutical and investigate the use of developed reactors with monopolar and bipolar arrangements to further enhance its efficiency and effectiveness.

CRediT authorship contribution statement

Farideh Malekdar: Writing – original draft, Software. **Kiran Kumar H S.**: Writing - original draft and Data curation. **B. Lokeshappa:** Writing – original draft, Formal analysis, Data curation, Conceptualization. **Abideen Idowu Adeogun:** Writing – original draft, Formal analysis, Data curation. **Suhas Sapate:** Writing – original draft, Formal analysis, Data curation. **Lalit Goswami:** Writing – original draft. **Sharanappa Chapi:** Writing – original draft. **Sayedali Mirkhalafi:** Writing – review & editing, Writing – original draft, Validation. **Mika Sillanpää:** Writing – review & editing. **Prashant Basavaraj Bhagawati:** Writing – review & editing, Writing – original draft, Funding acquisition, Formal analysis, Data curation, Conceptualization.

Data availability

Data will be made available on request.

Declaration of Competing Interest

No potential conflict of interest was reported by the author(s).

References

[1] Dubey A. A study on factors affecting exports of leather footwear as a strong initiative of make In India. J Surv Fish Sci 2023:1558–65.
[2] El-Bestawy EA, Al-Fassi FA, Amer RA, Aburokba R. Biological treatment of leather-tanning industrial wastewater using free living bacteria. Adv Life Sci Technol 2013;12:46–65.
[3] Banuraman S., editor Treatability Study of Tannery Effluent by Enhanced Primary Treatment 2013.
[4] Hansen É, de Aquim PM, Gutterres M. Current technologies for post-tanning wastewater treatment: A review. J Environ Manag 2021;294:113003.
[5] Belay AA. Impacts of chromium from tannery effluent and evaluation of alternative treatment options. J Environ Prot 2010;1(01):53.
[6] Farasati Far B, Naimi-Jamal MR, Jahanbakhshi M, Khalafvandi SA, Alian M, Razeghi Jahromi D. Decontamination of Congo red dye from aqueous solution using nanoclay/chitosan-graft-gelatin nanocomposite hydrogel. J Mol Liq 2024;395:123839.
[7] Abdollahi SA, Pourabadeh A, Alishiri M, Sodagartojgi A, Ranjbar SF, Ehghaghi MB, Talati F. Modeling and optimization of efficient removal of diclofenac and naproxen based on chemometric approaches. Water Resour Ind 2024;31:100238.
[8] Apaydin Ö, Kurt U, Gonullu M. An investigation on the treatment of tannery wastewater by electrocoagulation. Glob NEST J 2009;11(4):546–55.
[9] Swathi M, Sathya S, Aravind S, Ashi S, Gobinath R, Saranya DD. Adsorption studies on tannery wastewater using rice husk. Sch J Eng Tech 2014;2(2B):253–7.
[10] Zouboulis AI, Peleka EN, Ntolia A. Treatment of tannery wastewater with vibratory shear-enhanced processing membrane filtration. Separations 2019;6(2):20.
[11] Ramírez-Estrada A, Mena-Cervantes V, Fuentes-García J, Vazquez-Arenas J, Palma-Goyes R, Flores-Vela A, et al. Cr (III) removal from synthetic and real tanning effluents using an electro-precipitation method. J Environ Chem Eng 2018;6(1):1219–25.
[12] Arukula D, PP, Tanwi P, Hariraj S, Vijay LM, Brijesh KM. Treatment of tannery wastewater using aluminium formate: influence of the formate over sulphate based coagulant. Issue 2018;3.
[13] Raj R, Tripathi A, Das S, Ghangrekar M. Removal of caffeine from wastewater using electrochemical advanced oxidation process: a mini review. Case Stud Chem Environ Eng 2021;4:100129.
[14] Elabed A, El Abed S, Ibnsouda S, Erable B. Sustainable approach for tannery wastewater treatment: bioelectricity generation in bioelectrochemical systems. Arab J Sci Eng 2019;44(12):10057–66.
[15] Le Luu T, Stephane DDF, Minh NH, Canh ND, Thanh BX. Electrochemical oxidation as a post treatment for biologically tannery wastewater in batch reactor. Water Sci Technol 2019;80(7):1326–37.
[16] Mousazadeh M, Khademi N, Kabdaşlı I, Rezaei S, Hajalifard Z, Moosakhani Z, et al. Domestic greywater treatment using electrocoagulation-electrooxidation process: optimisation and experimental approaches. Sci Rep 2023;13(1):15852.
[17] Mousazadeh M, Naghdali Z, Al-Qodah Z, Alizadeh S, Niaragh EK, Malekmohammadi S, et al. A systematic diagnosis of state of the art in the use of electrocoagulation as a sustainable technology for pollutant treatment: An updated review. Sustain Energy Technol Assess 2021;47:101353.
[18] Shakeri E, Mousazadeh M, Ahmadpari H, Kabdasli I, Jamali HA, Graca NS, et al. Electrocoagulation-flotation treatment followed by sedimentation of carpet cleaning wastewater: optimization of key operating parameters via RSM-CCD. Desalin Water Treat 2021;227:163–76.
[19] Bazrafshan E, Moein H, Kord Mostafapour F, Nakhaie S. Application of electrocoagulation process for dairy wastewater treatment. J Chem 2013;2013.
[20] Bhagawati PB, Shivayogimath C. Separation of pollutants from pulp mill wastewater by electrocoagulation. Int J Energy Technol Policy 2017;13(1-2):166–76.
[21] Mousazadeh M, Naghdali Z, Kabdaşlı I, Sandoval MA, Titchou FE, Malekdar F, et al. Reclamation of forward osmosis reject water containing hexavalent chromium via coupled electrochemical-physical processes. Environ Technol 2024;45(5):888–901.
[22] Mousazadeh M, Niaragh EK, Usman M, Khan SU, Sandoval MA, Al-Qodah Z, et al. A critical review of state-of-the-art electrocoagulation technique applied to COD-rich industrial wastewaters. Environ Sci Pollut Res 2021;28(32):43143–72.
[23] Gholami Shirkoohi M, Tyagi RD, Vanrolleghem PA, Drogui P. A comparison of artificial intelligence models for predicting phosphate removal efficiency from wastewater using the electrocoagulation process. Digit Chem Eng 2022;4:100043.
[24] Farzin S, Nabizadeh Chianeh F, Valikhan Anaraki M, Mahmoudian F. Introducing a framework for modeling of drug electrochemical removal from wastewater based on data mining algorithms, scatter interpolation method, and multi criteria decision analysis (DID). J Clean Prod 2020;266:122075.
[25] Shirkoohi MG, Tyagi RD, Vanrolleghem PA, Drogui P. Artificial intelligence techniques in electrochemical processes for water and wastewater treatment: a review. J Environ Health Sci Eng 2022;20(2):1089–109.
[26] Kothari MS, Vegad KG, Shah KA, Hassan AA. An artificial neural network combined with response surface methodology approach for modelling and optimization of the electro-coagulation for cationic dye. Heliyon 2022;8(1).
[27] Wang S, Huang X, Liu P, Zhang M, Biljecki F, Hu T, et al. Mapping the landscape and roadmap of geospatial artificial intelligence (GeoAI) in quantitative human geography: An extensive systematic review. Int J Appl Earth Obs Geoinf 2024;128:103734.
[28] Merzouk B, Gourich B, Madani K, Vial C, Sekki A. Removal of a disperse red dye from synthetic wastewater by chemical coagulation and continuous electrocoagulation. A comparative study. Desalination 2011;272(1-3):246–53.
[29] Tiaiba M, Merzouk B, Mazour M, Leclerc J, Lapicque F. Study of chemical coagulation conditions for a disperse red dye removal from aqueous solutions. Membr Water Treat 2018.
[30] Emamjomeh MM, Jamali HA, Naghdali Z, Mousazadeh M. Carwash wastewater treatment by the application of an environmentally friendly hybrid system: an experimental design approach. Desalin Water Treat 2019;160:171–7.
[31] Das D, Nandi BK. Removal of Fe (II) ions from drinking water using Electrocoagulation (EC) process: Parametric optimization and kinetic study. J Environ Chem Eng 2019;7(3):103116.
[32] Vepsäläinen M, Sillanpää M. Electrocoagulation in the treatment of industrial waters and wastewaters. Advanced water treatment. Elsevier; 2020. p. 1–78.
[33] Khaled B, Wided B, Béchir H, Elimame E, Mouna L, Zied T. Investigation of electrocoagulation reactor design parameters effect on the removal of cadmium from synthetic and phosphate industrial wastewater. Arab J Chem 2019;12(8):1848–59.
[34] Darmadi D, Lubis MR, Hizir H, Chairunnisak A, Arifin B. Comparison of palm oil mill effluent electrocoagulation by using Fe-Fe and Al-Al electrodes: Box-Behnken design. Asean J Chem Eng 2018:30–43.
[35] Amri I, Meldha Z, Herman S, Karmila D, Ramadani MF. Effects of electric voltage and number of aluminum electrodes on continuous electrocoagulation of liquid waste from the palm oil industry. Mater Today: Proc 2023;87:345–9.
[36] Chavalparit O, Ongwandee M. Optimizing electrocoagulation process for the treatment of biodiesel wastewater using response surface methodology. J Environ Sci 2009;21(11):1491–6.
[37] Ngamlerdpokin K, Kumjadpai S, Chatanon P, Tungmanee U, Chuenchuanchom S, Jaruwat P, et al. Remediation of biodiesel wastewater by chemical- and electrocoagulation: a comparative study. J Environ Manag 2011;92(10):2454–60.
[38] Khandegar V, Saroha AK. Electrocoagulation for the treatment of textile industry effluent–a review. J Environ Manag 2013;128:949–63.
[39] Tegladza ID, Xu Q, Xu K, Lv G, Lu J. Electrocoagulation processes: a general review about role of electro-generated flocs in pollutant removal. Process Saf Environ Prot 2021;146:169–89.
[40] Bhagawati PB, Adeogun AI, Shivayogimath CB, Kadier A. Gum Arabic tree biomass derived activated carbon for fluoride sequestration in batch and fixed bed processes: kinetics, thermodynamics and column adsorption modeling. J Dispers Sci Technol 2023:1–9.
[41] Kadier, Wang A, Chandrasekhar J, Abdeshahian K, Islam MA P, Ghanbari F, et al. Performance optimization of microbial electrolysis cell (MEC) for palm oil mill effluent (POME) wastewater treatment and sustainable Bio-H2 production using response surface methodology (RSM). Int J Hydrog Energy 2022;47(34):15464–79.
[42] Kiran Kumar HS, Lokeshappa B, MRM R. Treatment of tannery wastewater by electrocoagulation using aluminium and iron electrodes. Int J Recent Technol Eng 2019;8(4).
[43] Emamjomeh MM, Mousazadeh M, Mokhtari N, Jamali HA, Makkiabadi M, Naghdali Z, et al. Simultaneous removal of phenol and linear alkylbenzene sulfonate from automotive service station wastewater: optimization of coupled electrochemical and physical processes. Sep Sci Technol 2020;55(17):3184–94.
[44] Bhatti MS, Reddy AS, Kalia RK, Thukral AK. Modeling and optimization of voltage and treatment time for electrocoagulation removal of hexavalent chromium. Desalination 2011;269(1-3):157–62.
[45] Elazzouzi M, Haboubi K, Elyoubi M, El Kasmi A. Development of a novel electrocoagulation anode for real urban wastewater treatment: experimental and modeling study to optimize operative conditions. Arab J Chem 2021;14(1):102912.
[46] Villaseñor-Basulto DL, Kadier A, Singh R, Navarro-Mendoza R, Bandala E, Peralta-Hernández JM. Post-tanning wastewater treatment using electrocoagulation: optimization, kinetics, and settlement analysis. Process Saf Environ Prot 2022;165:872–86.
[47] Agarwal S, Singh AP, Mathur S. Removal of COD and color from textile industrial wastewater using wheat straw activated carbon: an application of response surface and artificial neural network modeling. Environ Sci Pollut Res Int 2023;30(14):41073–94.
[48] Li B, Lu C, Zhao J, Tian J, Sun J, Hu C. Operational parameter prediction of electrocoagulation system in a rural decentralized water treatment plant by interpretable machine learning model. J Environ Manag 2023;333:117416.

Political Flower Pollination Optimizer for age-related macular degeneration detection enabled Deep Maxout network using OCT images

[1,2*]Mr. Rahul Sukumar Nejkar and [3]Dr. Shabnam Farook Sayyad

[1*]Research Scholar, Department of Computer Engineering, AISSMS College of Engineering (Savitribai Phule Pune University), Pune, Maharashtra 411 001, India

&

[2*]Assistant Professor, Sanjeevan Engineering And Technology Institute, Panhala, Maharashtra 416201, India

[1,2*]rahul.nej@gmail.com

[3]Associate Professor, Department of Computer Engineering, AISSMS College of Engineering (Savitribai Phule Pune University), Pune, Maharashtra 411 001, India

Abstract

Age-related Macular Degeneration (AMD) is the eye state, which influences most elder people. An accurate cause of AMD is yet not understood fully, but it is referred to as multi-factorial with increasing age as the most reliable factor. Thus, AMD prevalence is increasing owing to the aged population in the community. Hence, earlier AMD detection is required to avoid vision loss in the elderly. The detection of AMD in earlier stages at most perils of development permits more appropriate treatment and protection. Even though, arranging a complete eye examination for detection of AMD in the elderly is challenging and laborious. Hence, this research introduces the Political Flower Pollination Optimizer_Deep Maxout network (PFPO_DMN) for AMD detection. Here, median filter is used to pre-process the OCT images. The layers in considered input optical coherence tomography (OCT) images are

segmented in the layer segmentation phase utilizing ensemble U-Net. The ensemble U-Net training is accomplished by employing PFPO which is formed by amalgamating the Political Optimizer (PO) with the flower pollination algorithm (FPA). After that, feature extraction is done including texture features, reflectivity, statistical features, thickness and curvature. Lastly, AMD detection is performed using DMN, where DMN is trained by PFPO and hence, detected output is obtained. Furthermore, PFPO_DMN achieved high specificity, sensitivity and accuracy values about 91.6%, 92.9% and 92%.

Keywords: Deep Maxout network (DMN), Political Optimizer (PO), Ensemble U-Net, Age-related Macular Degeneration (AMD), Flower Pollination Algorithm (FPA),.

1. Introduction

AMD is considered a highly prevalent eye disorder, which leads to blindness. An important portion of the retina has a smaller oval-formed pigment termed a macula. Normally, the macula senses the finest visual information, the light intensity of nerve cells and colour. Furthermore, the retina takes in every detail from the macula and passes it to the brain by optical nerve. Thus, the retina should encrypt a light in the macula portion to consistent neural signals. The common feature, which affects the safety of the macula, is AMD and it is frequently found in aged people. The foremost causes of low vision in the United States (US) are principally age-related eye diseases, including cataracts, AMD, Diabetic Retinopathy (DR), and glaucoma. The AMD is a fourth widespread visual syndrome, which causes blindness, however, an appropriate screening process helps to reduce the early stage blindness [1]. Furthermore, AMD is a common eye disease, which causes progressive degeneration of dominant vision in many countries [10]. Meanwhile, AMD is a difficult retinal ailment that generates from an amalgamation of dangerous features namely environment, lifestyle and genetics. Besides, it causes loss of vision because of irregular

blood vessel evolution by Bruch's Membrane (BM), hence it directs fluid leakage into the retina [11]. Moreover, fluid portions in the retina are regarded as the main features of AMD. The position and dimension of the fluid region are the most significant biomarkers for AMD development [7]. AMD usually affects aged persons [12], and is generated through various genetic and environmental features [9].

OCT is a specific imaging modality, which permits volumetric and cross-sectional imaging of biological tissues at micrometer resolution [13]. The OCT model dimensions are attained using a less coherent interferometric model, and it gathers light that is reflected from a tissue samples are different lowest points. These reflected signals are exhibited as cross-sectional images named B-scans based on a log false colour scale [14]. In general, B-scan images attained from the OCT system highlight the morphological aspects of tissue microstructures [15]. These images have demonstrated that it is effective for finding plaque in heart arteries, motoring cerebral hemodynamics, detecting eye imaging [34] and skin tissues, detecting neurological pathologies and identification of stomach cancer from the gastrointestinal area [16]. Moreover, OCT is the tool for detecting the retinal diseases, namely AMD in ophthalmology. Even though, there are two important challenges for OCT-based detection. An initial OCT images are corrupted along with a speckle noise. It happens owing to optical backscattering of less coherence imaging light through retinal tissues [17]. The quality of OCT image is affected by noises and it affects the diagnostic effectiveness. The next issue happens because of involuntary eye movement [35] for head movements, fixation, like microsaccades, tremors and drifts, as well as body jitters produced through the cardiorespiratory system. In addition, these involuntary motions produce motion artefacts in OCT images [18]. Besides, severe failure of OCT image also occurred owing to eye blinking. These artifacts can produce imprecise clinical interpretation of OCT images [19] [2].

Several researchers have detected various OCT-driven features for finding the AMD level and its development [20]. The most common OCT features are sub-retinal deposits or reticular pseudo drusen, intra-retinal hyper-reflective foci, heterogeneous internal reflectivity in lesions as well as sophisticated central drusen measurements that are found to be connected with many risks for the development of progressive AMD. Besides, various methods are designed for automated evaluation of AMD-enabled features on OCT like Geographic Atrophy (GA), intra-sub-retinal fluid, pigment epithelial detachment and drusen. Besides [21], most of these approaches are mainly intensive on analyzing and detecting AMD features from a single time point. The evaluation of likelihood development from intermediate and early AMD to exudative AMD as well as employed drusen is explicated to make the determination [21]. In recent days, there has been more interest in Deep learning (DL)-based approaches for the automatic identification of eye diseases, like AMD [22] [6]. Moreover, evaluating the images using DL model. It is mainly depends on handcrafted features during the identification of pathologies, which is compared with conventional machine learning techniques. Generally, DL is proficient in illustrating hidden difficult features by employing neural network structures with different hidden layers. Besides, DCNN displays hierarchies of feature as well as learns the features of augmenting difficulty and concept with collective network power. Furthermore, it is frequently criticized for its “black box” character, while CNN driven model attained state-of-the-art performance in various AMD evaluation tools [6].

The significant purpose is to introduce PFPO_DMN for AMD detection. AMD is a progressive eye ailment that damages the retina and it causes impairment in vision. The detection of earlier stages at high danger of progression allows many timely treatments and preserves sight. In this research, median filter is pre-processed to the input OCT images. The input OCT image is given to layer segmentation stage to the detection of AMD. Further, the

layers are segmented using ensemble U-Net. The ensemble U-Net is tuned using a devised PFPO that is designed by integrating PO with FPA. Afterwards, features are extracted from segmented images in a phase of feature extraction. The features, which are extracted include statistical features specifically correlation, energy, mean, entropy, skewness as well as kurtosis, reflectivity, thickness, curvature and texture features namely local binary pattern (LBP) and shape index histogram. Lastly, AMD detection is conducted utilizing DMN and training of DMN is carried out using PFPO. Thus, AMD detected output is acquired employing a devised approach.

The eminent contribution is defined beneath.

Proposed PFPO_DMN for AMD detection: Here, an effectual method called PFPO_DMN is designed for the detection of AMD. The AMD detection is done by DMN, which is trained utilizing PFPO. Moreover, PFPO is designed newly by an incorporation of PO with FPA.

The residual parts are ordered in a manner: Section 2 describes a literature survey of traditional methods based upon AMD detection whereas the methodology of this work is expounded in Section 3 and Section 4 explicates results attained by PFPO_DMN for AMD detection whereas Section 5 interprets the conclusion of PFPO_DMN.

2. Motivation

AMD is considered an irrevocable and constant clinical stage that is caused by the deterioration of the cells in the macula that are accountable for central vision. The earlier treatment and detection process of AMD may assist in preventing the development of disease. Hence, an automatic AMD diagnosis may decrease the screening time of clinicians. This motivated me to propose a method for the detection of AMD. The papers taken for review according to AMD detection, that is explained in this part with their limitations.

2.1 Literature Survey

Anju Thomas., *et al*. [1] devised Multi-scale CNN for AMD detection utilizing OCT images. Owing to fewer complications and few learnable parameters, it can be executed in real-world applications, but this method was trained only by the Mendeley dataset. Vineeta Das., *et al*. [2] utilized a Generative Adversarial Network (GAN) for improved diagnosis of AMD. It assisted ophthalmologists in better planning of treatments and diagnosis. This model concentrated the diagnosing of AMD only through super-resolution (SR). Marwa Hani., *et al*. [3] designed a Support Vector Machine (SVM) algorithm for AMD identification utilizing OCT images. This was proven as an effective way to improve recognition for accurate and fast ophthalmology diagnostics, though it did not consider diverse kinds of features for improving classification procedures. Jefferson Alves Sousa., *et al*. [4] introduced U-Net and DexiNed for automated segmentation of retinal layers in the OCT images along with AMD. It showed high ability and robustness, but still, it did not enhance the process of layer segmentation to improve model performance.

Hyun-Lim Yang., *et al*. [5] utilized the CNN model for the detection of AMD obtaining high accuracy and lower cost. In this method, hyperparameters are not optimized and hence it affects system performance. Sajib Saha., *et al*. [6] CNN visualization strategy for visualizing AMD progression. Intrinsic image features that contribute to the progression of the disease can be known utilizing this method, but still, it did not consider large as well as several groups of images for enhancing the output performance of disease. Zailiang Chen., *et al*. [7] employed DL for automated segmentation of fluid areas in OCT of AMD. This method proved to be highly efficient for segmenting fluid areas in OCT, but it needed several iterations in the training procedure. Zailiang Chen., *et al*. [8] developed a Deep forest for layer segmentation (DF-LS), which was robust not only for healthier retinas but also for

severe and moderate pathology. This approach did not consider other types of eye disease including central serous retinopathy and diabetic macular edema.

2.2 Challenges

The papers reviewed according to AMD detection confronted a few challenges for detection that are described as follows.

- In [1], Multi-scale CNN devised for AMD detection utilizing OCT images had better capability for classifying AMD and normal images, but this method had higher computational complexity problems.
- The GAN utilized in [2] for improved diagnosing of AMD was highly appropriate for rapid and accurate diagnosing, even though the applicability of this system was not evaluated for other retinal diseases under inadequate as well as unpaired training data circumstances.
- CNN visualization strategy was developed in [6] for the AMD detection process, but this method failed to find more specific imaging features responsible for disease evolution.
- In [7], an automatic deep learning method was developed for classifying the OCT B-scan images, even though this method failed to segment fluid regions in OCT B-scan images of other kinds of eye diseases, such as diabetic macular edema, and central serous retinopathy.
- AMD is a general ophthalmic situation that may have fewer symptoms in its earlier stage but progresses to visual disabilities. There are no treatments for earlier stage diagnosing whereas there are several modalities for treating advanced disease. For the increasing occurrence of the disease, there are numerous cost-efficiency assessments of AMD therapy, even though approaches and techniques differ broadly.

3. Proposed PFPO_DMN for detection of AMD

AMD is the main reason for enduring vision loss and hence earlier detection of AMD is significant. An earlier AMD is hugely unidentified in the population owing to a deficiency of visual symptoms in affected persons. When the symptoms are present, this disease has regular growth to the last stage. It is vital to monitor the person for detecting AMD as soon as possible. Here, PFPO_DMN is newly designed for AMD detection. In this work, the input images are pre-processed by using median filter. That input OCT image is given to layer segmentation, where the layers are segmented by ensemble U-Net. The U-Net training is performed using PFPO which is an amalgamation of PO and FPA. Then, features like thickness, curvature, reflectivity, statistical and texture features are extracted. At last, AMD detection is conducted utilizing DMN, which is also tuned by PFPO. Figure 1 indicates a diagrammatic view of PFPO_DMN for AMD detection.

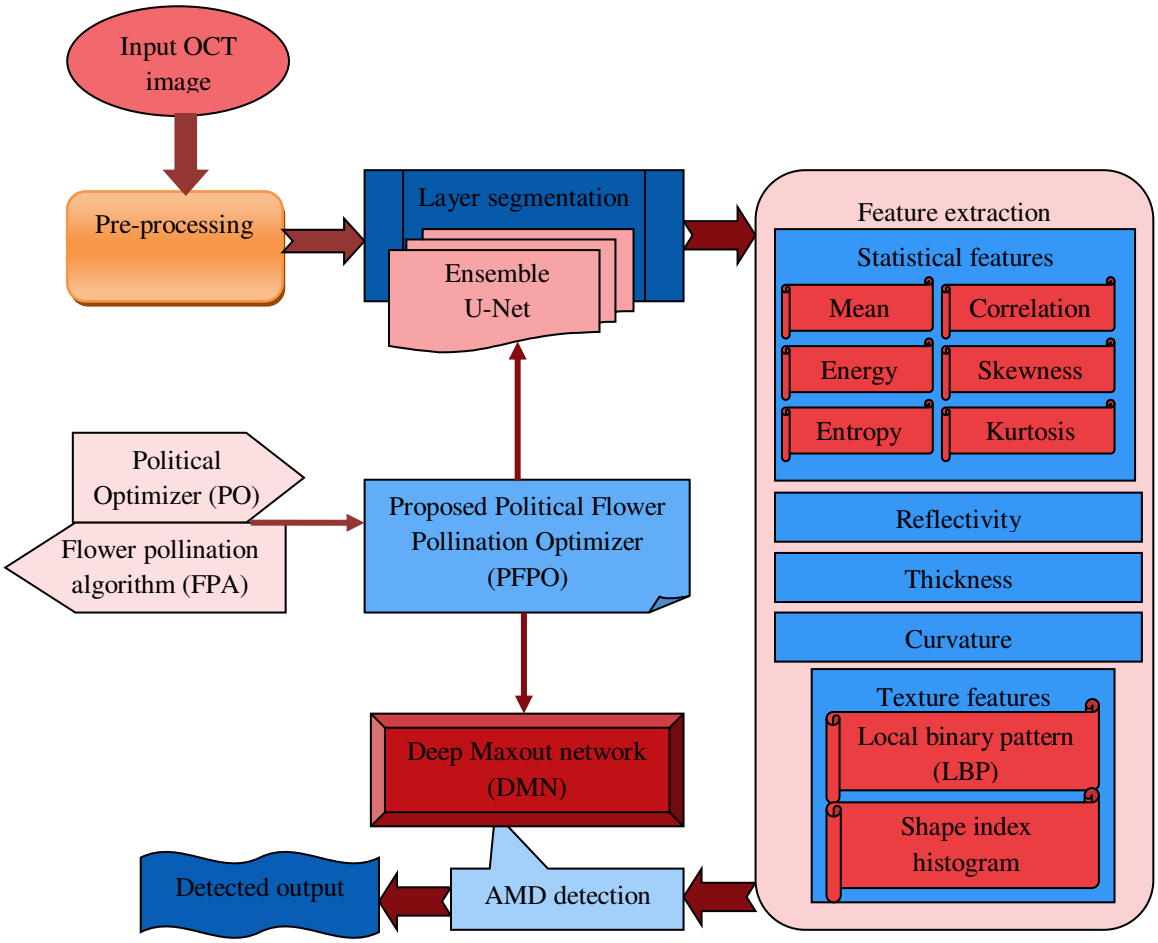

Figure 1. Diagrammatic view of PFPO_DMN for AMD detection

3.1 Acquisition of an image

The detection of AMD is performed by considering an OCT image that is obtained from a specific dataset stated in [33] that can be represented by,

$$A = \{A_1, A_2, ...A_m ...A_d\} \quad (1)$$

Where the amount of OCT images comprised in the database A is implied as A_d and A_m signifies m^{th} input image.

3.2 Pre-processing

In PFPO_DMN for AMD detection, median filter is used to pre-processing the image. The median filter is a non-linear digital filtering technique, which often used to remove noise from an image [36]. To improve the result of later processing, typical pre-processing step of noise reduction is used. The input OCT images are pre-processed by median filter technique. Further, the pre-processed image is given to the layer segmentation process.

3.3 Layer segmentation utilizing ensemble U-Net

The layers segmentation is vital in several automated assessment approaches based on retinal OCT images. Individual retinal layer thickness and position are acquired by an outcome of layer segmentation approaches and then by assessing resemblances and variations amongst layer index of the examined image as well as the referenced image, several problems including lesion position and detection can be found. Here, layer segmentation is done utilizing ensemble U-Net, where the training process is done by PFPO. To perform layer segmentation input image A_m is taken.

3.3.1 Architecture of Ensemble U-Net

The ensemble U-Net [29] [30] utilized here comprises three networks namely LadderNet, Big-U Small- (BUSU-Net) and Light BUSU.U-net, which has achieved much success in several medical image segmentation applications.

(i) LadderNet: It is a multiple-branched CNN having chains of U-Net for layer segmentation, consists of skipping connections among network levels and other than U-Net, the features obtained from branches of the encoder are concatenated with features attained from decoder branches, wherein features are added from these branches. A LadderNet is developed as an ensemble of numerous FC networks. Each path is viewed as the variance of the FC network and overall count of ways that grow up exponentially along with a count of decoder and encoder pairs as well as spatial levels. It states that LadderNet is efficient for recording complex features and yields high accuracies.

(ii) BUSU-Net: An actual model of BUSU-Net comprises 108 layers that are made up of chaining the two BCDU-Net, wherein the initial one is closer than the second one. Particularly, Big-U is closer than the actual BCDU-Net whereas Small-U is of a similar dimension as the actual.

(iii) Light BUSU-Net: This network is the lightest version of the BUSU-Net comprising 43 layers, wherein the Small-U as well as Big-U is less closer than in BCDU-Net and BUSU-Net. Light BUSU-Net intends to elucidate the strength of a lightweight system that could be utilized in conditions with fewer resources like space, computing abilities and memory.

(iv) Model ensemble: The output is fused appropriately and hence they complement one another and jointly explore the benefits. As the entire variance is constant, it is equal to maximize an addition of squared deviations among points in diverse clusters that pursue from law of overall variance. The ensemble model can be given by,

$$U = \sum_{l=1}^{p} W_l * K_l \qquad (2)$$

Here, U specifies the output matrix of the ensemble model, p represents the count of models, W_l denotes the weight of the model l and K_l indicates the prediction probability map of the model l. The segmented output from the layer segmentation phase is indicated by E_m. The architecture of the ensemble U-Net is represented in Figure 2.

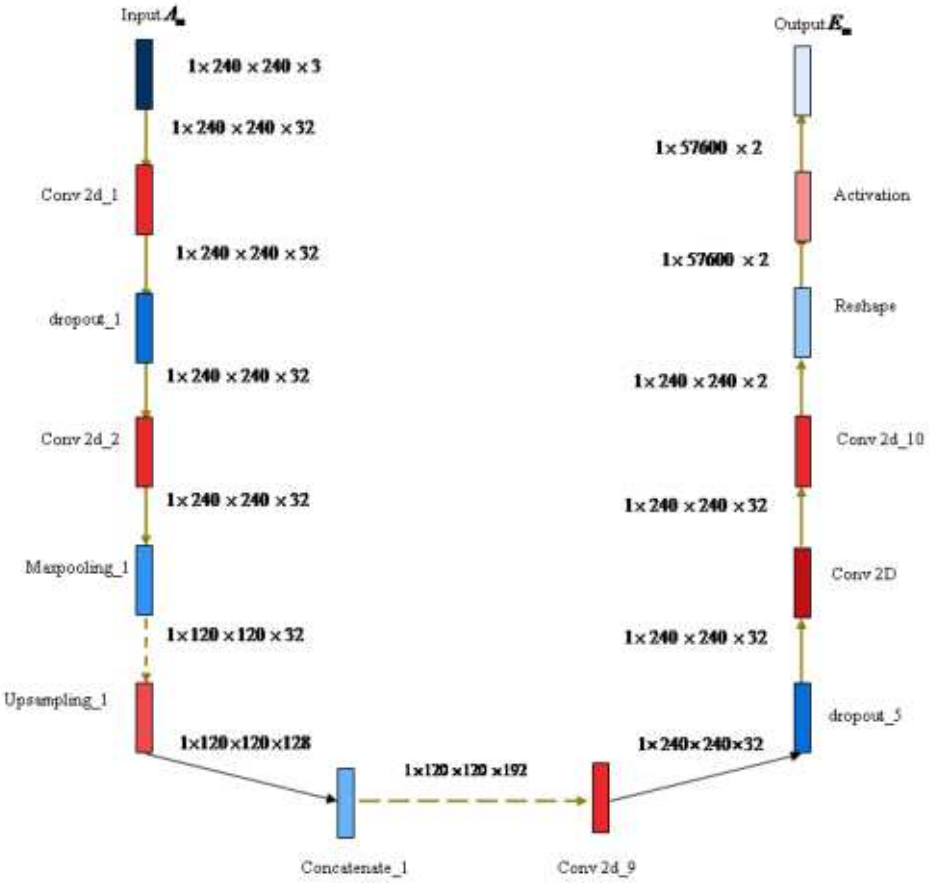

Figure 2: Architecture of ensemble U-Net

3.3.2 Training of ensemble U-Net utilizing PFPO

PO [25] is enthused by multiple-phased processes of the politics. It is a mathematical mapping of every significant phase of politics like party switching, election of constituency allocations, inter-parties, parliamentary affairs and election campaigns. PO algorithm is

invariant to the function shifting as well as executes constantly in higher-dimension search space. FPA [24] is stimulated by the process of pollination by flowers. An interaction and interchange of vital elements and choosing of better solution ensures that FPA is highly effective. Here, U-Net for layer segmentation is trained by PFPO, which is more suitable for the segmentation process. Furthermore, PFPO is the combination of PO with FPA.

Political position encoding

In search space ϖ, the finest solution is obtained wherein the ensemble U-Net learning parameter is signified by δ, in such a manner $\varpi = 1 \times \delta$.

Fitness measure

An estimation of fitness measure is performed by assessing differences among results of the target and ensemble U-Net that can be expressed by,

$$\hbar_1 = \frac{1}{d}\sum_{m=1}^{d}\left[\mathrm{T}_m - E_m\right]^2 \tag{3}$$

Here, overall images are denoted by d whereas the target output is symbolized by T_m and ensemble U-Net output is implied by E_m.

PFPO pursues beneath explicated steps for obtaining the best solution.

Step 1: Solution initialization

Firstly, the initialization step begins with initializing a solution and it is expressed as shown below,

$$a = \left\{a_1, a_2, ..., a_z, ..., a_g\right\} \tag{4}$$

Here, a_z indicates z^{th} the candidate solution, a symbolizes population and a_g denotes total variables.

Step 2: Objective function assessment

Objective function assessment can be done by evaluating the difference between ensemble U-Net and targeted outputs that are computed employing Eq. (3).

Step 3: Formation of party and constituency allocation

A population a is separated into y political parties as modelled in Eq. (5). Individual parties are comprised of y members or candidates as mentioned in Eq. (6). Each q^{th} member P_z^q is regarded as the potent solution that is j -dimension vector as represented in Equation 7.

In Eq. (7), a value j denotes the count of input variables in the problem that is being resolved and $a_{z,x}^q$ implies P_z^q .

$$a = \left\{a_1, a_2, a_3, ..., a_y\right\} \tag{5}$$

$$a_z = \left\{\mathrm{P}_z^1, \mathrm{P}_z^2, \mathrm{P}_z^3, ..., \mathrm{P}_z^y\right\} \tag{6}$$

$$\mathrm{P}_z^q = \left[a_{z,1}^q, a_{z,2}^q, a_{z,3}^q, ..., a_{z,j}^q\right]^Q \tag{7}$$

Besides being a part of the party member, the probable solution is to perform as an election candidate. This is considered as there are y constituencies as expressed in Equation 8 and q^{th} members of individual party conflict election from q^{th} the constituency τ_q as represented in Equation 9.

$$\tau = \left\{\tau_1, \tau_2, \tau_3, ..., \tau_y\right\} \tag{8}$$

$$\tau_q = \left\{\mathrm{P}_1^q, \mathrm{P}_2^q, \mathrm{P}_3^q, ..., \mathrm{P}_y^q\right\} \tag{9}$$

The fittest candidate of the party is acknowledged as a party leader, which is decisive afterwards the actual election. The selection of party leader is formulated in Equation 11, which P_z^* indicates the leader of z^{th} the party and $\hbar\left(\mathrm{P}_z^q\right)$ evaluates fitness P_z^q .

$$k = \underset{1 \le q \le y}{\arg\min}\ \hbar\left(\mathrm{P}_z^q\right), \qquad \forall z \in \left\{1, ..., y\right\} \tag{10}$$

$$\mathrm{P}_z^* = \mathrm{P}_z^k \tag{11}$$

A set of every party leader is implied by a^* and can be given by,

$$a^* = \left\{\mathrm{P}_1^*, \mathrm{P}_2^*, \mathrm{P}_3^*, ..., \mathrm{P}_y^*\right\} \tag{12}$$

Afterwards the election, winners from every constituency become parliamentarians. Eq. (13), τ^* indicates the set of every parliamentarian which τ_q^* specifies the winner of q^{th} the constituency.

$$\tau^* = \left\{\tau_1^*, \tau_2^*, \tau_3^*, ..., \tau_y^*\right\} \quad (13)$$

Step 4: Election campaign (exploitation and exploration)

This step assists candidates in improving their performance in an election. The position is initially updated considering the party leader P_z^* and thereafter with consideration to constituency winner τ_q^*. The terms R s^* are utilized for updating candidate position whereas variable R denotes a range of random number is 0 and 1. They s^* initially hold a value of x^{th} the dimension of party leader $a_{z,x}^*$ and thereafter constituency winner $\tau_{q,x}^*$.

$$a_{z,x}(w+1) = a_{z,x}(w-1) + R\left(a_{z,x}(w) - a_{z,x}(w-1)\right) \quad (14)$$

$$a_{z,x}(w+1) = a_{z,x}(w-1) + Ra_{z,x}(w) - Ra_{z,x}(w-1) \quad (15)$$

$$a_{z,x}(w+1) = a_{z,x}(w-1)[1-R] + Ra_{z,x}(w) \quad (16)$$

The standard equation of FPA can be illustrated by,

$$a_{z,x}(w+1) = a_{z,x}(w) + N\left(a_{q,x}(w) - a_{c,x}(w)\right) \quad (17)$$

$$a_{z,x}(w) = a_{z,x}(w+1) - N\left(a_{q,x}(w) - a_{c,x}(w)\right) \quad (18)$$

Substitute Eq. (18) in Eq. (16),

$$a_{z,x}(w+1) = a_{z,x}(w-1)[1-R] + R\left[a_{z,x}(w+1) - N\left(a_{q,x}(w) - a_{c,x}(w)\right)\right] \quad (19)$$

$$a_{z,x}(w+1) = a_{z,x}(w-1)[1-R] + Ra_{z,x}(w+1) - RN\left(a_{q,x}(w) - a_{c,x}(w)\right) \quad (20)$$

$$a_{z,x}(w+1) - Ra_{z,x}(w+1) = a_{z,x}(w-1)[1-R] - RN\left(a_{q,x}(w) - a_{c,x}(w)\right) \quad (21)$$

$$a_{z,x}(w+1)[1-R] = a_{z,x}(w-1)[1-R] - RN\left(a_{q,x}(w) - a_{c,x}(w)\right) \quad (22)$$

The updated equation of PFPO can be represented as,

$$a_{z,x}(w+1)=\frac{1}{1-R}\left[a_{z,x}(w-1)[1-R]-RN\left(a_{q,x}(w)-a_{c,x}(w)\right)\right] \quad (23)$$

Where $a_{z,x}(w+1)$ symbolizes the location of z^{th} the solution in x^{th} dimension at an iteration $w+1$, N signifies a uniformly distributed random number, that is ranging among 0 and 1, q, c, z indicates q^{th}, c^{th} and z^{th} solutions whereas x signifies dimension.

Step 5: Switching of the party (Balancing exploitation and exploration)

In politics, this step performs parallel to an election campaign whereas in PO it is performed afterwards the election campaign phase. The adaptive parameter γ called as party switching rate is stated that starts from $\gamma_{\max}$ and reduces linearly to 0 throughout iterations. Individual members P_z^q are selected with a possibility γ and swapped to a few randomly chosen parties a_R , where it is exchanged or swapped with less fit members P_R^k of that party a_R. The estimation of the index k of less-fit members a_R is illustrated in the below equation.

$$k=\arg\max_{z\le q\le y}\hbar\left(\mathrm{P}_R^q\right) \quad (24)$$

Step 6: Election

An election is imitated to estimating the fitness of every candidate conflicting in the constituency and then declaring a winner. Eq. (26) τ_q^* specifies the winner of q^{th} the constituency (τ_q). As stated earlier, party leaders are updated afterwards the election utilizing Eq. (11).

$$k=\arg\min_{1\le z\le y}\hbar\left(\mathrm{P}_z^q\right) \quad (25)$$

$$\tau_q^*=\mathrm{P}_k^q \quad (26)$$

Step 7: Parliamentary affairs (convergence and exploitation)

The government is formed after an inter-party election, and party leaders as well as constituent parliamentarians or winners are decided utilizing Eq. (11) and Eq. (26). Each of

the parliamentarians τ_q^* that is a winner of q^{th} constituency updates the position regarding randomly chosen parliamentarian τ_R^*. If this causes any enhancement in fitness τ_q^*, then the status as well as fitness τ_q^* is updated.

Step 8: Termination

PFPO steps described above are repeatedly performed to achieving a best outcome for the detection of AMD. Algorithm 1 describes a pseudo code of PFPO.

Algorithm 1: Pseudo code of PFPO

SL. No	Pseudo code of PFPO
1	**Input:** $y, \gamma_{\max}, Q_{\max}$
2	**Output:** $a_{z,x}(w+1)$
3	**Begin**
4	Initialize a as represented in Eq. (5) to Eq. (9)
5	Evaluate and save the fitness of individual member a_z^q
6	Estimate a set of party leaders a^* utilizing Eq. (11)
7	Calculate a set of constituency winners τ^* utilizing Eq. (26)
8	$w = 1$
9	$a(w-1) = a;$
10	$\hbar(a(w-1)) = \hbar(a)$
11	$\gamma = \gamma_{\max}$;
12	***while*** $w \le Q_{\max}$ ***do***
13	$a_{temp} = a$
14	$\hbar(a_{temp}) = \hbar(a);$
15	***for each*** $a_z \in a$ ***do***
16	***for each*** $\mathrm{P}_z^q \in a_z$ ***do***
17	P_z^q =election campaign $(\mathrm{P}_z^q, \mathrm{P}_z^q(w-1), \mathrm{P}_z^*, \tau_q^*)$
18	Update the position of party leader utilizing Eq. (23)
19	***end***
20	***end***
21	Party switching (a, γ);
22	/* Election stage*/
23	Calculate and save the fitness of the individual member a_z^q
24	Evaluate a set of party leaders a^* utilizing Eq. (11)
25	Estimate a set of constituency winners τ^* utilizing Eq. (26)

26	Parliamentary Affairs $\left(\tau^{*}, a\right)$;
27	$a\left(w-1\right)=a_{temp}$;
28	$\hbar\left(a\left(w-1\right)\right)=\hbar\left(a_{temp}\right)$;
29	$\gamma=\gamma-\gamma_{\max}/Q_{\max}$;
30	$w=w+1$
31	***end***
32	**Terminate**

3.4 Feature extraction

The features are extracted by executing a few transformations of actual features for generating other features, which are highly significant. The feature extraction dimension of feature space can be frequently reduced without missing much information about the actual feature space. Here, a segmented image E_m is subjected as input to perform feature extraction. The extracted features are thickness, curvature, reflectivity, texture features and statistical features.

3.4.1 Statistical features

Mean, correlation, energy, skewness, entropy and kurtosis are the statistical features [28] considered for extraction.

(i) Mean: It reveals a measure of the average intensity of the image and can be expressed as shown below.

$$S_1=\sum_{v} I_v\,\rho\left(I_v\right) \tag{27}$$

Here, I_v specifies image intensity value whereas $\rho\left(I_v\right)$ indicates the probability value of an image intensity in the image.

(ii) Correlation: It signifies the measure of closeness that a pixel corresponds to neighbours. It can be illustrated as follows.

$$S_2=\sum_{\mu=1}^{\mathrm{M}}\sum_{\eta=1}^{\mathrm{M}}\left(\mu-\eta\right)^2\rho_{\mu\eta} \tag{28}$$

Where, $\rho_{\mu\eta}$ implies probability value of incidence by pixel, μ concerning pixel η.

(iii) Energy: It refers to the sum of the squared elements in a co-occurrence matrix and this energy can be computed by,

$$S_3 = \sum_{\mu=1}^{M}\sum_{\eta=1}^{M}\rho_{\mu\eta}^2 \qquad (29)$$

(iv) Skewness: It specifies a related decreasing level of a histogram curve on a certain image. The value of skewness may be positive or negative. It can be formulated as follows,

$$S_4 = \frac{1}{\sigma^3}\sum_{v}\left(I_v - S_2\right)^3\rho\left(I_v\right) \qquad (30)$$

(v) Entropy: Entropy defines a dimension of shape inconsistencies in the image and this can be modelled by,

$$S_5 = \sum_{v}\rho\left(I_v\right)^2\log\rho\left(I_v\right) \qquad (31)$$

(vi) Kurtosis: The kurtosis denotes the related tallness of the histogram curve in the image and it is given as follows.

$$S_6 = \frac{1}{\sigma^4}\sum_{v}\left(I_v - S_2\right)^4\rho\left(I_v\right) - 3 \qquad (32)$$

3.4.2 Reflectivity

A reflectivity is acquired from two areas per scanning, consisting thickest segments of the retina on the temporal and nasal sides of the foveal peak. The reflectivity feature is specified by S_7.

3.4.3 Thickness

The thickness of the retinal layers can be resolved by Euclidean distances among related points on lower as well as upper boundaries of individual layers and S_8 represents thickness.

3.4.4 Curvature

A curvature of the retinal layer integrates all curvature values computed for individual points over the layers afterwards local weighted polynomial smoothening of the surface. The curvature is specified as S_9.

3.4.5 Texture features

From an entire image, texture features are extracted without targeting specific regions. Here, texture features like LBP and shape index histogram are extracted.

(i) LBP: LBP [26] is the global texture-enabled feature descriptor, wherein these features label a value of a pixel by thresholding the neighbourhood of individual pixels and assessing the result as binary numbers. The LBP value of the pixel $(\varepsilon_b, \alpha_b)$ can be expressed by,

$$S_{10} = LBP_{(\varepsilon_b, \alpha_b)} = \sum_{t=0}^{1} P(\vartheta_t - \vartheta_b) * 2^t \tag{33}$$

$$P(\chi) = \begin{cases} 1 & if\ \chi \geq 0 \\ 0, & otherwise \end{cases} \tag{34}$$

Here, ϑ_b is an intensity of frame $F(\varepsilon_b, \alpha_b)$ and ϑ_t is utilized for neighbour pixels that aim ε_b as sample points distribution on the circle of a radius for α_b and evaluates LBP.

(ii) Shape index histogram: The shape index [27] is an image geometry that captures second-order image structures in continual intervals and permits to analysis of the curvature distribution in the histogram.

A shape index histogram is generated by selecting a set of e_ς bin centres $\varsigma_1, ..., \varsigma_{e_\varsigma}$ distributed uniformly along a shape index interval $[-\pi/2, \pi/2]$. For the bin B centred at ς, an overall contribution from the weighted sum is calculated utilizing spatial doughnut weighting X and curvedness measure ℓ,

$$S_{11} = \mathrm{B}(\sigma, \omega_0, \partial, i, \varsigma, \nu) = \frac{\sum_{\omega} X_{\ell} \exp\left(-\frac{(\varsigma - o)^2}{2\nu^2}\right)}{\sum_{\omega} X} \tag{35}$$

From a feature extraction phase, the feature vector symbolized as S_m is acquired, such that,

$$S_m = \{S_1, S_2, S_3, ..., S_{11}\} \tag{36}$$

3.5 AMD detection

It is a retinal disorder that affects the elderly as well as the community's aging person is becoming more and more prevalent. View of patients with earlier AMD is generally normal, even though central vision is damaged or might be lost if appropriate treatment is failed to be conducted. Hence, earlier diagnosing is mainly significant for preventing extra aggravation of AMD. Here, DMN is employed for detection of AMD and DMN is trained by PFPO. Moreover, PFPO is designed newly by a combination of PO with FPA. For conducting AMD detection, a feature vector S_m is considered as input.

3.5.1 Architecture of DMN

The max-out system is just a feed-forward structure like deep CNN or multilayer perceptrons that utilize a newer kind of activation function termed max-out unit. DMN [23] comprises numerous layers that generate hidden activations through the max-out function.

(i) Rectified linear unit (ReLU): It is firstly used in RBM that is defined by,

$$h_r = \begin{cases} \mathrm{X}_r, & if\ \mathrm{X}_r \geq 0 \\ 0, & if\ \mathrm{X}_r < 0 \end{cases} \tag{37}$$

Where, X_r represents input to neuron and h_r indicates an output. ReLU has attractive characteristics that neural node activations are scanty.

(ii) Maxout: It is a general version of ReLU, which acquires the max function on $\kappa(\kappa=2)$ trainable linear functions. For the known input $\mathrm{X}\in T^{C}$, where X is either the state vector or else raw input vector of the hidden layer? An output of max out unit is illustrated by,

$$\mathrm{E}_{r}(\mathrm{X})=\max_{u\in[1,\kappa]} Y_{ru} \tag{38}$$

Here, $Y_{ru}=\mathrm{X}^{Z}G_{\ldots ru}+B_{ru}$, $G\in T^{C\times\xi\times\kappa}$ are the trainable parameters. κ denotes the count of the linear sub-hidden units. In the CNN, max-out unit activation equals maximal over κ feature maps. However maxout unit is identical to the usually utilized spatial maxpooling in CNN, it obtains maximal value over similar input, where spatial maxpooling is associated with κ several inputs.

(iii) DMN: In multiple-layer configuration, DMN is considered a type of trainable activation function. For known input $\mathrm{X}\in T^{C}$, wherein X is either state vector or else raw input vector of the hidden layer, activation of the hidden unit is modelled by,

$$\Im^{1}_{r,u}=\max_{u\in[1,\kappa_{1}]}\mathrm{X}^{Z}\,G_{\ldots ru}+B_{ru} \tag{39}$$

$$\Im^{2}_{r,u}=\max_{u\in[1,\kappa_{2}]}\Im^{1}_{r,u}{}^{Z}\,G_{\ldots ru}+B_{ru} \tag{40}$$

$$\Im^{\xi}_{r,u}=\max_{u\in[1,\kappa_{\xi}]}\Im^{\xi-1}{}^{Z}_{r,u}\,G_{\ldots ru}+B_{ru} \tag{41}$$

$$\Im^{n}_{r,u}=\max_{u\in[1,\kappa_{n}]}\Im^{n-1}{}^{Z}_{r,u}\,G_{\ldots ru}+B_{ru} \tag{42}$$

$$\mathrm{E}_{r}=\max_{u\in[1,\kappa_{n}]}\Im^{n}_{r,u} \tag{43}$$

Here, κ_{ξ} implies the count of units in the ξ^{th} layer whereas n denotes overall layers that exist in DMN. It activates much stronger in approximating the arbitrary recurrent activation function than non-convex activation functions. The classical non-linear activation functions namely rectified linear and absolute value rectifier are approximated by DMN whilst κ is not lesser than 2. Still, an effective feature extraction needs a highly complex non-linear function,

DMN can approximate the arbitrary activation function by raising a parameter κ. A detected output is given D_m and the structure of the DMN network is diagrammatically modeled in Figure 3.

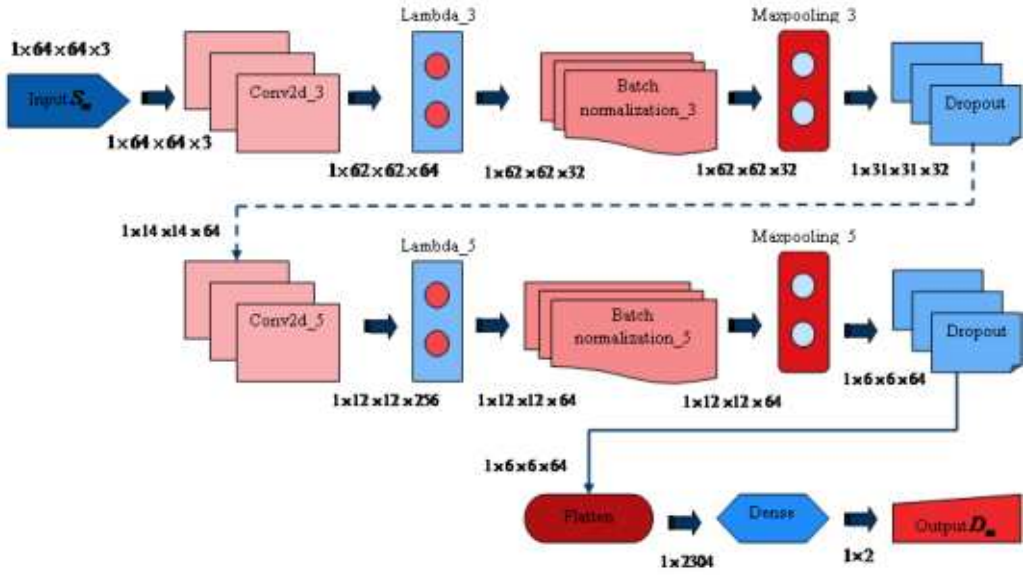

Figure 3. Architecture of DMN

3.5.2 Training of DMN utilizing PFPO

PO [25] allocates individual solution by dual function by dividing a population logically into the political parties as well as constituencies that facilitates individual candidate for updating the position regarding to party leader and constituency winner. This algorithm satisfies every constraint of the issue and identifies comparable outcomes in considerably fewer iterations than other approaches. The algorithm inspired by the pollination procedure of flowers is termed FPA [24]. This algorithm ensured that similar species of flowers were selected more often and hence ensured the convergence more rapidly. The training process of DMN is executed by PFPO which is a merging of PO and FPA. The PFPO is very effective and the steps pursued by the PFPO to acquire better solution is expounded in section 3.3.2.

Political position encoding

In the search space ϖ, the best solution is acquired wherein L implies the learning parameter of DMN, such that $\varpi = 1 \times L$.

Fitness measure

It is a measure that can be formulated by taking the difference between targeted and DMN output. The fitness can be stated by,

$$\hbar_2 = \frac{1}{d}\sum_{m=1}^{d}\left[\mathrm{T}_m - D_m\right]^2 \tag{44}$$

Here, comprising training images is specified by d, where target and DMN outputs are symbolized by T_m and D_m.

4. Results and discussion

The better results acquired by PFPO_DMN for AMD detection along with experimentation outcomes, description of dataset and assessments are explained in this portion.

4.1 Experimentation setup

A newly devised PFPO_DMN for AMD detection is implemented experimentally in the PYTHON tool.

4.2 Description of dataset

Optical Coherence Tomography Image Retinal Database [33] comprises AMD retinal OCT images. It has Fovea-centered OCT images of adult retinas diagnosed with DR. The file is of zip type with a size of 5.7MB. OCT images are capable of visualizing deep retinal layers, that is important for early detection of retinal diseases. More than 500 data base high-resolution images are categorized into different pathological conditions. The images are classified include Normal, Macular Hole, AMD, Central Serous Retinopathy, and Diabetic Retinopathy. The images are obtained with a 2 mm scan length and 512 × 1024 pixel

resolution. The proposed method included 25 normal OCT images with their corresponding ground truth delineations which can be used for an accurate evaluation of OCT image segmentation. In addition, user-friendly GUI can be used by clinicians for manual segmentation.

4.3 Experimentation outcomes

The result of PFPO_DMN are shown in the figure. Figure 4 a), b), and c) illustrates input image-1, segmented image-1 and extracted image-1 whereas input image-2, segmented image-2 and extracted image-2 are demonstrated in Figure 4 d), e) and f).

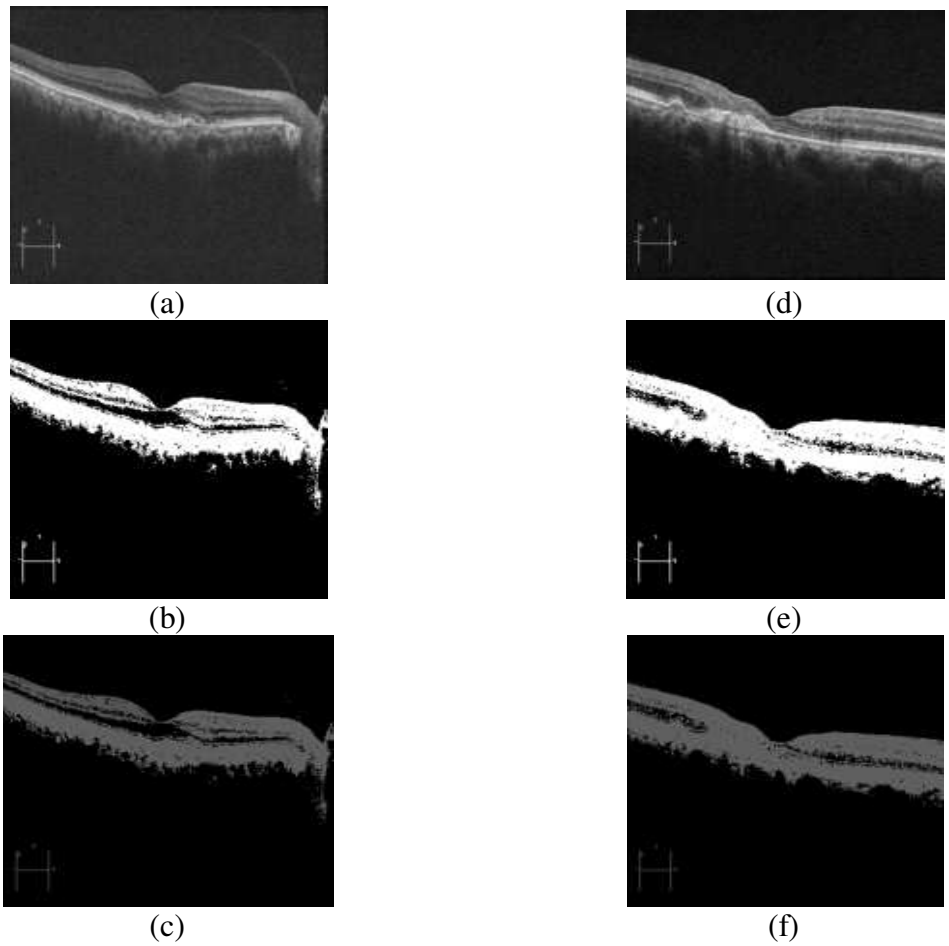

Figure 4: Experimental outcomes of PFPO_DMN, a) Input image-1, b) Segmented image-1, c) Extracted image-1, d) Input image-2, e) Segmented image-2, f) Extracted image-2

4.4 Performance metrics

Sensitivity, specificity and accuracy are the performance measures that are regarded for estimating PFPO_DMN.

4.4.1 Accuracy

It is defined as the percentage of corrected classification of affected as well as healthier patients that is illustrated as,

$$M_1 = \frac{PT + NT}{PT + NF + PF + NT} \tag{45}$$

Here, PT specifies true positive and NT specifies true negative whereas PF signifies positive false and NF symbolizes negative false.

4.4.2 Sensitivity

It specifies a probability of actually positive classes, which are detected accurately and can be given by,

$$M_2 = \frac{PT}{PT + NF} \tag{46}$$

4.4.3 Specificity

It states a probability of actually negative classes that are detected accurately and can be calculated by,

$$M_3 = \frac{NT}{NT + PF} \tag{47}$$

4.5 Performance evaluation

Table 1 demonstrates the analysis of PFPO_DMN based on measures by changing training data percentages with several epoches. In the proposed PFPO_DMN approach, the training data is 90% with epoch 100, which is considered to get the accuracy, sensitivity and specificity values obtained the better performance compared to all existing methods.

Table 1: Performance assessment of PFPO_DMN

Epoch/ Training data	Epoch 20	Epoch 40	Epoch 60	Epoch 80	Epoch 100
	Accuracy				
50	0.787	0.809	0.832	0.856	0.891
60	0.830	0.857	0.873	0.891	0.914
70	0.842	0.862	0.878	0.888	0.908
80	0.823	0.851	0.871	0.893	0.914
90	0.860	0.896	0.882	0.890	0.918
	Sensitivity				
50	0.789	0.803	0.825	0.859	0.891
60	0.833	0.860	0.877	0.880	0.910
70	0.847	0.862	0.872	0.887	0.906
80	0.833	0.852	0.873	0.891	0.914
90	0.887	0.902	0.908	0.897	0.929
	Specificity				
50	0.771	0.806	0.821	0.856	0.899
60	0.826	0.858	0.875	0.885	0.914
70	0.837	0.860	0.875	0.879	0.904
80	0.825	0.850	0.872	0.887	0.911
90	0.875	0.896	0.891	0.890	0.915

4.6 Comparative techniques

Multi-scale CNN [1], GAN [2], CNN visualization [6], DL [7], SVM [3] and U-Net+Dexi-Ned [4] are the techniques compared with PFPO_DMN for revealing its effectiveness.

4.7 Comparative assessment

The proposed PFPO_DMN is done with comparative schemes by altering training data and k-fold.

4.7.1 Evaluation based on training data

The proposed PFPO_DMN is evaluated by comparing existing methods considering measures by changing the training percentages is illustrated in Table 2. When the training percentage is 90, the proposed PFPO_DMN acquired an accuracy of 0.892, which is 11.547%, 9.417%, 4.821%, 2.130%, 1.457% and 1.121% improved than the Multi-scale CNN, GAN, CNN visualization, DL, SVM and U-Net + Dexi-Ned, respectively. PFPO_DMN achieved sensitivity value of 0.933 that shows the improvement in performance about 5.038%, 3.215%, 2.680%, 3.001%, 2.572% and 2.465% than all existing methods. Specificity achieved by PFPO_DMN is 0.920, which shows the better performance of about 4.614%, 2.826%, 3.913%, 4.239%, 3.587% and 3.043% improvement compare to all existing methods.

Table 2: Comparative estimation of PFPO_DMN based upon training data

Methods/ Training data	**Multi-scale CNN**	**GAN**	**CNN visualization**	**DL**	**SVM**	**U-Net+Dexi-Ned**	**Proposed PFPO_DMN**
	accuracy						
50	0.697	0.710	0.758	0.785	0.790	0.791	0.831
60	0.723	0.736	0.776	0.825	0.835	0.851	0.874
70	0.732	0.793	0.831	0.863	0.870	0.871	0.886
80	0.761	0.803	0.827	0.864	0.870	0.873	0.890
90	0.789	0.808	0.849	0.873	0.879	0.882	0.892
	sensitivity						
50	0.697	0.717	0.757	0.796	0.799	0.805	0.839
60	0.745	0.775	0.811	0.862	0.866	0.869	0.890
70	0.789	0.817	0.826	0.862	0.870	0.878	0.899
80	0.824	0.855	0.871	0.884	0.890	0.893	0.914
90	0.886	0.903	0.908	0.905	0.909	0.910	0.933
	specificity						
50	0.691	0.711	0.753	0.770	0.778	0.792	0.835
60	0.750	0.798	0.828	0.865	0.870	0.871	0.890
70	0.789	0.810	0.838	0.865	0.871	0.879	0.892
80	0.835	0.860	0.872	0.877	0.881	0.887	0.917
90	0.877	0.894	0.884	0.881	0.887	0.892	0.920

4.7.2 Evaluation based upon k-fold value

Table 3 displays an estimation of PFPO_DMN by comparing it with traditional techniques considering metrics by changing k-fold values. PFPO_DMN obtained an accuracy value of 0.916 which showed performance improvement about 9.934%, 6.769%, 4.367%, 2.620%, 2.074% and 1.747% than the existing methods such as Multi-scale CNN, GAN, CNN visualization, DL, SVM and U-Net+Dexi-Ned respectively for k-fold=9. The value of sensitivity obtained by PFPO_DMN is 0.929. It represents the performance improvement of PFPO_DMN by 3.660%, 3.014%, 4.090%, 3.229%, 4.198% and 3.122% than all existing methods. PFPO_DMN achieved specificity value of 0.920 while specificity obtained by the better performance about 5.978%, 2.283%, 2.609%, 2.935%, 2.500% and 2.174% compare to the existing methods for considered value of k-fold=9.

Table 3: Comparative assessment of PFPO_DMN based on k-fold value

Methods/ k-fold	**Multi-scale CNN**	**GAN**	**CNN visualization**	**DL**	**SVM**	**U-Net+Dexi-Ned**	**Proposed PFPO_DMN**
	accuracy						
5	0.723	0.745	0.771	0.807	0.810	0.821	0.846
6	0.747	0.753	0.816	0.866	0.873	0.878	0.894
7	0.787	0.817	0.840	0.866	0.878	0.880	0.887
8	0.787	0.815	0.827	0.873	0.880	0.887	0.899
9	0.825	0.854	0.876	0.892	0.897	0.900	0.916
	sensitivity						
5	0.748	0.750	0.826	0.869	0.871	0.876	0.899
6	0.787	0.804	0.821	0.862	0.875	0.880	0.897
7	0.837	0.853	0.876	0.890	0.894	0.898	0.917
8	0.874	0.892	0.886	0.893	0.897	0.899	0.917
9	0.895	0.901	0.891	0.899	0.890	0.900	0.929
	specificity						
5	0.732	0.793	0.815	0.862	0.866	0.870	0.893
6	0.827	0.855	0.876	0.880	0.881	0.888	0.915
7	0.831	0.857	0.875	0.884	0.887	0.893	0.908
8	0.831	0.857	0.874	0.890	0.891	0.898	0.915
9	0.865	0.899	0.896	0.893	0.897	0.900	0.920

4.8 Algorithmic assessment

The algorithms taken for assessing PFPO+DMN are Jaya [32]+DMN, CSO [31]+DMN, FPA [24]+DMN and PO [25]+DMN. The analysis is performed considering evaluation measures by varying swarm size.

Table 4 presents an algorithmic assessment of the PFPO+DMN algorithm regarding metrics by altering swarm size. PFPO+DMN attained an accuracy of 0.918 when swarm size=100, that signified enhancement of performance by 3.595%, 2.287%, 2.397% and 2.505%. For swarm size=100, sensitivity attained by PFPO+DMN is 0.918 that indicated performance improvement by 6.100%, 2.941%, 2.505% and 2.288%. PFPO+DMN obtained a specificity value of 0.911 Hence, the performance improvement of PFPO+DMN compared to other algorithms is 9.330%, 6.257%, 3.513% and 2.634%. From this algorithmic assessment, the PFPO+DMN algorithm is proven more effective than existing algorithms.

Table 4: Algorithmic evaluation of PFPO+DMN based upon swarm size

Methods/ Swam size	Jaya +DMN	CSO +DMN	FPA +DMN	PO +DMN	PFPO+DMN
	accuracy				
20	0.763	0.810	0.826	0.854	0.899
40	0.834	0.850	0.874	0.879	0.914
60	0.841	0.863	0.874	0.881	0.910
80	0.823	0.854	0.877	0.890	0.911
100	0.885	0.897	0.896	0.895	0.918
	sencitivity				
20	0.782	0.802	0.842	0.867	0.886
40	0.838	0.851	0.879	0.886	0.912
60	0.839	0.858	0.878	0.880	0.904
80	0.827	0.856	0.871	0.892	0.912
100	0.862	0.891	0.895	0.897	0.918
	specificity				
20	0.784	0.808	0.848	0.861	0.881
40	0.784	0.808	0.838	0.862	0.884
60	0.833	0.854	0.873	0.891	0.910
80	0.850	0.855	0.872	0.880	0.902

100	0.826	0.854	0.879	0.887	0.911

4.9 Comparative discussion

PFPO_DMN obtained better results while comparing with a few existing approaches that are interpreted in Table 5. It reveals PFPO_DMN attained maximal specificity, sensitivity and accuracy at about 92%, 92.9% and 91.6% for the value of k-fold =9.

Table 5: Comparative discussion of PFPO_DMN

Analysis based upon	**Metrics/ Methods**	**Multi-scale CNN**	**GAN**	**CNN visualization**	**DL**	**SVM**	**U-Net+Dexi-Ned**	**Proposed PFPO_DMN**
Training percentage =90%	*Accuracy*	78.9%	80.8%	84.9%	87.3%	87.9%	88.2%	**89.2%**
	Sensitivity	88.6%	90.3%	90.8%	90.5%	90.9%	91.0%	**93.3%**
	Specificity	87.7%	89.4%	88.4%	88.1%	89.7%	88.2%	**92.0%**
K-fold=9	*Accuracy*	82.5%	85.4%	87.6%	89.2%	89.7%	90.0%	**91.6%**
	Sensitivity	89.5%	90.1%	89.1%	89.9%	89.0%	90.0%	**92.9%**
	Specificity	86.5%	89.9%	89.6%	89.3%	89.7%	90.0%	**92.0%**

4.10 Statistical Analysis:

Table 6 represents the statistical analysis of PFPO_DMN. The process of collecting and analyzing large volumes of data to identify trends and develop valuable insights is called Statistical analysis. Here, the accuracy, sensitivity, and specificity of mean, variance and best in the six existing methods such as Multi-scale CNN, GAN, CNN visualization, DL, SVM, U-Net+Dexi-Ned are compared with the proposed method. The statistical analysis of PFPO_DMN method gets the best output than other comparative schemes.

Table 6: Statistical analysis of PFPO_DMN

Methods	**accuracy**			**sensitivity**			**Specificity**		
	Best	**Mean**	**Variance**	**Best**	**Mean**	**Variance**	**Best**	**Mean**	**Variance**
	Training percentage								

Multi-scale CNN	0.789	0.783	0.006	0.866	0.861	0.005	0.877	0.870	0.007
GAN	0.808	0.804	0.004	0.903	0.900	0.003	0.894	0.889	0.005
CNN visualization	0.849	0.844	0.005	0.908	0.904	0.004	0.884	0.880	0.004
DL	0.873	0.870	0.003	0.905	0.902	0.003	0.881	0.877	0.004
SVM	0.879	0.875	0.004	0.909	0.906	0.003	0.887	0.884	0.003
U-Net+Dexi-Ned	0.882	0.879	0.003	0.910	0.908	0.002	0.892	0.890	0.002
Proposed PFPO_DMN	0.892	0.890	0.002	0.933	0.932	0.001	0.920	0.919	0.001
	K-Fold								
Multi-scale CNN	0.825	0.820	0.005	0.895	0.890	0.005	0.865	0.859	0.006
GAN	0.854	0.850	0.004	0.901	0.897	0.004	0.899	0.895	0.005
CNN visualization	0.876	0.872	0.004	0.891	0.888	0.003	0.896	0.893	0.003
DL	0.892	0.889	0.003	0.899	0.896	0.003	0.893	0.890	0.003
SVM	0.897	0.895	0.002	0.890	0.886	0.004	0.897	0.895	0.002
U-Net+Dexi-Ned	0.900	0.898	0.002	0.900	0.897	0.003	0.900	0.898	0.002
Proposed PFPO_DMN	0.916	0.915	0.001	0.929	0.927	0.002	0.920	0.919	0.001

4.11 Analysis on Computational Time

The analysis on computational time is shown in Table 7. Here, the six methods, like Multi-scale CNN, GAN, CNN visualization, DL, SVM, and U-Net+Dexi-Ned are used to compare the computational time of the PFPO_DMN. The computational time of the PFPO_DMN is minimum when compared to the existing methods.

Table 7: Analysis on Computational Time

Methods	**Computational Time(sec)**

Multi-scale CNN	9.4257624
GAN	7.4458632
CNN visualization	6.7248544
DL	6.3368457
SVM	5.4856325
U-Net+Dexi-Ned	5.2964752
Proposed PFPO_DMN	4.5103648

5. Conclusion

One of the considerable retinal diseases, which affects older people, is termed AMD. An starting stage develops a blurring effect on eye vision and afterwards directs to central loss of eye sight. Many people unnoticed the starting stage of blurring and hence, converted to a complex stage. There is no appropriate treatment for curing this disease and therefore earlier AMD detection is significant for preventing the expansion to a complicated stage. In this research, PFPO_DMN is presented newly for the detection of AMD. Here, the median filter is used for pre-processing the input OCT images. That input OCT images are subjected to the layer segmentation stage. In layer segmentation, ensemble U-Net is utilized for segmenting layers. The tuning of ensemble U-Net is done by PFPO. PEPO is the combination of PO and FPA. Thereafter, features like texture features like LBP and shape index histogram, statistical features namely energy, mean, correlation, skewness, kurtosis and entropy, reflectivity, thickness and curvature are extracted. Finally, AMD detection is conducted utilizing DMN, wherein training of DMN is carried out by PFPO. Additionally, PFPO_DMN attained maximal specificity, sensitivity and accuracy of 92%, 92.9% and 91.6% when considering the value of k-fold is 9. More datasets will be utilized for validating the performance of designed approach and AMD classification as wet and dry AMD will be performed in the future work.

Declaration Statements:

Funding: This research did not receive any specific funding

Conflict of Interest: The authors declare no conflict of interest

Acknowledgements: I would like to express my very great appreciation to the co-authors of this manuscript for their valuable and constructive suggestions during the planning and development of this research work.

Informed consent: Not Applicable

Ethical approval: Not Applicable

Author Contribution: All authors have made substantial contributions to conception and design, revising the manuscript, and the final approval of the version to be published. Also, all authors agreed to be accountable for all aspects of the work in ensuring that questions related to the accuracy or integrity of any part of the work are appropriately investigated and resolved.

Data Availability Statement:

The data underlying this article are available in Optical Coherence Tomography Image Retinal Database*, at* https://www.openicpsr.org/openicpsr/project/108503/version/V1/view.

References

[1] Anju Thomas, Harikrishnan P. M., Adithya K. Krishna, Palanisamy P. and Varun P. Gopi, "A novel multiscale convolutional neural network based age-related macular degeneration detection using OCT images", Biomedical Signal Processing and Control, vol.67, pp.102538, May 2021.

[2] Vineeta Das, Samarendra Dandapat and Prabin Kumar Bora, "Unsupervised super-resolution of OCT images using the generative adversarial network for improved age-related macular degeneration diagnosis", IEEE Sensors Journal, vol.20, no.15, pp.8746-56, April 2020.

[3] Marwa Hani, Amine Ben Slama, Imen Zghal and Hedi Trabelsi, “Appropriate identification of age-related macular degeneration using OCT images”, Computer Methods in Biomechanics and Biomedical Engineering: Imaging & Visualization, vol.9, no.2, pp.146-56, March 2021.

[4] Jefferson Alves Sousa, Anselmo Paiva, Aristophanes Silva, Joao Dallyson Almeida, Geraldo Braz Junior, Joao Otavio Diniz, Weslley Kelson Figueredo and Marcelo Gattass, “Automatic segmentation of retinal layers in OCT images with intermediate age-related macular degeneration using U-Net and DexiNed”, Plos one, vol. 16, no.5, pp.e0251591, March 2021.

[5] Hyun-Lim Yang, Jong Jin Kim, Jong Ho Kim, Yong Koo Kang, Dong Ho Park, Han Sang Park, Hong Kyun Kim and Min-Soo Kim, “Weakly supervised lesion localization for age-related macular degeneration detection using optical coherence tomography images”, PloS one, vol.14, no.4, pp.e0215076, April 2019.

[6] Sajib Saha, Ziyuan Wang, Srinivas Sadda, Yogesan Kanagasingam and Zhihong Hu, “Visualizing and understanding inherent features in SD-OCT for the progression of age-related macular degeneration using deconvolutional neural networks”, Applied AI Letters, vol.1, pp.e16, October 2020.

[7] Zailiang Chena, Dabao Lia, Hailan Shena, Hailan Moa, Ziyang Zenga and Hao Wei, “Automated segmentation of fluid regions in optical coherence tomography B-scan images of age-related macular degeneration”, Optics & Laser Technology, vol.122, pp.105830, February 2020.

[8] Zailiang Chen, Dabao Li, Hailan Shen, Yufang Mo, Hao Wei and Pingbo Ouyang, “Automated retinal layer segmentation in OCT images of age-related macular degeneration”, IET Image Processing, vol.13, no.11, pp.1824-34, October 2019.

[9] K. Alsaih, M.Z. Yusoff, T.B. Tang, I. Faye and F. Meriaudeau, “Deep learning architectures analysis for age-related macular degeneration segmentation on optical coherence tomography scans”, Computer methods and programs in biomedicine, vol.195, pp.105566, October 2020.

[10] Laurence S Lim, Paul Mitchell, Johanna M Seddon, Frank G Holz and Tien Y Wong, “Age-related macular degeneration”, Lancet vol.379, no.9827, pp.1728–1738, 2017.

[11] Tapabrata Chakraborty, Brendan McCane, Steven Mills and Umapada Pal, "LOOP descriptor: encoding repeated local patterns for fine-grained visual identification of Lepidoptera", In Proc. Comput. Vis. Pattern Recognit, 2017.

[12] U Schmidt-Erfurth, S Klimscha, SM Waldstein and H Bogunovic, “A view of the current and future role of optical coherence tomography in the management of age-related macular degeneration”, Eye, vol.31, no.1, pp.26, 2017.

[13] Wolfgang Drexler and James G. Fujimoto, “Optical coherence tomography: technology and applications”, Springer Science & Business Media, 2008.

[14] Robert J. Zawadzki, Alfred R. Fuller, Mingtao Zhao, David F. Wiley, Stacey S. Choi, Bradley A. Bower, Bernd Hamann, Joseph A. Izatt and John S. Werner, “3D OCT imaging in clinical settings: toward quantitative measurements of retinal structures”, In Ophthalmic Technologies XVI, International Society for Optics and Photonics, vol.6138, pp.613803, March 2006.

[15] James G. Fujimoto, Costas Pitris, Stephen A. Boppart and Mark E. Brezinski, “Optical coherence tomography: an emerging technology for biomedical imaging and optical biopsy”, Neoplasia, vol.2, no.1-2, pp.9, 2000.

[16] A. Lay-Ekuakille, A. Trabacca, R. De Santis, M. Ciccarelli, P. Kapita Mvemba and R. Morello, “Extracting features from optical coherence tomography for measuring optical nerve

thickness", In 2018 IEEE International Symposium on Medical Measurements and Applications (MeMeA), pp.1-5, June 2018.

[17] SJ. M. Schmitt, S. H. Xiang and K. M. Yung, "Speckle in optical coherence tomography", Journal of biomedical optics, vol.4, no.1, pp.95-105, January 1999.

[18] Roy de Kinkelder, Jeroen Kalkman, Dirk J. Faber, Olaf Schraa, Pauline H. B. Kok, Frank D. Verbraak and Ton G. van Leeuwen, "Heartbeat-induced axial motion artefacts in optical coherence tomography measurements of the retina", Investigative ophthalmology & visual science, vol.52, no.6, pp.3908-13, May 2011.

[19] S. H. Yun, G. J. Tearney, J. F. de Boer and B. E. Bouma, "Motion artefacts in optical coherence tomography with frequency-domain ranging", Optics Express, vol.12, no.13, pp.2977-98, June 2004.

[20] Jianqin Lei, Siva Balasubramanian, Nizar Saleh Abdelfattah, Muneeswar G. Nittala and Srinivas R. Sadda, "Proposal of a simple optical coherence tomography-based scoring system for progression of age-related macular degeneration", Graefe's Archive for Clinical and Experimental Ophthalmology, vol.255, no.8, pp.1551-8, August 2017.

[21] Luis de Sisternes, Noah Simon, Robert Tibshirani, Theodore Leng and Daniel L. Rubin, "Quantitative SD-OCT imaging biomarkers as indicators of age-related macular degeneration progression", Investigative ophthalmology & visual science, vol.55, no.11, pp.7093-103, November 2014.

[22] Sajib Saha, Marco Nassisi, MoWang, Sophiana Lindenberg, Yogi Kanagasingam, Srinivas Sadda and Zhihong Jewel Hu, "Automated detection and classification of early AMD biomarkers using deep learning", Scientific reports, vol.9, no.1, pp.1-9, July 2019.

[23] Weichen Suna, Fei Sua and Leiquan Wang, "Improving deep neural networks with multi-layer max out networks and a novel initialization method", Neurocomputing, vol.278, pp.34-40, February 2018.

[24] Xin-She Yang and Mehmet Karamanoglu, "Nature-inspired computation and swarm intelligence: Algorithms, theory and applications", 2020.

[25] Qamar Askari, Irfan Younas and Mehreen Saeed, “Political Optimizer: A novel socio-inspired meta-heuristic for global optimization”, Knowledge-Based Systems, vol. 195, pp.105709, May 2020.

[26] B.H. Lohithashva, V.N. Manjunath Aradhya and D.S. Guru, "Violent Video Event Detection Based on Integrated LBP and GLCM Texture Features", Revue d' Intelligence Artificielle., vol.34, no.2, pp.179-187, 2020.

[27] P. Asha and Prof. R S Khule, "HEp-2 cell classification using shape index histograms with donut-shaped spatial pooling", IEEE transactions on medical imaging, vol.33, no.7, pp.1573-1580, 2014.

[28] Mentari Bella Al Rasyid, Yunidar, Fitri Arnia and Khairul Munadi, "Histogram statistics and GLCM features of breast thermograms for early cancer detection", In proceedings of 2018 International ECTI Northern section conference on electrical, electronics, computer and telecommunications engineering (ECTI-NCON), pp.120-124, February 2018.

[29] Yilong Li, Xingru Huang, Yaqi Wang, Zhaoyang Xu, Yibao Sun and Qianni Zhang, "U-net ensemble model for segmentation in histopathology images", 2019.

[30] Wei Hao Khoong, "BUSU-Net: an ensemble U-Net framework for medical image segmentation", arXiv preprint arXiv:2003.01581, 2020.

[31] Ran Cheng and Yaochu Jin, "A competitive swarm optimizer for large scale optimization", IEEE Transactions on Cybernetics, vol.45, no.2, pp.191-204, 2014.

[32] R. Venkata Rao, "Jaya: A simple and new optimization algorithm for solving constrained and unconstrained optimization problems", International Journal of Industrial Engineering Computations, vol.7, no.1, pp.19-34, 2016.

[33] Optical Coherence Tomography Image Retinal Database taken from, “https://www.openicpsr.org/openicpsr/project/108503/version/V1/view”, accessed on February 2023.

[34] Fatema Murshid AlBalushi, "Bat Optimization Assisted Diabetic Retinopathy Detection Framework", Multimedia Research, vol.3, no.2, 2020.

[35] Vilas S. Gaikwad, "Enhanced Whale Optimization Algorithm for the Eye Movement Recognition", Journal of Computational Mechanics, Power System and Control, vol.4, no.2, 2021.

[36] Young Jae Kim and Kwang Gi Kim , “Automated Segmentation Methods of Drusen to Diagnose Age-Related Macular Degeneration Screening in Retinal Images” **,** Computational and Mathematical Methods , 2018.

PAPER • **OPEN ACCESS**

Recent Trends and advances in deep learning techniques for the classification of landslides using satellite images: comprehensive survey

To cite this article: A Sharma *et al* 2024 *IOP Conf. Ser.: Earth Environ. Sci.* **1285** 012024

Recent Trends and advances in deep learning techniques for the classification of landslides using satellite images: comprehensive survey

A Sharma[1], **S R Chopra**[1], **S G Sapate**[2] and **P B Bhagawati**[3]

1 Electronics and communication department, Lovely Professional University, Jalandhar 144001, India akankshasharma2008@gmail.com
2. Computer science and engineering department, Sanjeevan engineering and technology institute, Panhala,416201, India shaktirchopra2008@gmail.com
3 Civil Engineering department, S.G. Balekundri Institute of Technology, Karnataka, India suhasgsapate@gmail.com

Abstract. A landslide is a geographical catastrophe that occurs frequently in monsoon season and has a formidable impact over a wide range to pose risks to human lives and infrastructure worldwide. Traditional methods to classify and identify landslides are more time-consuming and less reliable. In the past few years artificial intelligence algorithms mainly, deep learning algorithms were used in many fields to detect and identify automatic disasters like landslides and earthquakes. Numerous research and classification approaches have been implemented in satellite image processing for the detection and prediction of landslides. The most challenging task in the classification and prediction of landslides from satellite imagery is to train the model with appropriate techniques and datasets which predict "accurately". Limited work has been done on high-resolution satellite images using convolution techniques. This article presents a comprehensive study of recent deep-learning approaches based on convolutional neural networks to achieve efficient classification of landslide satellite images. A few selected research articles on deep learning approaches based on CNN for automatic detection of landside from peer reviews journals etc. are considered for this study. "The performance of all surveyed articles is evaluated using accuracy recall precision and F 1 score parameters". This study illustrates the viability of deep learning approaches in learning complex and high-resolution satellite images for the classification and prediction of landslides.

1. Introduction

1.1 History and background of landslide classification

Landslide is a common and frequent serious geological hazard in hilly areas, which cause damage to the environment, and human and socioeconomic conditions of many countries. The trigger factor of landslides is rainfall, soil, earthquake, seismic shaking and unplanned construction. To rescue and prevent the recurrence of landslides timely and reliable and accurate measures are required [1]. In Himachal Pradesh's Kothipura district Mandi on 12 August 2017 a debris flow type landslide took place causing 47 fatalities. In 1977 at the same site, huge landslide took place and was reactivated again on 13 august 2007. Tension carks, antecedent rainfall, rock mass, rise in soil moisture and increase in seismic activities were various causes. Still its reoccurrence chances are possible so continuous monitoring from satellite provides use information or early alarming of the event [2]. A number of

landslides have occurred in the Kinnaur district of Himachal Pradesh causing a number of deaths and property loss by heavy rainfall seismic activities and unplanned construction [3].

There are numerous case studies based on field surveys that are used for landslide detection and monitoring. All the traditional approaches to detecting classifying and monitoring landslides are reliable but very time-consuming. Automatic landslide classification, detection and monitoring are possible with the advancement in satellite image processing. For analysis of landslide detection aerial images have been widely used and provide good accuracy [4,5]. data from the Digital elevation model perform a pivotal role in the detection and prediction of landslides by providing topographic information [6]. For landslide classification and prediction-number of machine learning algorithms were used. Machine learning classification schemes are categorized as SVM classifiers, clustering-based classifiers, learning-based classifiers, fuzzy classifiers, and Bayesian classifiers [7,8]. In supervised machine learning methods labeled high-resolution data is required for training and testing for automatic detection and classification. These classification machine learning algorithms are based on low-level features which result in poor classification accuracy [9].

Deep learning is a subset of machine learning that has evidenced its efficiency in classification and prediction with satellite images in the past few years. In Deep learning, images can be processed with convolutional neural networks and achieve good results [10][11] Deep learning models such as deep convolutional networks and deep brief net have yielded good results in segmentation, object classification and detection [12].

Nowadays, development in infrastructure and weather conditions are triggering many parameters of landslide. So automatic detection and early alarming systems pay an important role to save life and infrastructure.

1.2 Stages of landslide classification

Landslide classification and prediction are mainly divided into two categories. One depends on the type of images used for training and testing and the other depends on the type of algorithm used for training and testing. The resolution of Earth-observing satellite images is an important feature to be considered in satellite image classification. Spatial, spectral, temporal, radiometric and geometric are five types of resolution.

1. Spatial resolution, pixel size of an image representing the size of surface area. Once an image is acquired its spatial resolution is frozen.
2. Spectral resolution is defined by wavelength discrete segments of electromagnetic space interval.
3. Time resolution is defined by the number of days that pass between a collection of two images.
4. Radiometric resolution recodes many levels of brightness.
5. Geometric resolution represents a portion of the earth's surface in a single pixel and is known as ground sample distance.

There are two types of approaches used in identification: pixel-wise and object-based image analysis. Pixel-based landslide identification defines pixel values and changes in pixel values. Attribute features are used in object-oriented identification [13].

To train the model semantic segmentation algorithms such as DeepLab,Mask R CNN, U-Net and fully convolution network(FCN) are used to pre-process the data. The choice of algorithm depends on the application and requirement. The model is trained with the algorithms of the Convolutional neural network. Finally, the trained model performance is tested with random datasets.

1.3 Motivation

From last few years remote sensing data was used to monitor changes on the earth surface, landslide detections, post and pre-images of landslide areas, forest monitoring and environment changes [14,15,16]. Satellite remote sensing offer information on a large area for a short period of time and is useful for the detection and relief of disasters like landslide, Earthquake and, flood [17 ,18]. Satellite remote sensing image-based databases have become very beneficial for object classification and

prediction in the last few years. In low and medium resolution satellite images have the ambiguity of overlapping in spectral curves. High-resolution data can achieve high accuracy as compared to medium and low spatial resolution. High-resolution Satellite images database become very much in demand for real-time events such as landslides [19].

1.4 Objectives

The primary objectives of this research work are

1. To identify the research gap in the literature available on deep learning models in landslide satellite image classification, object detection and prediction.
2. Compare the result of different deep learning algorithms performed on landslide identification on the basis of four parameters: accuracy, precision, recall and f1 score
3. Explore the effect of optimization to enhance the performance of CNN-based deep learning models for identification of landslides from satellite imagery database.

1.5 Article selection strategy

For this comprehensive study, we select research papers based on deep learning algorithms for the automatic identification of landslides from IEEE Explore, Springer, Remote sensing journal, landslide journal, IEEE and science direct etc. All the articles are based on landslide identification with deep learning for the last few years with common ground and parameters for comparison. Use a common strategy to compare different techniques. Research articles are covering the study of various landslide-prone areas all over the world which help researchers to understand changing trends of parameters and is helpful for proposing an advanced technique for automatic identification of the landside.

1.6 Organization of the Article

The article is organized into different sections: Section 2 covers the overview of the available data sets used by all the articles considered in this work. Section 3 elaborates on related work in this area. Observations and findings are discussed in Section 4 on the basis of the research gap identified in related work**.** Section 5 explains the proposed algorithm and Section 6 concludes the paper.

2. Related Work

This comprehensive survey provides an overview of various deep-learning models that have been used in the analysis and classification of landslide satellite images. The main agenda of this article is to discuss the current deep learning model for landslide classification and identification toward improving identification accuracy. The last few years of research work is compared with accuracy, precision, recall and F1 score. This work proposes the recent trends, advantages and performance of deep learning methods in the identification of landslides. Bijie Land Slide Dataset [20] and Global Landslide Catalog Export [21] landslide datasets have been used in many research related to the automatic detection of landslides with convolutional neural networks. Most of the researchers used data sets that are available publically. In neural networks, data set plays a very important role in training and testing. Accuracy in the detection of landslides depends on how accurately the network was trained. The tainting dataset should be full of accurate information so the training of the model is accurate.
A comprehensive review of a few selected articles on the identification landslides is presented below.

Ji S et al. [20] designed an attention module to emphasize the different features of a complicated background landslide. The paper was focused on developing an accurate and time-efficient inventory, based on the recognition of latent landslides. The work has been done on high-resolution optical satellite images with a CNN model to detect landladies. The attention mechanism which is based on a human visual system was developed with a number of landslides with complex backgrounds. Attention Mechanism was combined with CNN to boost the result of CNN to extract more features from the background of the landslide. Bijie landslide database with 770 images was created. Design and attention module which combine spatial and channel attention map and known 3D spatial channel attention

module (3D SCAM) was designed and used in this work. The proposed 3D SCAM was trained with two-thirds of the images and results are compared with other attention modules. A few deep learning architectures such as VGGNet, ResNet, Inception, and DenseNet were evaluated with four attention modules as SE module, BAM Module, CBAM module, 3D SCAM module. Experimental result shows that ResNet50 with the proposed 3D SCAM bossed CNN provide the best result in all the combination. This research claims 97.7 % accuracy, 0.97 precision, 0.94 recall and F1 score was 0.95. The accuracy of the model is high with the attention module. In this attention module model can learn the characteristics of landslides very clearly.

Yang S et al. [22] developed a semantic segmentation-based deep learning automatic model for the identification of landslides. Three selected semantic algorithms U-Net, DeepLab3+ and PSPNet were used with different deep learning algorithms such as ResNet 50, MobileNet etc. as the backbone. An open-source Bijie landslide dataset was used for training and testing the different combinations of semantic algorithms with a backbone deep learning model. Images on this dataset were pre-processed with an augmentation technique to enhance the data and data cleaning. In the deep learning model training plays, a very important role and depends on three points: accurate information in the data set, suitable parameters, and methods adopted for training. In this model, 90% data was used in training and 10% was used for the validation process. Experimental results were evaluated on six combinations of three semantic segmentation models (U-Net, DeepLab3+ and PSPNet) with two different deep learning architectures as the backbone (VGG, ResNet50, MobileNet, Xception). The pixel-type classification was used in this work. The freezing training method was adopted so the backbone of the model was frozen which was full with large batch size and learning rate. Experimental evaluation of PSPNet model with ResNet50 as backbone network yield 91.18 mIou (Jaccard Index) high accuracy, 96% recall and 93.76% precision. The work done by the researchers has significant practical use in real-time. This work will help geologists and disaster management to identify landslides automatically which will be more efficient than manual methods which are more time-consuming to save life. The accuracy of work still can increase by using more datasets. The algorithm can be trained with high-resolution images to improve the accuracy in the identification of landslides.

Lui T et al. [23] designed a landslide detection mapping (LDM) model based on residual neural networks and Dense convolutional neural networks. ResNet and DenseNet take high spectral resolution data and conditioning factors and 70 % of the data was used for training and 30%data was used for testing. To create database two cities of the chain was taken as steady object which is China's water conservancy project. CNN, ResNet and DenseNet were trained with nineteen conditional factors and found application in the field of LDM. In all these three algorithms DensNet with remote sensing (RS) images yielded the best result. All three trained algorithm claim accuracy above 95% and densNet with RS images and condition factor claim 99% accuracy and recall and F1 score for this particular dataset. The learning efficiency of the model was enhanced with conditional factor and yielded good results in landslide identification.

Fu R et al. [24] proposed a study on post-earthquake seismic landslides. To determine the size of post-earthquake few images of post-earthquake seismic landslide satellite imagery data were used. The database was created from Post-quake images of unmanned air vehicles (UAV) over Wenchuan country of China. The database has an average 2000 m altitude and 0.25m spatial resolution with an image size of 5616*3744 pixels. In pre-processing steps the database images were reduced in size to remove the complexity and textual information was added to these seismic landslide images. To increase the number of images in the dataset data augmentation was done with image rotation and image flip. For training, 70% of data was used, 20 % for validation and the remaining 10% was used for testing. Mask R CNN framework can scan the image and mark the region of a landslide as a target and proposes a mask according to the marked region of interest. For identification and prediction of landslides in the real world required a large number of datasets and by using transfer learning this requirement can be reduced.

Three architectures of convolutional neural networks ResNet 50, ResNet 101 and Swin transformer was used as backbone networks. Among three backbone Swis Transformer with Mask R-CNN claims 82.2% accuracy, 93.28% precision, 87.41% recall and 90.25%F1 score. This model needs to improve the accuracy in the identification and prediction of landslides. Accuracy can be enhanced with the quality of post-quake landslide images. Instead of using UAV images satellite images with high spatial and spectral resolution can be used.

Ullo S L et al. [25] presented a landslide detection method that uses Mask R-CNN with pixel-based segmentation to identify object layouts. ResNet50 and ResNet 101 was used as the backbone for the proposed method and the result was evaluated with accuracy, recall, precision and F1 score. The main objective of this research was to detect landslides with pertained mask RCNN with limited data set and Augmentation was used on the training dataset to increase the volume. The dataset that was used in training and testing was created from different resources. Images collected were high-resolution digital photographs collected from UAV, search engines. Two data sets A and B were created. Data set A contains total160 images, 101 images were used for training, 28 were used for validation and 31 were used for testing. Data set B contains total121 images, 62 images were used for training 28 were used for validation and 31 were used for testing different resources. Experimental result shows that ResNet101 have better accuracy, recall, precision and F1 score over ResNet 50. ResNet 101 yields 97% accuracy for dataset A and 90% accuracy for data set B. RestNet 101 has 1 precision, 93% recall, and 0.97 f1 score. The main advantage of this research was mask R CNN can provide segmentation and detection of landslide at the same time. The result shows that with the higher number of training samples accuracy was high.

Ghorbanzadeh O et al. [26] presented a model which fuses object-based image analysis (OBIA) with a Fully convolution network. ResUnet as the predominate FCN model was trained and tested with Sentinel 2 database and design an combination of FCN-OBIA segmentation and classification using knowledge-based rules. In OBIA image difference indices were calculated between pre and post landslide. The data set used in training and testing was created from sentinel-2 images of Eastern Iburi Japan. The experimental results show that ResU-Net yield 50.24 mIOu, 76.15 precision,60.01 recall and 66.62 F1 score where as ResU Net OBIA yield 72.49 mIOu, 85.5 precision, 82.6 recall and 84.03 F1 score. In this work, it is observed that the ResU-Net model detect landslide correctly but have high false positive results. The result was more accurate and had fewer false positives by adding rule-based OBIA for a landslide to train ResU-Net.

3. Observations and findings

The basic purpose behind the wide variety of selected articles in this study is to observe the performance of existing techniques for landslide identification and prediction using satellite data. Another important purpose is to identify the research gap and based on the gap propose a new technique to achieve high performance in terms of Accuracy, Precision, recall, F1 score. These two purposes and our outcomes are discussed in the subsections below.

3.1. Observations and Findings

During this research, some findings will be helpful for future research direction and these are summarized in this section:

- In all the architecture data collection was the major part. Training and testing of the proposed algorithm were done with a satellite dataset of landslides.
- High-resolution images and a good training process can produce landslide identifiers and predictors with good performance.
- Images should be of the same size in both the training and testing time of architecture.

- For deep learning architectures training process requires high-speed machines with a great number of datasets.

3.2. Research gap identified

Landslide is a real-time event and it is very difficult to create a database with a very high number of images. Landslide events depend on a number of factors like rain soil weather conditions. Need to design a model with Convolutional neural network which takes care of different factors of landslide. Deep neural networks are difficult to understand and with complex architecture of networks prediction is very difficult. Convolutional Neural network architecture has practical applications in images classification, object detection, and semantic segmentation [20]. Semantic segmentation with pixel-level segmentation provides good results in image segmentation [22].

The articles in this study have very effective results in terms of accuracy, precision, recall and F1 score for landslide detection. There are few potential research gaps as follows:

- Performance: Accuracy plays the main role in the performance of an automatic detection landslide model. Selected literature articles were compared with common parameters: accuracy, precision, recall and f1 score. The range of accuracy lies between 80% to 92%. Semantic segmentation model PSPNet with ResNet50 as backbone achieves the highest mIOU at 91.18% this can be further improved by exploring false results. [22]. The Swis Transformer as backbone network with Mask R-CNN claims 82.2% accuracy [24]
- Method used: Convolutional neural network architecture such as ResNet50, ResNet101, VGG, DensNet, Google Net were used as the backbone with different approaches and provide different results. CNN along with spatial channel attention mechanism and high-resolution optical images yield high accuracy. Need more investigation on the superiority of spatial channel attention mechanism [20].
- Database: Need is high-resolution remote sensing image dataset for improving accuracy. Models were trained for selected datasets. Bijie landslide dataset was used but it is limited with 770 images of landslide and nonlandslide images. Some Dataset was created from images of unmanned air vehicles which contain different images from different sources. Instead of using UAV images satellite images with high spatial and spectral resolution can be used and will provide good result. [25] Training is limited with the dataset is the biggest research gap.
- Different type of landslide has different characteristics. The model based on Mask R-CNN with pixel-based segmentation and ResNet at the backbone does not specify whether the model tested for different types of landslide. Results are only compared in between ResNet 50 and RestNet 101 rather than the other potential object detector deep learning architecture. [25].

4. Discussion

In the last few years, there has been research that provides automatic landslide identification and prediction with convolutional neural networks that claim good accuracy. Accuracy can be enhanced by increasing the number of datasets and by considering the condition factors. In Real-time events, it is difficult to collect more satellite images of a particular area. Augmentation techniques can be performed over available data set to increase the number of training sets. Semantic segmentation which labels each pixel in an image with the corresponding class label provides detail, unlike basic image segmentation techniques. Important stages of landslide identification and prediction are satellite image collection, pre-processing the image dataset and increasing the number of images in the dataset, Training the designed model with backbone CNN Networks such as: ResNet v50, ResNet 101, DensNet, Google Net, VGG etc. Finally, test the model with the dataset.

In the proposed model we can combine attention mechanism and optimization algorithms. The optimization algorithm can update the weights and attention layer to minimize the loss function. To enhance accuracy regularization techniques such as Dropout and batch normalization can be used. While

creating a dataset enough care should be taken on conditional factors of landslide. The flow chart of the proposed model is shown in Fig. 1.

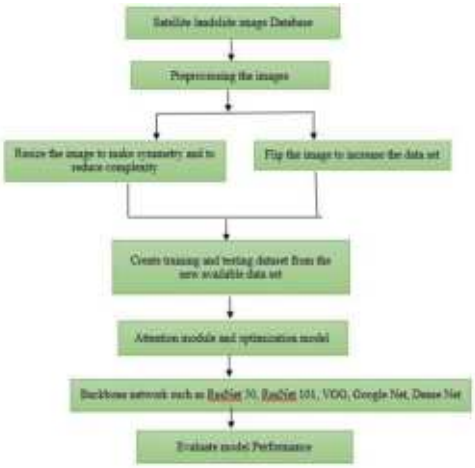

Fig. 1 Flow chart of proposed landslide detection model.

4.1. Dataset being used

Initially, we try our algorithm with open source Bijie landslide dataset which contains two sets of images one contains landslide images and the other is non landslide images. To increase the size of the dataset augmentation techniques can be applied. Later we try to test the model with practical events of landslides.

4.2. Expected outcomes

In our proposed model augmentation techniques will be used to increase the dataset and optimization and transfer learning will be used to enhance the accuracy of the detection of landslides. Enough care will be taken on the conditional factors of landslide to achieve accuracy between 93% to 96%. This model will be tested with inventory which will be created from the last two-year landslide events.

5. Conclusion

This comprehensive study proposed an automatic landslide detection model for a satellite landslide image database. Research gap has been identified in a number of automatic landslide detection models. Most of the selected landslide detection articles use the same backbone architecture of CNN such as ResNet 50, ResNet 101, DensNet, VGG etc., and are compared on four parameters: accuracy, precision, recall and f1 score. To collect the sufficient data for training and testing automatic or semiautomatic models is a challenging task in all the existing To overcome this problem real-time landslide event data can be increased with augmentation techniques. In the proposed model Attention mechanism can be used to enhance the accuracy of the identification and prediction of landslides. The work on the proposed method is to yield high accuracy in identification and prediction is in progress.

References

[1] Singhroy V 2009 Satellite Remote Sensing Applications for Landslide Detection and Monitoring.Sassa, K., Canuti, P. *Landslides – Disaster Risk Reduction.* (Berlin:Springer) p 143-158. https://doi.org/10.1007/978-3-540-69970-5_7

[2] Singh N, Gupta S and shukla D (2020) Analysis of landslide reactivation using satellite data:

a case study of kotrupi landslide, mandi, himachal pradesh, india. *ISPRS - International Archives of the Photogrammetry, Remote Sensing and Spatial Information Sciences* **XLII-3/W11** 137-142.

[3] kumar V , Gupta V, Jamir I and Chattoraj S L 2019 Evaluation of potential landslide damming: case study of urni landslide, kinnaur, satluj valley, india . *Geoscience frontiers* **10** (2) 753-767

[4] Keyport R N,Oommen T, Martha T R, K.S. SajinkumarK S and Gierke J S 2018 A comparative analysis of pixel- and object-based detection of landslides from very high-resolution images *International Journal of Applied Earth Observation and Geoinformation*, **64**(6) 1-11 2018 DOI: https://doi.org/10.1016/j.jag.2017.08.015

[5] Malviya U K and Gupta R 2021 Satellite Image Classification Method Using ELBP and SVM Classifier," *International Conference on Advances in Electrical, Computing, Communication and Sustainable Technologies (ICAECT)* (India: Bhilai) p 1-6

[6] Kakavas M P And Konstantinos G. Nikolakopoulos 2021 Digital Elevation Models of Rockfalls and Landslides: A Review and Meta-Analysis, *Geosciences* , **11**(6), 256 https://doi.org/10.3390/geosciences11060256

[7] Gavade A B and Rajpurohit V S 2019 Systematic analysis of satellite image-based land cover classification techniques: literature review and challenges *International Journal Of Computers And Applications* **43**(6) 1-9 DOI: 10.1080/1206212X.2019.1573946

[8] Sharma A and Sharma K K 2023 A review on satellite image processing of landslide detection *Artificial Intelligence and Machine Learning in Satellite Data Processing and Services* (Singapore: Springer) , *123*–129 DOI: https://doi.org/10.1007/978-981-19-7698-8_14

[9] Sarker I H 2021 Deep Learning: A Comprehensive Overview on Techniques, Taxonomy, Applications and Research Directions. *SN Computer* **2**, 420 DoI: https://doi.org/10.1007/s42979-021-00815-1

[10] Sharma, S. and Kumar, S., 2022. The Xception model: A potential feature extractor in breast cancer histology images classification. ICT Express, 8(1), pp.101-108.

[11] Kumar, S. and Sharma, S., 2022. Sub-classification of invasive and non-invasive cancer from magnification independent histopathological images using hybrid neural networks. Evolutionary Intelligence, 15(3), pp.1531-1543. SDD

[12] Pritt M, Chern G 2017 Satellite Image Classification with Deep Learning *IEEE Applied Imagery Pattern Recognition Workshop (AIPR)* (USA : Washington) p 1-7 DOI : 10.1109/AIPR.2017.8457969

[13] Lei T, Zhang Y, Lv Z , Li S, Liu S & Nandi A 2019. Landslide inventory mapping from bitemporal images using deep convolutional neural networks. *IEEE geoscience and remote sensing letters*. **16**(6) 1-5. DOI : 10.1109/lgrs.2018.2889307.

[14] Martire D, Confuorto P , Frezza A, Ramondini M, Lopez A, Rosso M P, Sebastianelli A and Ullo S 2018 X- and C-band SAR data to monitoring ground deformations and slow-moving landslides for the 2016 Manta and Portoviejo earthquake (Manabi, Ecuador). IEEE international conference on Environmental energy , 1-6

[15] Angelino C V ,Cicala L ,Parrilli S, Fiscante N, and Ullo S L 2020 Post-Fire assessment of burned areas with Landsat-8 and Sentinel-2 imagery together with MODIS and VIIRS active fire products, *2020 IEEE Int. Geoscience Remote Sensing. Sympo*,(USA: Waikoloa) p 6770–6773 DOI:10.1109/IGARSS39084.2020.9324512

[16] Napoli M D, Marsiglia P, Martire D D, Ramondini M, Ullo S L, and Calcaterra D 2020 Landslide susceptibility assessment of wildfire burnt areas through earth-observation techniques and a machinelearning-based approach, *Remote Sensing*. **12(**15) 2505

[17] Westen, C.J.. (2000). Remote sensing for natural disaster management. *International Archives of Photogrammetry and Remote Sensing* **33,** 1609-1617

[18] Sharma A, Sharma K K , Sapate S G 2022 A prototype model for detection and classification

of landslides using satellite data *4th International Conference on Intelligent Circuits and Systems*, *Journal of physics: conference series*, **2327**, IOP Science, DOI - 10.1088/1742-6596/2327/1/012029

[19] Gu Y, Wang Y, Li Y 2019 A Survey on Deep Learning-Driven Remote Sensing Image Scene Understanding: Scene Classification, Scene Retrieval and Scene-Guided Object Detection. *Appied. Science.***9**, 2110. https://doi.org/10.3390/app9102110

[20] Ji S, Dawen Y, Shen C, Li W and Xu Q 2020. Landslide detection from an open satellite imagery and digital elevation model dataset using attention boosted convolutional neural networks. *Landslides.* **17.** DOI https://doi.org/10.1007/s10346-020-01353-2

[21] Kirschbaum D, Stanley Tand Zhou Y 2015 Spatial and temporal analysis of a global landslide catalog. *Geomorphology* . **249**. DOI : 10.1016/j.geomorph.2015.03.016.

[22] Yang S, Yuzhu W, Panzhe W, Jingqin M, Shoutao J, Xupeng Z, Zhenhua W, Kaijian W, and Yueqin Z. 2022. Automatic Identification of Landslides Based on Deep Learning *Applied Sciences* **12** (16) 8153.DOI https://doi.org/10.3390/app12168153

[23] Liu T, Chen T, Niu R and Plaza A,2021 Landslide Detection Mapping Employing CNN, ResNet, and DenseNet in the Three Gorges Reservoir, China . *IEEE Journal of Selected Topics in Applied Earth Observations and Remote Sensing*,**14**, 11417-11428 doi: 10.1109/JSTARS.2021.3117975

[24] Fu R, He J, Liu G, Li W, Mao J, He M and Lin Y. 2022.Fast Seismic Landslide Detection Based on Improved Mask R-CNN *Remote Sensing* **14**(16) 3928. DOI: https://doi.org/10.3390/rs14163928

[25] Ullo S L, Amrita M, Sebastianelli A, Ahamed S, Kumar B, Dwivedi R and Sinha G 2021. A New Mask R-CNN Based Method for Improved Landslide Detection. *IEEE Journal of Selected Topics in Applied Earth Observations and Remote Sensing.* 14,3779-3810 DOI : 10.1109/JSTARS.2021.3064981.

[26] Ghorbanzadeh O, Gholamnia K and Ghamisi P 2022, The application of ResU-net and OBIA for landslide detection from multi-temporal sentinel-2 images. *In Big Earth Data*; 1–26.

Int. J. Advanced Networking and Applications
Volume: 15 Issue: 04 Pages:100-200 (2023) ISSN: 0975-0290 (Special Issue – ASCIS 2023)

Comprehensive Survey of Machine Learning Techniques for Ear Recognition System

Ulka P. Patil [1]
Assistant professor, Department of Computer Science
Vidnyan Mahavidyalaya, Malkapur(MH), India.
maheshulka@gmail.com
Dipak.N.Besekar[2]
Professor, Department of Computer Science
Shri Shivaji College, Akola, Maharashtra, India
dnbesekar@gmail.com
Suhas G. Sapate[3]
Professor, Department of CSE, Sanjeevan
Engineering and Technology Institute, Panhala
416201
suhasgsapate@gmail.com

----------ABSTRACT----------

Ear biometrics is non contacting and so it can be applied for identification of a human at a distance, making it a helpful supplement to facial recognition, law enforcement, crime investigation etc. Although ear detection and identification systems have rapidly improved to a certain extent, their success is still confined to specific circumstances such as an occlusion of hair. A major challenge for researchers nowadays is to recognize human based on ear with pose variations and occlusion.

This summarized survey aims at identifying the research gap which is helpful in proposing a novel machine learning approach as a pathway for budding researchers.

Most of the selected articles have common and a wide variety of preprocessing, feature extraction techniques such as SIFT, Gabor filter, shape features are gain. Performance of all surveyed methods is evaluated for comparison purposes using evaluation metrics such as Precision, Recall and Accuracy.

The challenges before an effective Ear recognition system are discuss. This comprehensive survey article will be useful for identifying research gaps as a pathway for the same researchers to get the idea regarding of Ear recognition system which further can be transformed into a marketable product. This article at the end presents the prototype model.

Date of Submission: 18 October 2023 Date of Acceptance:

1. INTRODUCTION

1.1 History and background of Ear Biometrics

In this world of uncertainty, reliability is a significant issue. The influence of biometrics in reliability has extended impetus due to its numerous advantages. In present day society, the biometric method based verification has become the most consistent and usually used method for automated individual identification in to variety of civilian applications. With the widespread usage of social media apps like Facebook, Google, Skype, WhatsApp, Instagram, Twitter, and Telegram on smart phones and the fact that most financial transactions are now done online (through online banking), it is crucial to establish a person's identification with accuracy. A trustworthy method of identifying persons is also needed for a number of law enforcement and military applications, for example decisive whether a person is a potential threat or a criminal suspect. Accomplishing higher recognition concerts in uncontrolled circumstances along the various biometric traits come to be a new class of biometrics due to their characteristics. In biometrics, various methods of identifying human beings are used: fingerprints, face, voice, iris, gait, etc. The reason for the particular interest in biometrics is the practicality for consumers and the difficulty of hacking compared to passwords and cards. The biometric systems categorized into two parts, active and passive. For example, face biometric is an active biometric technique. This biometric has poor identification performance because to shape and expression variance with time, as well as further difficult concerns like changing lighting, poor contrast, and user resistance. Several instances of forensic uses include Revolutionary identification, Criminal search, and mislaid person identification and on the other hand cyber commerce, law-enforcement agency, border crossing control, device access control, internet access, ATM security, driving license, social security, welfare disbursement, and everyday attendance are a number of emerging cases of civilian applications [1].

1.2 Significance of Ear as Biometric

Similar to how a facial image is easily acquired with a low resolution camera, ear images can also be obtained with little to no human input. The best emerging biometric method for human recognition has researchers' attention due to the ridiculousness of face recognition issues in comparison to a previous Ear shape. One of the most sophisticated and a unique use of human identification is Ear-based identification. The Ear has unique physiological and structural aspects. In surveillance systems, for example, it is

Int. J. Advanced Networking and Applications
Volume: 15 Issue: 04 Pages:100-200 (2023) ISSN: 0975-0290 (Special Issue – ASCIS 2023)

easier to recognize and identify an Ear than an eye. As a person ages, their ear undergoes little modifications. More crucially, ear biometrics can be passive since the person is not required to actively participate in the entire process and may not even be aware that the form of identification is being used. Technology for ear recognition may also be useful in the biometric toolbox. Using investigation videotapes to evaluate defendants in gas station robberies who had covered their faces but not their ears, forensic investigators in the Netherlands, for instance, used the Ear biometric to identify the suspects [1]. When French criminologist and biometrics researcher Alphonse Bertillon proposed utilizing the form of an individual's ears to identify criminals in the 1890s, the concept of ear biometrics first emerged [2]. A human Ear finds a constant structure which quite change significantly as an outcome of aging and perhaps regarded as one of the best unique human biometric traits since it possesses all of the aforementioned characteristics of uniqueness, collectability permanence and universality [3]. Human ears are unaffected by changes in facial expression, have a uniform hue, and have a constant shape from the age of eight to seventy and this is in contrast to the face. [4].

1.3 Ear Structure

Maternity causes the human ear to develop early, and by the time of delivery, it is fully developed. A sensitive part of the human body is the ear [5]. Sound detection, transmission, and transduction are its key concerns. Another crucial task carried out by the human ear is maintaining balance, and it has the distinctive structure seen in Figure 1 to accomplish this task. There are numerous forms and sizes for the outer ear. This framework contributes to the distinctive appearance that each of us has. Technically, the auricle or pinna is the term used to describe the exterior ear. Skin and bones make up the outer ear. The tragus, helix, and lobule are the three separate components of the outer ear. Because they vary from person to person in terms of structure, appearance, and relative positions, these structural cartilage formations can be used for identity and recognition.

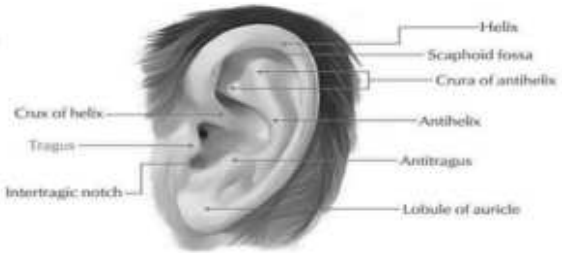

Figure 1. Ear Structure

1.4 Ear Recognition System

Figure 1 displays the block diagram for Ear identification system with different states. An appropriate camera is used to acquire images. Pre-processing is used to improve the image's quality. Preprocessing allows us to eliminate undesirable distortions and enhance certain qualities that are essential for the specific application we are developing. Those characteristics could vary according to the application. It will take less time to train models and take less time to infer models when image preprocessing is used. Decreasing the size of the input images will considerably decrease the amount of time it takes to train the model if the input images are extremely huge. Image segmentation is a technique for splitting up a digital image into different groupings of pixels called "Image Objects," which simplifies image analysis and decreases the complexity of the image. There are many image segmentation techniques available to isolate and classify a certain collection of pixels from the image. The most important process is feature extraction, which entails converting unprocessed data into numerical features that can be analyzed while maintaining the accuracy of the data in the original data collection. Compared to using machine learning on the raw data directly, it produced better outcomes. Classifiers classify data by analyzing the numerical properties of distinctive image features. Usually, classification algorithms have two processing stages: training and testing. However, it is fairly clear to examine the structure of the human ear before we attempt to understand various processing on the ear. The most important thing to process and analyze an image is to capture it. This is called Image Acquisition. The block diagram of common ear identification is shown in Figure 2.

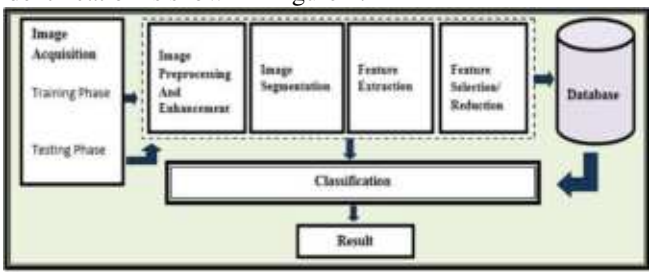

Figure 2. Ear Recognition System

1.5 Motivations

The rapid increase in popularity of biometric identification tools is largely due to how easily they solve the majority of concerns with standard identification methods. Ear biometric trait has various features such as unique structure, small shape compared to face, uniform color, and persistence over long period as well as higher user acceptance. That's why, eat biometric gains more attention by the research community. A remarkable progress has been reported in the related work over last two decades. However, major challenges of the ear biometrics include poor recognition performance due to illumination changes, low contrast, partial occlusion, and presence of noise.

1.6 Objectives

In this article, various feature extraction methods and machine learning algorithms are discussed with their accuracy. Basic preference of this article is to find out a proper machine learning algorithm for human ear identification and to extract significant features towards improving accuracy. Accuracy and performance of all surveyed approaches are highlighted for comparison purposes. This work is proposed to provide the research scholars a present status further scope of machine learning techniques in ear biometrics. In order to develop and implement new approaches and towards future research directions for accurate feature extraction methods, scholars will get the combined information of machine learning algorithms in this single article. This article will definitely be helpful to improve the accuracy with selecting modified feature extraction techniques and by improving the accuracy of classifiers with modified classification algorithms.

The specific objectives of this research work are as follows,

Int. J. Advanced Networking and Applications
Volume: 15 Issue: 04 Pages:100-200 (2023) ISSN: 0975-0290 (Special Issue – ASCIS 2023)

- To summarized the technical performances of the latest articles on ERS using machine learning techniques.
- To discuss the parameters or factors affecting the performance of ERS.

1.7 Article selection strategy and organization of article

For this study we identified several key concerns regarding this work, which encompass

1. Selecting appropriate and latest articles for last few years
2. Identify common ground and parameters for evaluating and comparing performances.
3. Use common strategy to compare different techniques.

For this comprehensive survey, we have chosen 11 machine learning techniques for ear biometrics from the sources such as peer reviewed international journals and proceedings of international conferences, book chapters from indexed books and some official websites to discuss in this article. In all we have selected 11 research articles based on machine learning algorithms for automatic and semiautomatic classification and recognition of human ear. Enough care is taken to ensure that the research articles are covering the variety of dataset from various countries all over the world. This will allow the researcher to understand the changing trend of datasets and techniques so that a new robust technique can be developed to identify the human from any test dataset accurately.

The rest of the article is organized as follows. The databases used by all the authors in selected articles are described in Section 2. Section 3 takes an overview of wide variety of the selected articles covering machine learning techniques for ear recognition. Principal findings and observations noted from all the articles are mentioned in Section 4. Based on the gap identified in section 4, a new approach for ear recognition is proposed in Section 5 and Section 6 concludes this article.

2. AVAILABLE DATABASES

This section includes a number of databases that have been utilized in articles considered in this study research. The majority of these datasets can either be shared publicly or with a license.

WVU database [6]: The West Virginia University (WVU) ear dataset includes 60 multi-sequences and 460 video sequences for roughly 400 individual people. Every video starts with the subject's left profile and ends with their right profile. In this dataset, there are individuals who wear earrings, eyeglasses, and partially occluded ears.

USTB Databases [5]: For academic study, the University of Science and Technology Beijing (USTB) databases 5 are accessible [USTB 2005].USTB I: 180 pictures of the 60 volunteers. Three photographs were taken of each subject: (a) a regular ear image; (b) an image rotated by a modest amount; and (c) an image taken in a different lighting scenario. The dataset comprises of 308 photographs of 77 volunteers from USTB II. Using the definition of the profile view (0°) as the angle at which the CCD camera is at right angles to the ear, the following four images were captured for each subject: (A) the profile image; (B) two photographs taken at different angles of 30° and 30°; and (C) one image taken with varying lighting. 79 participants in USTB III, IV, and USTB A camera setup with 17 CCD cameras was used to take pictures of 500 volunteers' faces and ears from various angles. The cameras were spaced 15 apart around the subject.

UMIST Database [6]: 20 persons are depicted in 564 photographs from the UMIST Face database 8 gently turning their heads from the front to the profile. A modest database called UMIST is freely accessible to the general public [Graham and Allison 1998; UMIST 1998]. The UMIST database has only been utilized in investigations involving ear detection in the literature.

IIT Delhi ear image database [7]: A database of ear images gathered by IIT Delhi students and staff in New Delhi, India, can be establish in the IIT Delhi Ear Image Database. Using a straightforward imaging setup, this database was collected at the IIT Delhi campus between October 2006 and June 2007 (continuously). With the use of a straightforward imaging setup, all images are taken remotely (non-contact) and indoors. There are currently 121 different subjects in the database, with each subject having at least three pictures of her ears. The database only contains people between the ages of 14 and 58. All 471 images in the database are in the JPEG format and are sequentially numbered with an integer ID/number for each user. The ear database recently expanded to include 754 automatically cropped and standardized images of the ears from 212 individuals.

The University of Notre Dame (UND) databases 1 [8]: For face and ear modalities, the UND database contains numerous collections. Collection E contains 464 left face side profile (ear) images from 114 subjects; Collection F contains 907 right face side profile (ear) images from 286 subjects; Collection G contains 738 3D profile (ear) images from 235 human subjects; and Collection J2 contains 1800 3D profile (ear) images from 415 human subjects. All of these collections were taken between 2003 and 2005.

Annotated Web Ears (AWE) database [9]: 100 subject photos may be found in the AWE dataset. The AWE dataset was compiled from web photos of well-known people of all ages, genders, and ethnicities, including actors, musicians, and politicians. A tight crop was applied to 10 photos for each subject. Every image has annotations, which are likewise kept in JSON files with the images.

3. LITERATURE SURVEY

We studied a number of ear recognition systems in all of the articles under this survey. The short comprehensive summary of the few selected articles is presented as below.

Iannarelli's system, which was created for the first time in 1949 [3], is one of the earliest ear recognition systems. Using the Voronoi neighbourhood graph, they created a classification invariant under affine transformations. They illustrated the issue of hair occlusion and suggested using a thermogram image to detect an ear through surface heat. However, because they did not include a scheme evaluation, the study was not comprehensive.

Asmaa Sabet Anwar et al [8] described a novel method for ear detection based on the extraction of geometrical data such as shape, mean, centroid, and Euclidean distance between pixels. All photos were initially pre-processed with the same size, and the ear was then detected using the snake contour detection model. The photos were then converted to

Int. J. Advanced Networking and Applications
Volume: 15 Issue: 04 Pages:100-200 (2023) ISSN: 0975-0290 (Special Issue – ASCIS 2023)

binary format after applying a median filter to reduce noise. After that, it made some picture enhancements using a clever edge detecting algorithm, computed the major boundary, and then created a distance matrix. Following this effort, the picture features were extracted. Last but not least, nearest neighbours by absolute error distance was used to classify the retrieved features. About 100 images as training, 50 images as testing from the IIT Delhi ear database, version 1.0, are used in the experiment. The author noticed in the related work that most scientists used their own databases rather than conventional databases due to accuracy. About 98% of the results from this investigation were obtained with greater accuracy. In order to evaluate the efficiency of this system in the future, it was planned to employ more datasets and increase the quantity of ear images. We will attempt to address issues like the ear's drop-down hair, which partially conceals them, in our future work.

M. Khamiss et.al. [10], Iterative Closest Point (ICP) and Stochastic Clustering Method (SCM) are combined to form the improved algorithm known as ICPSCM, which is recommended for ear recognition. These two strategies suggested reconstructing the ear surfaces from several scans, localizing locations, and using clustering techniques to achieve the best classification planning. The ICP algorithm and the SCM method are portable methodologies used in this study for feature extraction and pose variation in ear identification, respectively. The SURF Technique is used in this work to extract features. The proposed Multilayered Neural Network (MNN) strategy used in ear identification methods is used for ear classification and identification. The effectiveness of the analysis is defined by the criteria that were considered at various stages. The design of an ear identification system introduced a fully integrated sense of biometrics and integrative closest point based on an ear surface matching approach with features. The concept behind the ear identification technique blends the outcomes of ear matching using neural classifiers that focused on the outer ear points, data from the profile and shape of the ear, and density data generated from macro features. Integrative nearest points are used to start identifying the ear after the ear location has been extracted from the input image. This study makes use of the IITK, WPUTED, and USTB datasets. For this study, 500 images from each dataset are chosen. They draw their conclusions from the implementation phase's outcomes, including FAR and FRR. The experimental outcome in this work demonstrates 96.12% accuracy.

R. Dhivya et.al. [11], worked on Edge Detection and Feature Extraction for Ear Authentication. An enhanced technique for feature extraction, recognition, and ear edge detection is presented in this work. The accuracy of this work, which is carried out on the ear in a random orientation, is superior to that of the leading approaches at the moment. The accuracy of recognition is improved by eliminating noise from obtained ear shots and applying a novel new technique to work with online images. The Region of Interest used in this work is segmented using an active contour algorithm and a cunning edge detector, and the ear contours are then used for authentication. The entire procedure is carried out in Matlab. This method can be used to capture and handle the moving person's ear, and it can be drawn out more precisely than the current one. This software implementation for Ear Verification with the resulting steps of image acquisition, preprocessing, contour tracking, edge detection, feature extraction, and authentication is obtained in an efficient manner for the ROI. In this study, it can be expanded to match the inside curve of the ear and extract features from the inner part of the ear edge. For this investigation, the complete methodology was used on just one image. As a result, they did not find accuracy in this paper. Future implementation of any other method besides the clever edge detection method is within the purview of this study.

K. Mohanapriya et.al. [12], represented Ear Recognition by Feature Extraction using Force Field Transformation. This study identifies the use of an Ear Visual Biometric as a measure of identification for the Teaching Management System in Universities and Colleges. Teachers who use this study to instruct their pupils have a greatly reduced burden, and the system as a whole enhances the integrity and controllability of the data. For higher performance than existing edge detection algorithms, in this work, ear detection and recognition is carried out utilizing Feature Extraction techniques such Force Field Transformation and Chord Point Detection Algorithm. This technique was successful in taking advantage of the increase in test and attendance at lectures and exams. In this investigation, the force field method yields a classification accuracy rate of 99.2%.

Ahmed Kawther Hussein [13], analysed the performance of two classifiers for the detection of ears, one trained to execute HOG functions and the other to perform LBP functions. A dataset, the number of hidden neurons, and the activation function are all inputs in this study. In the first stage, the data is split into training and testing, and in the second stage, HOG and LBP are extracted. Afterwards in third step Normalize Train an ELM based on HOG, he call it ELM- HOG using Train and ELM based on LBP. The last step is to test an extreme learning machine - HOG using testing data and test extreme learning machine -LBP using testing data and then return testing accuracy. He used the dataset to include 180 images of 60 subjects, both students and teachers from USTB from 3 sessions in July and August 2002. The database includes images of the right ear from each subject. In this study to evaluate both HOG and LBP features, an ELM with a number of neurons equal to 10000 was created. The sigmoid function is used as an activation function. It was observed that the accuracy of HOG at 99.83% was superior to LBP with 99.87%. Future work is to examine the performance of other types of functions and use 3D images for the ears as input.

Bassam S. Ali et.al. [14], collected ear images from 100 test subjects, three right hand side using a 12- Megapixel digital camera under a steady lighting condition. In this work, an ear recognition system (ERS) with Match Region Localization (MRL) was applied. The MRL segmentation technique is used to pre-process and segment the captured ear pictures, which resulted in 96 sub images. The principle components analysis is applied to each segment individually in order to convert the segments into PCA spaces. Each segment is regarded as a unique image that represents a unique person according to the segments used. K-nearest

Int. J. Advanced Networking and Applications
Volume: 15 Issue: 04 Pages:100-200 (2023) ISSN: 0975-0290 (Special Issue – ASCIS 2023)

Neighbour algorithms and Euclidean distance calculations were used to categorize the data. The effectiveness of this method can be assessed using the FRR, FAR, and Recognition Accuracy metrics. (RA). The resulting algorithm is tested on additional freely available ear databases if users agree to cross-database comparisons. The MRL Ear Recognition System with PCA Recognition Accuracy of 97.07% and the other algorithm produced by Adeolu and Ademiluyi, with Recognition accuracy of 72.46%, performed better in this test than the ERS developed by Adeolu and Ademiluyi (2016). It was established from the trial that the system can function effectively as an identification system. The approach, method, or solution must be tested on an increasing number of photos, maybe more images from various datasets, and images with (hair-like) impediments on the ear, in order to be practically relevant.

Mangayarkarasi N et.al. [15], in their contour detection algorithm select a gray image as input. Setting a threshold number for Ear detection allows for the initial design of the masks for the ear image. The segmented final mask, which is in binary format, was obtained by convolving the mask with the gray picture. After applying the final mask to the input image, the bounding box then drawn around the ear portion. The bounding box was then drawn around the section of the ear after the final mask had been applied to the input image. Using Perceptive's bounding box dimensions, the ear is cropped, stored for feature extraction, and then the SIFT technique is utilised to identify the SIFT feature vectors. These feature vectors are saved for the conclusion after being extracted from each person's image during the training phase. This input test image goes through the same procedures as training images. The subject is identified using the Euclidean distance measure approach by assessing the SIFT vectors from both the training and testing phases. The two vectors are comparable if the space between them is as little as possible and thus, every person is recognized by using this value. With the Snake model some drawbacks like it do not solve the complete problem of finding contours in humans, since the method needs knowledge of the desired contour shape beforehand. As a result, they created a mask with 1s values starting at a threshold of 150 and increasing until the picture reached its maximum size. After that, the mask was convoluted, and the binary output of the segmented ear image was created. The bounding box is drawn around the ear after a subsequent application to the original RGB image to identify only the ear part. The ear portion is finally segmented out on its own and saved after learning the size of the bounding box. Reducing the feature values for better recognition systems will be the focus of future study.

Pre-processing and Feature Extraction in Ear Biometrics research work presented by Bhavani Petchiammal C et.al [16]. In this study, the RLBP algorithm and KNN classifier were utilized in conjunction with a straightforward technique for extracting ear information called Radon feature extraction to recognize objects. Image segmentation is done after image pre-processing to remove extraneous information from ear pictures. In this study's related work, a three-step technique was used that included a typical combinatorial feature selection algorithm, K-means clustering to reduce duplication, and a RELIEF filter to reduce irrelevancy. The RELIEF filter will provide training features with relevant values while eliminating the irrelevant features. The IIT Delhi database was employed for this study, and from it, 3 to 6 photographs of the same person's right and left ears were obtained. The median filter is utilized in this study to filter out undesired noise. 100 images from the dataset are used in this study's training set, and all 100 images are trained using the necessary pre-processing and feature extraction techniques. The system's estimation is provided with the use of a testing database that contains 46 photos. A classifier based on the KNN classifier is created, and it is then tested using Euclidean distance, to identify the ear images in the test and estimate datasets. The Radon feature extraction method has a higher accuracy rate while compared to RILBP. In order to accurately recognize a person in the future, classifiers like SVM, multi-class classifiers, and classifiers from neural networks were used.

Samik Chakraborty et.al [17], investigated the usage of ear-based biometrics for human identification. In this ear recognition system investigation, 10 people were used, and a geometrical solution was used to address the jewellery occlusion issue. When wearing no jewellery, the geometrical relationship between the image's points can be seen and determined. The information obtained in this way is noticeably close together. This information used to project a point from the area of the image that the jewellery has obscured. Following the discovery of this point, features that are similar to those in the original image are discovered. The tiny dataset meant that this had a 100% success rate. However, more research is required utilizing a larger database with additional objects, such as the existence of ear buds or hair and with dissimilar illumination experience.

Debbrota Paul Chowdhury et al. provided semantic ear feature reduction for source camera detection task [18]. By determining the source camera of the ear biometric photos, a semantic strategy to lowering this feature vector is debated in this study. The 36 energy components are a key component that is employed in the described study. This study also confirms that the presence of many different camera models lowers source recognition precision. The mechanism succeeds in classifying only a few distinct camera sources, and it is visible that it is now processing three sources. Before the bi orthogonal tunable wavelet filter is applied to the complete ear image for feature extraction, the ear image is divided into six blocks and the wavelet filter is applied to each block. This is done because jewellery, hair, or glasses may obscure some of the ear picture. The energy from each block is mined and used to produce the merged feature vector for the entire ear picture. Due to the lack of easily accessible datasets for camera source identification, the author combined three ear databases to create this. Three ear databases—IITDI, AMI, and WPUT—serve as the study's camera models I, II, and III, respectively. True positive, false positive, precision, recall, F-measure, the area under the receiver operating characteristic (ROC) curve, the area under the precision-recall curve, and accuracy are the parameters utilized in this study to gauge how well the system performs when the feature size is reduced. They chose 36 characteristics with the following performance metrics: True Positive (%) 99.3; False Positive (%) 0.4; Precision (%) 99.3; Recall (%) 99.3; F Measure (%) 99.3;

Int. J. Advanced Networking and Applications
Volume: 15 Issue: 04 Pages:100-200 (2023) ISSN: 0975-0290 (Special Issue – ASCIS 2023)

ROC Area (%) 100; PRC Area (%) 99.9; and Accuracy approximately 99.25%. The research is successful in identifying source cameras with significantly smaller feature sizes.

Abbas H. Hassin Alasadi et.al [19] proposed a machine learning approach for a human ear recognition system. The proposed system aims for use a probable skin detector to filter the ear image into skin and non-skin pixels. The static features of the ear are retrieved by using scale-invariant feature transform (SIFT). The initial image in the database and a new image are compared using the Euclidean Distance Measure (EDM). According to the three experiments presented in this research, the recognition rates for the various datasets when using the Gabor sampling filter method are 65%, 83% when using the Gabor mean feature extraction, and roughly 92% when using the SIFT feature approach in the proposed system. The enrolment phase and recognition phase are the two primary phases of the proposed system, which is a multistage procedure. Software called MATLAB is used to implement the suggested system. This study made use of the AMI ear database. In this study, the pre-processing algorithm is first used to an input side face image to produce an output ear color image. In the second iteration of the Morphological Operation algorithm closing operation. The third experiment tests a matching algorithm that determines if two provided data sets are similar or dissimilar. In the fourth experiment, the feature vector is used as the input for the identification mode algorithm, which is then used to verify the data. The accuracy rate of the proposed method decreases with an increase in number. In order to examine how ear print evidence is used in criminal investigations, the FearID research project was started in 2002 and ran until 2005. In this project, the usefulness of ear prints at crime scenes is investigated. In all 1229 donors were used in this project. From three different countries, three left and three right ear prints were obtained. The same error rate, which was 4% for lab-quality photos but increased to 9% for print versus mark comparisons, was employed for evaluation [28]. In Table 1, a summary of a few chosen articles from relevant work is listed.

4. PRINCIPAL FINDINGS

Basic preference of all selected research articles was to improve the performance on Ear Recognition, are analysed with the help of SIFT and machine learning techniques for the classification. During this study we came across different findings which are recorded for future research directions.

4.1 Challenges which are discussed

Many researchers have performed various automated systems for human ear identification with an additives technique and trying to increase the accuracy. The furthermost noticeable ones are in the data collection stage, where it is problematic to even crop an image containing an ear.

Table 1: Summary of some selected articles from related work

Referenc / Author	Preprocessing/ Segmentation	Feature Extraction Method	Classifier	Dataset	Performance metric, percentage
[24], Li Yuan, Zhichun Mu 2014	Preprocessing: ear detection using modified Adaboost algorithm and ear normalization Using Active Shape Model.	Gabor Feature Extraction	Full Space Kernel Discriminant Analysis	USTB dataset3 79 UND collection J2 150 subjects	96.46% 94.00%
[9],Asmaa Sabet Anwara et.al 2015	Preprocessing : Gaussian Filter, Median Filter, Global Threshold, Canny Edge detection	Geometrical Features	Naive classifier, nearest neighbor (distance type: Euclidean) and KNN (distance type: minimum absolute difference).	IIT 150	98.00%
[21], Lamis Ghoualmi et.al 2016	Artificial bees for ear image enhancement	scale in-variant feature transform (SIFT)	Euclidean Distance	IIT Delhi USTB USTB 2	99.6% 97.15% 94.79%
[15], Mangayarkarasi N,*, RaghuramanG, Nasreen A 2019	Preprocessing : resize the image and convert it into grayscale Segmentation : Contour Detection Algorithm	SIFT	Euclidean Distance	Own Dataset 545	96.00%
[19],Abbas H. Hassin Alasadi, Dheyaa Abbood Chyad 2021	Preprocessing : convert RGB to YCbCr, binary image conversion, Morphological Operation	SIFT	Matching algorithm	AMI 175	92.00%

Int. J. Advanced Networking and Applications
Volume: 15 Issue: 04 Pages:100-200 (2023) ISSN: 0975-0290 (Special Issue – ASCIS 2023)

Selection of proper feature extraction techniques is one of the interesting, complex and long-lasting domains of research from last two decades due to:

- As the number of dimensions increases, the feature extraction method will not work effectively.
- There is no special standard rule for validating classification results.

The exact performance rates of the study on any given dataset are merely a proof-of-concept; they are only of secondary significance. The progress of ear recognition system research is utterly dependent on the availability of new and more difficult public databases. New datasets for benchmarking Ear Biometrics should be compiled and published in order to maintain research in the field. Such a dataset might, for example, include left and right ears from the same person from different angles, as well as higher demographic variances. In addition to accelerating the pace of ear biometrics research, new datasets also present an opportunity to advance associated systems. In addition to the requirement for more difficult datasets, there are a few notable concerns with ear biometrics that are rarely brought up.

Most pre-processing algorithms are created to work on a single reference image before being applied to all the other datasets, which results in poor results. These concerns must be taken into consideration while creating new pre-processing methods.
Feature extraction algorithms cannot work well if dimensionality rises hence, there must be proper trade-off between classification accuracy and number of features. Using this literature survey our future work will highlight on accuracy improvement by extracting the suitable features from the human Ear, feature selection and integration of different classification algorithms to advance the classification results and try to implement an accurate system for ear recognition.

4.2 Challenges which are not discussed

Following are some of the points which are not discussed in this article due to limitation on text length.

- Reliable milestone detection in occlusion- and pose-varying ear pictures. Particularly the detection and masking of occluded regions would be an important contribution for ear recognition in surveillance scenarios.

- Classification accuracy of different survey methods is varying, hence the need to design a more precise segmentation algorithm to classify Ear more accurately.

4.3 Gap identified

An active area of study within the biometric community is automatic identification recognition from ear images. Significant advancements have been achieved in the subject over the past few years; however there are still unresolved research issues and no system for commercial use has yet to be created. A major challenge in face biometrics was the discordance between form and expression, whereas in the case of ear biometrics, the shape and look are constant. Biometrics for human identification is sometimes required by forensic and criminal justice technology used in everyday life. Numerous techniques, including face and fingerprint identification, have shown to be highly effective in computer vision-based human recognition systems.

4. PROPOSED PROTOTYPE

The research gap identified in the Section 5 encouraged us to propose a new approach towards ear based human recognition system. The proposed system architecture depicted in Figure 5 provides a broad overview of all the system modules and the process flow from data gathering to classification. Initially, photographs of various people's ears were collected and stored in a database. Similar to this, various picture datasets of the human ear have been amassed online. This data set comprises of pictures of each person's right and left ears from three different angles: the front, the down, and the back. The suggested system's flow is depicted in the diagram below.

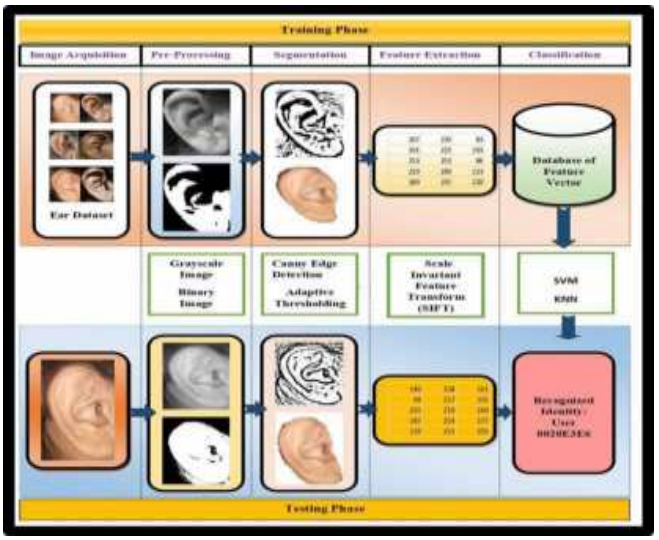

Figure 3.Proposed System architecture of Ear Recognition System

Step I: Image Acquisition

For the proposed method, a human ear dataset has been created. The basic idea of establishing this database was to simulate real scenes of real life. In this dataset the human ear image was taken at various angles of both right as well as left ear. The image acquisition step is the fundamental phase of every vision system. After the image has been captured, it is processed using a variety of ways to enhance its quality. Even by applying various image enhancing techniques, the proposed work might not be practical if the image was not

Int. J. Advanced Networking and Applications
Volume: 15 Issue: 04 Pages:100-200 (2023) ISSN: 0975-0290 (Special Issue – ASCIS 2023)

acquired properly. All of the photos in this work are in the .jpg format and have a 450 x 689 pixel resolution.

Figure 4. Some samples from the dataset

Step II: Pre-processing

Pre-processing is the ear recognition system's initial stage, in essence. It improves the images and gets rid of unwanted effects. Pre-primary processing's objective is to improve the image's quality so that we can analyse it more effectively [18, 29]. They must be standardized and cleaned up before being fed to machine learning (ML) techniques. Since the form in which an image is taken must be taken into consideration while writing a unique approach, when we acquire an image we typically renovate it into a form that enables a universal way to solve it, as demonstrated in the proposed system architecture. Pre-processing allows us to improve some qualities that are essential for the specific application we're working on while also smoothing out unwanted distortions. Various applications may require different person characteristics. Pre-processing makes sure that the image's essential characteristics are highlighted and that extraneous details, such noise, are removed. The two main types of picture pre-processing techniques are intensity-based and filter-based approaches [7].

Algorithm (1): Preprocessing Algorithm

Input: Side Face image

Output: Ear Binarized Image

Step 1: Select image from the dataset.

Step 2: Crop Ear Image from the above step.

Step 3: Resize the image.

Step 4: Convert the Resized image to a grayscale image.

Step 5: Convert the image from the previous step to Binary Image.

Figure 5. Algorithm of Pre-processing of Ear Image

The filtering technique can be used to improve or alter an image. You can use a filter, for instance, to highlight some components of an image while deleting others. Mean and median filters are used in filtering to smooth and reduce noise during image processing activities. For the purpose of enhancing the image for further analysis, some sharpening and edge enhancement techniques are also applied. Applications for the Log-Gabor filter include texture generation, image denoising, speech analysis, contour recognition, and picture enhancement. The sample ear images while applying Gaussian and median filter are shown in Figure 6.

Figure 6. Ear image with Filter-based approach

Colour is not required in any of the ear biometrics articles we reviewed to recognize and understand an ear image. Grayscale can be suitable for identifying some objects. Due to the fact that colour images are more information-rich than black and white ones. The sample ear images while applying intensity-based approach are shown in Figure 7.

Figure 7. Ear image with Intensity-based approach

Histogram normalization is another intensity-based technique. A new architecture for ear biometrics was introduced by Lamis Ghoualmi et al. [22]. To show more realistic 2D ear images with higher-detail content and 97.15% accuracy, they used a method for enhancing the contrast of ear images based on gray-level mapping with the ABC algorithm.

Step III: Ear Segmentation

In automated ear identification algorithms, ear segmentation is crucial. Image segmentation's primary goal is to make the image simpler for easy examination [22]. Segmentation is the process of giving labels to pixels, to put it simply. The system for object identification that is suggested employs a boundary-based strategy. Algorithms like point detection, edge detection, line detection, and others use a boundary-based approach to recognize the edges of unique pixels and isolate them from the rest of the picture. Thanks to adaptive thresholding, which sets a threshold value for each fractional section of the image, each fractional portion of the image has a distinct threshold value. This method provides the highest level of accuracy and is best suited for the following action.

Step IV: Feature Extraction

A large matrix is just an image. Features are traits which are mathematically retrieved from this matrix to serve as the foundation for additional processing, analysis, or recognition. Feature extraction is the process of identifying an image's key characteristics that help identify it specifically. Because just a limited subset of features is utilized to represent the complete image, the goal of feature extraction is dimensionality reduction [30]. Shape, colour, texture, and other features of an image that can be taken into account during feature extraction. The bulk of review studies used the SIFT Algorithm to detect and analyse the picture local features, such as rotation, scale, and viewpoints in computer

Int. J. Advanced Networking and Applications
Volume: 15 Issue: 04 Pages:100-200 (2023) ISSN: 0975-0290 (Special Issue – ASCIS 2023)

vision, based on their accuracy and processing complexity. Key characteristics are the output to identify the ear. For the purpose of recognition, it works better. The comparative analysis of reviewed articles is as follows.

Table 2. Comparative analysis of different Feature Extraction Techniques

Feature Extraction Techniques	**Accuracy**	**Computational Complexity**
Orthogonal log Gabor Filter	Moderate	Moderate
HOG and LBP	Average	Good
Geometrical Feature Extraction	good	Average
SIFT	Average	Average
Radon Feature Extraction and Texture based Feature	Moderate	Moderate

Step V: Storing Feature vector in a Database

In the database Feature vectors stored and then compared with testing phase outcome.

Step VI: Classification

The extracted features mentioned in Step V are applied to the machine learning algorithms for classification. In this research survey articles mostly used two machine learning algorithms known as SVM and KNN [31, 33]. The classification technique used as the last phase of the suggested methodology is a support vector machine (SVM) algorithm. The model was built faster using SVM, a well-known supervised machine learning method [23, 32].

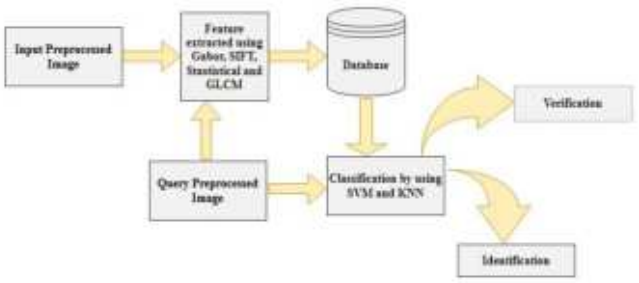

Figure 8. Ear feature extraction and classification

6. CONCLUSION

The primary objective of this comprehensive survey is to highlights challenges regarding design an automatic Ear Biometric System that can achieve better recognition performance in the uncontrolled scenarios. It can be used for real-time biometrics applications. In this paper we have taken the overview of a few selected research articles on ear recognition system using machine learning algorithms. The summary of the different techniques is enclosed in the table for better single view reading. The various classifiers are considered for comparison using a common ground of performance to the extent possible. The performance and accuracy of various methods enlisted may be useful for comparison and future direction purposes. The observations and lacunas found are enlisted properly. The research gap identified is then stated. Various methods proposed by researchers in literature reveal that there is still a research gap to design and develop a more accurate method of Machine Learning for Ear Biometric System by improving techniques of image processing pipe-line. At the end, the new approach for ear recognition system proposed with an altogether new dataset. The work on this proposed method to yield better classification accuracy is in progress.

In order to advance the accuracy of the classification, enhancement of the current classifier and selection of different classification techniques known like ensemble learning can be the future scope of research for the Ear Recognition System.

7. REFERENCES

1. Partha Pratim Sarangi, Bhabani Shankar Prasad Mishra, Satchidananda Dehuri (2018), ―Fusion of PHOG and LDP local descriptors for kernel-based‖, Springer Science+Business Media, LLC, part of Springer Nature,DOI:10.1007/s11042-018-6489-0, 2018
2. A. Bertillon, ―La Photographie Judiciaire, Avec un Appendice sur Classification l' identification Anthropométriques‖, Technical Report, Gauthier-Villars, Paris, France, 1890.
3. A. Iannarelli, ―Ear Identification‖, Paramount PublishingCompany, Freemont, California, 1989.
4. Marcolin F, Vezzetti E, ―Novel descriptors for geometrical 3D face analysis‖, Multimedia Tools & Applications, 76(12):13805–13834,DOI:10.1007/s11042-016-3741-3,2017
5. Ayman abaza et.al, ―A Survey on Ear Biometrics‖, ACM Computing Surveys, Vol. 45, No. 2, Article 22, DOI 10.1145/2431211.2431221 , February 2013
6. Aimee Booysens [1] and Serestina Viriri, ―Exploration of Ear Biometrics Using EfficientNet‖, Hindawi, Computational Intelligence and Neuroscience, Article ID 3514807, 14 pages, https://doi.org/10.1155/2022/3514807 ,2022
7. https://www4.comp.polyu.edu.hk/~csajaykr/IITD/Database_Ear.htm#:~:text=The%20IIT%20Delhi%20ear%20image,using%20a%20simple%20imaging%20setup.
8. Susan El-Naggar, Ayman Abaza, Thirimachos Bourlai, ―Ear Detection in the Wild using Faster R-CNN Deep Learning‖, IEEE/ACM

Int. J. Advanced Networking and Applications
Volume: 15 Issue: 04 Pages:100-200 (2023) ISSN: 0975-0290 (Special Issue – ASCIS 2023)

International Conference on Advances in Social Networks Analysis and Mining (ASONAM),2018

9. Asmaa Sabet Anwara, Kareem Kamal A.Ghanyb, HeshamElmahdy, ―Human Ear Recognition Using Geometrical Features Extraction‖, International Conference on Communication, Management and Information Technology ICCMIT 2015
10. M. khamiss*, S. Algabary, Khairuddin Omar, Md. Jan Nordin and SitiNorul Huda S Abdulla, ―Ear Identification Based on Improved Algorithm of ICPSCM‖, Journal of Applied Science 15(5):815.820, ISSN 1812-5654,2015
11. R. Dhivya1, R. Prakash2, ―Ear Authentication Using Edge Detection and Feature Extraction‖, ISSN:1995-0772 , Published BYAENSI Publication EISSN: 1998-1090, Published BYAENSI Publication EISSN: 1998-1090 ,http://www.aensiweb.com/ANAS (17): pages 89-94, 2016
12. K. Mohanapriya, Mr. M. Babu, ―Ear Recognition by Feature Extraction Using Force Field Transformation‖, International Journal Of Engineering And Computer Science ISSN:2319-7242 Volume 6 Issue 3 March 2017, Page No. 20742-20750 Index Copernicus value (2015): 58.10 DOI: 10.18535/ijecs/v6i3.61,2017
13. Ahmed Kawther Hussein, ―Histogram of Gradient and Local Binary Pattern with Extreme Learning Machine Based Ear Recognition‖, JOURNAL OF SOUTHWEST JIAOTONG UNIVERSITY, Vol. 54 No. 6, ISSN: 0258-2724, DOI : 10.35741/issn.0258-2724.54.6.31, Dec. 2019
14. Bassam S. Ali, Osman Nuri Ucan, Oguz BAYAT, ―Development of a Enhanced Ear Recognition System for Personal Identification‖, 5th International Conference for Convergence in Technology (I2CT) Pune, India. Mar 29-31, 978-1-5386-8075- 9/19/$31.00 ©2019 IEEE, 2019
15. Mangayarkarasi N , Raghuraman G, Nasreen A,―Contour Detection based Ear Recognition for Biometric Applications‖, International Conference On Recent Trends In Advanced Computing 2019, 10.1016/j.procs.2020.01.016,2019
16. Bhavani Petchiammal C1, Chithra P2, Ramesh P3, SowmyaLakshmi.R4, ―Preprocessing and Feature Extraction in Ear Biometrics‖, ISSN: 0976-8491 (Online) | ISSN: 2229-4333 (Print), IJECT Vol. 10, Issue 2, April - June 2019
17. Samik Chakraborty, Anumita Mitra, Sanhita Biswas and Saurabh Pal, ―Ear Based Biometric Analysis for Human Identification‖, Modelling and Simulation in Science, Technology and Engineering Mathematics, Advances in Intelligent Systems and Computing 749, https://doi.org/10.1007/978-3-319-74808-5_48, Springer Nature Switzerland AG 2019
18. Debbrota Paul Chowdhury,Sambit Bakshi,Pankaj Kumar Sa,,Banshidhar Majhi,―Semantic ear feature reduction for source camera identification‖, Multimedia Tools and Applications https://doi.org/10.1007/s11042-019-7665-6, Springer Science+Business Media, LLC, part of Springer Nature 2019
19. Abbas H. Hassin Alasadi, Dheyaa Abbood Chyad, ―Machine Learning System for Human Ear Recognition Using Scale Invariant Feature Transform", Artificial Intelligence & Robotics Development Journal Volume 1, Issue 1, pp 1-12, https://doi.org/10.52098/airdj.20217 ISSN: 2788-9696 January 2021
20. Suhas Sapate, Sanjay Talbar, Abhishek Mahajan, Nilesh Sable, Subhash Desai, Meenakshi Thakur, ―Breast cancer diagnosis using abnormalities on ipsilateral views of digital mammograms‖, Published by Elsevier B.V. on behalf of Nalecz Institute of Biocybernetics and Biomedical Engineering of the Polish Academy of Sciences, https://doi.org/10.1016/j.bbe.2019.04.008,2019
21. Ghoualmi, L., Draa, A., & Chikhi, S, ―An ear biometric system based on artificial bees and the scale invariant feature transform‖, Expert Systems with Applications, 57, 49–61. doi: 10.1016/j.eswa.2016.03.004, 2016.
22. Shivaji D. Pawar, Kamal Kr. Sharma b, Suhas G. Sapate, Geetanjali Y. Yadav, ―Segmentation of pectoral muscle from digital mammograms with depth-first search algorithm towards breast density classification‖, https://doi.org/10.1016/j.bbe.2021.08.005,2021
23. M. Alva, A. Sri nivasa raghavan and K. Sonawane, "A Review on Techniques for Ear Biometrics," 2019 IEEE International Conference on Electrical, Computer and Communication Technologies (ICECCT), pp. 1-6, doi: 10.1109/ICECCT.2019.8869450, 2019
24. Li Yuan, Zhichun Mu, ―Ear Recognition Based on Gabor Features and KFDA‖, Hindawi Publishing Corporation e Scientific World

Int. J. Advanced Networking and Applications
Volume: 15 Issue: 04 Pages:100-200 (2023) ISSN: 0975-0290 (Special Issue – ASCIS 2023)

Journal Volume, Article ID 702076, 12 pages http://dx.doi.org/10.1155/2014/702076, 2014

25. Shivaji D. Pawar, Suhas G. Sapate, Kamal Kr. Sharma, ―Machine Learning Approach towards Mammographic Breast Density Measurement for Breast Cancer Risk Prediction: An overview.‖ ,Proceedings of the 3rd International Conference on Advances in Science & Technology (ICAST) , http://dx.doi.org/10.2139/ssrn.3599187,2020
26. Yuan L, Zhichun M, Zhengguang X., ―Using Ear Biometrics for Personal Recognition. Advances in Biometric Person Authentication‖, LNCS; 3781: 221-228,2005
27. J.D.Bustard, M.S.Nixon, ―Toward sun constrained ear recognition from two dimensional images‖, IEEE Transactions on Systems, Man, and Cybernetics—Part C 40(3) ,486–494,2010
28. Maha Sharkas, ―Ear recognition with ensemble classifiers; A deep learning approach‖, Multimedia Tools and Applications, Vol. 81, pp- 43919–43945 , https://doi.org/10.1007/s11042-022-13252-w ,2020
29. Samira Abdul-Kader Hussain[1], Huda Al-Nayyef[2], Bassam AlKindy[*3], Samar Amil Qassir[4,] ―Human Earprint Detection Based on Ant Colony Algorithm‖ , IJISAE, 11(2), 513–517, 2023
30. Rahila Ayoub[1], Dr. Ashish Oberoi[2,] ―Study of Ear Biometrics Based Identification System Using Machine Learning‖, International Journal for Research in Applied Science & Engineering Technology (IJRASET) ISSN: 2321-9653; IC Value: 45.98; SJ Impact Factor: 7.429, Volume 9 Issue XII Dec 2021.
31. Resmi K. R.[1], Shijo M. Joseph[2], Raju G.[1], Debabrata Swain[3], Om Prakash Das[4], Biswaranjan Acharya[5,] ―Ear Recognition Using Rank Level Fusion of Classifiers Outputs‖, iJOE – Vol. 19, No. 03, https://doi.org/10.3991/ijoe.v19i03.36831, 2022
32. Naveena M, G. Hemantha Kumar, ―Classification of Human Ear by Extracting Hog Features and Support Vector Machine‖, International Journal of Computer Applications (0975 – 8887) Volume 177 – No. 40, February 2020
33. Prashanth G.K., M.A. Jayaram, ―Cascaded KNN-BPN for Classification of Ears based on Shape Measures for Person Identification‖, International Journal of Computer Applications (0975 – 8887) Volume 124 – No.8, August 2015

Dr. Dipak Besekar, completed his MCA in 1990, MPhil in 2009. He completed his Ph.D. in Sant Gadgebaba Amravati University, Amravati in 2014 as a full-time research scholar. He has published 45 research articles in international journals like Elsevier's Computer Methods, 15 book chapters in University, International and National conferences. His research domains include Digital Image Processing, Character Recognition and Web Mining. Dr. Dipak is approved Ph. D. Guide in Sant Gadgebaba Amravati University, Amravati, with 5 student are working under his supervision. He is expert in various bodies and subject expert of shankar dayal university Raipur, KBCNMU university. He has conducted Various PhD viva in shankar dayal university Jaipur, KBCNMU university. He has working in valuation of PhD thesis above universities.

Dr. Suhas Gajanan Sapate, completed his BE and ME in CSE in 2000 and 2007 respectively from WCE Sangli, Maharashtra. He completed his Ph.D. in CSE from SGGS IE&T, Nanded under SRTM University, Nanded in 2019 as a full-time research scholar. He has published 6 research articles in international journals like Elsevier's Computer Methods and programs in Biomedicine with IF 6.1 Citescore 10.1 and Elsevier's "Biocybernetics and Biomedical Engineering‖ IF 6.4 Citescore 11.6, Two book chapters in Springer and CRC press, 11 articles in International and 7 papers in National

Int. J. Advanced Networking and Applications
Volume: 15 Issue: 04 Pages:100-200 (2023) ISSN: 0975-0290 (Special Issue – ASCIS 2023)

conferences. His research domains include Digital Image Analysis, Artificial Intelligence and Computer Vision. Dr. Suhas is approved Ph. D. Co-supervisor in CSE department of Lovely Professional University, Punjab with 1 student completed Ph.D. while 2 are working under his supervision. He is also a Ph.D. Co-Supervisor at Visvesvaraya Technological University, Belagavi, Karnataka and one student is working under his supervision.

Prof. Punam Mahesh Ingale completed her M.Sc in 2008, MPhil in 2013 and currently pursuing PhD at Sant Gadgebaba Amravati University, Amravati. She is working as assistant Professor in Department of Computer Science at Vidnyan Mahavidyalaya, Malkapur (Maharashtra), District Buldhana.
Area of research: Digital Image Processing, Machine Learning

International Journal of Innovative Research of Science, Engineering and Technology (IJIRSET)

|www.ijirset.com | A Monthly Peer Reviewed & Referred Journal | e-ISSN: 2319-8753; p-ISSN: 2347-6710|

|Volume 13, Issue 6, June 2024|

|DOI: 10.15680/IJIRSET.2024.1306112|

Solar Based Automatic Grass Cutter

Sardar Patil[1], Vishwas Patil[2], Atharv Patil[3], Akash Warekar[4], Aarati Kadam[5], Pranav Kambale[6], Prof. N. S. Jadhav[7]

U.G. Student, Department of Electrical Engineering, SETI, Panhala, Kolhapur, Maharashtra, India[1-6]

Associate Professor, Department of Electrical Engineering, SETI, Panhala, Kolhapur, Maharashtra, India[7]

ABSTRACT: The goal of this research study is to improve sustainable lawn management through the construction of an autonomous grass cutter that runs on solar power and uses Arduino technology. The system is equipped with an Arduino microcontroller and Bluetooth module with mobile app for automatic operations, a rechargeable battery for energy storage, and a photovoltaic (PV) panel for harnessing solar energy. The grass cutter requires less human intervention to run because it is outfitted with sensors for obstacle identification and navigation as well as electric motors to drive the cutting blades. When compared to traditional gas-powered mowers, the integration of solar energy greatly lowers the carbon impact and operating expenses. The device's efficacy in tending to small to medium-sized lawns is validated by experimental results, underscoring its potential as an environmentally friendly substitute for automated lawn care. The feasibility of integrating intelligent automation and renewable energy sources to advance environmental sustainability and energy efficiency in daily applications is highlighted by this breakthrough.

KEYWORDS: Arduino UNO, Solar PV panel, Electric Motors, Sensors, etc.

I. INTRODUCTION

In light of the pressing environmental issues facing the world, finding sustainable and effective solutions to daily problems has become more and more important. The need for more environmentally friendly options is highlighted by the fact that traditional gas-powered lawn mowers, despite their effectiveness, contribute greatly to air pollution, noise pollution, and operating costs. In order to provide a greener and more effective method of lawn care, this research explores the construction of an Arduino-powered solar-powered autonomous grass cutter. The environmental effect of traditional lawn mowers can be greatly reduced by using solar energy, which is a plentiful, clean, and sustainable resource. The proposed grass cutter may function independently by utilizing photovoltaic (PV) panels to harvest energy, so decreasing its need on fossil fuels and mitigating greenhouse gas emissions. The Arduino microcontroller is the brains behind this innovation; it integrates different parts to ensure smooth operation and acts as the system's brain. Rechargeable batteries are used to store the electrical power generated by the photovoltaic panels as they absorb solar radiation. Electric motors and blades, which perform the cutting motion, are powered by this stored energy. Using effective algorithms to limit energy consumption and guarantee dependable performance in a range of environmental circumstances, the Arduino microcontroller orchestrates these activities. In order to ensure safe and efficient operation, the grass cutter must be able to handle obstacles and uneven terrain. This is made possible by sensors, such as infrared and ultrasonic detectors. This study has four key goals: to minimize the negative environmental effects of lawn care; to improve user convenience by automating tasks; to maximize solar energy use; and to guarantee the device's dependability and safety. The solar-powered lawnmower encourages people to embrace renewable energy sources in their daily lives by automating the process of mowing grass, saving time and effort. With the ability to spur wider uses of solar energy in automated systems, this project constitutes a noteworthy technological breakthrough in sustainable lawn care. In order to show the system's viability and efficacy as a green substitute for conventional lawn mowers, the ensuing sections of this article will offer a thorough review of its design, installation, and performance evaluation.

II. METHODOLOGY

To charge the battery, we utilize a solar panel. This system, which regulates the operation of every motor, is built using Arduino UNO microcontrollers. Additionally, we employ a Bluetooth module and a smartphone app to operate the grass cutter. The system is supplied with power from the battery. The Arduino UNO is utilized to control a motor by being connected between a battery and the motor. Here, we're also utilizing an ultrasonic sensor to find objects. If there are no obstacles in front of the car, the Arduino Uno microcontroller advances the motors. For the vehicle's safety, an

e-ISSN: 2582-5208
International Research Journal of Modernization in Engineering Technology and Science
(Peer-Reviewed, Open Access, Fully Refereed International Journal)
Volume:06/Issue:05/May-2024 Impact Factor- 7.868 www.irjmets.com

DESIGN & DEVELOPMENT OF PV MODULAR

Prof. Y. R. Naik*1, Pranavkumar Dinde*2, Omkar Gawade*3, Raviraj Ghewari*4, Samruddhi Kamble*5, Vaibhavi Patil*6

*1Assistant Professor, Electrical Engineering, Sanjeevan Engineering & Technology Institute, Panhala, Maharashtra, India.

*2,3,4,5,6UG Student, Electrical Engineering, Sanjeevan Engineering & Technology Institute, Panhala, Maharashtra, India.

ABSTRACT

solar PV modulator, there is solar it is mostly important Renewable energy sources, which gives tremendous or vast amount of energy but at cloudy, rainy atmosphere polar energy become a lower efficient. By using this method, we can collect solar energy with the help of solar panels but solar Panel most commonly situated at inclined position such as south at 30c to 45c most. But due to angle direction is at one side solar gives output efficiency is less, so we can provide some advance in this system to the Solar panel to increase output efficiency through DC gears motor, with sensors and Automation like PLC. To Through this we can. monitoring & controlling can achieve.

Keywords: Solar panel, Dc motors, PLC.

I. INTRODUCTION

What is photovoltaic (PV) technology and how does it work? PV materials and devices convert sunlight into electrical energy. A single PV device is known as a cell. An individual PV cell is usually small, typically producing about 1 or 2 watts of power. These cells are made of different semiconductor materials and are often less than the thickness of four human hairs. In order to withstand the outdoors for many years, cells are sandwiched between protective materials in a combination of glass and/or plastics.

To boost the power output of PV cells, they are connected together in chains to form larger units known as modules or panels. Modules can be used individually, or several can be connected to form arrays. One or more arrays is then connected to the electrical grid as part of a complete PV system. Because of this modular structure, PV systems can be built to meet almost any electric power need, small or large.

PV modules and arrays are just one part of a PV system. Systems also include mounting structures that point panels toward the sun, along with the components that take the direct-current (DC) electricity produced by modules and convert it to the alternating-current (AC) electricity used to power all of the appliances in your home.

II. LITERATURE REVIEW

Now days solar panel existing in a static position, but the process is only storing the solar energy at one direction. Through This project we are making operation by PLC in tilting position with axis.

Md. Shahariar Chowdhury [1] have studied An overview of solar photovoltaic panels' end-of-life material recycling. End-of-life (EOL) solar panels may become a source of hazardous waste although there are enormous benefits globally from the growth in solar power generation. Global installed PV capacity reached around 400 GW at the end of 2017 and is expected to rise further to 4500 GW by 2050. Considering an average panel lifetime of 25 years, the worldwide solar PV waste is anticipated to reach between 4%-14% of total generation capacity by 2030 and rise to over 80% (around 78 million tonnes) by 2050.

Therefore, the disposal of PV panels will become a pertinent environmental issue in the next decades. Eventually, there will be great scopes to carefully investigate on the disposal and recycling of PV panels EOL. At present, PV recycling management in many countries envisages to extend the duties of the manufacturers of PV materials to encompass their eventual disposal or reuse. However, further improvements in the economic viability, practicality, high recovery rate and environmental performance of the PV industry with respect to recycling its products are indispensable.

Xiao Yue Li [2] have studied Review and perspective of materials for flexible solar cells. Thin-film flexible solar

e-ISSN: 2582-5208
International Research Journal of Modernization in Engineering Technology and Science
(Peer-Reviewed, Open Access, Fully Refereed International Journal)
Volume:06/Issue:05/May-2024 Impact Factor- 7.868 www.irjmets.com

3 PHASE INDUCTION WITH SOFT START

Prof. Vinayak. Ghewari*1, Prathamesh Kamble*2, Sourabh Patil*3, Harshil Bodke*4

*1Professor, Department Of Electrical Engineering, Sanjeevan Engineering Technical Institute, Kolhapur, Maharashtra, India.

*2,3,4Students, Department Of Electrical Engineering Sanjeevan Engineering Technical Institute, Kolhapur, Maharashtra, India.

DOI:https://www.doi.org/10.56726/IRJMETS58450

ABSTRACT

This project explains how a 3phase induction motor starts smoothly and softly. When the three-phase induction motor first starts, it draws far more current than it can handle, which causes the motor to accelerate to its maximum speed right away. This causes the motor's windings to experience high electrical stress and a mechanical jerk. The windings may burn occasionally. The prototype was created to provide an induction motor with a gentle start through the use of SCR firing, which is activated by a significantly delayed firing angle during starting. As a result, there is low voltage at startup and gradually high voltage. As a result, the motor begins slowly and increases gradually to its maximum speed. The working prototype consists of a six anti-parallel SCRs, two for each phase, the output of which is connected to a set of lamps representing the coils of a 3phase induction motor, capacitors, comparators, opto-isolators to trigger the SCRs. The implementation of hardware model has been discussed in this paper.

Keywords: Firing Angle Delay, Opto Isolators, Scr Triggering, Motor Current Control.

I. INTRODUCTION

The project's goal is to give a three-phase induction motor a gentle, seamless start. When the three-phase induction motor first starts, it draws far more current than it can handle, which causes the motor to accelerate to its maximum speed right away. This causes the motor's windings to experience high electrical stress and a mechanical jerk. The windings may burn occasionally. For a safer operation, the induction motor should start smoothly and increase in speed gradually. The goal of this project is to gently start the induction motor using SCR firing, which is triggered by a firing angle that is significantly delayed during starting. The delay is then gradually reduced until it reaches zero voltage triggering.

As a result, there is low voltage at startup and gradually high voltage. As a result, the motor begins slowly and increases gradually to its maximum speed. The six anti-parallel SCRs in this project—two for each phase—have their outputs connected to a series of LEDs that symbolize the coils of a three-phase induction motor. Capacitor charging and discharging are interfaced to comparators, which causes delayed firing pulses at first, which are subsequently progressively reduced until the motor reaches its maximum speed. To activate the SCRs, the comparators' output is routed through OPTO-isolators. provide a gentle induction motor start. Three-phase induction motors have a low power factor and require a significant amount of current when they first start. Motor torque content fluctuates and transients as a result of excessive current. The mechanical life of the rotor decreases as a result of transients and torque pulsation causing the motor shaft to jerk. An increasingly common technique to lessen the negative effects of beginning current and torque pulsation in induction motors is electronically controlled soft starting. Typically, soft starters—which are accomplished by raising stator frequency—are employed to prevent these issues. Both the induction motor's performance and the load torque characteristics are enhanced when a soft starter is used.

Because of its regulated soft-starting capability with limited beginning current, power semiconductor-based ac motor starters are replacing conventional reduced-voltage starters and electromagnetic line starters more frequently. The employment of THYRISTOR-based soft starters is a workable answer to the induction motor (IM) starting issue since they are inexpensive, straightforward, dependable, and take up less space. Whether an IM is controlled by a soft starter or a direct-online starter, it can cause significant pulsations on the electromechanical torque depending on the first switching instants of all three phases to the supply.

e-ISSN: 2582-5208
International Research Journal of Modernization in Engineering Technology and Science
(Peer-Reviewed, Open Access, Fully Refereed International Journal)
Volume:06/Issue:06/June-2024 Impact Factor- 7.868 www.irjmets.com

SOLAR WIND HYBRID ELECTRIC VEHICLE

Sandip Gurav*1, Digvijay Patil*2, Sammed Patil*3, Sourav Jadhav*4, Surabhi Pusalkar*5, Atul Powar*6, Prof. A. M.Bhandare*7

*1,2,3,4,5,6DBATU, Electrical Engg, Seti, Panhala, Kolhapur, Maharashtra, India.

*7Department of electrical engineering, Sanjeevan engineering technology Institute panhala, kolhapur, Maharashtra, India.

DOI : https://www.doi.Org/10.56726/IRJMETS58560

ABSTRACT

In order to address issues with energy security and mitigate the effects on the environment, a shift to sustainable energy sources is imperative. The Solar-Wind Hybrid Electric Vehicle (S-WHEV), which combines solar and wind energy harvesting systems with electric vehicle (EV) technology to improve efficiency and lessen reliance on traditional energy sources, is one innovative concept in this field that shows promise. An extensive summary of the design, functionality, and possible advantages of the S-WHEV is provided in this abstract.The S-WHEV produces power using a small wind turbine and solar panels, which is then stored in an onboard battery system. Photovoltaic cells in the solar panels, which are usually mounted on the top of the car, absorb sunlight and transform it into electrical energy. Concurrently, the wind turbine—which is positioned to capture airflow during vehicle motion—provides further power. This two-pronged harvesting

Keywords: Wind Energy, Solar Energy, Hybrid Vehicle, Maximum Power Point Tracking.

I. INTRODUCTION

Utilizing solar energy to charge the electric vehicles (EVs) during daytime is an interesting concept gaining much attention among the masses. This allows for the operating of EVs with net zero greenhouse gas emissions, provided the solar panels and ESS equipment are themselves mass-produced in an environmentally benign manner, which is already the case. However, for electric vehicles only charged with solar energy, a forecasted Solar Power Production Profile (SPPP) is not sufficient to guarantee the workload and opportunistic driving of the green mobility option. As solar batteries are the primary energy storage capacity within the car, their state of charge most likely depends on weather and usage scenarios. There are many other mathematical and technical hurdles to clear in defining a "solar-powered car" more accurately. This includes defining motor–generator efficiencies within the vehicle and considering energy costs for different types of propulsion, etc. Furthermore, the run times of a car on the solar energy sourced by the last SPPP set actually exceed the utility of this energy in certain cases. Utility waste could be due to reduced battery charging/discharge efficiencies, potentially using solar electricity from elsewhere (e.g., friends' places near destination cities), or the lack of energy prices and sources in the last forecasted SPPP set. Especially because of operating errors, such scenarios could be much unpredictable due to unsustainable battery state of charge and solar power delivered. Therefore, for solar-charged electric vehicles, more direct and compact performance indicators for green mobility opportunity at a certain point in time are desirable [1].

Humanity is currently witnessing a shift towards renewable energy across various sectors in their effort to minimize their carbon footprint. As part of this renewable energy integration, electric vehicles (EVs) are gaining incredible attention and favor around the world [2]. The drop in prices of renewable energy technologies and the advancement in the efficiency and performance of energy storage systems (ESS) are some major reasons behind this transition.

II. INTEGRATION OF SOLAR WIND

In order to address issues with energy security and mitigate the effects on the environment, a shift to sustainable energy sources is imperative. The Solar-Wind Hybrid Electric Vehicle (S-WHEV), which combines solar and wind energy harvesting systems with electric vehicle (EV) technology to improve efficiency and lessen reliance on traditional energy sources, is one innovative concept in this field that promise. The S-WHEV produces power using a small wind turbine and solar panels, which is then stored in an onboard battery system. Photovoltaic cells in the solar panels, which are usually mounted on the top of the car, absorb

e-ISSN: 2582-5208
International Research Journal of Modernization in Engineering Technology and Science
(Peer-Reviewed, Open Access, Fully Refereed International Journal)
Volume:06/Issue:05/May-2024 Impact Factor- 7.868 www.irjmets.com

TO MODIFIED AND DESIGN SOLAR POWERED BASED ENERGY EFFICIENT PORTABLE WASHING MACHINE

Prof. V.T. Metkari*1, Nadim Devlekar*2, Prashant Kurane*3, Prashant Patil*4, Ubed Chougle*5, Payal Bunde*6

*1Head Of Department, Dept. Of Electrical Engg, Sanjeevan Engineering And Technology Institute, Panhala, Kolhapur, Maharashtra, India.

*2,3,4,5,6Undergraduate Students, Dept. Of Electrical Engg, Sanjeevan Engineering And Technology Institute, Panhala, Kolhapur, Maharashtra, India.

DOI : https://www.doi.org/10.56726/IRJMETS58470

ABSTRACT

It is necessary to build some energy-efficient electronic equipment for that model, which is readily available and energy-efficient, in order to minimize the energy cruisers in India. To catch solar energy, for example, this system uses solar panels. It then stores the energy in a battery for later use. It is propelled by a DC motor that is run by a battery that powers the washing machine. To meet the needs of both the washing and rinsing processes, the machine features two wash buckets. In terms of convenience, the machine has buttons for choosing washing cycles, starting and halting the machine, and controlling the motor through the use of a microcontroller. The integration of SMPS ensures that the battery is charged, either from the grid or elsewhere as needed, providing flexibility and dependability. This portable washing machine is affordable in terms of electricity usage, eco-friendly, and equipped with functions designed specifically for locations without power.

Keywords: Solar Panel, Buckets, Grid, Battery, Etc.

I. INTRODUCTION

One excellent illustration of this technical development is the portable washing machine. It is perfect for people who live in tiny places or are always on the road because of its compact and portable design. The washer is made up of a few essential parts that function as a unit to give a sustainable and effective washing experience[1]. First of all, a solar panel attached to the washing machine is in charge of capturing solar energy[1]. The appliance's solar panel is positioned to optimize exposure to sunshine and ensure maximum energy output. The washing machine is powered by electricity that is produced by the solar panel[2]. Additionally, a battery for energy storage is included with the portable washing machine to guarantee continuous operation. The extra energy produced by the solar panel throughout the day is stored in this battery, which serves as a backup power supply. When solar power is inadequate, the washing machine may still operate thanks to the stored energy, which can be used at night or during periods of low sunlight[3].

A complex SMPS (Switched-Mode Power Supply) system is also linked to the appliance. When solar power is insufficient, this method is essential in charging the battery from the grid. It keeps the washing machine powered on all the time by smartly switching between utility and solar power [4]. This function not only increases the appliance's dependability but also maximizes energy use, making it extremely efficient.

II. EASE OF USE

A. Simple Setup

- Plug and play solar panel: The solar panel comes with user-friendly connectors that can be easily plugged into the charge controller and battery system, eliminating the need for any technical knowledge or expertise.
- Integrated components: By combining the battery, charge controller, and SMPS into one compact unit, the setup of multiple components is made easier, eliminating the need for separate installations.

B. Automated cycles

- Pre-programmed cycles: The machine's washing and rinsing cycles can be easily started by pressing a single button.

e-ISSN: 2582-5208
International Research Journal of Modernization in Engineering Technology and Science
(Peer-Reviewed, Open Access, Fully Refereed International Journal)
Volume:06/Issue:06/June-2024 Impact Factor- 7.868 www.irjmets.com

SOLAR BASED GPS TRACKING HANDICAPPED TRICYCLE

Rutuja Bobade*1, Neha Mensagare*2, Pravin Digekar*3, Omkar Narute*4, Prof. N.S. Jadhav*5

*1,2,3,4Student, Department Of Electrical Engineering, Sanjeevan Engineering & Technology Institute, Panhala, Kolhapur, India.

*5Assistant Professor, Department Of Electrical Engineering, Sanjeevan Engineering & Technology Institute, Panhala, Kolhapur, India.

ABSTRACT

Transportation is the biggest source of natural contamination as comes about of carbon outflow. Which advances nursery impact that can quicken worldwide warming. In this report show plan and creation of sun oriented fuelled tricycle; transportation gadget with three wheels to advantage sun powered as a renewable vitality assets. To coordinated sun powered PV framework within the tricycle, the major component required are electrical stack, battery, sun oriented PV board and sun based charge controller. The plan prepare begins with the era of design concepts which coming about within the last plan concept and a specialized drawing of the model. At that point, creation prepare is start which includes the tricycle outline and body earlier to establishment of mechanical components. After portray, the sun powered PV framework are coordinates into the tricycle, coming about in wrap up item of sun based control tricycle model. The model is effectively useful with sun based control; in this way, it can be concluded that the plan of sun based control tricycle can be utilized to advance green and economical transportation.

Keywords: GPS Tracking Tri-bicycle, PV, Solar Charger, Controller.

I. INTRODUCTION

In today's world, saddling renewable vitality sources like sun powered control has ended up basic for economical improvement. One such inventive application is the integration of sun based innovation with GPS following frameworks, especially in incapacitate tricycles. By combining these innovations, we will make a arrangement that not as it were makes a difference in route but moreover upgrades security and openness for people with versatility challenges. Let's investigate how this solar-based GPS tracking system can revolutionize the utilization of disable tricycles within the domain of electric portability. The improvement of a solar-based and electricity-powered GPS following tricycle speaks to a critical development in maintainable transportation and coordination. This sort of tricycle leverages renewable vitality and progressed innovation to offer an eco-friendly, productive, and flexible arrangement for individual and commercial utilize.

Sun powered and Electric Control Integration: By combining sun oriented boards and rechargeable electric batteries, the tricycle can diminish dependence on fossil fills, bringing down carbon emanations and operational costs. The sun based boards tackle daylight to charge the batteries amid the day, guaranteeing that the vehicle remains operational indeed in farther or off-grid ranges. This double control framework upgrades the tricycle's run and unwavering quality, making it a practical choice for urban conveyances, last-mile coordination, and individual versatility.

GPS Tracking Capabilities: Joining GPS following innovation into the tricycle offers various points of interest. Real-time following improves course optimization, moving forward conveyance productivity and decreasing fuel utilization. For individual clients, GPS following gives security highlights such as course observing, burglary recuperation, and geo-fencing, which can send alarms on the off chance that the vehicle clears out a assigned zone.

II. LITERATURE REVIEW

In organize to perform this expand, composing overview has been made from diverse sources like journal, books, article and others. This chapter joins all basic considers which have been done as of now by other explore work. It is importance to do the composing overview a few time as of late doing the expand since we are ready execute in case there are information that related to this expand. The first basic thing a few time as of late starting the wander we must clearly get it roughly the subject that we got to do. So by doing the composing

e-ISSN: 2582-5208
International Research Journal of Modernization in Engineering Technology and Science
(Peer-Reviewed, Open Access, Fully Refereed International Journal)
Volume:06/Issue:06/June-2024 Impact Factor- 7.868 www.irjmets.com

SMART SOLAR AUTOMATION

Nagesh Jagganwar*1, Urmila Varpe*2, Sakshi Miraje*3, Sampada Shinde*4, Prajakta Yeloore*5, Prof. Y.R. Naik*6

*1,2,3,4,5Student, Department Of Electrical Engineering, Sanjeevan Engineering & Technology Institute, Panhala, Kolhapur, India.

*6Assistant Professor, Department Of Electrical Engineering, Sanjeevan Engineering & Technology Institute, Panhala, Kolhapur, India.

ABSTRACT

This project introduces an innovative design for Smart Solar Automation, focusing on a cost-effective and wireless Internet of Things (IoT) based home automation system. The system is capable of controlling various household components via the internet or automatically adjusting to ambient conditions. Key to this development is the creation of firmware for smart control, aimed at minimizing human interaction while ensuring the efficient operation of all electrical devices in the home. Utilizing Node MCU, a widely-used open-source IoT platform, the project facilitates automation processes. Each component within the system employs distinct transmission modes to communicate user commands via the Node MCU to the relevant appliances. Central to this system is the implementation of wireless technology, allowing remote access through a smartphone. By leveraging a cloud server-based communication model, the project enhances practicality by enabling users to control their appliances from any location. The designed network ensures robust data transmission, strengthening the automation process. This system aims to control household electrical appliances with a focus on affordability, user-friendliness, and ease of installation. Additionally, it provides real-time appliance status and control through an Android interface. The system is tailored to support the needs of the elderly and disabled, while the integration of smart solar technology enhances living standards in homes and offices.

Keywords: Automation, Solar, IoT.

I. INTRODUCTION

The development of energy efficiency and renewable energy technologies is growing worldwide, prompting increased interest from numerous countries. Universities are actively engaging in this technological advancement through student competitions aimed at raising awareness. Among these competitions is the Solar Decathlon, which has been held in the United States and various other countries. A recent addition to this landscape is the Solar Decathlon Middle East (SDME), established in the Middle East with the inaugural event taking place in Dubai in 2018. Qatar University's participation in the SDME 2018 competition has facilitated the formation of a diverse team of students collaborating on the design and construction of environmentally friendly, intelligent, portable, and cost-effective solar buildings. These structures are energy-efficient and fully monitored and automated through Internet of Things (IoT) technologies.

This project concentrates on the development of an economical Wireless Smart Automation System (WSAS) utilizing IoT and the Android operating system, harnessing Wi-Fi, Bluetooth technology, and solar power to operate electrical devices. By incorporating Intel Galileo, it seamlessly integrates cloud networking and wireless communication, empowering users to remotely control lighting, ventilation, and appliances. Prioritizing energy conservation, the system adjusts its operations based on sensor feedback and securely stores data in the cloud. With its utilization of Wi-Fi technology, this home automation solution stands out for its remote accessibility, affordability, and potential for expansion.

II. LITERATURE REVIEW

Wireless Smart Automation system using IoT: This system allows for basic home control and automation via mobile devices or computers, accessible worldwide over the internet. Known as a smart home, its primary aim is to save energy and simplify tasks. The proposed configuration consists of a distributed home automation system with a server, Wi-Fi module, and sensors. The server oversees and monitors these sensors and is easily expandable to accommodate additional hardware interfaces. An Arduino board with a built-in Wi-Fi module

e-ISSN: 2582-5208
International Research Journal of Modernization in Engineering Technology and Science
(Peer-Reviewed, Open Access, Fully Refereed International Journal)
Volume:06/Issue:06/June-2024 Impact Factor- 7.868 www.irjmets.com

AUTOMATIC POWER FACTOR CONTROLLER

Prof. Basawaraj Hebbale*1, Pranav Madan Patil*2, Yuvraj Yashawant Desai*3, Vaibhav Vasant Kamble*4, Anil Dasharath Bavane*5

*1,2,3,4,5Sanjeevan Engineering & Technology Institute, Panhala, Maharastra, India.

DOI : https://www.doi.org/10.56726/IRJMETS58886

ABSTRACT

Power factor correction (PFC) is a technique for mitigating the unwanted effects of electric loads that result in a power factor less than unity. Power factor correction can be used by an electrical power transmission utility to increase the stability and efficiency of the transmission network, or by individual electrical customers to minimize the costs imposed by their electricity supplier. This paper discusses the design and implementation of an automated power factor correction (APFC) system employing solid state switching capacitors and a microprocessor. The major goals are to reduce line loss, reduce reactive power flows on the line, and avoid switching surge overvoltage caused by turning on/off capacitors.

Keywords: Power Factor, LCD, C language, Microcontroller.

I. INTRODUCTION

Power is extremely valuable in the a current technology revolution, and the power a system is growing more and more complicated every day. As a result, it becomes essential to transmit every unit of power produced over longer distances with the least amount of power loss. But as the number of inductive loads, load volatility, etc., has increased, so too have the losses. Therefore, it is now wise to identify the reasons behind power outages and enhance the power infrastructure. The load power factor significantly drops as inductive loads are used more frequently, increasing system losses and decreasing system efficiency. By utilizing an internal timer to determine the delay in the arrival of the current signal relative to the voltage signal from the source, an automatic power factor correction device determines power factor from line voltage and line current with high precision. The phase angle lag (ø) between the voltage and current signals is determined, and the related power factor (cosø) is subsequently found.

After that, the microcontroller determines how much compensation is needed and activates the necessary number of capacitors from the capacitor bank in order to bring the power factor close to unity. Techniques for automatic power factor adjustment can be used to stabilize power systems, homes, and industrial equipment.

As a result, the system stabilizes and the apparatus's overall efficiency rises. As a result, using a microcontroller-based power factor corrector lowers total costs for both electrical energy suppliers and customers. Reducing reactive power consumption with capacitor banks maximizes electrical system efficiency while minimizing losses. This technique is known as power factor correction. Single phase capacitor banks for residential and commercial applications have been developed in response to concerns about power conservation and reactive power control. The goal of this project is to create a microprocessor-based control system that will improve and increase the performance of single-phase capacitor banks.

II. LITERATURE REVIEW

Solar panels are currently in a static posture, however the process only stores solar energy in one direction. With this project, we are able to operate a PLC in an axis-tilted position. Power Factor Improvement Based on Micro Controller Using APFC Panel has been explored by

[1]Chanchad Vishal

The Power Factor can be increased and brought closer to 0.9 to 0.95 by adding power capacitors of the right size to the circuit. This reduces line losses and boosts a plant's efficiency. This APFC system greatly increases the system's efficiency. Solid state switches are used in place of mechanical relays to produce a consistent and effective result. This highly effective method uses capacitors of varying sizes to trigger switches that were programmed to manage the loads. As a result, it is strongly advised to maximize the advantages of the system that will be built in the manner previously described.

www.ijprems.com
editor@ijprems.com

INTERNATIONAL JOURNAL OF PROGRESSIVE RESEARCH IN ENGINEERING MANAGEMENT AND SCIENCE (IJPREMS)

Vol. 04, Issue 05, May 2024, pp: 1964-1970

e-ISSN : 2583-1062

Impact Factor: 5.725

DESIGN AND DEVELOPMENT OF SIGN LANGUAGE TO SPEECH CONVERSION

Prof. P. D. Pange[1], Mr. P. A. Jadhav[2], Mr. R. N. Jadhav[3], Mr. A. B. Latwadekar[4], Mr. P. S. Jagtap[5], Mr. N. I. Jamadar[6]

[1]Project Guide, Department Of Electrical Engineering, Sanjeevan Knowledge City, Somwar Peth, Panhala, Kolhapur - 416201, Maharashtra, India.

[2,3,4,5,6]Sanjeevan Engineering And Technology Institute Sanjeevan Knowledge City, Somwar Peth, Panhala, Kolhapur - 416201, Maharashtra, India.

DOI: https://www.doi.org/10.58257/IJPREMS34545

ABSTRACT

This project focuses on the design and development of an innovative Sign Language to Speech Conversion System (SLSCS) aiming to facilitate communication between individuals proficient in sign language and those who use spoken language. Leveraging advanced computer vision techniques, the system interprets and recognizes diverse sign language gestures. Natural Language Processing (NLP) algorithms are employed to convert these gestures into intelligible spoken language. The abstract emphasizes the project's commitment to inclusivity, user-friendliness, and continuous improvement through iterative refinement, ensuring a seamless and effective communication experience for users across different sign languages.

Keywords: Firing angle delay, Motor current control, Opto-couplers, Opto-isolators, SCR triggering, Zero voltage

1. INTRODUCTION

This report is about a glove that can help people who have trouble speaking. These people often communicate through hand gestures, but it can be hard for others to understand them. The glove has sensors that can read the hand gestures and convert them into speech and text. It is affordable and easy to use. We use a computer program called Python to make it work. The glove has been tested and calibrated using American Sign Language. The glove has the potential to make communication easier for people who are speech-impaired. In the future, we hope to improve the glove even more.

Communicating through hand gestures is one of the most common forms of non- verbal and visual communication adopted by speech-impaired populations all around the world. The problem existing now is that most people are not able to comprehend hand gestures or convert them to k enough for the listener to understand. A large fraction of India's population is speech impaired. In addition to this communication to sign language is not a very easy task. This problem demands a better solution that can assist the speech-impaired population in conversation without any difficulties. As a result, reducing the communication gap for the speech impaired.

This paper proposes an idea that will assist in removing or at least reducing this gap between the chaired people research going on in this area mostly focusing on image-processing approaches. However, a cheaper and user-friendly approach has been used in this paper. The idea is to make a glove that can be worn by speech-impaired people which will further be used to convert sign language into speech and text. Our prototype involves Arduino Uno as a microcontroller which is interfaced with flex sensors an accelerometer, gyroscopic sensor for reading hand gestures. Furthermore, to perform better execution, we have incorporated an algorithm for better data interpretation and to produce more accurate results. Thereafter, we use Python to interface Arduino Uno with a microprocessor and finally converting into speech. The prototype has been calibrated by ASL.

2. LITERATURE REVIEW

This report proposes an idea which will assist in removing or at least reducing this gap between the chaired research going on in this area mostly focusing on image- processing approaches. However, a

cheaper and user-friendly approach has been used in this paper. The idea is to make a glove that can be worn by speech-impaired people which will further be used to convert sign language into speech and text.

Review of Literature

Deena Nath, Jitendra Kurami and Deveki Nandan Shukla

Is studies have suggested that mindfulness meditation can have a positive impact on mental health, including reducing symptoms of anxiety and depression. One study found that individuals who practiced mindfulness meditation had reduced symptoms of anxiety and improved overall well-being. Overall, the literature suggests that mindfulness

e-ISSN: 2582-5208
International Research Journal of Modernization in Engineering Technology and Science
(Peer-Reviewed, Open Access, Fully Refereed International Journal)
Volume:06/Issue:06/June-2024 Impact Factor- 7.868 www.irjmets.com

SOLAR POWER CHARGE CONTROLLER USING ARDUINO

Prof. Baswaraj Hebbale*1, Nikhil Dakare*2, Venkatesh Haval*3, Rohit Basare*4

*1Professor, Department Of Electrical Engineering, Sanjeevan Engineering Technical Institute, Kolhapur, Maharashtra, India.

*2,3,4Students, Department Of Electrical Engineering, Sanjeevan Engineering Technical Institute, Kolhapur, Maharashtra, India.

DOI : https://www.doi.org/10.56726/IRJMETS58793

ABSTRACT

Integrating solar energy into power systems has gained significant attention due to its environmental benefits and potential to alleviate energy crises. A crucial component in solar power systems is the charge controller, which regulates the charging and discharging of batteries to optimize energy utilization and ensure battery longevity. In this project, we propose designing and implementing a Solar Power Charge Controller (SPCC) utilizing Arduino microcontroller technology. The SPCC is designed to efficiently manage the charging process of batteries connected to solar panels. Utilizing Arduino's versatility, the controller employs hardware and software components to monitor parameters such as battery voltage, solar panel voltage, and current flow. The controller dynamically adjusts the charging parameters by processing this data to maximize energy harvesting while preventing overcharging and deep discharge.

Keywords: Photovoltaic (PV) panel, Arduino, Maximum Power Point Tracking (MPPT).

I. INTRODUCTION

The utilization of solar energy has emerged as a promising solution to address the ever-growing energy demands while mitigating environmental concerns associated with traditional energy sources. Solar power systems, equipped with photovoltaic (PV) panels, harness sunlight to generate electricity, offering a sustainable and renewable energy alternative. However, the efficient management of solar power systems poses a significant challenge, particularly concerning battery charging and maintenance. A critical component in solar power systems is the charge controller, responsible for regulating the charging and discharging of batteries connected to the solar panels. The charge controller ensures optimal charging efficiency, prevents overcharging, and safeguards batteries from deep discharge, extending their lifespan. Traditionally, particularly concerning battery charging and maintenance.

A solar-powered battery charging system using an Arduino can be an excellent project for those who want to learn about renewable energy and microcontroller programming. Here are the basic steps to create such a system. Choose the solar panel: The first step is choosing the right one. The discussion should be able to produce enough power to charge the battery. You can use online calculators to determine the solar panel size needed. Choose the battery: The battery should have enough capacity to store the energy produced by the solar panel. Choose a battery compatible with the Arduino and can be charged using the solar panel. Connect the solar panel to the battery: Connect the solar panel to the battery using a charge controller. The charge controller ensures the battery is charged at the correct voltage and current levels. Connect the Arduino to the battery: Connect the Arduino to the battery using a voltage regulator. The voltage regulator ensures that the Arduino is powered at the correct voltage level. Programming Arduino: The program should monitor the battery voltage and current levels and adjust the charging current accordingly.

The project is designed to Solar power as a renewable and environmentally friendly source of energy, which has gained widespread attention and adoption in recent years. With the growing global demand for sustainable energy solutions, solar power systems are becoming increasingly popular for both residential and commercial applications. However, effective monitoring and management of solar power systems are critical to optimize their performance and ensure reliable operation. In this research paper, we present an integrated solution for solar power monitoring using NodeMCU, an open-source Internet of Things(IoT) platform and deploying it onto the ThingSpeak cloud server. We discuss the design, implementation, and evaluation of a solar power monitoring system that leverages the capabilities of NodeMCU along with voltage sensors to collect, process, and visualize real-time data from solar panels, and other system components. Our system provides a

International Journal of Innovative Research of Science, Engineering and Technology (IJIRSET)

|www.ijirset.com | A Monthly Peer Reviewed & Referred Journal | e-ISSN: 2319-8753; p-ISSN: 2347-6710|

|Volume 13, Issue 6, June 2024|

|DOI: 10.15680/IJIRSET.2024.1306219|

Vertical Injection Plastic Moulding Machine

Prof. A.M.Bhandare[1], Sairaj Patil[2], Abhijeet Mithari[3], Sushant Pawar[4], Aniket Patil[5], Sonali Jadhav[6], Sonali Chand[7], Sharvari Patil[8], Deepshree Prabhavalkar[9]

Assistant Professor, Department of Electrical Engineering, Sanjeevan Engineering & Technology Institute, Panhala, Maharashtra, India[1]

Department of Electrical Engineering, Sanjeevan Engineering & Technology Institute, Panhala, Maharashtra, India[2-9]

ABSTRACT: In today's rapidly advancing industrial landscape, plastic has become increasingly vital. Products made of plastic, both small and large, are widely utilized. We utilize this approach to manufacture Vertical Injection Plastic Moulding Machines, which are more efficient than other machines, reducing production time, improving product quality, and increasing output. Vertical injection plastic moulding machines are designed to produce delicate and intricate plastic parts through the injection moulding process. This abstract outlines the key features, benefits, and applications of these machines. Compared to horizontal machines, vertical machines have a smaller footprint, provide easier mold changes, and utilize gravity to aid in the injection process. These machines are well-suited for creating a diverse range of plastic components due to their flexibility and compatibility with various molds and materials. They are widely used in industries such as automotive, electronics, consumer goods, and medical devices. Vertical injection plastic moulding machines are crucial for industrial applications that demand consistent quality and reliability, as they can produce high-precision products with tight tolerances. In summary, vertical injection plastic moulding machines are exceptionally efficient and versatile for manufacturing complex plastic parts. Their compact size, precision, and adaptability make them essential for various types of production.

KEYWORDS: Plastic, injection, moulding, etc

I. INTRODUCTION

The vertical injection plastic moulding machine operates using a high-pressure hydraulic cylinder, making it more efficient compared to non-automatic machines. This type of machine is an ideal choice for industrial applications due to its compact size and reduced manpower requirements. The process involves melting plastic and injecting the molten material into a die under high pressure, resulting in improved production speed and product quality. This fully automatic process reduces production time and enhances precision, ensuring that even small parts are produced accurately. Additionally, the machine allows for recycling used plastic to create new products. Injection moulding, a common manufacturing technique, involves injecting molten plastic into a mould cavity to form the desired shape, which then cools and hardens. This method is widely used in various industries, including consumer products, automotive, electronics, and medical devices, due to its versatility, efficiency, and cost-effectiveness. The operation begins with designing a mould, typically made of steel or aluminum, with two halves to shape the final product. The mould is mounted on the injection moulding machine, which feeds plastic pellets from a hopper into a heated barrel, where they are melted and injected into the mould cavity.

II. LITERATURE REVIEW

Paper [1]: This paper explores a screw-type injection plastic moulding machine, using a screw mechanism to press material into the mould. It details the design and manufacture of a bench top injection moulding machine for educational use. The machine features a vertical plunger-type injection system with a clamping mechanism, a 290 cc barrel, and a 60 mm injection plunger, making it suitable for labs. The design process and preliminary tests show that increasing motor speed raises the flow rate while decreasing packing time. At 2500 rpm, the flow rate is 0.42 m/s, and packing time is 15 seconds. In Paper [2] the study examines the impact of design parameters on the plastic injection moulding process, focusing on a machine using a handle piston to press material into the mould. With the growing use of plastics in various industries, injection moulding machines are essential for producing diverse plastic items. The paper emphasizes the importance of design parameters on product quality and cost. Prototypes are tested for mechanical and functional performance using Pro E software. Results show that vertical

INTERNATIONAL JOURNAL OF HYDROGEN ENERGY 48 (2023) 37944-37953

Available online at www.sciencedirect.com

ScienceDirect

journal homepage: www.elsevier.com/locate/he

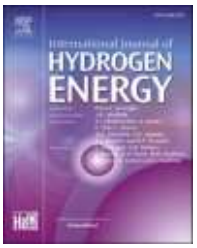

Performance analysis of sodium alanate hydride reactor with different nanofluids

Rahul U. Urunkar[*], *Sharad D. Patil*

Department of Mechanical Engineering, RIT, Rajaramnagar, Affiliated to Shivaji University, Kolhapur, Maharashtra, India

HIGHLIGHTS

- Developed and validated mathematical model of sodium alanate based hydride reactor.
- Used nanofluid as a heat exchange fluid.
- Presented performance for Al_2O_3/HTF, CuO/HTF and MgO/HTF Nanofluids.
- Absorption time is improved by 14% for given conditions.
- Reported up to 10% enhancement in the heat exchange rate for CuO/HTF nanofluid.

ARTICLE INFO

Article history:
Received 31 July 2022
Received in revised form
3 February 2023
Accepted 27 February 2023
Available online xxx

Keywords:
Hydrogen
Hydride bed reactor
Heat transfer
Sodium alanate
Nanofluid

ABSTRACT

The thermal management of the hydride based hydrogen storage reactor is the key factor to realize the complete storing potential of hydrides. In this regards a hydride reactor filled with sodium alanate in multiple tubes is numerically analyzed for absorption process. Based on various governing equations, a mathematical model of hydride reactor is developed and validated with the help of ANSYS Fluent. The hydride reactor uses mainly water or oil for heat exchange during hydrogen sorption. In the present study conventional heat transfer fluid (HTF) is replaced with the nanofluid since it has a greater heat exchange properties. The CuO/HTF, Al_2O_3/HTF and MgO/HTF nanofluids are selected based on previous studies and results of numerical experiment are recorded. The outcomes are attained for various parameters such as material and concentration of nanoparticles, supply pressure of hydrogen and inlet temperature of heat exchange fluid. The CuO/HTF nanofluid with concentration of 5 vol% exhibited better rate of absorption in comparison with other vol% concentrations and other selected nanofluids. It shows improvement in hydrogen absorption time up to 14% under selected conditions. Additionally, it is observed that CuO/HTF nanofluid with 5 vol% concentration is thermodynamically superior to other selected nanofluids; as a result it enhances the rate of the heat exchange up to 10% for hydride reactor. It is realized that the performance of CuO/HTF nanofluid with 5 vol% concentration is superior among picked nanofluids. Therefore for the hydride reactor the use the nanofluid is advantageous.

* *Corresponding author.*
E-mail addresses: rahul.urunkar1991@gmail.com (R.U. Urunkar), p2sharad@yahoo.com, sharad.patil@ritindia.edu (S.D. Patil).
https://doi.org/10.1016/j.ijhydene.2023.02.105